DURATION-TUNED NEURONS IN THE VERTEBRATE AUDITORY MIDBRAIN

MECHANISMS AND RESPONSE PROPERTIES OF DURATION-TUNED NEURONS
IN THE VERTEBRATE AUDITORY MIDBRAIN

By BRANDON AUBIE, B.Math

A Thesis
Submitted to the School of Graduate Studies
in Partial Fulfillment of the Requirements for the
Degree Doctor of Philosophy

McMaster University DOCTOR OF PHILOSOPHY (2012) Hamilton, Ontario
Department of Psychology, Neuroscience & Behaviour

TITLE:	Mechanisms and Response Properties of Duration-Tuned Neurons in the Vertebrate Auditory Midbrain
AUTHOR:	Brandon Aubie, B.Math (University of Waterloo)
SUPERVISORS:	Dr. Paul A. Faure & Dr. Suzanna Becker
NUMBER OF PAGES:	xviii, 206

Abstract

This thesis aims to elucidate the mechanisms and response characteristics of neural circuits in the vertebrate brain capable of responding selectively to stimulus duration. The research within focused on, but is not limited to, auditory neurons; however, most of the results extend to other sensory modalities. These neurons are known, appropriately, as duration-tuned neurons (DTNs). Duration-tuned neurons tend to prefer stimulus durations similar to the duration of species-specific vocalizations and have preferred durations ranging from 1 ms up to over 100 ms across species.

To study the mechanisms underlying DTNs, biologically inspired computational models were produced to explore previously hypothesized mechanisms of duration tuning. These models support the mechanisms by reproducing the responses of *in vivo* DTNs and predicting additional *in vivo* response characteristics. The models demonstrate an inherent flexibility in the mechanisms to extend across a wide range of durations and also reveal subtleties in response profiles that arise from particular model parameters.

To quantify the encoding efficiency of *in vivo* DTNs, information theoretic measures were applied to the responses of 97 DTNs recorded from the auditory midbrain (inferior colliculus) of the big brown bat. Stimulus duration encoding robustness, as measured by stimulus-specific information, tended to align with the stimulus durations that produce the largest responses. In contrast, stimulus durations with the most sensitivity to changes in stimulus duration, as measured with an approximation of the observed Fisher information, tended to be stimulus durations shorter or longer than the duration evoking the largest response. Remarkably, both optimal and non-optional Bayesian decoding methods were able to accurately recover stimulus duration from population responses, including durations that lacked neurons dedicated to best representing that duration. These results suggest that DTNs are excellent at encoding stimulus duration, a feature that has been generally assumed but not previously quantified.

This thesis is dedicated to my loving wife, Rachel.
Thank you for everything.

Acknowledgements

The first science experiment I can remember performing was from a book of experiments my parents bought for me. I was four years old. Holding a spoon over the steam from a kettle, I watched the vapor form into liquid water and learned about the states of matter. My parents, Brian and Heather Aubie, instilled in me a drive for discovery that persists to this day. For their years of encouragement, confidence, and never ending support, I am both lucky and extremely grateful.

When I first arrived at McMaster University, I knew I was going to be working with *data* from bats, but I truly did not picture myself climbing roofs and into dusty attics to find bats, hand feeding bats, or assisting in the delivery of bat pups. But I did and I did it with the never ending support from my supervisor, Paul Faure. Paul's enthusiasm for science, for bats, and for life has forever made me a better person. As I took on new projects and new directions of research, I never heard the word 'No'. Of the many, many, many things I have learned these past five years, a phrase I will take with me forever is "Say what you mean, and mean what you say".

I am grateful to Sue Becker, my co-supervisor, who has provided more than generous support to me while pursuing my research. I have been afforded every opportunity to travel the world, meet incredible people, and present my research at a host of scientific meetings. I am thankful for Sue's confidence in me and support from the very beginning.

Deda Gillespie and Ian Bruce have been invaluable members of my committee. I thank them both for their support. I had the opportunity to work closely on a project with Deda and I am very thankful for the time and resources she has provided for me, but especially for the challenges. I thank Ian for always bringing forth new ideas and perspectives of my research and always being supportive. I am also appreciative of Dan Goldreich, who supervised a side project of mine and has offered valuable feedback and support, especially for my latest research endeavours.

I owe a tremendous thank you to my fellow lab members. In the Faure lab, Riziq Sayegh took the time to teach me everything he knew about electrophysiology. His hard work the years prior and his patience and commitment to teach let me jump right in to a brand new field, one of my best experiences in graduate school. Heather Mayberry's hard work in our lab kept us on track. I have always valued her cheerful greetings and remarkable will to climb tall buildings to catch bats. I also thank all of the undergraduate students I've had the

Table of Contents

List of Figures

List of Tables

Abbreviations

5-HT	5-hydroxytryptamine
aEIF	Adaptive Exponential Integrate-and-Fire
AMPA	2-Amino-3-(5-Methyl-3-Oxo-1,2- Oxazol-4-yl)Propanoic Acid
BD	Best Duration
BEF	Best Excitatory Frequency
CN	Cochlear Nucleus
CNS	Central Nervous System
dB	Decibel
DTN	Duration-Tuned Neuron
EPSP	Excitatory Post-Synaptic Potential
FI	Fisher Information
FM	Frequency Modulated
FSL	First-Spike Latency
GABA	γ-Aminobutyric Acid
IC	Inferior Colliculus
ICc	Central Nucleus of the Inferior Colliculus
IPSP	Inhibitory Post-Synaptic Potential
JND	Just-Noticeable Difference
NLL	Nucleus of the Lateral Lemniscus
NMDA	*N*-Methyl-D-Aspartic Acid
PTSH	Peri-stimulus time histogram
SE	Standard Error *or* Sustained Excitation
SI	Sustained Inhibition
SOC	Superior Olivary Complex
SPL	Sound Pressure Level
SSI	Stimulus-Specific Information
TS	Torus Semicircularis

Declaration of Academic Achievement

Chapter 1 - Introduction

Author: Brandon Aubie

Chapter 2 - Computational Models of Millisecond Level Duration Tuning in Neural Circuits

Authors: Brandon Aubie, Suzanna Becker, Paul A. Faure
Publication: Journal of Neuroscience (2009) 29:9255-9270
Comments: This manuscript was conceived by BA, SB and PAF. BA programmed the computational models, performed all data analysis, wrote the original manuscript drafts and produced all of the figures. Subsequent drafts were edited by BA and PAF. Reprinted with permission.

Chapter 3 - Duration Tuning across Vertebrates

Authors: Brandon Aubie, Riziq Sayegh, Paul A. Faure
Publication: Journal of Neuroscience (2012) 32:6373-6390
Comments: This manuscript was conceived by BA and PAF. BA programmed the computational models, performed all data analysis, wrote the original manuscript drafts and produced all of the figures. *In vivo* big brown bat extracellular recordings were performed by BA and RS. Subsequent drafts were edited by BA, RS and PAF. Reprinted with permission.

Chapter 4 - Estimating stimulus duration from neurons in the auditory midbrain of the big brown bat, *Eptesicus fuscus*

Authors: Brandon Aubie, Riziq Sayegh, Thane Fremouw, John H. Casseday, Ellen Covey and Paul A. Faure

Publication: In preparation for submission

Comments: This manuscript was conceived by BA and PAF. BA performed all data analysis, wrote the manuscript and produced all of the figures. *In vivo* big brown bat extracellular recordings were performed by BA, RS, TF, JHC, EC and PAF. This manuscript will undergo further revisions by all co-authors to be submitted for publication at a later date.

Chapter 5 - Discussion

Author: Brandon Aubie

Appendices

Author: Brandon Aubie

Introduction

1

*What then is time? If no one asks me, I know: if I wish to explain
it to one that asketh, I know not.*

— ST. AUGUSTINE OF HIPPO, *Confessions*

Preamble

Within the vertebrate brain are neurons that tell time. In particular, neural circuits culminate at a class of neurons called duration-tuned neurons (DTNs) to systematically produce duration selective spiking responses. The aim of this dissertation is to elucidate both the mechanism and the efficiency of these neural circuits. The research within is focused on, but not limited to, neurons that respond to sounds; however, many of the results extend to other sensory modalities.

This chapter first provides brief introductions to the physics of sound and the mammalian auditory system to ensure an appropriate background for readers. Next, a history of research on DTNs is provided to give context to the research presented in later chapters. Finally, an overview of all chapters within the dissertation is given.

1.1 Background Material

1.1.1 Physical Properties of Sound

Sound waves are series of longitudinal density condensations and rarefactions propagating through an elastic medium such as water or air. The peak amplitude of a sound wave, A, is the maximum level of condensation and rarefaction of the density relative to the medium at rest. The frequency of a pure tone, f, is the rate at which the medium density changes over time. Let $p(t, x)$ be the amplitude of a particular sound wave at time t and distance from the sound source, x. A pure tone is a simple sound wave composed of a single frequency, f_0. The amplitude of this wave, p, can be described by the equation

$$p(t, x) = A \sin(f_0 t - cx + \theta)$$

where A is the maximum amplitude, c is the speed of sound within the medium, and θ is the phase offset. An example pure tone waveform with relative molecular densities is illustrated in Figure 1.1. Actual sounds are complex sound waves, composed of the linear summation of a series of simple waves or pure tones. Complex sound waves can be represented as the summation of multiple frequencies that produce a single complex pressure wave represented by

$$p(t, x) = \sum_i A_i \sin(f_i t - cx + \theta_i).$$

2

In fact, all[1] complex waveforms can be decomposed into a linear summation of simple sine waves, regardless of their complexity, as proven by Fourier's Theorem (Courant, 1961).
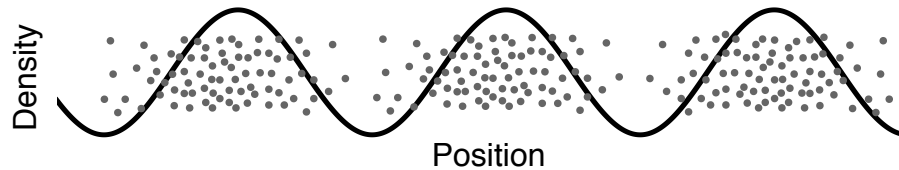
Figure 1.1: A pure tone longitudinal waveform shown both as a sine wave and as molecular densities.

When the molecular density within a region of a medium is increased, there is a force exerted by the molecules as they try to return to a stable density. Similarly, when the molecular density decreases, there is a force exerted by the molecules as they try to fill in the less dense area. Therefore, the rarefactions and condensations within a sound wave are described in terms of pressure (force over area and why p was used in the sound wave equations above). Physiologically relevant sound pressure levels (SPL) can vary over several orders of magnitude so it is convenient to use a relative log scale to represent sound pressure instead of absolute pressure values. A bel is defined as the log ratio of two values; however, the smaller unit of decibel (dB; 1/10th of a bel) is more commonly used and is defined as $10 \log_{10}(p_1^2/p_0^2) = 20 \log_{10}(p_1/p_0)$, where p_1 is the RMS sound pressure of a sound pressure wave and p_0 is a reference pressure level. The most popular reference pressure level is 20 micropascals (μPa) – the lowest pressure level required for an average young adult to detect a 1000 Hz sinusoid pressure wave – and is denoted with the units "dB SPL" (Yost, 2007).

The majority of *in vivo* experiments described in this dissertation were performed with pure tone stimuli. Perfect pure tones are impossible to produce with mechanical speakers due to the inability to produce instantaneous changes in air pressure. Therefore, the pure tone stimuli generated by our speakers ramp up in amplitude following a squared cosine function over 0.4 to 0.5 ms. Similarly, stimuli ramp down in amplitude at the end of a tone instead of instantaneously turning off. Such amplitude ramps are required because approximating instantaneous pressure changes would require combining a large number of

---

[1]As long as the waveform is *sectionally smooth* – that is, sectionally continuous (continuous within $-\pi \leq x \leq \pi$ except for a finite number of discontinuities) and its first derivative is also sectionally continuous. Discontinuities are joined by letting the point of discontinuity, x_0 be the mean of the left-hand and right-hand limits of $\lim_{x \to x_0} f(x)$ (Courant, 1961).

frequencies. Mechanical speakers are limited in frequency range and thus would produce an undesired audible click (spectral "splatter"). Such a stimulus could produce a startle effect in an animal and/or evoke response from neurons with a wide range of best excitatory frequencies. Speakers also tend to produce frequencies in addition to the desired pure tone frequency (harmonics) with low amplitudes; however, such frequencies tend to be too quiet to produce an experimental effect. In the next section, the mammalian auditory system is introduced to describe how physical pressure waves are transduced from mechanical energy into neural signals.

1.1.2   Mammalian Auditory System[2]

Outer and Middle Ear

For many mammals, sound pressure waves first encounter the body at the outer ear where an external portion, the pinna, helps to direct pressure waves into the external auditory canal. At the end of the external canal rests the tympanic membrane (or ear drum), a thin piece of fibrous tissue that is malleable to incoming air pressure changes. Connected to the medial side of the tympanic membrane are three tiny bones called the middle ear ossicles. The malleus is a mallet like structure with its manubrium (handle) attached to the tympanic membrane and its head jointed with the middle ossicle, the incus. The incus then joins with the stapes which itself connects to the inner ear via the oval window. Together, the outer and middle ears transfer and amplify external sound pressure waves into the inner ear where the waves are eventually transduced into neural signals.

Inner Ear

The inner ear begins at the oval window[3] where the stapes oscillates with changes in air pressure at the outer ear. The oval window separates the middle ear from the fluid filled cochlea – a small spiral bone structure home to the basilar membrane and hair cells. As the oval window oscillates, pressure waves are sent through the fluid and around the spiral until they reach the apex, or helicotrema. Changes in the fluid pressure cause the basilar

---

[2]Unless otherwise noted, the content in this section was synthesized from Pickles (1988), Møller (2000) and Yost (2007).

[3]The inner ear also contains the semicircular canals that contribute to the vestibular system (balance) (Yost, 2007). Vestibular mechanisms share several similarities with auditory mechanisms but will not be discussed here.

membrane to vibrate with a travelling wave that follows the pressure wave. Mechanical properties of the basilar membrane differ over the membrane's length (e.g. size and rigidity) to produce frequency and position dependent wave amplitudes. In particular, high frequency oscillations produce larger mechanical wave amplitudes at the base of the membrane whereas low frequency oscillations produce larger wave amplitudes at the apex. This results in a series of bandpass frequency filters distributed along the basilar membrane and enables the auditory system to separate complex sound waves into a series of simpler frequency components.

The passive transduction of this travelling wave into neural signals is known as von Békésy's model (von Békésy, 1960; Dallos, 1992). Sitting on the basilar membrane are hair cells (one row of inner hair cells and three rows of outer hair cells) with tiny stereocilia protruding from their apical ends. Some of the stereocilia directly contact and are embedded in the tectorial membrane above them, while others are loosely influenced by fluid movements between their tips and the surface of the tectorial membrane. As the basilar membrane vibrates, the stereocilia bend against the tectorial membrane, causing ion channels to open and positive ions to flow into the hair cell below. The hair cell depolarization cascades into the opening of calcium specific channels that permit calcium ions to enter and trigger the release of glutamate onto nerve cells to activate post-synaptic AMPA receptors (Moser et al., 2006). These nerve cells make up the afferent cochlear nerve (part of the 8th cranial nerve) and carry auditory signal information to the brain as a series of action potentials. These action potentials are the sole means of acoustic signal representation available to the brain and are primarily facilitated by inner hair cells that are highly innervated with afferent nerve fibers.

The mammalian ear enhances mechanical transduction of sound energy into neural signals with an actively amplifying feedback process facilitated by the three rows of outer hair cells. Unlike the inner hair cells that receive dense afferent innervation, the outer hair cells receive only single afferent nerve fibers in addition to large efferent inputs from the medial superior olivary complex (Dallos, 1992). Even though the inner hair cells are innervated by 90-95% of all cochlear afferent nerves, the loss of outer hair cell function results in significant hearing loss; suggesting that outer hair cells have an important role separate from the passive transduction process (Gold, 1948; Dallos, 1992). It is now understood that an active electromechanical process takes place in the outer hair cells that elongates and shortens outer hair cells in concert with the travelling wave by way of the

voltage sensitive motor protein prestin (Zheng et al., 2000; Liberman et al., 2002; Dallos, 2008). This somatic electromotility effectively increases acoustic sensitivity by 40 - 50 dB (Dallos and Harris, 1978) via an amplifying feedback mechanism. The strongest frequencies produce the strongest amplitude deflections of stereocilia, producing voltage changes in the outer hair cells that result in changes in the structure of the cell due to prestin transformation that further enhance the amplitude of the travelling wave. Stronger initial waves will produce stronger amplifications and thus result in a sharpening of the frequency tuning curves within the cochlea. The mammalian ear therefore depends on both passive and active processes to produce the exquisite ability to encode complex acoustic signals into neural signals.

Neural Afferent Auditory Pathway

The central auditory nervous system is composed of several nuclei that are functionally subdivided further (Fig. 1.2). For simplicity, only the major auditory nuclei and pathways will be described here. Nucleus subdivisions that contribute to the mechanisms studied in this dissertation will be discussed within the relevant chapters. The cochlear nerve maintains the frequency separation generated by the basilar membrane and innervates the ipsilateral cochlear nucleus in the brainstem where a spatial map of frequency (tonotopic map) is preserved. From the cochlear nucleus, nerves project to both the ipsilateral and the contralateral nuclei such as the superior olivary complex where important computations such as sound source location analysis are performed. The superior olivary complexes relay signals to both the ipsilateral and the contralateral inferior colliculus (IC) either through or around the lateral lemniscus. The IC is the first location where DTNs are found and is the focus of the majority of this dissertation. Further detail on the connections to the IC from other auditory nuclei are listed in Table 1.1. The IC projects nerve fibers to both the opposite (contralateral) IC and to the medial geniculate body, also known as the auditory thalamus. From the medial geniculate body, neural signals are projected into the ipsilateral auditory cortex. As discussed in Chapters 2 and 3, it is yet known which nuclei are directly responsible for DTN responses. Due to the vast heterogeneity of response profiles throughout the auditory pathway, no particular auditory nucleus can yet be excluded as possible inputs to DTNs.

The tonotopic map created in the cochlea is somewhat preserved throughout the auditory pathway but with increasing variance the further from the brainstem a nucleus is. For

example, although frequency tuning is approximately tonotopic in the IC, the spatial map tends to be discontinuous when measured with fine enough spatial resolution (Schreiner and Langner, 1997; Malmierca et al., 2008). The auditory cortex exhibits, on average, a smooth tonotopic map; however, detailed frequency distribution analysis reveals high levels of local heterogeneity between nearby neurons exhibiting significantly different preferred stimulus frequencies (Bandyopadhyay et al., 2010; Rothschild et al., 2010). In fact, neighboring dendritic spines on a single dendritic shaft can receive synaptic inputs tuned to vastly different stimulus frequencies (Chen et al., 2011). This suggests that the smoother tonotopic map created in the cochlea undergoes vast amounts of manipulation and processing by the time it reaches the auditory cortex. These results are evidence that the auditory pathway progressively abstracts away the physical features of sounds (e.g. frequency and amplitude) to produce higher order representations of behaviourally relevant acoustic objects such as communication signals which may rely more on relative acoustic features rather than absolute physical parameters.

1.2 History of Duration-Tuned Neuron Research

1.2.1 Discovery

Duration-tuned neurons were first reported by Potter (1965) from the torus semicircularis (TS; analog to the mammalian IC) of the bullfrog. **?** found at least five DTNs and illustrated an example DTN that responded weakly to 13 ms pure tone stimuli, produced increased spike counts for longer stimuli up to 32 ms, and then decreased in spike count as the stimulus duration increased to 80 ms. Although this study was focused more on response characterization than mechanisms, **?** hypothesized that DTNs arose from "a summation of excitation produced by the onset and the termination of the stimulus". Ten years later, Straughan (1975) reported DTNs from the TS of the Pacific tree frog and the California tree frog with preferred durations of 25 – 35 ms. Two additional frog studies followed by Narins and Capranica (1980) and Gooler and Feng (1992) that further characterized DTN response properties and produced hypotheses on the neuroethology of duration selectivity.

The first study to report DTNs in mammals was published by Jen and Schlegel (1982) who characterized a series of DTNs in the IC of the big brown bat. Further analysis of the mechanisms underlying mammalian DTNs was performed by Casseday et al. (1994) who
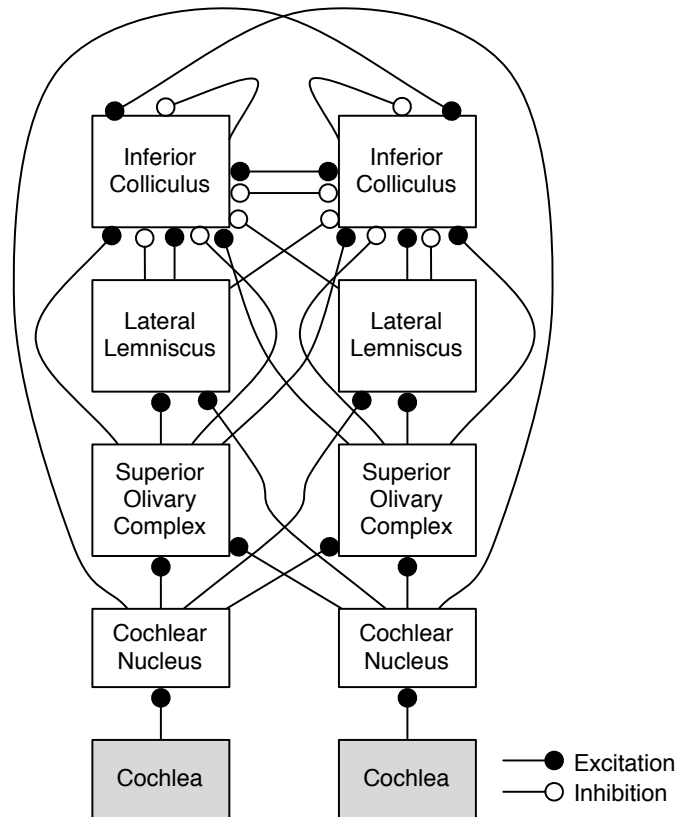
Figure 1.2: Schematic diagram of the major nuclei in the subcortical mammalian afferent auditory pathway. Projections to lateral lemniscus (Kelly et al., 2009), other connections (Yost, 2007). Further details on projections to the IC are available in Table 1.1.

reported a vast array of findings including pharmacological manipulation and whole-cell patch clamp recordings that were later expanded in a series of papers published over the next decade. Following shortly thereafter, recordings from DTNs in cats (He et al., 1997), chinchillas (Chen, 1998), mice (Brand et al., 2000; Xia et al., 2000; Tan and Borst, 2007), guinea pigs (He, 2002), rats (Pérez-González et al., 2006) and most recently the southern green stink bug (Zorović, 2011), the first invertebrate report of DTNs, were published (Fig. 1.3). Despite the range of mammalian species with reported DTNs, 58% of DTN literature published since 1982 has focused on bat species (29 / 50 publications).

1.2.2 Proposed Mechanisms

The mechanism underlying DTN responses proposed by **?** remains the foundation of hypothesized mechanisms supported by recent studies. Fundamentally, an excitatory event

Table 1.1: Mammalian brainstem nuclei inputs to the inferior colliculus with the active neurotransmitters and known response patterns to pure tone acoustic stimuli. Response types not listed may certainly still exist within the specific nucleus.

	Ipsilateral IC	Contralateral IC
Cochlear Nucleus - Onset and Sustained[1]	–	Glutamate[2,18]
Medial Superior Olive - Onset and Offset[3,4,5]	Glutamate[2,18]	–
Lateral Superior Olive	Glycine[2]	Glutamate [2,6,18]
Superior Paraolivary Nucleus - Sustained[7] - Onset and Offset[8]	GABA[9]	–
Nuclei of the Lateral Lemniscus - Onset[10,11]	GABA[12,13,14,18] Glycine[12,13,14] Glutamate [13]	GABA[15,18]
Inferior Colliculus	GABA[16] Glutamate[17]	GABA[14] Glutamate[14]

[1] Rhode et al. (2010)   [2] Oliver et al. (1995)   [3] Guinan et al. (1972)   [4] Grothe et al. (1997)
[5] Grothe et al. (2001)   [6] Loftus et al. (2004)   [7] Behrend et al. (2002)   [8] Kulesza et al. (2003)
[9] Pollak et al. (2011)   [10] Nayagam et al. (2005)   [11] Vater et al. (1997)   [12] Covey and Casseday (1991)
[13] Wagner (1996)   [14] Moore et al. (1998)   [15] Shneiderman et al. (1993)   [16] Faingold et al. (1991)
[17] Saldaña and Merchán (1992)   [18] Kelly et al. (2009)

linked to the onset of a sound stimulus is delayed in time to coincide with an excitatory event linked to stimulus offset. Casseday et al. (1994) were the first of many to demonstrate that the presence of inhibition is also crucial. When inhibition was blocked, excitatory inputs produced responses in DTNs regardless of stimulus duration. Fuzessery and Hall (1999) later proposed an alternative mechanism for DTNs tuned for short stimulus durations that required only a delayed onset-evoked excitation and sustained inhibition lasting the duration of the stimulus. At short durations, the excitation arrives at the DTN after the inhibition and produces spikes. At long durations, the inhibition overlaps with the excitation and quenches all spiking. These two mechanisms form a basis for the range of theoretical mechanisms hypothesized to underlie DTN responses and are known in the literature, appropriately, as the "coincidence detection mechanism" and the "anti-coincidence mechanism", respectively. Variations on these two mechanisms have been proposed that replace transient inputs with
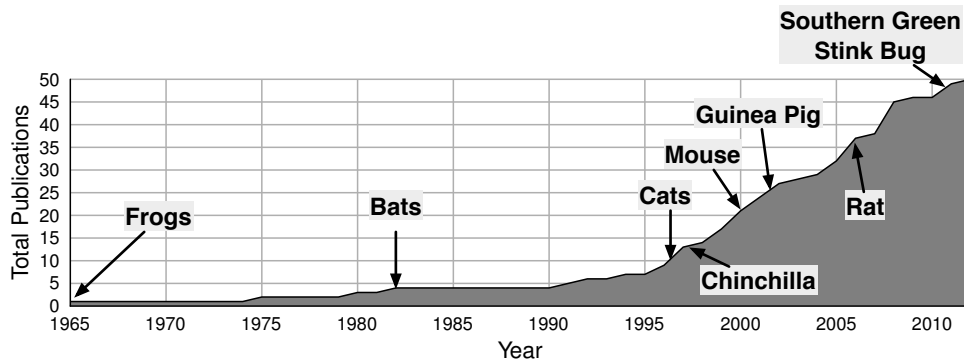
Figure 1.3: Total DTN related publications from 1965 through to 2012 and labels for different species at the year where DTNs were first reported from that species.

multiple sustained inputs (Casseday et al., 2000) or suggest multiple onset-evoked events to account for DTNs tuned for two stimulus durations (Mora and Kössl, 2004); however, the fundamental mechanisms of onset- and offset-evoked excitatory coincidence or excitatory anti-coincidence with inhibition remain present. Chapter 2 presents a generalization of duration tuning that encompasses all such synaptic mechanisms.

The aforementioned synaptic mechanisms are well supported by *in vivo* extracellular and intracellular studies; nevertheless, evidence for these specific mechanisms does not preclude the possibility of additional mechanisms. Hooper et al. (2002) observed that the coincidence detection mechanism did not scale to long stimulus durations given physiological constraints on neural delays (>50 ms). To alleviate this issue, they proposed a mechanism of duration selectivity that required only inhibition and hyperpolarization activated membrane conductances with slow kinetics. During the duration of a stimulus, inhibition is provided to the DTN and the hyperpolarization activated depolarizing current, I_h, increases in strength. At the offset of the stimulus, inhibition is removed and the I_h current drives the membrane potential towards spiking threshold and post-inhibitory rebound spiking can occur, a mechanism similar to that observed in the burst response of thalamic neurons (Llinás and Steriade, 2006). A model DTN can be tuned for long duration stimuli by having the I_h mediated depolarization be too weak to evoke spikes at short stimulus durations but strong enough for spiking at long stimulus durations. Spiking to long duration stimuli can be reduced by slowly removing inactivation of the transient potassium current, I_A. Without I_A, the I_h current is able to produce spikes but with sufficient availability of I_A, post-inhibitory rebound spiking is prevented. Therefore, the combination of I_h and I_A is able to produce

10

spikes to only a select range of stimulus durations. This model scales well to long duration stimuli ($>$1000 ms) and reproduces several of the response properties observed from *in vivo* DTNs; however, DTNs without excitatory inputs have yet to be observed in the auditory midbrain *in vivo* (further discussion is presented in the *Discussion* section of Chapter 2). Regardless, similar mechanisms most likely contribute to duration-tuned responses at long timescales. For example, O_2 sensors in *C. elegans* with slow adaptation properties appear to alter behaviour depending on whether the duration of O_2 exposure is short (seconds) or long (minutes) (Busch et al., 2012). Further comparisons of this model, the coincidence detection and the anti-coincidence mechanisms of duration tuning are discussed in Chapter 2.

Prior to the work presented in this dissertation, only two computational models of neural tuning to stimulus duration, including the slow conductance mechanism (Hooper et al., 2002), had been published. The second model produced by Singh and Mountain (1997) instantiates a form of the coincidence detection mechanism using rate level coding model neurons. Instead of modelling the membrane potentials of neurons and action potentials, neurons were modelled as continuous response values and synaptic inputs were modelled by summing the response value of the input neurons. Although lacking biological plausibility, this model was the first to demonstrate the robustness of the coincidence detection mechanism for selecting for different stimulus duration ranges.

1.3   Dissertation Overview

The goal of this dissertation is to explore both the mechanisms and roles of DTNs. Computational models are used to validate and explore synaptic mechanisms of duration tuning while revealing complexities and subtleties not previously considered. Electrophysiological recordings of DTNs from the big brown bat were collected in collaboration with Riziq Sayegh and Paul A. Faure at McMaster University to further characterize the response profiles of DTNs *in vivo* and allow for an investigation into how the responses of DTNs could be interpreted by the brain.

- Chapter 1, the present chapter, introduces fundamentals of the mammalian auditory system important for understanding the mechanisms studied throughout this dissertation. A history of DTN research is presented to contextualize the research presented herein.

- Chapter 2 instantiates biologically plausible computational models of three mechanisms believed to drive DTN responses. The models are able to reproduce a wide array of response characteristics observed *in vivo* without having been designed to do so. A theoretical model framework is proposed that encompasses multiple specific mechanisms under a single mechanistic class.

- Chapter 3 extends the computational work from the previous chapter to a wider range of temporal response profiles spanning four vertebrate species. Close inspection of the mechanisms reveal novel insights into the subtleties of the coincidence detection mechanism.

- Chapter 4 explores how the responses of DTNs could be used by the brain for determining the duration of a stimulus. By assuming the role of an optimal (and non-optimal) Bayesian observer, responses from *in vivo* big brown bat DTNs are decoded individually and as a population into estimations of the stimulating stimulus duration. This chapter includes *in vivo* data collected by McMaster University personnel, including the author, and by University of Washington personnel.

- Chapter 5 provides a summary of the findings in this dissertation and briefly suggests further avenues of research.

- Appendix A provides additional details on the modelling software written for the simulations performed in Chapter 2.

- Appendix B provides additional details on the modelling software used for the simulations performed in Chapter 3.

- Appendix C provides additional details and analysis from the dataset used in for Chapter 4.

- Appendix D provides an overview of software written to aid in electrophysiological data analysis that was used for the analysis in Chapter 4.

  The references for chapters 2, 3 and 4 are contained at the end of those manuscript chapters. The references for chapters 1, 5 and appendices A, B, C and D are contained directly after chapter 5.

2

Computational Models of Millisecond Level Duration Tuning in Neural Circuits

Preamble

This chapter previously appeared in the Journal of Neuroscience in 2009 and is reproduced with permission. Material added for this thesis has been appended to the text as footnotes.

Aubie B, Becker S, Faure PA (2009) Computational models of millisecond level duration tuning in neural circuits. *J Neurosci* 29:9255-9270.

The model source code is available from ModelDB:

http://senselab.med.yale.edu/modeldb/ShowModel.asp?model=144509

2.1 Abstract

Discrimination of stimulus duration on the order of milliseconds has been observed in behavioural and neurophysiological studies across a variety of species and taxa. Several studies conducted in mammals have found neurons in the auditory midbrain (inferior colliculus) that are selective for signal duration. Duration selectivity in these cells arises from an interaction of excitatory and inhibitory events occurring at particular latencies from stimulus onset and offset. As previously shown in barn owls, coincidence of delayed, excitatory events can be employed by the central nervous system to respond selectively to specific stimuli in auditory space. This study formulates several computational models of duration tuning that combine existing conceptual models with observed physiological responses in the auditory brainstem and midbrain to evaluate the plausibility of the proposed neural mechanisms. The computational models are able to reproduce a wide range of *in vivo* responses including best duration tuning, duration-selective response classes, spike counts, first-spike latencies, level tolerance to changes in signal amplitude, and neuropharmacological effects of applying inhibitory neurotransmitter antagonists to duration-tuned neurons. A unified model of duration tuning is proposed that enhances classic models of duration tuning, emphasizes similarities across the models, and simplifies our understanding of duration tuning across species and sensory modalities.

2.2 Introduction

Stimulus duration can encode information about a signal's source and meaning. To utilize temporal information, the central nervous system (CNS) employs mechanisms that can discriminate temporal intervals over several orders of magnitude. Numerous neurophysiological studies in frogs (Potter, 1965; Gooler and Feng, 1992; Leary et al., 2008), rats (Pérez-González et al., 2006), mice (Brand et al., 2000; Xia et al., 2000; Tan and Borst, 2007), guinea pigs (Wang et al., 2006), cats (He et al., 1997) and bats (Ehrlich et al., 1997; Casseday et al., 2000; Faure et al., 2003; Mora and Kössl, 2004; Fremouw et al., 2005) reveal the presence of auditory duration-tuned neurons (DTNs) with precise millisecond level response discrimination (tuning) to stimulus durations typical of species-specific vocalizations. Visually oriented DTNs have also been reported in areas 17 and 18 of the cat visual cortex (Duysens et al., 1996). Duration-tuned neurons were first observed in the torus semicircularis of amphibians (Potter, 1965) and later in the inferior colliculus (IC) of mammals (Casseday et al., 1994). Their physiological responses can be characterized by having a maximum spike count at a best duration (BD) and a temporal response bandwidth, typically to pure tones or species-specific frequency modulated (FM) signals (Casseday et al., 1994, 2000; Fremouw et al., 2005).

Temporal selectivity in the CNS can be conceptualized to arise out of internal state changes in neural networks between two temporally separated events such as a stimulus onset and offset (Buonomano and Maass, 2009). For example, a counting mechanism coupled to an internal clock has been hypothesized to provide temporal discrimination on the order of seconds to minutes (Roberts, 1981; Church, 1984; Meck, 2006). Singh and Mountain (1997) demonstrated millisecond level selectivity for band-pass duration tuning using rate coded model neurons and a coincidence detection mechanism of delayed onset- and offset-evoked excitatory events.

Whole-cell patch and extracellular recordings in the amphibian and mammalian auditory midbrain provided evidence that duration tuning results from the interaction of early post-synaptic inhibition and delayed post-synaptic excitation (Fuzessery and Hall, 1999), and/or from the interaction of sustained post-synaptic inhibition and multiple post-synaptic excitations (Covey et al., 1996; Casseday et al., 2000; Faure et al., 2003; Leary et al., 2008). A similar coincidence detection mechanism has been described for microsecond level timing in the nucleus laminaris of barn owls (Carr and Konishi, 1990), suggesting the mechanism

may be employed generally by the CNS to encode and discriminate temporal signals.

Here we amalgamate conceptual models of duration tuning with observed neuronal response characteristics to produce formal, detailed, and biologically plausible computational models of DTNs. Our goals were to evaluate the plausibility of each model and to explore their response dynamics. We propose that each conceptual model can be described by a single, overarching model, and then demonstrate how each duration tuning response class can arise by simple parameter adjustments in the unified model.

2.3 Methods and Materials

2.3.1 Conceptual Models

Responses of DTNs can be divided into three electrophysiological response classes (e.g. Jen and Zhou, 1999; Faure et al., 2003). (1) Short-pass DTNs have spike counts that peak at BD and drop to ≤50% of the peak at durations longer than BD, whereas stimuli shorter than BD continue to elicit strong spiking. (2) Band-pass DTNs also have a peak spike count to a BD, but their spike counts drop to ≤50% of the peak count at durations both shorter and longer than BD. (3) Long-pass DTNs do not have a BD and are characterized by responding only when the stimulus exceeds a minimum duration. Moreover, the minimum stimulus duration required to elicit a response does not continue to decrease as signal energy increases (Brand et al., 2000; Faure et al., 2003; Pérez-González et al., 2006) even though central auditory neurons tend to respond with more spikes at a short latency to higher amplitude stimuli (Kiang, 1965). Spikes for short-pass and band-pass DTNs typically occur after stimulus offset, whereas spikes for long-pass cells can occur during the ongoing portion of the stimulus (Faure et al., 2003; Pérez-González et al., 2006).

Three conceptual models have been proposed to explain the neural mechanisms underlying short-pass, band-pass and long-pass duration tuning in the auditory midbrain of amphibians and mammals, and all rely on the temporal interaction of synaptic excitation and inhibition (Fig. 2.1). The first model is a coincidence detection mechanism that suggests a transient, onset-evoked excitation coinciding with an offset-evoked excitation could produce cells with responses tuned to specific stimulus durations. If the onset-evoked excitation arrived either before or after the offset-evoked excitation, there would be no temporal coincidence of the excitations and the DTN would fail to respond (Potter, 1965; Narins and

Capranica, 1980). Whole-cell patch recordings indicated that DTNs received an onset-evoked, inhibitory post-synaptic potential (IPSP) that preceded an onset-evoked, excitatory post-synaptic potential (EPSP) (Casseday et al., 1994; Covey et al., 1996). Paired tone stimulation experiments confirmed that DTNs received inhibition that preceded excitation, and that the inhibition was sustained for as long or longer than the duration of the stimulus (Faure et al., 2003). Many DTNs lost their selectivity and responded to all stimulus durations when inhibition to the cell was blocked with neurotransmitter antagonists (Casseday et al., 1994). The cells also changed the timing of their spikes from offset-following to a fixed latency from stimulus onset (Fuzessery and Hall, 1999; Casseday et al., 2000). Because *in vivo* single-unit recordings and neuropharmacological experiments revealed that many DTNs received a supra-threshold, onset-evoked excitation (Casseday et al., 2000; Faure et al., 2003), this contradicted the original coincidence detection mechanism of duration tuning that assumed both the onset- and offset-evoked excitations were sub-threshold.

Here we propose a new version of the coincidence detection model of duration tuning that is consistent with the *in vivo* data. Our model employs supra-threshold, onset-evoked excitation at all but the shortest stimulus duration (i.e. 1 ms); however, this excitation can be rendered sub-threshold when it interacts (coincides) with inhibition. Later we demonstrate that inhibition is crucial for controlling the temporal specificity (i.e. window of temporal coincidence) for the onset- and offset-evoked EPSPs. In our new version of the band-pass coincidence detection model, a DTN fails to spike at 1 ms because there is insufficient stimulus energy to evoke reliable firing in the cells providing the onset- and offset-evoked excitations. In the new version of the short-pass coincidence detection model, the spiking threshold of the cells providing the onset-evoked excitation was lowered and this permitted responses from the DTN at 1 ms.

The second conceptual model is an anti-coincidence mechanism described specifically for short-pass duration tuning (Fuzessery and Hall, 1999). This model suggests a short latency, onset-evoked IPSP, lasting the duration of the stimulus, occurs at a fixed-latency from stimulus onset, and that a delayed, supra-threshold, onset-evoked EPSP arrives after the IPSP when the stimulus is shorter than some duration. When the stimulus duration is longer, the IPSP now overlaps with the delayed EPSP and this prevents the DTN from reaching spike threshold. The anti-coincidence model does not rely on an offset-evoked response or the coincidence of excitatory events (i.e. EPSPs).

The third model, also an anti-coincidence mechanism, is specific to long-pass duration
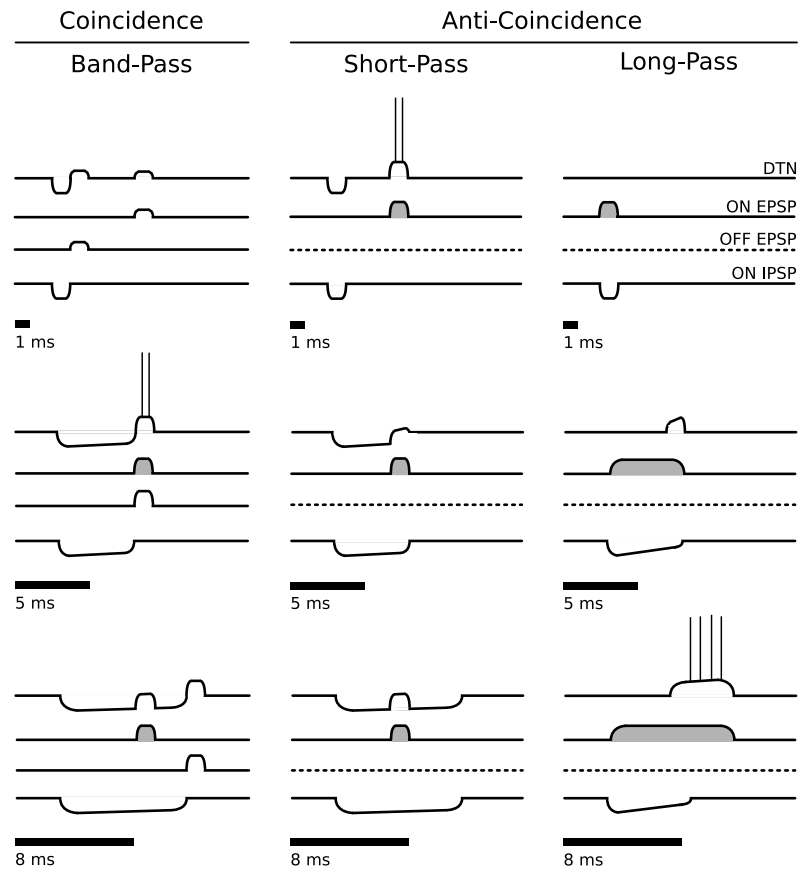
Figure 2.1: Coincidence and anti-coincidence conceptual models for the creation of band-pass, short-pass and long-pass duration-tuned neurons (DTNs). Four traces are shown above each stimulus (*black bars*). The top traces show the membrane potentials from the summation of synaptic inputs and, if supra-threshold, the spike output of the DTN. The second, third, and bottom traces represent hypothetical synaptic inputs to a DTN. Each model has two or three inputs illustrated as excitatory post-synaptic potentials (EPSPs) or inhibitory post-synaptic potentials (IPSPs): (1) onset-evoked EPSP (*ON EPSP*, second trace); (2) offset-evoked EPSP (*OFF EPSP*, third trace, coincidence detection model only); (3) onset-evoked IPSP (*ON IPSP*, bottom trace). In the coincidence detection model, the DTN spikes only when the ON EPSP coincides with the OFF EPSP. This occurs for the 5 ms stimulus but not for the 1 ms or 8 ms stimuli. For the 1 ms stimulus, the ON and OFF EPSPs are absent or weak. For the 8 ms stimulus, the ON and OFF EPSPs do not coincide and the ON EPSP is rendered subthreshold by the ON IPSP. In the anti-coincidence models, the DTN spikes only when the ON EPSP does not coincide with the sustained ON IPSP. In the short-pass anti-coincidence model, this occurs for the 1 ms stimulus but not for the 5 ms or 8 ms stimuli. For the long-pass anti-coincidence model, this occurs only for the 8 ms stimulus. In the long-pass model, the ON EPSP is sustained whereas the ON IPSP adapts. Supra-threshold EPSPs illustrated with gray shading. The OFF EPSP is absent in both anti-coincidence models (*dashed lines*). Models adapted and modified from Fuzessery and Hall (1999), Faure et al. (2003) and Leary et al. (2008).

19

tuning and suggests that a supra-threshold, onset-evoked EPSP provides sustained excitation to the DTN throughout the stimulus (Brand et al., 2000; Faure et al., 2003; Pérez-González et al., 2006). A strong, onset-evoked IPSP is also present and overlaps with the supra-threshold EPSP, and this prevents action potentials in the DTN for the first several milliseconds. When the IPSP ends, or when its strength decreases (adapts), the supra-threshold EPSP evokes action potentials in the DTN for the remainder of the stimulus. Because the DTN spikes only when there is no significant interaction between the EPSP and IPSP, this model is also classified as anti-coincidence.

2.3.2 Computational Model Components

Our computational models simulate cells from sub-populations of neurons in the mammalian central auditory system that differ in their physiological response properties. For convenience, we have suggested possible anatomical locations for these neural populations although the performance of the models are not dependent on their exact locations. Model performance is also independent of stimulus frequency but we assume that all input populations are excited at their characteristic frequency. Furthermore, we only consider monaural auditory pathways at this time because the majority of *in vivo* data on the responses of DTNs have been collected using monaural, contralateral acoustic stimulation (i.e. acoustic stimuli were presented to the ear contralateral to the electrode recording site).

Each model cell population, other than the single DTN in the inferior colliculus (IC) and the afferent input population in the cochlear nucleus (CN), was composed of ten model neurons. Sound input to the system was modelled by simulating driven (evoked) CN activity with 25 Poisson distributed random spiking processes with a mean firing rate (μ) that exceeded 0 Hz during the stimulus (25 Poisson processes each with mean spiking rate μ is equivalent to a single Poisson process with mean spiking rate of 25μ)[1]. We incorporated a larger number of neurons in the CN input responses so that individual spiking rates could be described at physiologically plausible rates. An initial burst of spikes lasting 2 ms that grows with stimulus amplitude was modelled to mimic the onset burst response of auditory nerve

---

[1]The response of the model is not dependent on the Poisson spiking statistics of the input neurons. To verify this, additional simulations have been performed since the publication of this manuscript using phase-locked stimuli that ranged from 500 to 2000 Hz. We found that the post-synaptic current functions (Fig. 2.2) "blurred" out at the particular spiking statistics at the level of the neural circuit and what mattered most was the spiking *density*, or in other words, the total number of spikes produced over an average time period of several milliseconds.

fibers (Kiang, 1965) and CN neurons (Rhode and Greenberg, 1992). Additionally, a 0.2 ms onset and offset ramp was applied to μ to simulate the energy envelope of mechanically generated acoustic signals.

The complete input firing rate for simulated CN evoked activity is characterized for 100 Hz $< \mu <$ 500 Hz by the equations below, where t is time in milliseconds relative to stimulus onset, μ_0 is the mean firing rate of a CN neuron after its initial onset burst of activity, d is the stimulus duration, $r(t)$ is a linear energy envelope ramp function of 0.2 ms, and $\mu_r(t)$ is the mean spiking rate after the onset burst and ramp functions have been applied.

$$\mu(t) = \begin{cases} \mu_0 + (1000 - \mu_0)\sqrt{\frac{\mu_0 - 100}{400}} & \text{if} & 0 < t < 1 \\ \mu_0 + (500 - \mu_0)\sqrt{\frac{\mu_0 - 100}{400}} & \text{if} & 1 \leq t < 2 \\ \mu_0 & \text{if} & 2 \leq t < d \\ 0 & \text{otherwise} \end{cases}$$

$$\mu_r(t) = r(\mu(t))$$

An example peri-stimulus time histogram (PSTH) of the Poisson process for the simulated evoked CN activity is shown in Figure 2.2A. For rates $>$500 Hz, the initial onset burst of spikes was capped at a firing rate of 1000 Hz. While auditory neurons are known to phase lock to stimulus frequency, this ability is greatly diminished at carrier frequencies $\geq$3 kHz (Covey and Casseday, 1999). Because *in vivo* DTNs show little to no spontaneous activity (Casseday et al., 1994; Faure et al., 2003), our models have, for the most part, ignored spontaneous input; however, for instances in which we wished to model a DTN with spontaneous activity, we included an additional population of Poisson spiking processes to excite the DTN directly for the entire simulation (e.g. see *Anti-Coincidence Model*).

Although rate-level functions of mammalian CN neurons vary, for consistency of comparison, our chosen values of 350 Hz, 400 Hz, 450 Hz and 500 Hz were used for all simulations. These values are on the same order as for CN neurons from Horseshoe bats, *Rhinolophus ferrumequinum* (Vater, 1982), and correspond to an input stimulus dynamic range of ca. 30-40 dB.

An adaptive exponential integrate-and-fire (aEIF) single neuron model (Brette and Gerstner, 2005) was used for all other model neurons with parameters set so that model output was qualitatively comparable to response characteristics observed for *in vivo* and *in*
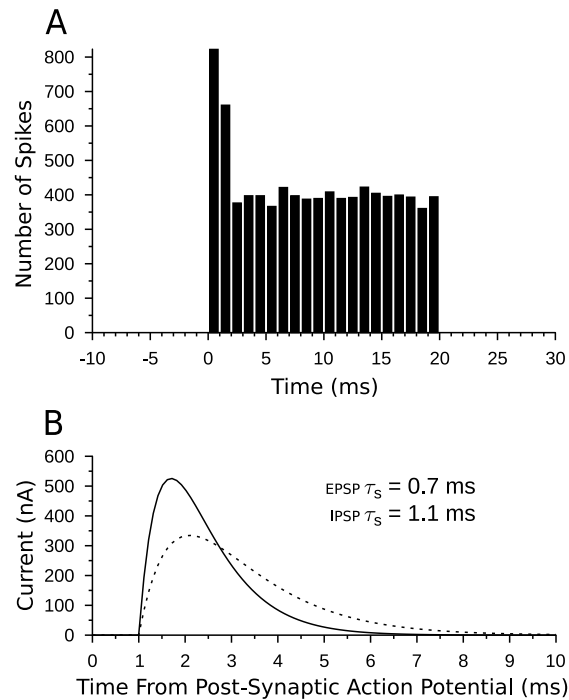
Figure 2.2: Model Cochlear Nucleus (CN) afferent input and post-synaptic α-functions. (A) Peri-stimulus time histogram (PSTH) of spike counts for 25 model CN Poisson neurons over 40 trials with a mean firing rate μ_0 of 400 Hz. The stimulus occurs from 0 to 20 ms. Each time bin is 1 ms and there are $25 \times 40 = 1000$ neuron trials per bin, so the spike count can be interpreted as an averaged, instantaneous firing rate in Hz. The onset burst in the CN neurons is easily seen in the first and second bins. (B) The model's α-function with $\tau_s = 0.7$ ms (EPSP; *solid line*) and $\tau_s = 1.1$ ms (IPSP; *dashed line*) plotted as a function of time since the post-synaptic neuron generated an action potential. A 1 ms delay was added to simulate the axonal delays of each neuron in the circuit. Each function is normalized to an area of 1 before being scaled by q to ensure the same total energy for each spike regardless of τ_s. Increased or decreased levels of current can be implemented by multiplying the α-functions by a scaling factor (connection weight).

vitro neurons[2]. Parameters for each model neuron within a population were often drawn from a normal distribution with a mean (μ) and variance (σ) to simulate the varying nature of real neural systems. Each population was fully and uni-directionally connected with neurons between populations. The connection strength was characterized by a weight, W, that was divided evenly between each individual connection. This allowed a population to have an arbitrary number of model neurons without changing the total summed connection strength. The membrane potentials of post-synaptic cells were modified with a current injecting α-function (Fig. 2.2B), multiplied by W, as described in Gerstner and Kistler (2002). Full implementation details are given in the *Appendix*.

The aEIF model is defined by the differential equations:

$$C\frac{dV}{dt} = -g_L(V - E_L) + g_L s(V) - w + I$$

$$s(V) = \Delta_T \exp\left(\frac{V - V_T}{\Delta_T}\right)$$

$$\tau_w \frac{dw}{dt} = a(V - E_L) - w$$

where C is the cell membrane capacitance, V is the membrane potential, t is time, g_L is the leak conductance, E_L is the leak reversal potential, w is an adaptation parameter with dynamics characterized by time constant τ_w, a is a sub-threshold adaptation value, I is the input current, and $s(V)$ is an exponential spiking mechanism characterized by a slope factor, Δ_T, and a threshold value, V_T. An exponential spiking mechanism is said to reach threshold when the rate of change in membrane voltage approaches infinity. In practice, spikes in our model were triggered when the membrane potential reached an absolute value of +20 mV because the rate of change was always satisfactorily steep at this point. Changing this hard threshold only modifies spike times by a fraction of a millisecond (Gerstner and Kistler, 2002). To confirm this, we re-ran several simulations with a hard threshold of -20 mV and no differences in spike timing or response characteristics were observed. When a spike

---

[2]The decision to use an aEIF was made because the aEIF model provided parameter settings to produce a wide range of response profiles including transient, onset-evoked responses, post-inhibitory rebound, and bursting. Other neuron models that produce these types of responses could also have been substituted with minimal changes to the results of this study because the response of the model DTNs are primarily functions of the timing and strength of inhibitory inputs. The exact mechanisms that produce those response profiles (onset, offset, sustained, adapting) are not important for describing the mechanisms underlying duration selectivity at the level of the DTN. Prior to this manuscript, simple leaky integrate-and-fire model neurons with onset and offset evoked inputs were used to successfully model the coincidence detection mechanism of duration selectivity.

occurred, the time was recorded and the membrane potential was reset to a predetermined value, V_R.

2.3.3 Coincidence Detection Model

The coincidence detection model defines three events responsible for causing a DTN to selectively produce action potentials in response to a stimulus of appropriate duration (Faure et al., 2003; Leary et al., 2008): (1) a short latency, onset-evoked inhibition (IPSP) that is sustained for at least the duration of the stimulus; (2) a longer latency (delayed), onset-evoked excitation (EPSP); and (3) an offset-evoked excitation (EPSP). At the shortest stimulus duration (1 ms), the onset- (2) and offset-evoked EPSPs (3) are either absent or sub-threshold. At longer durations ($\geq$2 ms), the onset-evoked EPSP is supra-threshold on its own, but is rendered sub-threshold when interacting with the onset-evoked IPSP (1). The offset-evoked EPSP is sub-threshold. When events (2) and (3) coincide, the neuron's membrane potential is likely to rise above the spike generation threshold, resulting in action potentials in the DTN. In Figure 2.1 we illustrate (3) as an independent offset-evoked EPSP, but this event could also be modelled as post-inhibitory rebound excitation in the model DTN, and later we explicitly explore this possibility (see *Relevance of Model Components*). This model is naturally conducive to producing band-pass duration tuning because short stimulus durations cause the the onset- and offset-evoked EPSPs to be weak or absent and long signal durations cause the offset-evoked EPSP (3) to occur after the delayed, onset-evoked EPSP (2).

A schematic illustrating the network connections of our band-pass coincidence detection model is shown in Figure 2.3A. First, the CN excites two populations of neurons that for our purposes have been hypothesized to reside in the Nucleus of the Lateral Lemniscus (NLL) due to its inhibitory connections to the IC (Schofield, 2005); however, neurons with similar response characteristics and inhibitory connections to the IC are also found in the superior olivary complex (SOC) (Schofield, 2005). Hence, the model is not dependent on input from particular auditory nuclei. The first population provides sustained inhibition (SI) to its target cells: an onset-evoked population of cells (ON) in the NLL, an offset-evoked population of cells (OFF) in the IC, and to the single model DTN in the IC. When the stimulus ends, the sustained inhibition ends and the targets of the SI units are released from inhibition. This results in post-inhibitory rebound spikes in the population of OFF cells that provide

sub-threshold excitation to the model DTN, and also marks the offset of the stimulus. For additional details on the physiological characteristics of post-inhibitory rebound of *in vitro* IC neurons, see Peruzzi et al. (2000) and Sun and Wu (2008). Offset responding cells have also been found in the SOC of bats (Grothe, 1994) and rabbits (Kuwada and Batra, 1999), and in the superior paraolivary nucleus of rats (Kadner et al., 2006). The sustained inhibitory input to the DTN prevents action potentials from being evoked during the stimulus and plays a key role in refining the duration tuning curve (see *Relevance of Model Components*).

The CN also drives a population of onset responding cells (ON) that provide a transient, onset-evoked inhibition to a population of delayed onset responding cells (ON_{Delay}) in the IC. When ON_{Delay} cells are released from inhibition, they rebound with one or two action potentials that provide supra-threshold excitation to the DTN for durations ≥ 2 ms; however, when coinciding with inhibition from the SI population, the post-inhibitory rebound excitation is rendered sub-threshold. Because the response characteristics of the ON population are largely independent of stimulus duration, the ON_{Delay} population will be released from inhibition at a fixed latency from stimulus onset. Each cell in the ON population produces only one or two action potentials at stimulus onset and then ceases to fire for the remainder of the stimulus. Inhibition from the SI population ensures that ON cells do not produce action potentials after their initial onset burst of spikes. Onset cells in the band-pass coincidence model were tuned with a higher spiking threshold and required stimulus durations ≥ 2 ms before producing spikes. For an overview of onset responses of *in vivo* NLL neurons, see Covey and Casseday (1991). Onset-bursting cells with similar behaviour are also found in the IC (Xie et al., 2008).

To illustrate responses of each cellular population, Figure 2.4A shows the membrane voltage traces of each neuron in the coincidence detection model for a single stimulus presentation at the network's BD (in this case, 5 ms). Figure 2.4B demonstrates the model's response to a longer stimulus (15 ms) that is not at BD, and clearly shows a lack of spiking in the model DTN when responses from the ON_{Delay} and OFF cells fail to coincide.

Assuming the first-spike latency of OFF cells (re stimulus offset) is consistent across all durations, then it is the response latency of the ON_{Delay} cells (re stimulus onset) that ultimately determines the BD of the coincidence detection network. The temporal bandwidth of duration tuning is determined by the duration and strength of the ON_{Delay} and OFF EPSPs as these define the window of coincidence. The DTN produces spikes only when the stimulus is long enough to evoke spikes in the ON population and short enough such
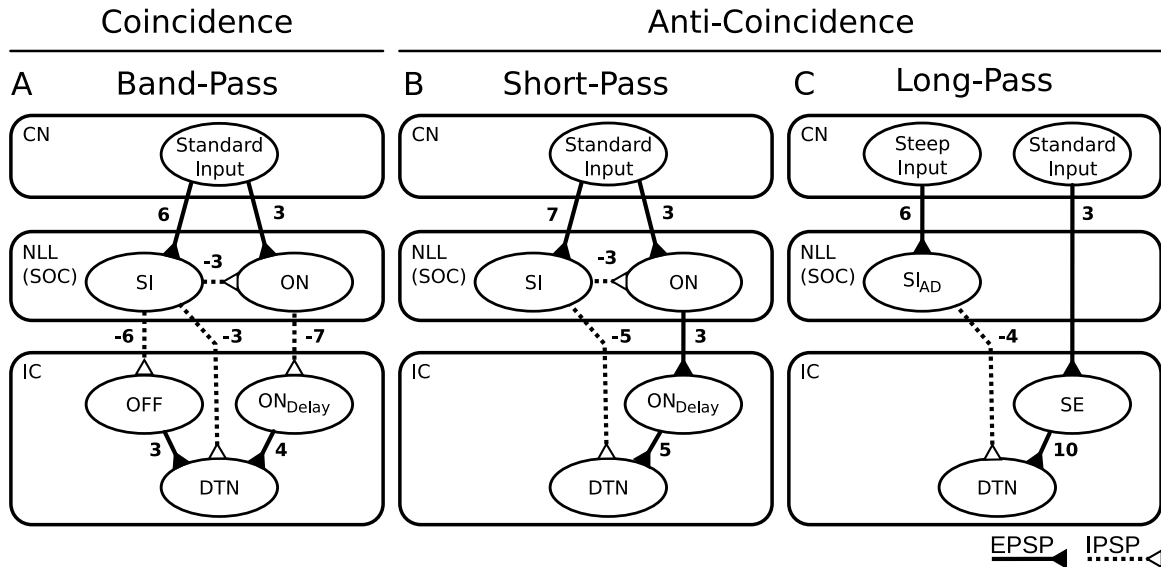
Figure 2.3: Network flow diagrams for three computational models of duration tuning. Rectangles define nuclei of the mammalian central auditory system where the proposed model components may exist *in vivo*. *Solid lines* with *filled triangles* connecting populations represent EPSPs, and *dashed lines* with *open triangles* represent IPSPs, with connection weights as shown. *Ovals* represent sub-populations of neurons that share similar response characteristics. Standard Input: acoustic input implemented as a Poisson spiking process in CN afferents (see Fig. 2.2A); Steep Input: acoustic input to inhibitory components in the long-pass model implemented as a Poisson spiking process with a mean firing rate that grows steeply as stimulus intensity increases; SI: cells that provide sustained inhibition during a stimulus; ON: cells that respond with 1 or 2 spikes to stimulus onset; OFF: cells that respond with 1 or 2 spikes to stimulus offset via a post-inhibitory rebound mechanism; ON_{Delay}: onset cells that respond with 1 or 2 spikes after some delay; SI_{AD}: cells that provide adapting sustained inhibition during a stimulus; SE: cells that provide sustained excitation during a stimulus; DTN: duration tuned neuron. (A) In the band-pass coincidence detection model, the DTN responds only when the stimulus duration results in the production of spikes in the ON cells and EPSPs from the ON_{Delay} and OFF cells coincide. (B) In the short-pass anti-coincidence model, the DTN responds only when the EPSP from the ON_{Delay} cells does not coincide with the IPSP from the SI cells. (C) In the long-pass anti-coincidence model, the DTN responds only when the EPSP from the SE cells is not suppressed by the adapting IPSP from the SI_{AD} cells. CN: Cochlear Nucleus; NLL: Nucleus of the Lateral Lemniscus; SOC: Superior Olivary Complex; IC: Inferior Colliculus.

Figure 2.4: Band-pass coincidence detection duration tuning. Shown are model neuron responses to a single standard input stimulus from the Cochlear Nucleus at 400 Hz for a duration of (A) 5 ms and (B) 15 ms to illustrate model responses to a best duration (BD) stimulus and a longer duration stimulus. Membrane potential (voltage) traces of every neuron in the model are shown with action potentials truncated for improved sub-threshold clarity. Action potentials from the Cochlear Nucleus Poisson spiking processes are drawn as instantaneous spikes. (A) The Duration Tuned Neuron produced action potentials when there was a coincidence of spikes from the Delayed Onset and Offset populations. (B) When excitations from the Delayed Onset and Offset populations did not coincide, the membrane potential of the DTN remained sub-threshold and no action potentials were produced. Stimulus duration illustrated as *black bars* on the time axis.

that the ON_{Delay} and OFF EPSPs coincide. Our computational model is similar to the coincidence detection model originally postulated by Potter (1965) and later by Narins and Capranica (1980) but differs in one key characteristic. In the new model, the onset-evoked EPSP is always supra-threshold except when it coincides with inhibition or for a 1 ms stimulus when it is weak or absent. Classic presentations of the coincidence detection model suggested that the onset-evoked EPSP was always sub-threshold and did not include a role for inhibition. As shown later, these modifications were critical for reproducing results from *in vivo* neuropharmacological experiments (see *Relevance of Model Components*).

2.3.4 Anti-coincidence Model

The anti-coincidence model suggests a mechanism where supra-threshold, onset-evoked excitation causes action potentials in the model DTN only if it arrives after the onset-evoked, sustained inhibition (Fig. 2.1). Thus, the anti-coincidence model defines two key events responsible for producing selectivity to short stimulus durations (Fuzessery and Hall, 1999): (1) a short latency, onset-evoked inhibition (IPSP) that is sustained for at least the duration of the stimulus, and (2) a longer latency (delayed), supra-threshold, onset-evoked transient excitation (EPSP). When event (2) occurs *after* event (1), the DTN's membrane potential is likely to rise above the spike generation threshold, resulting in action potentials. At longer durations, the sustained IPSP coincides with the onset-evoked EPSP and this suppresses supra-threshold activity in the model DTN.

The network structure of an anti-coincidence short-pass duration-tuned neural circuit is shown in Figure 2.3B. Simply removing the offset excitation component from the coincidence detection model in Figure 2.3A without other modifications caused the model DTN to respond with few or no spikes. This was because excitation from the ON_{Delay} population was rendered sub-threshold when combined with the sustained inhibition. In the short-pass anti-coincidence model, we increased the ON_{Delay} to DTN connection weight from 4 to 5 to provide supra-threshold excitation to the DTN even when a small amount of inhibition coincided with the arrival of the EPSP at shorter durations. At longer durations when the inhibition was stronger, the ON_{Delay} was still rendered sub-threshold. In the band-pass coincidence detection model, the ON population was tuned with a high spiking threshold to prevent spiking to short stimulus durations. To permit sensitivity to short stimulus durations in the short-pass anti-coincidence model, ON cells were tuned with a lower spiking threshold

by changing the leak reversal potential (E_L) and spike threshold (V_T) parameters by 2 mV. We found that the onset bursting behaviour of the input CN population was critical for evoking spikes in DTNs at short (1-2 ms) stimulus durations. At longer stimulus durations ($\geq$3 ms), the onset bursting behaviour in the CN afferents was less critical. We also changed the inhibitory connection between the ON and the ON_{Delay} population to an excitatory connection. The reason for doing this was to account for the shorter first-spike latencies and sharper temporal response bandwidths observed in many *in vivo* short-pass DTNs (Faure et al., 2003).

A post-inhibitory rebound mechanism in the ON_{Delay} population, as described in the coincidence detection model, could also be implemented in an anti-coincidence model to produce a short-pass DTN. The post-inhibitory rebound would delay the arrival of supra-threshold excitation to the DTN, hence longer duration stimuli would be required before sustained inhibition from the SI population would overlap with the EPSP from the ON_{Delay} population. This would result in a short-pass DTN with a wider temporal response bandwidth and longer first-spike latency (data not shown).

Many *in vivo* DTNs generate several action potentials in response to short duration stimuli, and the spikes tend to be spread apart by several milliseconds (Faure et al., 2003). To account for this, we hypothesized that such cells received sub-threshold, spontaneous activity acting as an additional source of excitation (i.e. EPSPs) riding on top of the excitation from the onset-evoked EPSP to produce longer latency action potentials at short durations. To model this, we generated random Poisson spikes for the entire run of the simulation in a population of five neurons, each with a mean firing rate of 50 Hz. This population synapsed directly on the DTN with an excitatory connection weight of 1.

In the anti-coincidence model of duration tuning, the ON population excited the ON_{Delay} population after stimulus onset, and the ON_{Delay} population provided supra-threshold excitation to the DTN. Figure 2.5 shows the membrane potential traces of each neuron in a short-pass anti-coincidence model to a single stimulus presentation at BD (1 ms) and at a longer duration (8 ms). The SI population provided sustained inhibition to the model DTN beginning shortly after stimulus onset and lasting throughout the stimulus. At short durations, spiking was evoked in the SI population for only a short time period. As a result, inhibition from the SI population ended before excitation from the ON_{Delay} population arrived. This allowed for the production of action potentials in the model DTN. When the duration of the stimulus was lengthened, sustained inhibition from the SI population coincided with

excitation from the ON_{Delay} population and this prevented action potentials in the model DTN.

2.3.5   Long-pass Model

Unlike typical sensory neurons that show a decrease in first-spike latency in response to increasing stimulus intensity (e.g. Kitzes et al., 1978; Heil, 1997), some long-pass DTNs in the mammalian IC show an *increase* in first-spike latency at higher SPLs (Faure et al., 2003; Pérez-González et al., 2006). The response characteristics of long-pass DTNs differ both qualitatively and quantitatively from band-pass and short-pass DTNs in that: (1) spikes are evoked by the onset of the stimulus; (2) spikes occur during the ongoing portion of the stimulus; and (3) the number of spikes tends to increase with stimulus duration. To model these responses, we instantiated an anti-coincidence tuning mechanism proposed by Brand et al. (2000), Faure et al. (2003) and Pérez-González et al. (2006) with the components illustrated in Figure 2.3C.

The long-pass model used our standard CN Poisson input spiking process to provide excitation throughout the duration of the stimulus to sustained excitation (SE) cells in the IC, which then relayed excitation to the model DTN in the IC. Additionally, a second population of CN afferents with a steeper rate-level function (i.e. afferents with a larger increase in spiking rate as a function of stimulus magnitude) excited cells in the NLL (or SOC) that provided adapting, sustained inhibition (SI_{AD}) to the DTN. We used two different CN rate-level functions (standard and steep) to account for the *in vivo* responses of long-pass DTNs at higher SPLs. For a stimulus of fixed duration, the strength of inhibition received by the model DTN grew faster than the strength of the excitation as stimulus magnitude increased, resulting in decreased spike counts and longer first-spike latencies as observed *in vivo*. Recruiting afferent input to the model at different rates is biologically plausible because a wide variety of rate-level functions exist in the mammalian central auditory system (see Kiang (1965) for auditory nerve fibers; Rhode and Greenberg (1992) for CN afferents).

The long-pass model incorporates neurons with adapting, sustained inhibition (SI_{AD}) to inhibit the model DTN. This is in contrast to the short-pass and band-pass models which used non-adapting inhibitory inputs. Neurons with adapting responses are referred to as "primary-like" and have been observed in the NLL (Covey and Casseday, 1991) and the SOC (Guinan et al., 1972).
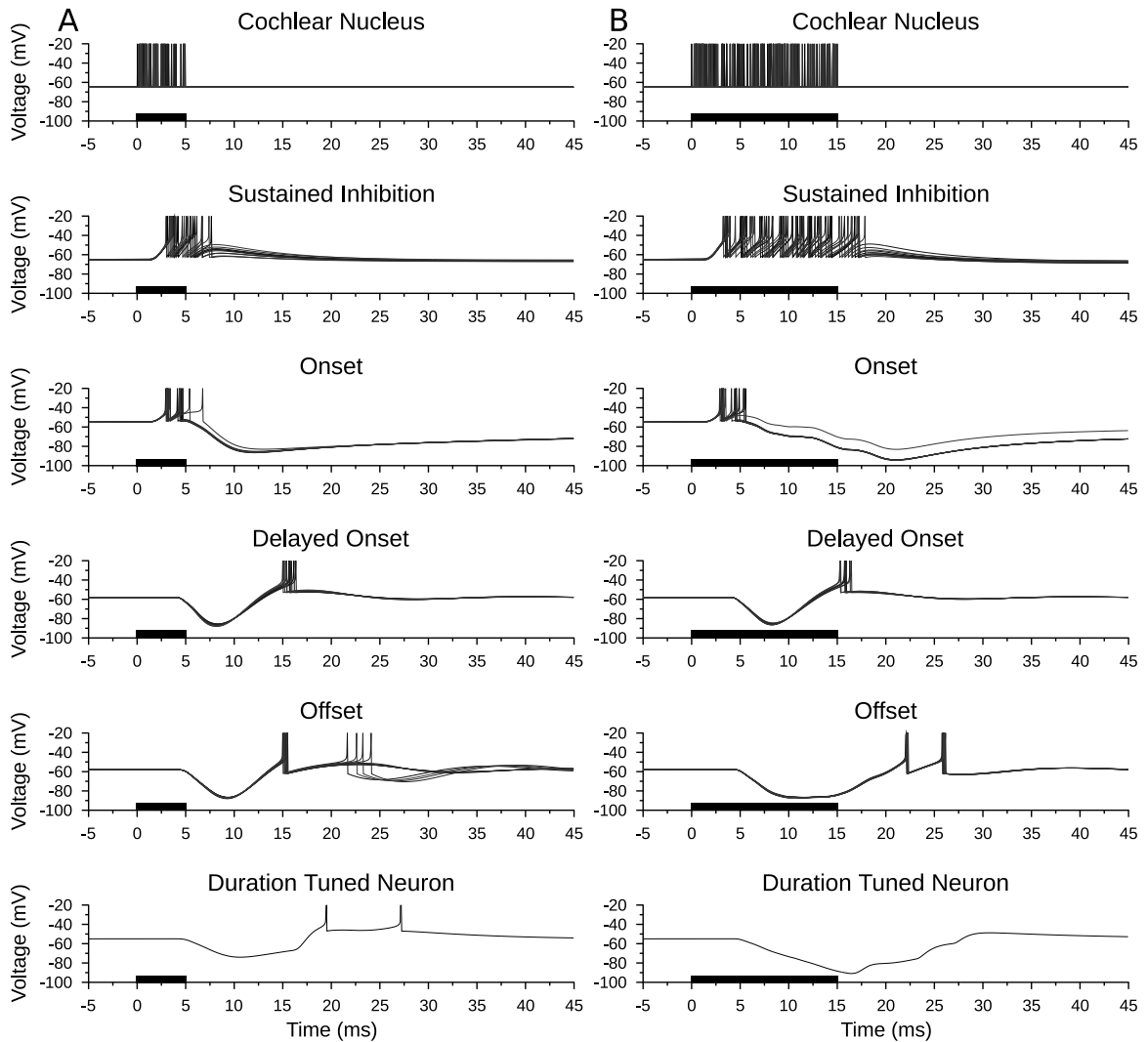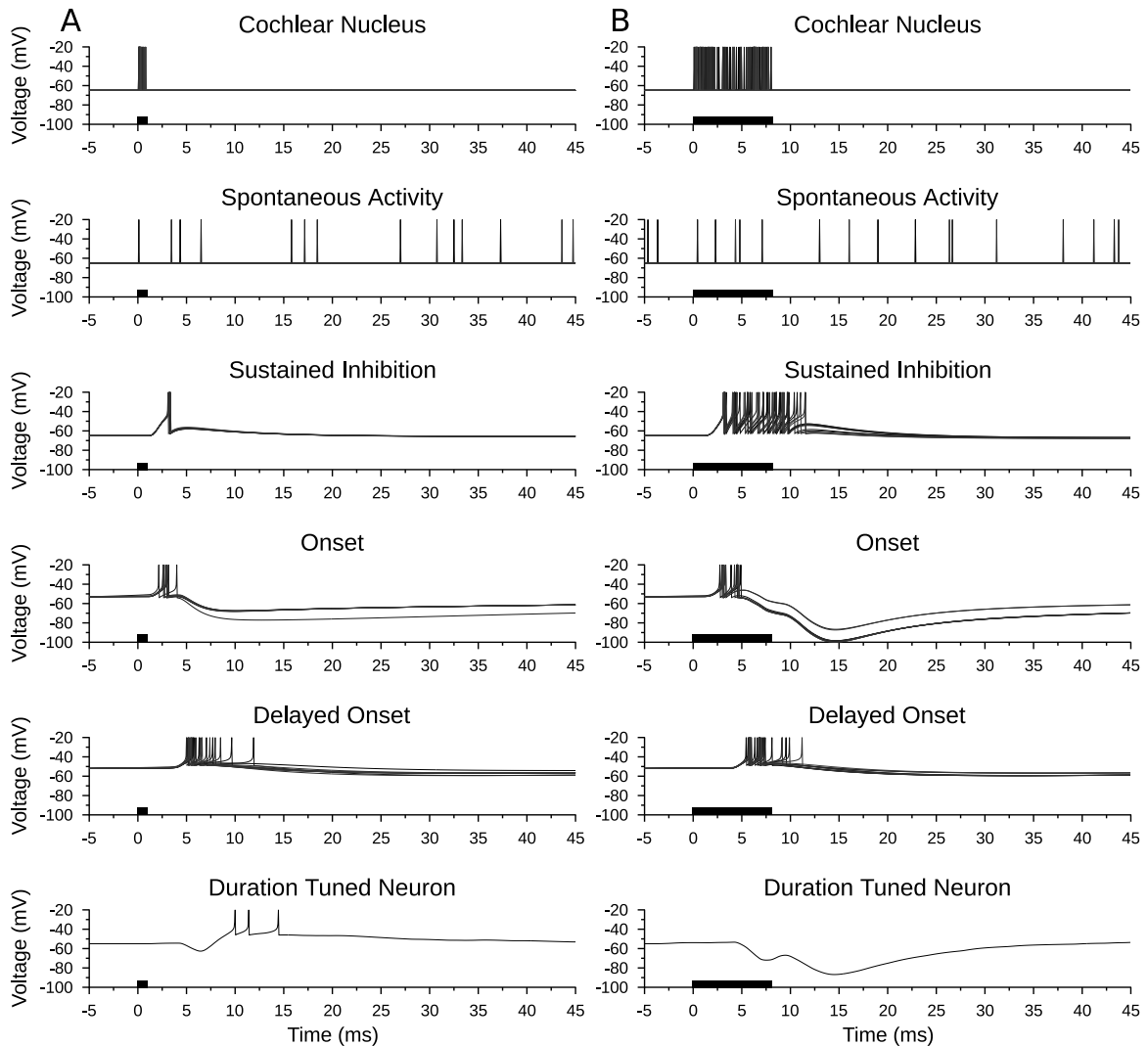
Figure 2.5: Short-pass anti-coincidence duration tuning. Shown are model neuron responses to a single standard input stimulus from the Cochlear Nucleus at 400 Hz for a duration of (A) 1 ms and (B) 8 ms to illustrate model responses to a BD stimulus and a longer duration stimulus. Spontaneous activity to the DTN from five Poisson spiking processes each with a mean firing rate of 50 Hz is also shown. Membrane potential (voltage) traces of every neuron in the model are shown with action potentials truncated for improved sub-threshold clarity. Action potentials from the Cochlear Nucleus Poisson spiking processes and from Spontaneous Activity are drawn as instantaneous spikes. (A) Excitation from the Delayed Onset cells was supra-threshold unless it overlapped with inhibition. Therefore, the Duration Tuned Neuron produced action potentials when there was an anti-coincidence of spikes in the Sustained Inhibition and Delayed Onset populations. (B) When responses of the Delayed Onset and Sustained Inhibition populations overlapped, the membrane potential of the Duration Tuned Neuron remained sub-threshold and no action potentials were produced. Stimulus duration illustrated as *black bars* on the time axis.

Figure 2.6A shows the membrane potential traces of each neuron in the long-pass model in response to a 5 ms stimulus. Inhibition from the SI_{AD} population was strong and suppressed spiking that might otherwise have been induced in the DTN by excitation from the SE population. Figure 2.6B shows the membrane potential traces of the same long-pass model network in response to a 15 ms stimulus. Starting at approximately 10 ms after stimulus onset, the SI_{AD} population had adapted sufficiently so that excitation from the SE cells was able to evoke action potentials in the DTN. Note the sub-threshold change in the membrane potential of the model DTN from 4 to 8 ms after stimulus onset caused by the SI_{AD} cells overpowering the sustained excitation. Faure et al. (2003) and Pérez-González et al. (2006) observed longer first-spike latencies in some long-pass DTNs as stimulus magnitude increased. To account for this, we hypothesized that CN afferent input to the SI_{AD} population grew more quickly than CN afferent input to the SE population; thus, increasing stimulus energy caused the SI_{AD}-evoked inhibition to lengthen in duration and overlap with the initial portion of the onset-evoked EPSP. This resulted in longer first-spike latencies in the model cell, reproducing the so-called "paradoxical latency shift" (Heil, 2004) that has been observed in some long-pass DTNs and other IC neurons (Wang et al., 2007).

Alternatively, long-pass selectivity could arise from a duration-dependent enhancement of excitation rather than through a reduction of inhibition as proposed above. For paradoxical latency shift to occur in this case, there would also need to be an inverse relationship between stimulus input energy and the strength of excitation to the DTN; as stimulus energy increased, the strength of the excitatory input to the long-pass cell would need to decrease (to a point), resulting in fewer spikes at longer latencies.

2.4   Results

To evaluate the biological plausibility of our computational networks, we compared responses of model neurons to responses of *in vivo* extracellular recordings of DTNs from the IC of the big brown bat, *Eptesicus fuscus* (Casseday et al., 2000; Faure et al., 2003). *In vivo* responses were measured with pure tones or linear frequency modulated (FM) sweeps that were randomly varied in duration and presented at 10 to 40 dB above threshold at the DTN's characteristic frequency. Acoustic stimuli were presented monaurally to the ear contralateral to the recording site. To simulate increases in SPL for model input, we chose CN rate-level
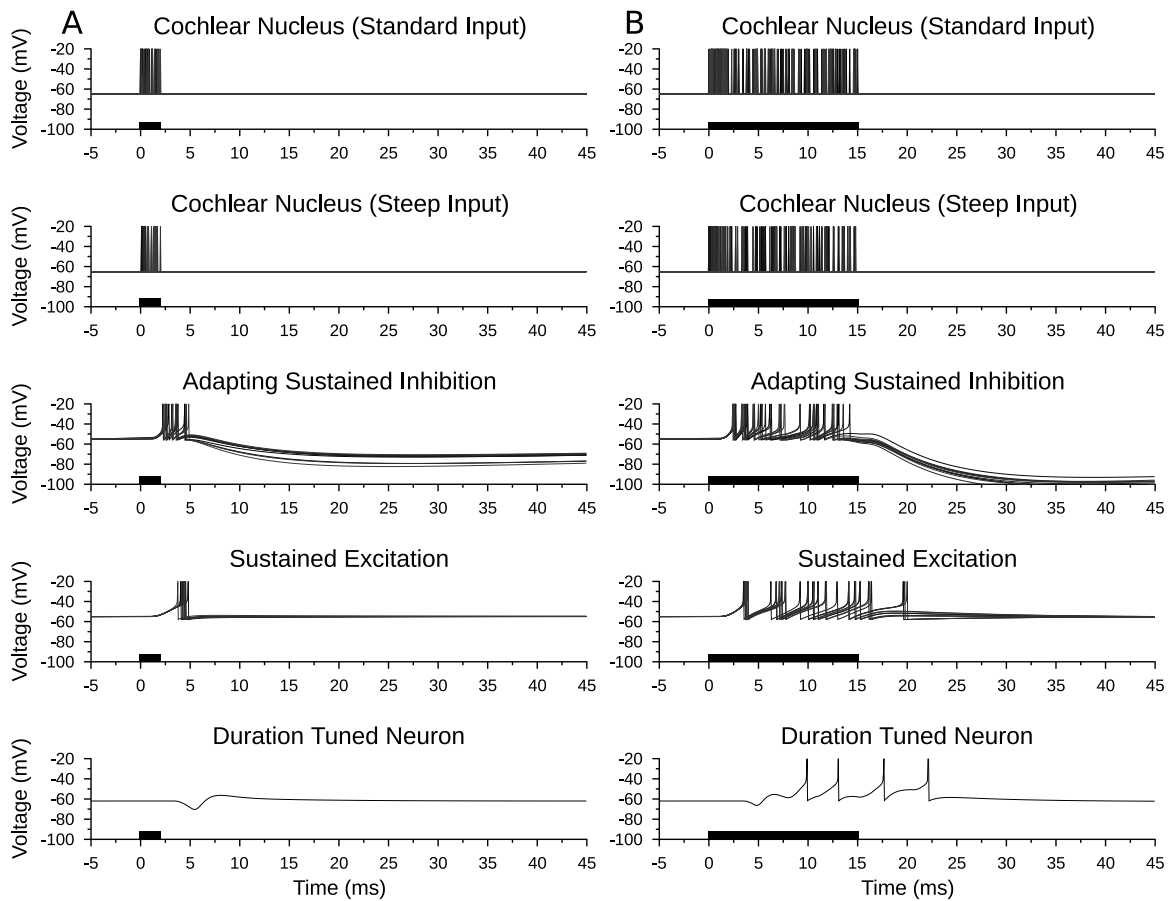
Figure 2.6: Long-pass anti-coincidence duration tuning. Shown are model neuron responses to a single input stimulus that recruits standard input at 400 Hz and steep input at 250 Hz from the Cochlear Nucleus to illustrate model responses to (A) a 2 ms (short) stimulus and (B) a 15 ms (long) stimulus. Membrane potential (voltage) traces of every neuron in the model are shown with action potentials truncated for improved sub-threshold clarity. Action potentials from the Cochlear Nucleus Poisson spiking processes are drawn as instantaneous spikes. (A) Excitation from the Sustained Excitation cells was supra-threshold unless it overlapped with inhibition. Therefore, the Duration Tuned Neuron did not fire action potentials when there was a coincidence of spikes from the Adapting Sustained Inhibition and Sustained Excitation populations. (B) When inhibition from the Adapting Sustained Inhibition population decreased, excitation from the Sustained Excitation population broke through and produced action potentials in the Duration Tuned Neuron. Note how the membrane potential of the DTN at 7 ms (both stimuli) was raised by excitatory input from the Sustained Excitation population but did not reach threshold. Sustained Excitation neurons driven by the standard Cochlear Nucleus Poisson spiking process; Adapting Sustained Inhibition neurons driven by the steep Cochlear Nucleus Poisson spiking process (see Fig. 2.3C). Stimulus duration illustrated as *black bars* on the time axis.

functions appropriate for bats (see *Methods and Materials*).

2.4.1 Transitioning Between Short-Pass and Band-Pass Responses

Historically, the labels "short-pass" and "band-pass" were used to describe the temporal selectivity and response classes of DTNs in a manner analogous to the filter frequency selectivity of resonant electronic circuits. A coincidence detection mechanism was suggested to produce cells in both classes (Ehrlich et al., 1997; Faure et al., 2003) while an anti-coincidence mechanism was suggested for short-pass responses (Fuzessery and Hall, 1999). In this section, we demonstrate that neither mechanism is necessarily mutually exclusive and that hybrid models can produce short-pass and band-pass duration-tuned responses by modifying various model connection weights and response parameters.

To demonstrate that an anti-coincidence mechanism can produce model neurons with band-pass duration tuning, we changed the original band-pass coincidence detection model into a band-pass anti-coincidence model by removing the OFF population and increasing the ON_{Delay} to DTN connection weight from 4 to 8. As in our band-pass coincidence detection model, very short stimulus durations (i.e. 1 ms) failed to evoke spikes in the ON population and thus the DTN did not respond. Therefore, a minimum stimulus duration was required to evoke spikes in the DTN in both the coincidence detection and anti-coincidence band-pass models. At longer stimulus durations (i.e. ≥ 10 ms), inhibition from the SI population was strong and rendered the supra-threshold excitation from the ON_{Delay} population sub-threshold. At stimulus durations near the model cell's BD (ca. 5 ms), supra-threshold excitation from the ON_{Delay} population was not sufficiently coincident with inhibition from the SI population, and therefore the model DTN was able to produce action potentials.

To demonstrate that a coincidence detection mechanism can produce model neurons with short-pass duration tuning, we transformed the original short-pass anti-coincidence model into a short-pass coincidence detection model by reducing the ON_{Delay} to DTN connection weight from 5 to 4, adding a population of offset (OFF) responding cells with parameters equivalent to the OFF population in our band-pass coincidence detection model (along with the afferent and efferent connections), and by removing the spontaneous afferent input that was included in the short-pass anti-coincidence model (see *Anti-coincidence Model*). In the original short-pass anti-coincidence model, supra-threshold excitation from the ON population was capable of producing spikes in the DTN at durations of 1-4 ms even when

there was a small overlap with inhibition. In the short-pass coincidence detection model, the ON_{Delay} to DTN connection weight was reduced so the ON_{Delay} excitation was now rendered sub-threshold by inhibition from the SI population for stimulus durations $\geq$2 ms. At 1 ms, the ON_{Delay} excitation could still evoke spikes in the DTN on its own because the overlap with inhibition was insignificant. At stimulus durations $\geq$2 ms, the ON_{Delay} excitation required coincidence with the OFF excitation to evoke spikes in the DTN. Therefore, this alternative model of short-pass duration tuning was a hybrid of anti-coincidence and coincidence detection mechanisms. We refer to this model as a coincidence detection model because the majority of responses (stimulus durations $\geq$2 ms) required coincidence of the ON_{Delay} and OFF excitations. In contrast to the short-pass anti-coincidence model, the short-pass coincidence detection model produced more spikes at longer stimulus durations (see *Model Response Characteristics*). This was due to the window of coincidence being sufficiently wide to facilitate coincidence at stimulus durations up to 9 ms. Increasing the SI to DTN connection weight strengthened inhibition to the DTN, and this narrowed the window of coincidence between the onset- and offset-evoked excitations but also decreased the number of spikes at all durations.

2.4.2   Model Response Characteristics

For each figure in this section, two types of plots are presented. The first shows a dot raster display of the spikes evoked by a DTN in response to stimuli that were randomly varied in duration from 1 to 25 ms at a constant mean Poisson input rate or acoustic SPL. The ordinate shows stimulus duration and the abscissas shows time relative to stimulus onset. Black lines represent the duration of the stimulus, and dots represent the time of occurrence of individual spikes. The second plot shows the mean $\pm$ standard error (SE) number of spikes per stimulus at each duration and stimulus level. Model and *in vivo* band-pass plots were composed of 20 trials per stimulus whereas short-pass and long-pass plots were comprised of 15 trials per stimulus. This was done so that the number of trials was the same when comparing model and *in vivo* responses.

First we compare band-pass responses from the coincidence detection and anti-coincidence models with band-pass responses from an *in vivo* DTN (Fig. 2.7). Notice how both the coincidence detection and anti-coincidence models accurately reproduced the spike counts, first-spike latencies, and amplitude tolerance of the *in vivo* band-pass DTN (compare Figs.

2.7A&B with Fig. 2.7C). At durations above ca. 11 ms, the models failed to spike even though the *in vivo* band-pass neuron occasionally produced action potentials, especially at the highest stimulus amplitudes (compare Figs. 2.7D&2.7E to 2.7F). Although the +40 dB raster data from Figure 2.7F are not shown, the few additional spikes that were evoked by stimulus durations $\geq$11 ms consistently occurred between 20 and 30 ms re stimulus onset and did not follow stimulus offset, thus confirming the existence of an onset-evoked excitation. The default parameters we used did not reproduce onset breakthrough in our models; however, slight modifications permit for such occurrences (see Fig. 2.11E). A primary difference between responses from the band-pass coincidence detection and anti-coincidence model neurons was in first-spike latency; due to the offset component in the coincidence detection model, spikes followed the offset of the stimulus more faithfully than in the anti-coincidence model. This difference is discussed further in *Relevance of Model Components*. The temporal response bandwidth was also 1-2 ms larger in the coincidence detection model DTN.

Figure 2.8 compares short-pass model responses from the coincidence detection and anti-coincidence models with short-pass responses from an *in vivo* DTN. Although the coincidence detection model reproduced the first-spike latency and amplitude tolerance of the *in vivo* short-pass DTN, it also produced spikes at longer stimulus durations (i.e. 5 to 8 ms) whereas the anti-coincidence model did not (compare Figs. 2.8A&D with Figs. 2.8C&F). This is because the window of coincidence between the ON_{Delay} and OFF populations was wide enough to evoke supra-threshold responses to durations <10 ms. To narrow the window of coincidence, the offset excitation would either have to be shorter in duration or weaker in amplitude than in our model network. The brief increase in spike count in the coincidence model at 4 and 5 ms was caused by a stronger offset response to longer stimulus durations, but at 6 ms there was less coincidence between the onset- and offset-evoked EPSPs so spike counts again decreased.

Neural responses similar to the output of the coincidence detection and anti-coincidence short-pass models have been observed from *in vivo* DTNs exhibiting a wide range of temporal bandwidths (e.g. Jen and Zhou, 1999; Fremouw et al., 2005). The anti-coincidence model accurately reproduced the spike counts, first-spike latencies, and amplitude tolerance of the *in vivo* short-pass cell (compare Figs. 2.8B&E with 2.8C&F). The inclusion of spontaneous input directly to the DTN in the short-pass anti-coincidence model (see *Methods and Materials*) caused additional action potentials at latencies longer than 15 ms re stimulus
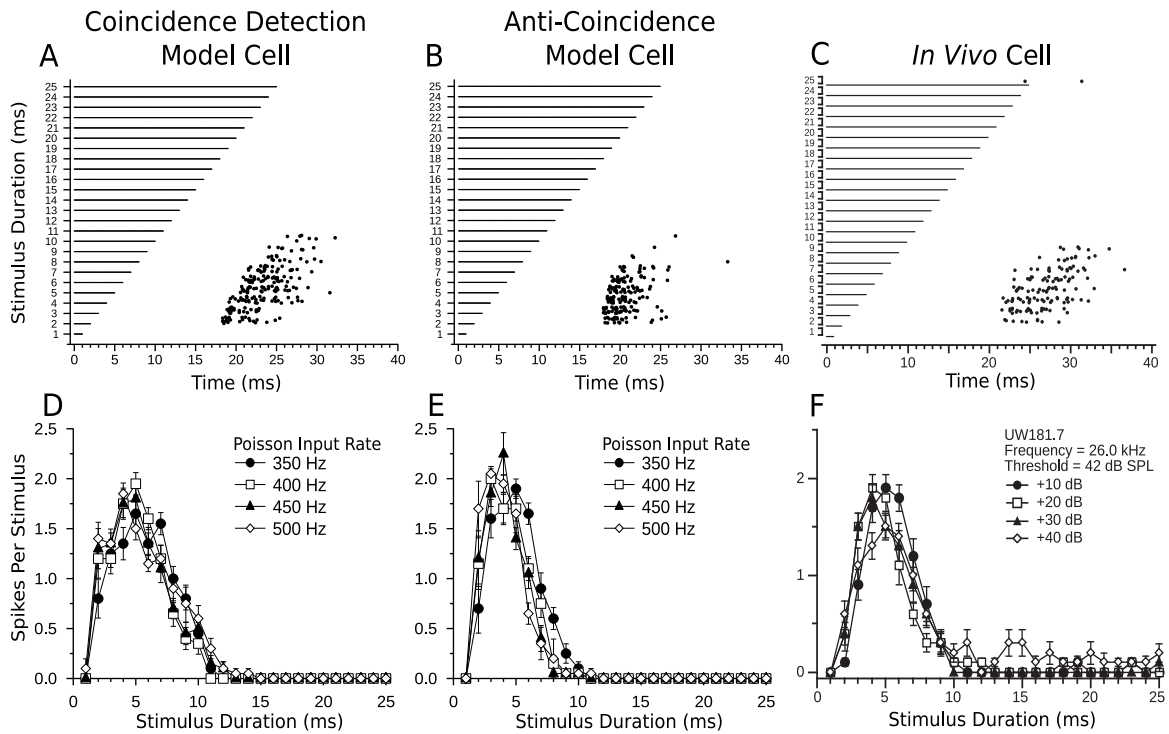
Figure 2.7: Comparison of model and *in vivo* band-pass duration tuning. Dot raster displays of the responses of a band-pass coincidence detection (A) and anti-coincidence (B) model cell to different stimulus durations (20 trials per stimulus; mean Poisson input firing rate = 400 Hz). Model cells have a BD of 5 ms. (C) Dot raster display of the responses of an *in vivo* band-pass DTN with a BD of 5 ms to variable duration pure tones presented at the cell's characteristic frequency (20 trials per stimulus; 30 dB above threshold). (D,E,F) Mean ± standard error (SE) spikes per stimulus as a function of stimulus duration (i.e. duration tuning curves) at four different CN Poisson input firing rates (D,E) or different sound pressure levels (SPLs) relative to threshold (F). Four different Poisson firing rates were chosen to be analogous to four different acoustic SPLs. Refer to *Methods and Materials* for additional details. Note the response tolerance to changes in stimulus magnitude in both model and *in vivo* cells. Coincidence detection model responses follow offset of the stimulus more faithfully than anti-coincidence model responses and have a slightly wider temporal bandwidth. Panels C and F reprinted with permission (Faure et al., 2003, Fig. 4B).
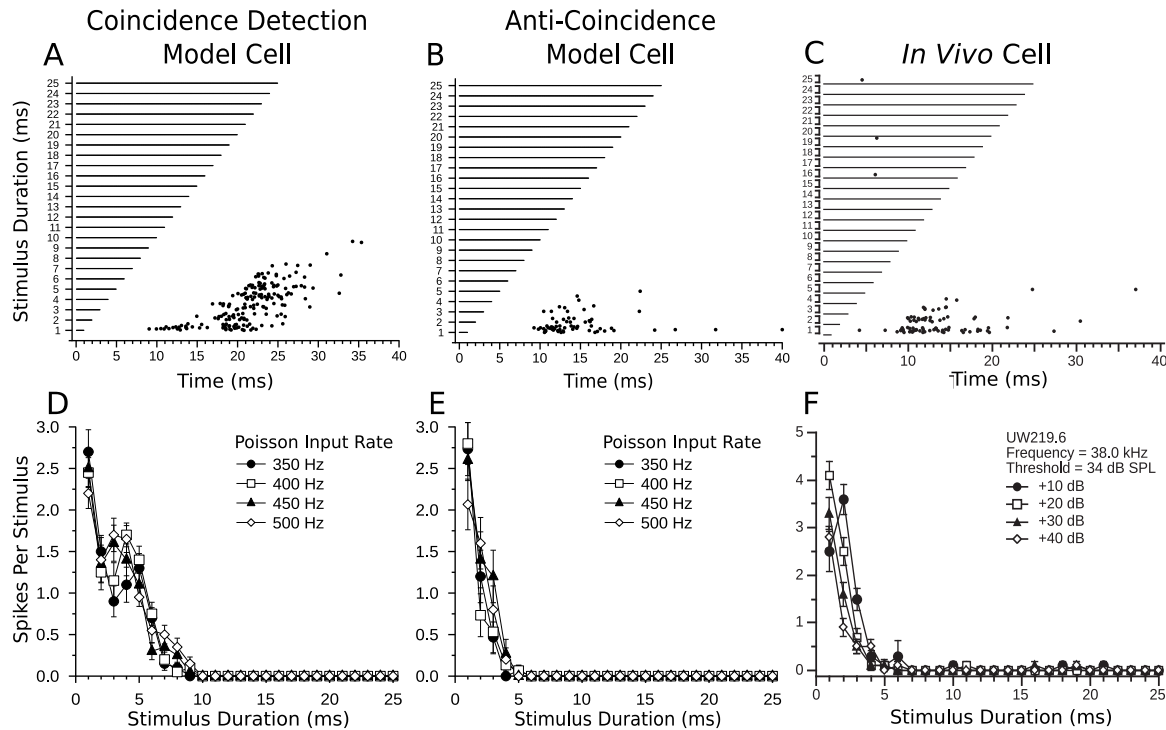
Figure 2.8: Comparison of model and *in vivo* short-pass duration tuning. Dot raster displays of the responses of a short-pass coincidence detection (A) and anti-coincidence (B) model cell to different stimulus durations (15 trials per stimulus; mean Poisson input firing rate = 400 Hz). Model cells have a BD of 1 ms. (C) Dot raster display of the responses of an *in vivo* short-pass DTN with a BD of 1 ms to variable duration pure tones presented at the cell's characteristic frequency (15 trials per stimulus; 30 dB above threshold). (D,E,F) Mean ± SE spikes per stimulus as a function of stimulus duration at four different CN Poisson input firing rates (D,E) or different SPLs relative to threshold (F). Four different Poisson firing rates were chosen to be analogous to four different acoustic SPLs. Refer to *Methods and Materials* for additional details. Note the response tolerance to changes in stimulus magnitude in both model and *in vivo* cells. Coincidence detection model DTN has a wider temporal response bandwidth than the anti-coincidence model neuron. Panels C and F reprinted with permission (Faure et al., 2003, Fig. 4A).

onset. This mirrors the *in vivo* responses of some short-pass DTNs (Faure et al., 2003). Removal of the spontaneous activity resulted in fewer spikes at the model neuron's BD.

Long-pass model responses and *in vivo* long-pass data are compared in Figure 2.9. The model cell accurately reproduced the spike counts and first-spike latencies of the *in vivo* long-pass cell (Figs. 2.9A-D). Sustained excitation resulted in linearly increasing spike counts in the model DTN with increasing stimulus duration. The delay in first-spike latency in the model long-pass DTN at high stimulus amplitudes (shown explicitly in Fig. 2.13B) occurred because the strength of the adapting sustained inhibition from the SI_{AD} cells grew more rapidly for increases in stimulus magnitude than the sustained excitation from the SE cells. As the SI_{AD} cells adapted, the sustained excitation (driven by the standard CN input) broke through the adapting sustained inhibition (driven by the steep CN input), and action potentials were produced. This resulted in paradoxical latency shift that has been observed for some long-pass DTNs in the IC of the bat (Faure et al., 2003) and rat (Pérez-González et al., 2006).

2.4.3   Relevance of Model Components

To assess the relevance of various components, we ran simulations with each model while varying a single parameter across a range of values. In both the coincidence detection and anti-coincidence models, inhibition from the SI population played a key role in defining spike counts and temporal response bandwidths of DTNs. To study the role of inhibition in duration tuning, Casseday et al. (2000) iontophoretically applied two types of inhibitory neurotransmitter antagonists while simultaneously recording acoustically-evoked responses from DTNs in the IC of the bat. Responses were recorded before, during, and after the blocking of synaptic inhibition at the DTN with bicuculline, a $GABA_A$ antagonist, and strychnine, a glycine antagonist. They found that when inhibition was blocked, duration selectivity vanished in 71% of cells tested with bicuculline and in 40% of cells tested with strychnine. In the remaining units, the temporal bandwidth of the duration tuning curve broadened or no changes were observed.

To simulate the effects of applying inhibitory neurotransmitter antagonists, we modified the coincidence detection and anti-coincidence models by adjusting the inhibitory connection weight between the SI population and the DTN (see Fig. 2.3A,B). This effectively blocked some or all inhibition to the model DTN. Figures 2.10A&B compare coincidence detection
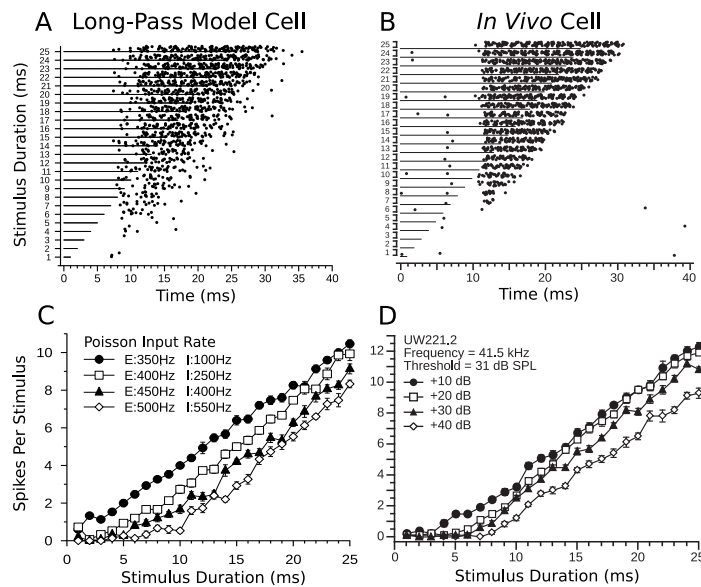
Figure 2.9: Comparison of model and *in vivo* long-pass duration tuning. (A) Dot raster display of the responses of a long-pass anti-coincidence model cell to different stimulus durations (15 trials per stimulus; mean standard input Poisson firing rate = 400 Hz, mean steep input Poisson firing rate = 250 Hz). (B) Dot raster display of the responses of an *in vivo* long-pass DTN to variable duration pure tones presented at the cell's characteristic frequency (15 trials per stimulus; 30 dB above threshold). (C,D) Mean $\pm$ SE spikes per stimulus as a function of stimulus duration at four different CN Poisson input firing rates (C) or different SPLs relative to threshold (D). Four different Poisson firing rates were chosen to be analogous to four different acoustic SPLs. The legend in (C) lists the standard CN input Poisson firing rates driving the Sustained Excitation cells (prefaced with an E) and the steep CN input Poisson firing rates driving the Adapting Sustained Inhibition cells (prefaced with an I). Refer to *Methods and Materials* for additional details. Note the decreased spike counts of both the model and *in vivo* long-pass DTNs as the stimulus magnitude increases. Panels B and D reprinted with permission (Faure et al., 2003, Figure 4C).

model cell responses with decreasing levels of inhibition to *in vivo* responses of a band-pass DTN when inhibition was blocked iontophoretically. As the inhibitory connection weight in the coincidence model decreased, the temporal selectivity of the DTN decreased. Eventually, its band-pass tuning was abolished when inhibition was removed completely. This occurred because all onset excitation to the model DTN evoked spiking. Therefore, inhibition was critical for ensuring the onset-evoked excitation remained sub-threshold. The BD of the network, however, remained fairly stable, increasing only slightly from 5 to 7 ms when inhibition was present. This happened because peak spiking still occurred when the onset- and offset-evoked excitations coincided. Again, the model DTN did not respond to 1 ms stimuli when inhibition was completely removed because of the high spiking threshold of the ON population (see *Coincidence Detection Model*). Casseday et al. (2000) reported that blocking inhibition with bicuculline resulted in either a broadening of the duration tuning curve (e.g. Fig. 2.10B) or loss of temporal selectivity.

As inhibition was removed in the anti-coincidence model, the duration turning curve of the short-pass model cell broadened and eventually its temporal selectivity was abolished (Fig. 2.10C). This occurred because spiking from the ON$_{Delay}$ population provided supra-threshold excitation to the model DTN at a fixed latency from stimulus onset at all durations when inhibition was no longer available to render it sub-threshold. Again, our simulations mirrored the *in vivo* results of Casseday et al. (2000) who reported that some short-pass cells bathed in bicuculline and/or strychnine lost their temporal response specificity (e.g. Fig. 2.10D). When spikes were observed for *in vivo* cells, they tended to occur at a fixed latency from stimulus onset.

The standard parameters of our band-pass coincidence detection model produced a DTN with a BD tuned between 4 and 6 ms, whereas the standard anti-coincidence model resulted in a short-pass cell with a BD of 1 or 2 ms. These BDs are typical for DTNs recorded in the IC of bats (Faure et al., 2003) and mice (Brand et al., 2000). When *in vivo* DTNs with longer BDs were reported, they typically had a wider temporal response bandwidth. That is, the width at half-height of the duration tuning function was wider and shifted toward longer durations (Fremouw et al., 2005). As seen in our simulations, dampening inhibition in the coincidence detection and anti-coincidence models produced similar behaviour. Therefore, we conclude that inhibition plays a critical role in determining the BD of both model and *in vivo* DTNs.

Onset excitation breakthrough has been observed in as many as 49% of DTNs (Faure et
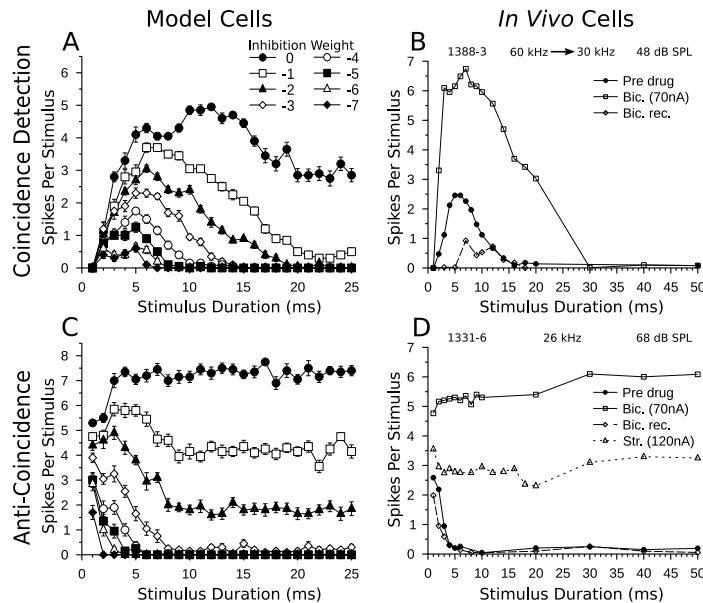
Figure 2.10: Blocking inhibition in model and *in vivo* DTNs. (A,C) Mean $\pm$ SE and (B,D) mean spikes per stimulus as a function of stimulus duration. (A) Duration tuning curves of a band-pass coincidence detection model neuron (20 trials per stimulus; mean Poisson input firing rate = 400 Hz) with the SI to DTN connection weight varied from -7 to 0 (see Fig. 2.3A). As inhibition decreased, spike counts increased, the BD of the neuron remained fairly stable, and the temporal response bandwidth increased until eventually duration tuning was lost. (B) Duration tuning curves of an *in vivo* band-pass DTN in response to downward frequency modulated sweeps (60 to 30 kHz) before, during, and after application of bicuculline, a GABA$_A$ antagonist that blocks inhibition. Before drug application (*solid circles*), the cell had a BD of 5 or 6 ms and did not respond reliably to sounds longer than 14 ms. During application of bicuculline (*open squares*), spike counts grew considerably, BD remained unchanged and the temporal response bandwidth increased. (C) Duration tuning curves of a short-pass anti-coincidence model neuron (20 trials per stimulus; mean Poisson input firing rate = 400 Hz) with the SI to DTN connection weight varied from -7 to 0 (see Fig. 2.3B). Once again, as inhibition decreased, spike counts increased and short-pass duration tuning was eventually lost. (D) Duration tuning curves of an *in vivo* short-pass DTN in response to pure tones (characteristic frequency = 26 kHz) at varying stimulus durations before (*closed circles*), during (*open squares*), and after (*open diamonds*) application of bicuculline, and during application of strychnine, a glycine antagonist (*open triangles*). When inhibition was blocked, spike counts increased considerably and duration tuning was eventually abolished. Panels B and D reprinted with permission (Casseday et al., 2000, Figure 5A, 2A).
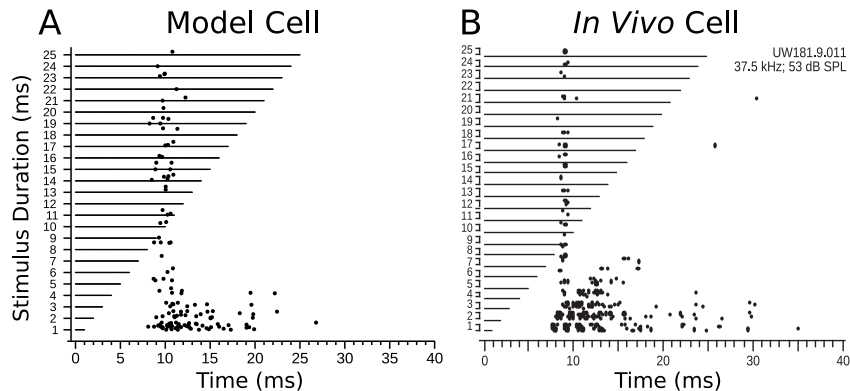
Figure 2.11: Onset excitation breakthrough in model and *in vivo* DTNs. (A) Dot raster display of an onset breakthrough response in a short-pass anti-coincidence model neuron (BD = 1 ms) with the SI to DTN connection weight decreased from -5 to -4.3 and the SI to DTN axonal delay increased from 1 to 2.8 ms (15 trials per stimulus; mean Poisson input firing rate = 400 Hz). (B) Dot raster display of an onset breakthrough response in an *in vivo* short-pass DTN (BD = 1 ms; 15 trials per stimulus; 30 dB above threshold). Panel B reprinted with permission (Faure et al., 2003, Figure 6B).

al., 2003). The breakthrough was interpreted as evidence for an onset-evoked excitation that was able to break through a weaker, sustained inhibition during the stimulus, resulting in spikes with a (more or less) constant first-spike latency re stimulus onset rather than a latency that tracks stimulus offset. To reproduce this behaviour in the short-pass anti-coincidence model neuron, we decreased the magnitude of the SI to DTN inhibitory connection weight from -5 to -4.3 and increased the axonal delay from 1 to 2.8 ms (i.e. we weakened and delayed synaptic inhibition to the DTN; Fig. 2.3B) while keeping all other model parameters unchanged. Figure 2.11 compares the results of a modified short-pass anti-coincidence model cell to an *in vivo* short-pass DTN exhibiting onset-excitation breakthrough. By slightly weakening the onset-evoked sustained inhibition to the model DTN, we were able to reproduce the onset-evoked excitation breakthrough that has been observed *in vivo*.

In the coincidence detection model, the latency of the offset-evoked EPSP (re stimulus onset) increases with stimulus duration. Indeed, it is the timing of the offset-evoked excitation that determines when a DTN will spike because the onset-evoked excitation occurs at a fixed latency (re stimulus onset). To evaluate how the strength of the offset-evoked excitation affected responses of the band-pass coincidence detection model, we varied the OFF to DTN connection weight from 0 to 5 (with 3 being the value in the standard model; see Fig. 2.7A). When the connection weight was 0 (i.e. the offset-evoked excitation was removed),

spiking in the DTN was effectively abolished (Fig. 2.12A) despite the onset-evoked EPSP being supra-threshold in the absence of inhibition (see Fig. 2.10A). Even at short durations, when the sustained inhibitory input to the DTN had ended before the arrival of the supra-threshold, onset-evoked EPSP, the excitation was still rendered sub-threshold because the model neuron's recovery from inhibition was not instantaneous. *In vivo* recordings from IC neurons have shown that the effects of inhibition can persist beyond the duration of the stimulus (e.g. Klug et al., 1999). This emphasized the need for a coincidence between the onset- and offset-evoked EPSPs. When the connection weight was 1 (Fig. 2.12A), responses from the model DTN started to become band-pass. Figures 2.12B and C show dot rasters when the OFF to DTN connection weights were 2 and 5, respectively. Increasing the offset connection weight caused the sub-threshold, offset-evoked EPSP to become supra-threshold, resulting in spikes that followed stimulus offset at all durations, although peak counts still occurred when the onset- and offset-evoked EPSPs coincided. Additional spikes also occurred when the SI to DTN inhibitory connection weight was decreased (see Fig. 2.10A), but in this case, the relative timing of the spikes differed. As inhibition to the DTN was weakened, the onset-evoked EPSP was no longer rendered sub-threshold by the sustained inhibition. Therefore, the additional spikes occurred at a fixed latency from stimulus onset (see Fig. 2.11A) rather than from stimulus offset.

It is also plausible that the offset excitation observed from *in vivo* recordings of DTNs does not arise from an external synaptic input, but instead arises from a post-inhibitory rebound mechanism. Post-inhibitory rebound, likely facilitated by an I_h current, has been observed in the mammalian IC (Peruzzi et al., 2000; Koch and Grothe, 2003; Tan et al., 2007; Sun and Wu, 2008). To examine response characteristics of model DTNs with post-inhibitory rebound, we removed the OFF population from the coincidence detection model and increased the sub-threshold adaptation parameter (a) of the model DTN (see Brette and Gerstner, 2005). Figures 2.12D-F show spike counts and dot raster displays for several values of a. With a small amount of adaptation ($a = 44$ nS), the model cell produced band-reject duration tuning. That is, the cell reliably responded only to short (2 - 4 ms) or long signals ($\geq$15 ms). For stimulus durations between 5 and 14 ms, there were few or no spikes. At short durations, the model DTN was not sufficiently hyperpolarized to evoke post-inhibitory rebound spiking unless excitation from the delayed onset-evoked EPSP coincided with the rebound. This occurred between 2 and 4 ms. At durations $\geq$15 ms, the model cell was hyperpolarized for a sufficient time such that the post-inhibitory rebound was
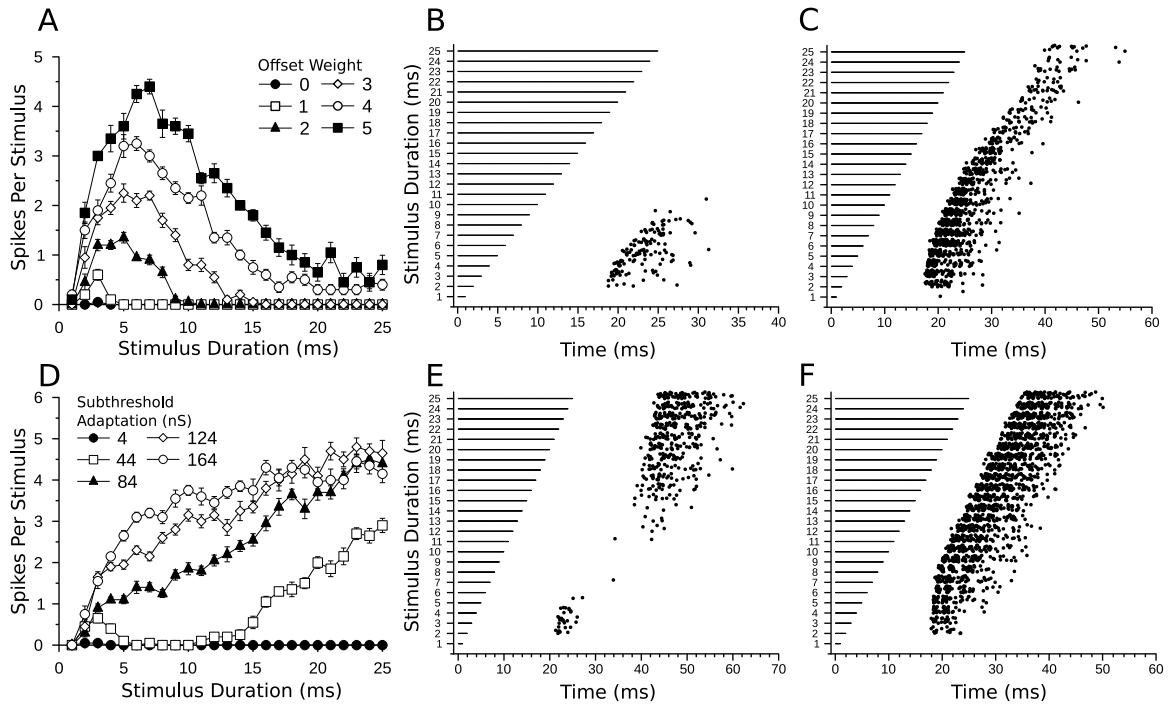
Figure 2.12: Offset excitation in the band-pass coincidence detection model. (A) Mean ± SE duration tuning curves of a band-pass coincidence detection model cell with the OFF to DTN connection weight varied from 0 to 5 (see Fig. 2.3A) and a mean Poisson input rate = 400 Hz (20 trials per stimulus). (B,C) Dot raster displays showing responses of the band-pass coincidence model with the OFF to DTN connection weight set to 2 (B) and 5 (C). (D) Mean ± SE duration tuning curves of a band-pass coincidence model with post-inhibitory rebound and increasing levels of sub-threshold adaptation in the model neuron (see *Relevance of Model Components*). (E,F) Dot raster displays showing responses of the band-pass coincidence model with post-inhibitory rebound and sub-threshold adaptation levels of 44 nS (E) and 164 nS (F). In (E), note the bimodal pattern of action potentials. The model cell reliably spiked in response to stimulus durations between 2 and 4 ms and at durations >15 ms. The band-reject selectivity resulted from the model cell's failure to produce spikes from post-inhibitory rebound at short durations unless the rebound coincided with the onset-evoked excitation; however, at longer durations, the rebound was strong and spikes were produced in the model DTN. In (F), the high level of sub-threshold adaptation allowed the model cell to spike via post-inhibitory rebound at all but the shortest duration, hence the cell lost its duration selectivity.

stronger and produced action potentials in the model DTN, even in the absence of coincident excitation from the onset-evoked EPSP. Therefore, for a post-inhibitory rebound mechanism to replace the offset excitation in the coincidence detection model and reproduce typical *in vivo* responses, the rebound must be sub-threshold at all durations. Leary et al. (2008) found no evidence of post-inhibitory rebound in short-pass DTNs in amphibians, although it may still play a role in the DTNs of mammals.

Finally, we examined first-spike latencies in each duration tuning model. Figure 2.13A shows first-spike latencies of band-pass and short-pass model DTNs implemented with coincidence detection and anti-coincidence mechanisms. Both short-pass and band-pass model cells had first-spike latencies that tracked stimulus offset. This was expected for the coincidence detection models because the overlap between the onset- and offset-evoked excitations would occur later in time as stimulus duration increased. We also found that both anti-coincidence models produced first-spike latencies that tracked stimulus offset. This was somewhat surprising because conceptually, the kinetics of the anti-coincidence mechanism depend primarily on a single, fixed-latency, onset-evoked EPSP. We hypothesized that the offset following response in both the short-pass and band-pass anti-coincidence networks resulted from sustained inhibition; because the duration of the sustained IPSP increased with stimulus duration, this increased first-spike latencies in both the short-pass and band-pass anti-coincidence networks. In short, the spikes were delayed by the DTN's recovery from hyperpolarization. Not surprisingly, we found that the shortest first-spike latencies occurred in short-pass DTNs for the anti-coincidence network when the onset-evoked excitation was early and supra-threshold (Fig. 2.13A). The coincidence detection models of duration tuning had consistently longer first-spike latencies because spikes in these models explicitly required the coincidence of onset- and offset-evoked EPSPs. Longer first-spike latencies were also observed in the band-pass anti-coincidence model because spikes in the ON_{Delay} cells were evoked by a post-inhibitory rebound mechanism and this delayed the arrival of onset-evoked excitation to the model DTN.

Variability of first-spike latency between different computational models was consistent with *in vivo* data where a wide range of first-spike latencies has been observed between but not within cells tuned to similar BDs. Leary et al. (2008) reported first-spike latencies from ca. 55 to 150 ms in frog DTNs with BDs tuned from 10 to 12 ms. Faure et al. (2003) found that DTNs of big brown bats had first-spike latencies ranging from 8 to 27 ms in cells with a 2 ms BD, and 13 to 24 ms in cells with a 5 ms BD. Such large variation in
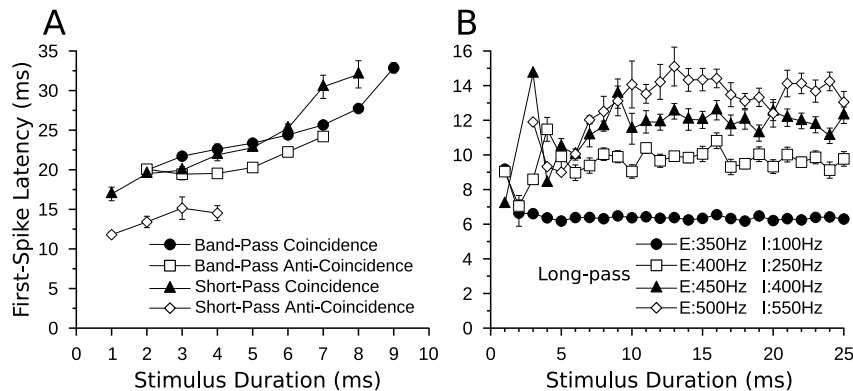
Figure 2.13: Mean $\pm$ SE first-spike latencies of the (A) coincidence detection, anti-coincidence and (B) long-pass duration tuning models. (A) Responses of the coincidence and anti-coincidence model cells followed the offset of the stimulus. In the anti-coincidence models, the sustained inhibition to the model DTN caused a longer first-spike latency even though the onset-evoked EPSP arrived at approximately the same time at all durations. The coincidence detection models followed signal offset more reliably than the anti-coincidence models (see *Relevance of Model Components*). (B) First-spike latencies of the long-pass model at four Poisson input firing rates. Note how first-spike latency increased with stimulus magnitude at durations ca. ≥ 6 ms. Action potentials occurred less frequently and with more variable timing at shorter durations (see Fig. 2.9). Each model was run 20 times with a mean Poisson input rate = 400 Hz (A) or as shown in the legend (B).

first-spike latency between cells with the same BD suggests the existence of multiple neural mechanisms underlying *in vivo* duration selectivity, and/or that there is variability within a single mechanism across networks.

First-spike latencies in the long-pass model of duration tuning clearly showed a paradoxical latency shift at stimulus durations >10 ms (Fig. 2.13B). At shorter durations, action potentials were infrequent and first-spike latencies had more variable timing. Recall that paradoxical latency shift occurred in our long-pass model because inhibitory inputs increased in strength faster than excitatory inputs.

2.5 Discussion

In general, the computational models presented here support previously hypothesized conceptual models proposed for creating duration-selective neural responses in the auditory system of amphibians (Leary et al., 2008) and mammals (Casseday et al., 1994, 2000; Mora and Kössl, 2004). One notable advancement is the introduction of a supra-threshold,

onset-evoked excitation that can be rendered sub-threshold by onset-evoked inhibition when it does not coincide with sub-threshold, offset-evoked excitation. This is in contrast to the original versions of the coincidence detection model where it was explicitly stated that the onset- and offset-evoked excitations were sub-threshold even in the absence of inhibition (e.g. Casseday et al., 1994; Faure et al., 2003; Mora and Kössl, 2004). With this simple enhancement, our new version of the coincidence detection model was able to reproduce a wider range of *in vivo* response characteristics.

The power of these computational models is their simplicity and biological plausibility in both the individual neuron response characteristics and the proposed neuroanatomical network connections. To showcase the predictive and concordant responses of each model, comparisons were made to *in vivo* data. First, the number of action potentials evoked by model neurons were on the same order as those observed for *in vivo* DTNs. Second, model DTNs had first-spike latencies that tracked signal offset as reported for *in vivo* DTNs in both the amphibian and mammalian auditory midbrain (Brand et al., 2000; Casseday et al., 2000; Leary et al., 2008) and the mammalian (cat) visual cortex (Duysens et al., 1996). We demonstrated that variation in first-spike latency, which correlates with neuronal BD and the strength of leading inhibition *in vivo* (Faure et al., 2003), can easily be altered by simple changes to excitatory or inhibitory connection weights (e.g. compare band-pass coincidence detection model with short-pass anti-coincidence model in Fig. 2.3). Our computational models were also capable of reproducing the variation in first-spike latency that is observed between cells tuned to similar BDs. Third, responses from our model neurons were robust to changes in stimulus input firing rates (analogous to changes in acoustic SPL) and showed amplitude tolerance similar to *in vivo* DTNs (Zhou and Jen, 2001; Fremouw et al., 2005). Fourth, we found that the strength and timing of inhibition and excitation could be tuned to produce model cells with a range of neuronal BDs and temporal response bandwidths. Fifth, our models were capable of replicating additional *in vivo* neurophysiological responses such as onset excitation breakthrough and the effects of blocking local synaptic inhibition with neuropharmacological agents.

2.5.1 Comparison to Other Timing Mechanisms

Significant behavioural and neurophysiological research has been conducted on the perception of stimulus duration in human and non-human animals. The pacemaker-accumulator

model (reviewed in Buhusi and Meck, 2005) proposes that an internal clock (e.g. spiking neurons) provides regularly spaced pulses that accumulate over time. In this model, the duration of an event is calculated by multiplying the number of pulses received during an event by the discharge frequency of the internal clock. This simple model has been successful in explaining many behavioural results on a timescale of hundreds or thousands of milliseconds, but fails to explain the millisecond level discrimination observed for *in vivo* DTNs. Additionally, because spike counts in most auditory midbrain neurons (but not all DTNs) tend to increase with stimulus amplitude (Potter, 1965; Covey and Carr, 2005), this would hinder a pacemaker-accumulator mechanism because it relies on a constant spiking frequency to calculate the duration of an event.

Carr and Konishi (1990) described a coincidence detection timing mechanism that used axonal delay lines of cochlear nucleus magnocellularis neurons to facilitate microsecond, interaural interval tuning in the nucleus laminaris of barn owls (*Tyto alba*). The coincidence detection mechanism described by our models is similar in that it requires two excitatory inputs to coincide, although it is unlikely that simple axonal delays can explain first-spike latencies of 20+ ms observed for *in vivo* DTNs (Faure et al., 2003).

A previous model of duration tuning, the slow conductance model, suggested that duration-selective responses resulted from slowly changing ionic currents induced in a cell by hyperpolarization (Hooper et al., 2002). This model was especially tailored for sound durations >50 ms and relied on inhibition that was sustained throughout the stimulus. The slow conductance model and our network models are not mutually exclusive mechanisms because they invoke explanations at different levels of analyses. Both models produce offset responding cells tuned to a range of BDs, and both predict that the range of excitatory durations (i.e. temporal bandwidth) increases as a function of BD. However, the slow conductance model does not reproduce several key *in vivo* results observed in DTNs with BDs <50 ms. First, onset- and (sometimes) offset-evoked excitatory inputs are known to occur in midbrain DTNs of amphibians (Leary et al., 2008) and mammals (Covey et al., 1996; Casseday et al., 2000; Faure et al., 2003); the slow conductance model includes an offset-evoked rebound excitation (i.e. post-inhibitory rebound) but does not include an onset-evoked excitation. Second, Fuzessery and Hall (1999) and Casseday et al. (2000) showed that pharmacologically blocking inhibition increased spike counts and broadened or abolished the duration-selective responses of some DTNs. The slow conductance model should cease responding entirely when inhibition is removed because the only input is an

IPSP that lasts for the duration of the stimulus. Third, first-spike latencies of *in vivo* DTNs with the same BD can be quite variable, ranging from 7 to 27 ms after stimulus onset in bats (Faure et al., 2003). Variation in first-spike latency of DTNs in the IC of the bat also correlates with the magnitude of leading inhibition (i.e. the difference in time between when the onset-evoked IPSP and the onset-evoked EPSP arrives at the DTN; (Faure et al., 2003)). The slow conductance model does not explicitly account for variation in first-spike latency of DTNs with the same or with different BDs.

2.5.2 Model Generalization

The coincidence detection and anti-coincidence models in no way limit the range of stimulus durations that can be successfully discriminated; however, neural instantiations restrict their use to short timescales (i.e. millisecond to tens of milliseconds). For both the coincidence and anti-coincidence models to discriminate long duration stimuli, the latency of the onset-evoked events would have to scale proportionally. That is, for a neuron to have a BD of 50 ms, the onset-evoked excitation (re stimulus onset) would have to be delayed by approximately 50 ms. Accounting for such a long delay would necessitate mechanisms not included in the present computational models, such as slowly changing ionic currents (Hooper et al., 2002) or unrealistic axonal delays. The long-pass model, however, may be able to explain preferences for long duration stimuli. Increasing the adaptation time of the onset-evoked inhibition in the long-pass model could produce a DTN with a preference for arbitrarily long duration stimuli.

2.5.3 Unifying The Conceptual Models

Duration-tuned neurons are among the most complex cells in the central auditory pathway because they are tuned to stimulus frequency, amplitude and duration. Three conceptual models were proposed to describe the underlying neural mechanisms of duration selectivity, and in this study we have formulated each model computationally. Here we combine the models into a single, unified conceptual model that encompasses all duration tuning response classes.

The unified model consists of three components (inputs) to the DTN, each with parameters that can be tuned to produce different response characteristics: (1) onset-evoked excitation; (2) offset-evoked excitation (which may be an external synaptic connection to

the DTN or rebound from inhibition within the DTN); and (3) onset-evoked inhibition. Parameters to adjust in all three components include: the synaptic connection strength to the DTN, the latency of the component relative to other components, the duration and rate of adaptation of the component, and the minimum stimulus energy required for evoking the component (i.e. low or high spiking threshold). Table 2.1 suggests how the unified model's parameters may be tuned generally to create each duration tuning response class.

Short-pass duration tuning can arise when the supra-threshold, onset-evoked excitation (component 1) has a low spiking threshold (i.e. the neurons providing this input spike with low stimulus input energy) and occurs after the onset-evoked inhibition (component 3). This is the anti-coincidence mechanism of short-pass duration tuning. Alternatively, if the onset-evoked excitation (1) is rendered sub-threshold at short durations by sustained, onset-evoked inhibition (3), then it must also coincide with sub-threshold, offset-evoked excitation (component 2) to produce spikes in the DTN. This is the coincidence detection mechanism of short-pass duration tuning.

Band-pass duration tuning can arise when supra-threshold, onset-evoked excitation (1) has a high spiking threshold (i.e. the neurons providing this input spike only with high stimulus input energy) and occurs after the onset-evoked inhibition (3). This is the anti-coincidence mechanism of band-pass duration tuning. If the onset-evoked excitation (1) is rendered sub-threshold by sustained, onset-evoked inhibition (3), then it must also coincide with sub-threshold, offset-evoked excitation (2) to produce spikes in the DTN. This is the coincidence detection mechanism of band-pass duration tuning.

Long-pass duration tuning can arise when supra-threshold, onset evoked excitation (1) persists for as long or longer than the duration of the stimulus and is rendered sub-threshold for the first several milliseconds of a stimulus by onset-evoked inhibition (3). For this to occur, either the onset-evoked inhibition (3) must adapt and weaken over time, or the onset-evoked excitation (1) must strengthen over time. This is the anti-coincidence mechanism of long-pass duration tuning.

In all cases, the connection strength of the excitatory events (components 1 and 2) can vary as a function of the inhibitory connection strength (component 3). Hybrid mechanisms might employ an anti-coincidence mechanism for short stimulus durations and a coincidence detection mechanism for longer durations. Increasing stimulus energy can decrease spike counts in the DTN if the input to the onset-evoked inhibition has a steeper rate-level function than to the onset-evoked excitation. This is explicitly formulated in the long-pass model but

Table 2.1: Parameters of the unified conceptual model to produce three classes of duration tuning. *Supra-*: supra-threshold synaptic input to the DTN; *Sub-*: sub-threshold input to the DTN (i.e. requires coincidence with an additional excitatory event); *Low*: low spiking threshold (i.e. neurons providing this input spike with low stimulus input energy); *High*: high spiking threshold spiking (i.e. neurons providing this input spike only with high stimulus input energy); *Transient*: duration of the synaptic input is transient; *Sustained*: synaptic input lasting as long or longer than the stimulus; *Augmenting*: input strengthens over time; *Adapting*: input weakens (adapts) over time.

	Onset EPSP	Offset EPSP	Onset IPSP	Conceptual Model
Short-pass	Supra-; Low; Transient	None	Sustained	Anti-Coincidence
	Supra-; Low; Transient	Sub-; Low; Transient	Sustained	Coincidence
Band-pass	Supra-; High; Transient	None	Sustained	Anti-Coincidence
	Supra-; High; Transient	Sub-; High; Transient	Sustained	Coincidence
Long-pass	Supra-; Low/High; Sustained	None	Sustained	Coincidence
	Supra-; Low/High; Sustained	None	Sustained; Adapting	Anti-Coincidence
	Supra-; Low/High; Sustained; Augmenting	None	Sustained	Alt. Anti-Coincidence

could also exist in the short-pass and band-pass models.

Encompassing each conceptual model of duration tuning under a single, unifying model simplifies our understanding of neural selectivity for stimulus duration. Rather than distinct mechanisms for each class of duration tuning, we present a gradient across models, unified with common components and parameters. With such an understanding, it is now possible to investigate how duration tuning could generalize within and across species and sensory modalities. Indeed, simple parameter adjustments to the model can reproduce the variation observed within and between duration tuning response classes, both within and across species (e.g. DTNs in bats *versus* mice *versus* frogs). This is the subject of a future investigation.

2.6   Appendix

2.6.1   Neural Model

The goal of our computational models was to evaluate the plausibility of previously proposed conceptual models of duration tuning in the central auditory system (Potter, 1965; Narins and Capranica, 1980; Fuzessery and Hall, 1999; Faure et al., 2003). To model neuronal circuits with realistic temporal dynamics while retaining tractability and simplicity, we employed individual neuron models that have an adaptive exponential integrate-and-fire (aEIF) mechanism (Brette and Gerstner, 2005), except for the stimulus input to the cochlear nucleus which was modelled with Poisson spiking processes. The aEIF model is a single compartment cellular model extending the classic integrate-and-fire model with exponential spike generation, sub-threshold adaptation and spike adaptation. It is defined by the differential equations

$$C\frac{dV}{dt} = -g_L(V - E_L) + g_L s(V) - w + I$$

$$s(V) = \Delta_T \exp\left(\frac{V - V_T}{\Delta_T}\right)$$

$$\tau_w \frac{dw}{dt} = a(V - E_L) - w$$

with model parameters for each model shown in Tables 2.2, 2.3 and 2.4. The V_T parameter, unlike a standard integrate-and-fire model, is not a hard set spiking threshold. Instead, it defines a point where the membrane potential begins to rise rapidly, similar to a real action

potential. Formally, a spike is said to have occurred when the membrane potential, V, rises rapidly to infinity. The exact spike threshold is a function of V_T and Δ_T, which defines the slope of the exponential curve immediately before a spike is triggered. Following Brette and Gerstner (2005), we defined a spike to have occurred when the membrane potential reached an absolute value of +20 mV, but the exact value was not critical because it changed spike times by only a fraction of a millisecond. After spiking, the neuron's membrane potential was set to V_R. The w term provides both the sub-threshold adaptation and spike adaptation. For spike adaptation, the value of w was increased by b immediately after each spike. The initial values of the free variables were $w = 0$ and $V = E_L$.

Differential equations were solved in a C++ program compiled with GCC 4.3.2 via the fourth-order Runge-Kutta method and a constant time step of 0.05 ms. To obtain the source code, please contact the corresponding author.

2.6.2 Network Modelling

Except for Poisson spiking processes in the CN afferents, membrane potential changes in model neurons were evoked by action potentials in "synaptically" connected neurons. When a model neuron produced an action potential, the time was recorded in memory. The current induced in a post-synaptic neuron was then calculated by an α-function (equations below), which takes the time interval between a simulation time step and a spike time and returns the magnitude of the post-synaptic input current for that time step and spike, where s is (current time - spike time), W is the connection weight, Δ^{ax} is the axonal delay, q is the scaling factor, and τ_s is the rise/fall time constant (Gerstner and Kistler, 2002). All models used a constant axonal delay of 1 ms (unless otherwise stated), a scaling factor of $q = 1000$, and a time constant (τ_s) of 0.7 ms for EPSP connections and 1.1 ms for IPSP connections (see Fig. 2.2B).

$$\alpha(s, W, \Delta^{\text{ax}}) = Wq\frac{(s - \Delta^{\text{ax}})}{\tau_s^2} \exp\left(\frac{-(s - \Delta^{\text{ax}})}{\tau_s}\right) \Theta(s - \Delta^{\text{ax}})$$

$$\Theta(x) = \begin{cases} 1 & \text{if} \quad x > 0 \\ 0 & \text{if} \quad x \leq 0 \end{cases}$$

Table 2.2: aEIF parameters for the coincidence detection model chosen from a normal distribution with parameters (μ,σ) and when not shown, $\sigma = 0$.

Parameter		SI	ON	ON$_{Delay}$	OFF	DTN
C (pF)	membrane capacitance	(220,5)	(200,2)	(250,10)	(250,5)	260
g_L (nS)	leak conductance	30	30	30	30	30
E_L (mV)	leak reversal potential	(-65,1)	-55	-58	-58	-55
V_T (mV)	spike threshold	(-52,3)	(-52,1)	-50	-55	-48
V_R (mV)	spike reset level	-63	-54	-53	-62	-47
Δ_T (mV)	slope factor	2	2	2	2	2
τ_w (ms)	rise/fall time constant	250	100	10	10	30
a (nS)	sub-threshold adaptation	40	10	(200,2)	(200,2)	4
b (nA)	spike-triggered adaptation	(10,2)	400	500	1000	10

Table 2.3: aEIF parameters for the anti-coincidence model chosen from a normal distribution with parameters (μ,σ) and when not shown, $\sigma = 0$.

Parameter		SI	ON	ON$_{Delay}$	DTN
C (pF)	membrane capacitance	(220,5)	(200,5)	(250,5)	280
g_L (nS)	leak conductance	30	30	30	30
E_L (mV)	leak reversal potential	-65	-53	-52	-55
V_T (mV)	spike threshold	(52,1)	(-50,1)	(-50,1)	-48
V_R (mV)	spike reset level	-63	-54	-49	-46
Δ_T (mV)	slope factor	2	2	2	2
τ_w (ms)	rise/fall time constant	250	100	100	30
a (nS)	sub-threshold adaptation	40	10	10	4
b (nA)	spike-triggered adaptation	(10,2)	400	100	1

Table 2.4: aEIF parameters for the long-pass model chosen from a normal distribution with parameters (μ,σ) and when not shown, $\sigma = 0$.

Parameter		SI$_{AD}$	SE	DTN
C (pF)	membrane capacitance	(220,10)	(280,7)	260
g_L (nS)	leak conductance	30	30	30
E_L (mV)	leak reversal potential	-55	-55	-62
V_T (mV)	spike threshold	(-51,1)	(-50,1)	-52
V_R (mV)	spike reset level	-56	-58	-62
Δ_T (mV)	slope factor	2	2	2
τ_w (ms)	rise/fall time constant	250	250	30
a (nS)	sub-threshold adaptation	40	40	4
b (nA)	spike-triggered adaptation	(300,20)	0	4

2.7   References

Brand A, Urban A, Grothe B (2000) Duration tuning in the mouse auditory midbrain. *J Neurophysiol* 84:1790–1799.

Brette R, Gerstner W (2005) Adaptive exponential integrate-and-fire model as an effective description of neuronal activity. *J Neurophysiol* 94:3637–3642.

Buhusi CV, Meck WH (2005) What makes us tick? Functional and neural mechanisms of interval timing. *Nature Rev Neurosci* 6:755–765.

Buonomano DV, Maass W (2009) State-dependent computations: spatiotemporal processing in cortical networks. *Nature Rev Neurosci* 10:113–125.

Carr CE, Konishi M (1990) A circuit for detection of interaural time differences in the brain stem of the barn owl. *J Neurosci* 10:3227–3246.

Casseday JH, Ehrlich D, Covey E (1994) Neural tuning for sound duration: role of inhibitory mechanisms in the inferior colliculus. *Science* 264:847–850.

Casseday JH, Ehrlich D, Covey E (2000) Neural measurement of sound duration: control by excitatory-inhibitory interactions in the inferior colliculus. *J Neurophysiol* 84:1475–1487.

Church RM (1984) Properties of the internal clock. *Ann NY Acad Sci* 423:566–582.

Covey E, Carr CE (2005) The auditory midbrain in bats and birds In Winer Ja, Schreiner CE, editors, *The Inferior Colliculus*, pp. 493–536. New York: Springer.

Covey E, Casseday JH (1991) The monaural nuclei of the lateral lemniscus in an echolocating bat: parallel pathways for analyzing temporal features of sound. *J Neurosci* 11:3456–3470.

Covey E, Casseday JH (1999) Timing in the auditory system of the bat. *Annu Rev Physiol* 61:457–476.

Covey E, Kauer JA, Casseday JH (1996) Whole-cell patch-clamp recording reveals sub-threshold sound-evoked postsynaptic currents in the inferior colliculus of awake bats. *J Neurosci* 16:3009–3018.

Duysens J, Schaafsma SJ, Orban GA (1996) Cortical off response tuning for stimulus duration. *Vision Res* 36:3243–3251.

Ehrlich D, Casseday JH, Covey E (1997) Neural tuning to sound duration in the inferior colliculus of the big brown bat, *Eptesicus fuscus*. *J Neurophysiol* 77:2360–2372.

Faure PA, Fremouw T, Casseday JH, Covey E (2003) Temporal masking reveals properties of sound-evoked inhibition in duration-tuned neurons of the inferior colliculus. *J Neurosci* 23:3052–3065.

Fremouw T, Faure PA, Casseday JH, Covey E (2005) Duration selectivity of neurons in the inferior colliculus of the big brown bat: tolerance to changes in sound level. *J Neurophysiol* 94:1869–1878.

Fuzessery ZM, Hall JC (1999) Sound duration selectivity in the pallid bat inferior colliculus. *Hear Res* 137:137–154.

Gerstner W, Kistler W (2002) *Spiking Neuron Models: Single Neurons, Populations, Plasticity* Cambridge University Press, Cambridge, UK.

Gooler DM, Feng AS (1992) Temporal coding in the frog auditory midbrain: the influence of duration and rise-fall time on the processing of complex amplitude-modulated stimuli. *J Neurophysiol* 67:1–22.

Grothe B (1994) Interaction of excitation and inhibition in processing of pure tone and amplitude-modulated stimuli in the medial superior olive of the mustached bat. *J Neurophysiol* 71:706–721.

Guinan J, Guinan S, Norris B (1972) Single auditory units in the superior olivary complex: I: responses to sounds and classifications based on physiological properties. *Int J Neurosci* 4:101–120.

He J, Hashikawa T, Ojima H, Kinouchi Y (1997) Temporal integration and duration tuning in the dorsal zone of cat auditory cortex. *J Neurosci* 17:2615–2625.

Heil P (1997) Auditory cortical onset responses revisited. I. first-spike timing. *J Neurophysiol* 77:2616–2641.

Heil P (2004) First-spike latency of auditory neurons revisited. *Curr Opin Neurobiol* 14:461–467.

Hooper SL, Buchman E, Hobbs KH (2002) A computational role for slow conductances: single-neuron models that measure duration. *Nat Neurosci* 5:552–556.

Jen PHS, Zhou XM (1999) Temporally patterned pulse trains affect duration tuning characteristics of bat inferior collicular neurons. *J Comp Physiol A* 185:471–478.

Kadner A, Kulesza RJ, Berrebi AS (2006) Neurons in the medial nucleus of the trapezoid body and superior paraolivary nucleus of the rat may play a role in sound duration coding. *J Neurophysiol* 95:1499–1508.

Kiang NYS (1965) *Discharge patterns of single fibers in the cat's auditory nerve* MIT Press, Cambridge, MA.

Kitzes LM, Gibson MM, Rose JE, Hind JE (1978) Initial discharge latency and threshold considerations for some neurons in cochlear nuclear complex of the cat. *J Neurophysiol* 41:1165–1182.

Klug A, Bauer EE, Pollak GD (1999) Multiple components of ipsilaterally evoked inhibition in the inferior colliculus. *J Neurophysiol* 82:593–610.

Koch U, Grothe B (2003) Hyperpolarization-activated current (I_h) in the inferior colliculus: distribution and contribution to temporal processing. *J Neurophysiol* 90:3679–3687.

Kuwada S, Batra R (1999) Coding of sound envelopes by inhibitory rebound in neurons of the superior olivary complex in the unanesthetized rabbit. *J Neurosci* 19:2273–2287.

Leary CJ, Edwards CJ, Rose GJ (2008) Midbrain auditory neurons integrate excitation and inhibition to generate duration selectivity: an *in vivo* whole-cell patch study in anurans. *J Neurosci* 28:5481–5493.

Meck WH (2006) Neuroanatomical localization of an internal clock: a functional link between mesolimbic, nigrostriatal, and mesocortical dopaminergic systems. *Brain Res* 1109:93–107.

Mora EC, Kössl M (2004) Ambiguities in sound duration selectivity by neurons in the inferior colliculus of the bat *Molossus molossus* from Cuba. *J Neurophysiol* 91:2215–2226.

Narins PM, Capranica RR (1980) Neural adaptations for processing the two-note call of the Puerto Rican treefrog, *Eleutherodactylus coqui*. *Brain Behav Evol* 17:48–66.

Pérez-González D, Malmierca MS, Moore JM, Hern a ndez O, Covey E (2006) Duration selective neurons in the inferior colliculus of the rat: topographic distribution and relation of duration sensitivity to other response properties. *J Neurophysiol* 95:823–836.

Peruzzi D, Sivaramakrishnan S, Oliver DL (2000) Identification of cell types in brain slices of the inferior colliculus. *Neuroscience* 101:403–416.

Potter HD (1965) Patterns of acoustically evoked discharges of neurons in the mesencephalon of the bullfrog. *J Neurophysiol* 28:1155–1184.

Rhode WS, Greenberg S (1992) Physiology of the cochlear nuclei In N PA, Fay RR, editors, *The mammalian auditory pathway: neurophysiology*, pp. 94–152. Springer-Verlag, New York.

Roberts S (1981) Isolation of an internal clock. *J Exp Psychol [Anim Behav]* 7:242–268.

Schofield BR (2005) Superior olivary complex and lateral lemniscal connections of the auditory midbrain In Winer Ja, Schreiner CE, editors, *The Inferior Colliculus*, pp. 132–154. Springer New York.

Singh S, Mountain DC (1997) A model for duration coding in the inferior colliculus In *Proceedings of the annual conference on Computational neuroscience: Trends in research*, pp. 497–503. New York: Plenum.

Sun H, Wu SH (2008) Physiological characteristics of postinhibitory rebound depolarization in neurons of the rat's dorsal cortex of the inferior colliculus studied *in vitro*. *Brain Res* 1226:70–81.

Tan ML, Borst JGG (2007) Comparison of responses of neurons in the mouse inferior colliculus to current injections, tones of different durations, and sinusoidal amplitude-modulated tones. *J Neurophysiol* 98:454–466.

Tan ML, Theeuwes HP, Feenstra L, Borst JGG (2007) Membrane properties and firing patterns of inferior colliculus neurons: an *in vivo* patch-clamp study in rodents. *J Neurophysiol* 98:443–453.

Vater M (1982) Single unit responses in cochlear nucleus of horseshoe bats to sinusoidal frequency and amplitude modulated signals. *J Comp Physiol* 149:369–388.

Wang J, van Wijhe R, Chen Z, Yin S (2006) Is duration tuning a transient process in the inferior colliculus of guinea pigs? *Brain Res* 1114:63–74.

Wang X, Galazyuk AV, Feng AS (2007) FM signals produce robust paradoxical latency shifts in the bat's inferior colliculus. *J Comp Physiol A* 193:13–20.

Xia YF, Qi ZH, Shen JX (2000) Neural representation of sound duration in the inferior colliculus of the mouse. *Acta Otolaryngol* 120:638–643.

Xie R, Gittelman JX, Li N, Pollak GD (2008) Whole cell recordings of intrinsic properties and sound-evoked responses from the inferior colliculus. *Neuroscience* 154:245–256.

Zhou X, Jen PH (2001) The effect of sound intensity on duration-tuning characteristics of bat inferior collicular neurons. *J Comp Physiol A* 187:63–73.

Duration Tuning Across Vertebrates

3

Preamble

This chapter previously appeared in the Journal of Neuroscience in 2012 and is reproduced with permission.

Aubie B, Sayegh R, Faure PA (2012) Duration tuning across vertebrates. *J Neurosci* 32:6373–6390.

The model source code is available from ModelDB:

http://senselab.med.yale.edu/modeldb/ShowModel.asp?model=144511

3.1 Abstract

Signal duration is important for identifying sound sources and determining signal meaning. Duration-tuned neurons (DTNs) respond preferentially to a range of stimulus durations and maximally to a best duration (BD). Duration-tuned neurons are found in the auditory midbrain of many vertebrates, though studied most extensively in bats. Studies of DTNs across vertebrates have identified cells with BDs and temporal response bandwidths that mirror the range of species-specific vocalizations. Neural tuning to stimulus duration appears to be universal among hearing vertebrates. Herein we test the hypothesis that neural mechanisms underlying duration selectivity may be similar across vertebrates. We instantiated theoretical mechanisms of duration tuning in computational models to systematically explore the roles of excitatory and inhibitory receptor strengths, input latencies and membrane time constant on duration tuning response profiles. We demonstrate that models of duration tuning with similar neural circuitry can be tuned with species-specific parameters to reproduce the responses of *in vivo* DTNs from the auditory midbrain. To relate and validate model output to *in vivo* responses, we collected electrophysiological data from the inferior colliculus of the awake big brown bat, *Eptesicus fuscus*, and present similar *in vivo* data from the published literature on DTNs in rats, mice and frogs. Our results support the hypothesis that neural mechanisms of duration tuning may be shared across vertebrates despite species-specific differences in duration selectivity. Finally, we discuss how the underlying mechanisms of duration selectivity relate to other auditory feature detectors arising from the interaction of neural excitation and inhibition.

3.2   Introduction

The wide variation of sounds relevant to different species has led to specialized neural circuits for analyzing and interpreting species-specific acoustic signals. Neural specializations for representing spectral (frequency) and temporal (timing) components of sound are found from the auditory periphery to the auditory cortex. Mammals first determine sound frequencies in the cochlea where mechanical properties of the basilar membrane produce a spatial (tonotopic) map of frequency that is preserved throughout the auditory brainstem, midbrain, thalamus and cortex (Brugge, 1992). Neurons within the central auditory pathway are often specialized for species-specific acoustic processing. For example, New World mustached bats (*Pteronotus parnellii*) emit multi-harmonic echolocation calls composed of a long duration constant frequency tone near 60 kHz followed by a short duration downward frequency modulated (FM) sweep (Pollak and Bodenhamer, 1981). Mustached bats adjust the constant frequency component of their vocalizations to compensate for flight-induced Doppler shifts in received echoes (Jen and Kamada, 1982). Doppler-shift compensation behaviour is facilitated by having an auditory fovea with mechanical and physiological specializations of the cochlea and an over-representation of narrowly tuned neurons in the peripheral (Suga et al., 1975; Kössl and Vater, 1985) and central auditory system (Suga and Jen, 1976; Pollak and Bodenhamer, 1981).

Temporal components of acoustic signals are extracted and represented throughout the central auditory pathway. Signal onset and offset are encoded in the periphery by the onset and offset of cochlear afferent spike trains. Higher order temporal features, such as gap and signal duration, are analyzed by upstream auditory nuclei. In particular, cells tuned to stimulus duration, known as duration-tuned neurons (DTNs), are found first in the auditory midbrain of amphibians (Narins and Capranica, 1980) and mammals (Jen and Schlegel, 1982; Casseday et al., 1994; Chen, 1998; Fuzessery and Hall, 1999; Brand et al., 2000; Pérez-González et al., 2006; Wang et al., 2006). Auditory DTNs exist across vertebrate species and taxa and vary widely in their preferred range of signal durations (see Sayegh et al., 2011, for review). The existence of visual DTNs in the mammalian cortex suggests that neural mechanisms of duration selectivity may be shared across vertebrates and sensory modalities (Duysens et al., 1996).

To address this hypothesis and explore the flexibility of neural mechanisms proposed to produce duration selectivity, we developed computational models of duration-tuned neural

circuits. To validate our models and demonstrate how responses of DTNs in different vertebrates are reproduced by similar synaptic mechanisms tuned with species-specific model parameters, we analyzed *in vivo* electrophysiology data from the central nucleus of the inferior colliculus (ICc) of the big brown bat (*Eptesicus fuscus*) and present similar data from the published literature on rats (Pérez-González et al., 2006), mice (Brand et al., 2000) and frogs (Leary et al., 2008). Our results support the hypothesis that neural tuning for stimulus duration results from a complex interaction of excitation and inhibition, and that the proposed mechanisms are flexible enough to account for duration selectivity across vertebrates. We then discuss how duration tuning fits into a larger class of stimulus evoked auditory responses attributable to complex temporal interactions of neural excitation and inhibition.

3.3 Methods

3.3.1 Computational Modelling

We modelled DTNs with a single-compartment model in NEURON 7.2 (Carnevale and Hines, 2006) via the Python scripting interface (Hines et al., 2009) using simulation time-steps of 0.05 ms. The model cell was a spherical neuron with a diameter of 13 μm that contained glutamate activated AMPA (α-amino-3-hydroxy-5-methyl-4-isoxazole propanoic acid) and NMDA (N-methyl-D-aspartic acid) receptor mediated depolarizing currents and GABA (γ-aminobutryic acid) activated GABA$_A$ receptor mediated hyperpolarizing currents. Receptor kinetics were based on the simplified versions of post-synaptic currents from Destexhe et al. (1998). Briefly, pre-synaptic spikes triggered a 1 ms release of 1 mM neurotransmitter that activated post-synaptic receptor currents with kinetics determined by the equations in Table 3.1. The time of a spike was defined as the time-step in which the membrane potential of the model neuron crossed 0 mV. The rates of neurotransmitter binding (α) and unbinding (β) determined the rise and decay kinetics of each post-synaptic receptor conductance (g_{AMPA}, g_{NMDA}, g_{GABA_A}). Fitted parameter values for α and β were previously determined from whole-cell current recordings (Destexhe et al., 1998). NMDA receptors exhibited a voltage dependent Mg^{2+} block characterized by the function $B(V)$ defined in Table 3.1 (Jahr and Stevens, 1990). The membrane of the model cell also contained passive channels that conduct leak current (I_{leak}), and channels for fast Hodgkin-Huxley type sodium

(Na; I_{Na}) and potassium (K; I_K) currents based on the kinetics described by Traub and Miles (1991) and implemented by Destexhe et al. (1996) (see Table 3.2). Voltage dynamics of the model cell membrane potential ($\frac{dV}{dt}$) were determined by

$$C_m \frac{dV}{dt} = -I_{\text{leak}} - I_{\text{Na}} - I_K - I_{\text{AMPA}} - I_{\text{NMDA}} - I_{\text{GABA}_A},$$

where C_m is the membrane capacitance, I_{leak} is the passive membrane leak current, I_{Na} is the sodium channel current, I_K is the potassium channel current, and I_{AMPA}, I_{NMDA}, I_{GABA_A} are the corresponding receptor mediated currents.

Excitatory Inputs to the Model DTN

Pre-synaptic spikes that activated glutamatergic AMPA and NMDA receptors on the model DTN were generated by two single-compartment neurons: one providing excitation timed relative to stimulus onset (onset-evoked) and the other providing excitation timed relative to stimulus offset (offset-evoked). Neurons with transient, onset-evoked responses are found throughout the central auditory pathway, including the cochlear nucleus (Pfeiffer, 1966; Haplea et al., 1994) and (medial) superior olive (Guinan et al., 1972; Grothe et al., 1997, 2001). Offset responding neurons have also been observed in the (medial) superior olivary complex (Guinan et al., 1972; Grothe et al., 1997, 2001), where dense excitatory projections lead into the ICc (Oliver et al., 1995). GABAergic offset responding neurons in the superior paraolivary complex are not candidates for providing offset-evoked excitatory input to the inferior colliculus (IC) but may still contribute to duration tuning by suppressing excitatory offset responses at some durations (Kadner et al., 2006). Another possible source of offset-evoked excitation comes from within the IC or even a DTN itself via post-inhibitory rebound following sustained inhibition (Casseday et al., 1994). Our model is not dependent on and does not presume a particular anatomical location for these inputs.

Pre-synaptic neurons were modelled with fast spiking kinetics (see Table 3.3) such that a 1 ms, 0.1 nA injected current pulse produced exactly one spike in the neuron. Pre-synaptic neurons activated post-synaptic receptors on the model DTN. In our initial (default) model, the onset-responding pre-synaptic neuron was activated 10 ms after stimulus onset and the offset-responding pre-synaptic neuron was activated 6 ms after stimulus offset (Fig. 3.3*E*). We also explored the effect of input latency on duration tuning by running simulations with a range of onset-evoked excitation latencies (see *Onset-Evoked Excitatory Input Latency*).

66

Table 3.1: Post-synaptic glutamatergic and GABAergic receptor current parameters of the default model DTN. The AMPA and NMDA receptors were modelled with a single synapse per input, whereas the GABA$_A$ receptors had 10 synapses per input. r, proportion of open channels; dt, simulation time-step; [T], neurotransmitter concentration; $[Mg^2+]_o$, Mg^2+ concentration outside of the cell; $E_{\text{AMPA,NMDA,GABA}_A}$ receptor reversal potential; α, receptor activation rate constant; β, receptor deactivation rate constant. Conductance ($\bar{g}$) values are written as the total conductance combined over all inputs of that type. Equation and parameter values for each receptor from Destexhe et al. (1998). The Mg^{2+} block function, $B(V)$, was first derived by Jahr and Stevens (1990).

AMPA Receptors	
I_{AMPA}	$\bar{g}_{\text{AMPA}} r (V - E_{\text{AMPA}})$
$\bar{g}_{\text{AMPA}}$	4 nS
$\frac{dr}{dt}$	$\alpha[T](1-r) - \beta r$
[T]	1.0 mM for 1 ms
E_{AMPA}	0 mV
α	1.1 /ms mM
β	0.19 /ms
NMDA Receptors	
I_{NMDA}	$\bar{g}_{\text{NMDA}} B(V) r (V - E_{\text{NMDA}})$
$\bar{g}_{\text{NMDA}}$	20 nS
Mg^{2+} Block; $B(V)$	$(1 + \exp(-0.062V)[Mg^{2+}]_o/3.57)^{-1}$
$[Mg^{2+}]_o$	1.0 mM
$\frac{dr}{dt}$	$\alpha[T](1-r) - \beta r$
[T]	1.0 mM for 1 ms
E_{NMDA}	0 mV
α	0.072 /ms mM
β	0.0066 /ms
GABA$_A$ Receptors	
I_{GABA_A}	$\bar{g}_{\text{GABA}_A} r (V - E_{\text{GABA}_A})$
$\bar{g}_{\text{GABA}_A}$	2.5 nS
$\frac{dr}{dt}$	$\alpha[T](1-r) - \beta r$
[T]	1.0 mM for 1 ms
E_{GABA_A}	-80 mV
α	5.0 /ms mM
β	0.18 /ms

Inhibitory Inputs to the Model DTN

Previous work has demonstrated that neural inhibition is necessary for creating DTNs in the IC. Blocking receptors of inhibitory neurotransmitters via neuropharmacological agents abolishes or greatly diminishes duration-tuned responses (Jen and Feng, 1999; Fuzessery and Hall, 1999; Casseday et al., 2000; Jen and Wu, 2005; Yin et al., 2008). Intracellular (whole-cell patch clamp) (Covey et al., 1996; Tan and Borst, 2007; Leary et al., 2008) and extracellular (single-unit) recordings (Faure et al., 2003) suggest that inhibitory inputs usually precede excitatory inputs to the DTN and persist for as long or longer than the duration of the stimulus. Potential sources of sustained inhibitory input to the IC are from the nuclei of the lateral lemniscus (Covey and Casseday, 1991; Nayagam et al., 2005) where both GABAergic and glycinergic neurons with sustained spiking exist (Vater et al., 1997). Furthermore, neurons in the columnar division of the ventral nucleus of the lateral lemniscus in the big brown bat produce transient, onset-evoked responses with a glycinergic input to the IC that could account for the presence of a strong, onset-evoked inhibition that mainly affects the early portion of a stimulus-evoked response (Covey and Casseday, 1991; Vater et al., 1997). Neuropharmacologically blocking either GABA$_A$ or glycine receptors produces a similar effect on the responses of *in vivo* DTNs (Casseday et al., 2000). Therefore, we chose to model all inhibitory post-synaptic potentials with GABA$_A$ receptor kinetics to simplify both the model description and analysis (see *Model Limitations and Future Enhancements* for a discussion of additional receptor types).

Inhibitory pre-synaptic inputs to the model DTN were generated by a population of ten single-compartment neurons with fast spiking kinetics (see Table 3.4) that activated GABA$_A$ receptors on the model DTN. Ten neurons were chosen so that the pre-synaptic input would approximate a continuous inhibitory conductance in the model DTN (Fig. 3.1*A*). The current injected to each pre-synaptic neuron was in the form of discrete 1 nA square pulse events. Each event lasted for the duration of a simulation time-step (0.05 ms) and followed a Poisson distribution with a mean probability of 0.05 events per time-step (i.e. on average, each pre-synaptic neuron received 1 nA of current for 0.05 ms per 20 simulation time-steps). This resulted in a mean spiking rate of ca. 250 Hz in each pre-synaptic input neuron. In the default model the inhibitory pre-synaptic inputs had a latency of 9 ms (re stimulus onset) and their input lasted for the duration of the stimulus. This latency corresponds to that of the leading inhibition observed in the big brown bat (approximately 4 to 12 ms; Covey et
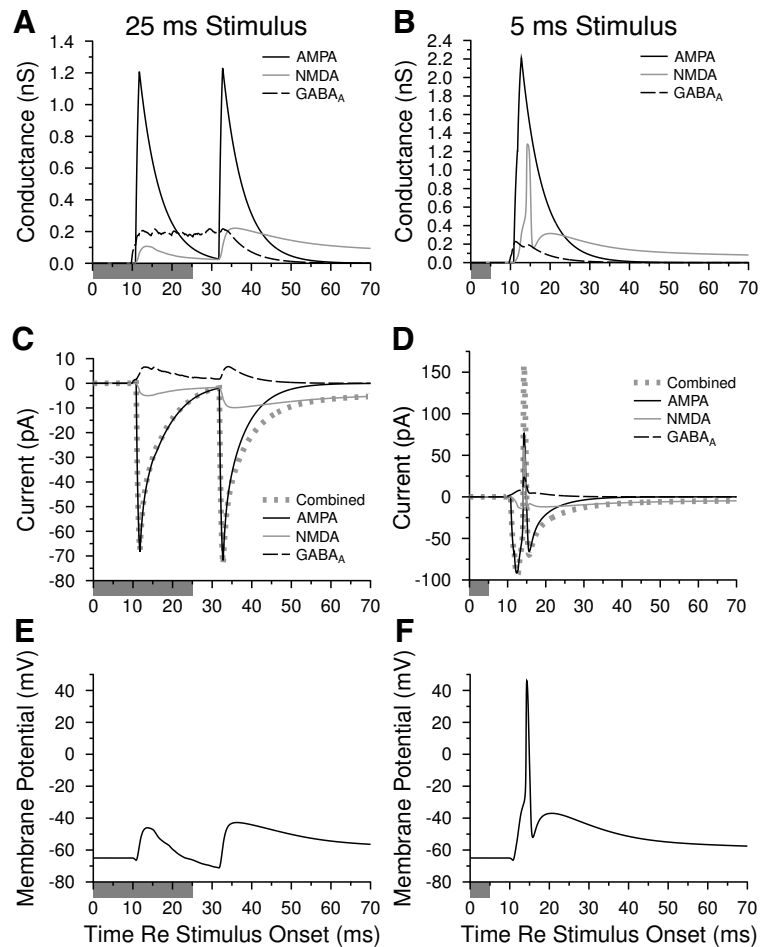
Figure 3.1: Conductances (***A,B***) and current (***C,D***) of AMPA, NMDA and GABA$_A$ receptors and resulting membrane voltage (***E,F***) over time for single stimulus presentations to the default computational model employing the coincidence detection mechanism of duration tuning. Shown are model inputs and responses to a long (25 ms) stimulus that does not evoke spikes (***A,C,E***), and a short (5 ms) stimulus that always evokes a spike (***B,D,F***). Stimulus duration represented by grey bars on time axes.

al., 1996; Faure et al., 2003). Due to the random timing of inhibitory pre-synaptic spikes, the precise time course of the inhibition acting on the DTN varied slightly for each stimulus presentation. Simulations were therefore repeated 20 times and the mean $\pm$ standard error (SE) results are reported. Dynamic model parameters were allowed to settle for 25 ms before stimulus presentation to ensure that each simulation began from a stable network state.

Default Model Response

Figure 3.1 illustrates the simulated receptor conductances, inward currents and membrane potential of the DTN in the default model. For comparison, we show responses of the model DTN for both a long (25 ms) duration stimulus that did not evoke spiking (Fig. 3.1 *left column*) and a short (5 ms) stimulus that reliably evoked one spike per trial (Fig. 3.1 *right column*). The conductance changes over time for the AMPA, NMDA and GABA$_A$ receptors in the default model are shown in Figure 3.1*A,B*. The two peaks observed in the AMPA and NMDA receptor conductances in response to the long duration stimulus correspond to the onset- and offset-evoked excitatory pre-synpatic inputs (see *Excitatory Inputs to the Model DTN*). These peaks are also present in response to the short duration stimulus but are less evident because they temporally overlap, as evidenced by the two-fold increase in AMPA evoked conductance and by the even larger increase in NMDA conductance owing to a significantly reduced Mg^{2+} block ($B(V)$) during the action potential of the DTN. Although the maximum NMDA receptor conductance was greater than the maximum AMPA receptor conductance (see Table 3.5), the realized NMDA conductance, and thus NMDA-mediated current, was substantially smaller due to the Mg^{2+} block. Our maximum conductance values were chosen so that single, pre-synaptic, excitatory spikes evoked sub-threshold depolarizations in the DTN when they were coincident with pre-synaptic inhibition, but they evoked supra-threshold depolarizations when they were temporally coincident with the other excitatory input (see *Coincidence Detection Mechanism*). In the absence of inhibition, the excitatory input spikes were supra-threshold and produced spikes in the DTN (see *Onset-Evoked Excitatory Input Latency*). The maximum conductance parameter values represent approximately 4 - 10 synapses per input (Destexhe et al., 1998) and nicely reproduced the sharp, short-pass duration selectivity observed in the ICc of bats (e.g. Zhou and Jen, 2001; Fremouw et al., 2005). The GABA$_A$ receptor conductance (Table 3.5), and therefore inhibitory current, was noisy due to the random arrival times of the pre-synaptic inhibitory input spikes. Later, we explore the effect of varying AMPA, NMDA and GABA$_A$ receptor conductances on duration selectivity (see *Maximum Receptor Conductance*).

The AMPA, NMDA and GABA$_A$ receptor-mediated currents are shown in Figure 3.1*C,D*. Inward current, responsible for depolarizing the membrane potential, is shown as negative (downward) values and outward current, responsible for hyperpolarizing the membrane potential of the DTN, is shown as positive (upward) values. Because the NMDA receptor

conductance decays slowly, the second (offset-evoked) excitatory input results in a facilitated conductance, and thus a larger receptor-mediated current, compared to the first (onset-evoked) excitatory input. When both excitatory inputs overlapped, the summated current produced an action potential ca. 15 ms from stimulus onset (Fig. 3.1*D*). Notice also that the AMPA and NMDA currents reversed direction during the action potential (Fig. 3.1*D* at 14 ms) when the membrane potential of the model DTN rose above the 0 mV reversal potential of the AMPA and NMDA receptors (Fig. 3.1*F* at 14 ms).

Receptor currents are a complex function of channel activation kinetics, receptor activation kinetics and passive model parameters. We measured the ratio of peak NMDA current to peak AMPA current in the default model for a single excitatory input spike to be 0.0732 (NMDA : AMPA; 5.00 pA : 68.28 pA). Ma et al. (2002b) found that late (NMDA) and early (AMPA) currents in the rat IC had an average ratio of 0.58 (late : early) with a range of approximately 0.08 to 1.8. We predict that the NMDA to AMPA current ratio could be lower in bats, and thus more similar to our default model, due to the requirement for faster temporal processing. The resulting membrane potentials of the model DTN in response to both long and short duration stimuli are shown in Figure 3.1*E,F*. When the excitatory inputs failed to overlap, the membrane potential depolarized slightly but remained sub-threshold (Fig. 3.1*E*). When the excitatory inputs coincided, an action potential was produced (Fig. 3.1*F*).

3.3.2 Electrophysiology

Surgical Procedures

Electrophysiological recordings were obtained from the ICc of 21 awake big brown bats (*Eptesicus fuscus*) of either sex. Prior to recording, a stainless steel post was affixed to the skull with cyanoacrylate superglue (Henkel Loctite Corporation) to ensure a fixed head position could be precisely replicated between sessions. Prior to the head-posting surgery, bats were given a subcutaneous injection of buprenorphine (0.03 mL; 0.045 mg/kg). Bats were then placed in a small (9.7 cm $\times$ 11.6 cm $\times$ 9.6 cm; l $\times$ w $\times$ h) anesthesia induction chamber where they inhaled a 1 to 5% isoflurane:oxygen mixture (1 L/min). Anesthetized bats were then placed in a foam-lined body restraint within a surgical stereotaxic alignment system with a custom mask for continuous gas inhalation (David Kopf Instruments Model 1900). The hair covering the skull was shaved and the skin was disinfected with Betadine.

Local anesthetic (0.2 mL bupivicaine; 5 mg/mL) was injected subcutaneously prior to making a midline incision in the scalp. The temporal muscles were reflected to reveal the dorsal surface of the skull which was then scraped clean and swabbed with 70% ethanol. After drying, the post was glued to the skull over the cortex using superglue hardened with liquid cyanoacrylate accelerator (Pacer Zip Kicker®). A chlorided silver wire attached to the headpost was positioned under the right temporal muscle and served as the reference electrode.

Electrophysiological Recordings

Recordings began 1 to 3 days after surgery and continued for 1 to 6 sessions on separate days. Each session lasted 4 to 6 hours and was terminated if the bat showed signs of discomfort. Prior to recording, bats were subcutaneously administered a neuroleptic (0.3 mL; 1:1 mixture of 0.05 mg/mL fentanyl citrate and 2.5 mg/mL droperidol; 19.1 mg/kg). Bats were then placed in a foam-lined body restraint that was suspended by springs within a small animal stereotaxic frame customized for bats (ASI Instruments). The entire apparatus was mounted atop an air vibration table (TMC Migro-g). The bat's head was immobilized by securing the headpost to a stainless steel rod attached to a micromanipulator (ASI Instruments) mounted on the stereotaxic frame. A scalpel was used to cut a small hole in the skull and dura matter over the dorsal surface of the IC. Single-unit extracellular recordings were made with thin-wall borosilicate glass microelectrodes with a capillary filament (o.d. = 1.2 mm; A-M Systems, Inc.) filled with 3M NaCl. Electrodes were made with a Flaming/Brown style micropipette puller (Model P-97; Sutter Instrument Co.). Typical electrode resistances ranged from 15 to 30 MΩ. Electrodes were visually positioned over the dorsal surface of the IC with manual manipulators (ASI Instruments) and advanced into the brain at 1 μm intervals with a stepping hydraulic micropositioner (Kopf Model 2650). Action potentials were recorded with a neuroprobe amplifier (A-M Systems Model 1600) whose 10x output was bandpass filtered and further amplified (500 to 1000x) by a Tucker Davis Technologies spike pre-conditioner (TDT PC1; low-pass $f_c = 7$ kHz; high-pass $f_c = 300$ Hz). Spike times were logged to a computer by passing the PC1 output to a spike discriminator (TDT SD1) and an event timer (TDT ET1) synchronized to a timing generator (TDT TG6). Between recording sessions the skull was covered with a piece of contact lens and Gelfoam coated in Polysporin. Bats were individually housed in a temperature- and humidity-controlled room.

All procedures were approved by the McMaster University Animal Research Ethics Board and were in accordance with the Canadian Council on Animal Care.

Stimulus Generation and Data Collection

Stimulus generation and online data collection were controlled with custom software that displayed spike-times as dot rasters ordered by the acoustic parameter that was varied during stimulus presentation (see Faure et al., 2003; Fremouw et al., 2005). Briefly, sound pulses were digitally generated with a two-channel array processor (TDT Apos II; 357 kHz sampling rate) optically interfaced to two digital-to-analog (D/A) converters (TDT DA3-2) whose individual outputs were fed to a low-pass anti-aliasing filter (TDT FT6-2; $f_c = 120$ kHz), two programmable attenuators (TDT PA5) and two signal mixers (TDT SM5) with equal weighting. The output of each mixer was fed to a manual attenuator (Leader LAT-45) before final amplification (Krohn-Hite Model 7500). Stimuli were presented monaurally to the ear contralateral to the IC being recorded using a Bruel & Kjær 1/4 inch condenser microphone (Type 4939; protective grid on) modified for use as a loudspeaker by a transmitting adaptor (B&K Type UA-9020) to correct for nonlinearities in the transfer function (Frederiksen, 1977). The loudspeaker was positioned ca. 1 mm in front of the external auditory meatus. The output of the speaker, recorded with a B&K Type 4138 1/8 inch condenser microphone (90º incidence; grid off) connected to a measuring amplifier (B&K Type 2606) and bandpass filter (K-H Model 3500), was measured relative to a sound calibrator (B&K Type 4231) and expressed in decibels sound pressure level (dB SPL re 20 μPa) equivalent to the peak amplitude of continuous tones of the same frequency (Stapells et al., 1982). The loudspeaker transfer function was flat ±6 dB from 28 to 119 kHz, and there was at least 30 dB attenuation at the ear opposite the source (Ehrlich et al., 1997). All stimuli had rise/fall times of 0.4 - 0.5 ms shaped with a square cosine function and were presented at a rate of 3 Hz.

Single units were found by searching with a paired stimulus consisting of a short duration (3-4 ms) and long duration (20-25 ms) pure tone of the same frequency separated by 110 ms. Upon isolation, a neuron's best excitatory frequency (BEF), duration selectivity profile, and acoustic threshold were determined by presenting 10-20 repetitions of pure tone stimuli randomly varied in frequency, duration, or amplitude, respectively. First, we defined BEF as the frequency (1 kHz resolution) that evoked the maximum spike count in the cell using a stimulus duration and amplitude that resulted in robust spiking. Next, the duration selectivity

profile of the cell was measured by presenting a series of BEF tones (at the same amplitude as BEF testing) randomly varied in duration from 1 to 25 ms (1 ms resolution). Best duration (BD) was defined as the stimulus duration that evoked the maximum spike count in the cell (Casseday et al., 1994). Finally, acoustic threshold was determined by presenting a series of BEF, BD pulses that were randomly varied in amplitude (10 dB resolution) over a 70 dB range of attenuation.

3.4   Results

3.4.1   Characterizing Duration-Tuned Neurons

Duration-tuned neurons can be classified into one of three response classes based on the temporal tuning profile of the cell when stimulated with variable duration pure tones at BEF. (1) Shortpass DTNs respond maximally to short duration stimuli and eventually have a ≥50% reduction in spike count at durations longer than BD. (2) Bandpass DTNs respond maximally at BD and eventually have a ≥50% reduction in spike count at durations both shorter and longer than BD. (3) Longpass DTNs differ from shortpass and bandpass DTNs by not having a BD; they respond only when the stimulus exceeds a minimum duration. Moreover, unlike typical sensory neurons that integrate stimulus energy, the minimum duration for evoking a response in a longpass DTN does not decrease with increasing stimulus amplitude/energy (Faure et al., 2003; Sayegh et al., 2011). Some longpass DTNs respond with fewer spikes at a longer first-spike latency (FSL) to increasing stimulus amplitude/energy (e.g. Faure et al., 2003), a phenomenon characterized as "paradoxical" latency shift (Covey et al., 1996; Galazyuk and Feng, 2001; Hechavarría et al., 2011). It is paradoxical because most sensory neurons produce more spikes and shorter FSLs with increasing stimulus amplitude/energy (e.g. Kiang, 1965). To summarize, the responses of DTNs are temporally selective and do not reflect the simple integration of stimulus energy.

3.4.2   Conceptual Mechanisms of Duration Tuning

Various neural mechanisms have been proposed to explain the responses of DTNs. Some are circuit based models that rely on the temporal interaction and integration of excitatory and inhibitory synaptic inputs at the DTN (Casseday et al., 1994, 2000; Fuzessery and Hall, 1999;

74

Aubie et al., 2009). Another proposes that slowly changing ionic conductances, induced solely by sustained hyperpolarization (i.e. sustained inhibition), result in duration-dependent currents and duration selective responses (Hooper et al., 2002). The slow conductance mechanism, while biologically possible, lacks empirical support because DTNs in the auditory midbrain continue to fire action potentials even when inhibition is neuropharmacologically blocked (see below). Here we investigate how variations of two circuit based mechanisms, employing both excitatory and inhibitory synaptic inputs, can reproduce the shortpass and bandpass responses observed from *in vivo* recordings in the auditory midbrain of the bat, rat, mouse and frog.

Coincidence Detection Mechanism

The coincidence detection mechanism of duration tuning was first suggested by Potter (1965) who hypothesized that neurons tuned for stimulus duration in the frog's torus semicircularis would spike only after the summation of excitations evoked by the onset and offset of a stimulus. This mechanism was further described by Narins and Capranica (1980) who postulated that an onset-evoked excitation would temporally coincide with an offset-evoked excitation and produce spikes in a DTN when the onset-evoked excitation had a delay (latency) equal to the preferred stimulus duration. This model was later augmented to include inhibitory inputs when it was shown that blocking inhibition at the DTN severely reduced (or abolished) the cell's temporal selectivity (Casseday et al., 1994; Jen and Feng, 1999; Casseday et al., 2000; Jen and Wu, 2005; Yin et al., 2008). Therefore, the coincidence detection mechanism requires three inputs to the DTN: (1) onset-evoked excitation; (2) offset-evoked excitation; and (3) onset-evoked inhibition that is sustained for as long or longer than the duration of the stimulus. In the presence of inhibition, neither the onset-evoked nor offset-evoked excitations are supra-threshold on their own and cannot evoke spiking in the DTN; however, when the onset- and offset-evoked excitations temporally coincide, or their effects sufficiently overlap, the summed excitation can overcome inhibition and evoke spiking in the DTN (Fig. 3.2*A,B*). Because the arrival time (latency) of the offset-evoked excitation varies with stimulus duration, the response of the DTN will be selective to specific durations. A symmetrical window of coincidence will naturally result in a bandpass duration-tuned response (Fig. 3.2*A,B*); however, the coincidence detection mechanism can also produce shortpass duration-tuned responses when the excitatory inputs

maximally coincide at the shortest stimulus durations (Aubie et al., 2009).

Anti-Coincidence Mechanism

Fuzessery and Hall (1999) noticed that many shortpass DTNs in the IC of the pallid bat had responses locked to stimulus onset rather than stimulus offset, suggesting these neurons lacked an offset-evoked excitatory input. They proposed an alternative mechanism that had only one onset-evoked excitatory input and predicted that a DTN would respond when excitation and inhibition failed to coincide. This anti-coincidence mechanism of duration tuning requires two inputs to the DTN: (1) onset-evoked excitation; and (2) onset-evoked inhibition that is sustained for as long or longer than the duration of the stimulus (Fuzessery and Hall, 1999). In the absence of inhibition, the onset-evoked excitation is supra-threshold and can evoke spikes in the DTN. When the onset-evoked excitation has a latency longer than the offset (end) of the inhibition, as may occur at short stimulus durations, it can evoke spiking in the DTN. At longer stimulus durations the sustained inhibition will eventually overlap the onset-evoked excitation and spiking will be extinguished (Fig. 3.2*C,D*). Therefore, the anti-coincidence mechanism naturally results in shortpass duration-tuned responses; however, modified anti-coincidence mechanisms can also produce bandpass duration tuning when the excitatory input is weak or absent at the shortest stimulus durations (Aubie et al., 2009).

3.4.3   Default Model

Response Profile

Our default computational model produced a shortpass DTN with a BD of 1 ms. Figure 3.3*A* illustrates the membrane potential of the DTN in the default model for single stimulus presentations from 1 to 9 ms in duration relative to the timing of spikes arriving at the DTN from the onset- and offset-responding excitatory input neurons. Panel *B* is a dot raster display of the default model over 20 trials, with the mean spike count and FSL (re stimulus onset) over all trials summarized in panels *C* and *D*, respectively. A network diagram of the default model inputs and their synaptic latencies is shown in Panel *E*. In this simulation, one or two spikes were evoked in the DTN for stimuli ≤4 ms, one or no spikes were evoked for stimuli between 5 and 8 ms, and no spikes were evoked at durations >8 ms (Fig. 3.3*A*-
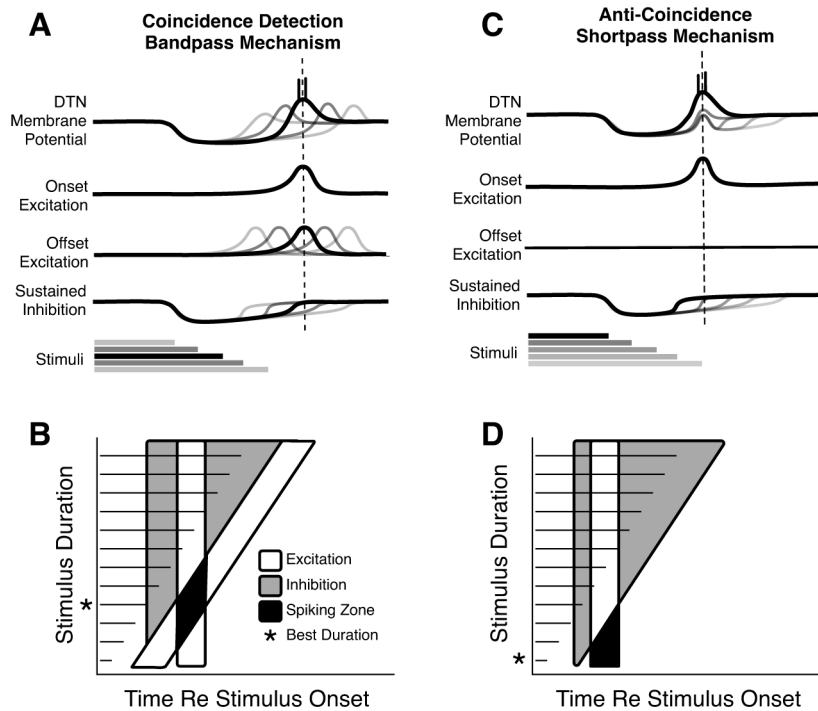
Figure 3.2: Two representations of the coincidence detection and anti-coincidence mecha-nisms of duration tuning. *A,C*, The top trace represents the membrane potential of the model DTN in response to a BD stimulus (*bold trace*) and to stimuli not at BD (*shades of grey*, with lighter greys corresponding to responses evoked by stimuli further from BD). The lower three traces represent the magnitude and timing of synaptic inputs to the DTN at BD (*bold*) and not at BD (*shades of grey*). Inputs are: an onset-evoked transient excitation (*second trace*), an offset-evoked transient excitation (*third trace*) and an onset-evoked sustained inhibition (*fourth trace*) that grows with stimulus duration. Stimulus duration represented by horizontal bars below traces. *Black bars* represent the BD stimulus; *grey bars* represent stim-uli not at BD, with lighter greys corresponding to stimuli further from BD. Excitatory input latencies in the coincidence detection mechanism were set so that the maximum temporal coincidence (*vertical dashed line*) occurred at an intermediate stimulus duration resulting in a bandpass DTN. For the anti-coincidence mechanism, the *vertical dashed line* is the first point when there is no temporal coincidence between the excitatory and inhibitory inputs. *B,D*, Schematic dot raster displays illustrating how temporal interaction of excitatory and inhibitory inputs result in offset spiking responses in the bandpass and shortpass DTNs. The latency and time course of excitatory (*white*) and inhibitory (*grey*) inputs, and the zone of high spiking probability by the DTN (*black*), are illustrated for a range of stimulus durations. Maximum spiking (*) occurs to the BD stimulus. Stimulus durations shown as *horizontal black lines*. Axes intentionally unlabelled to highlight the timescale invariance of the models.

77

C). For stimulus durations ≤4 ms, the spike from the onset-responding excitatory input neuron arrived at the model DTN prior to (1-3 ms) or exactly coincident with (4 ms) the spike from the offset-responding excitatory input neuron, whereas for stimulus durations ≥5 ms the spike from the offset-responding input neuron arrived after the spike from the onset-responding input neuron. The timing of excitatory inputs to the DTN is also evident in the dot raster display (Fig. 3.3*B*). The FSL of the model DTN increased more quickly at stimulus durations ≥5 ms because spikes followed the latency of the offset-evoked excitatory input (Fig. 3.3*D*).

Because the two excitatory inputs were maximally coincident in response to the 4 ms stimulus, the coincidence detection mechanism of duration tuning would predict the default model DTN to have a BD of 4 ms; however, the observed BD was 1 ms. The discrepancy between the predicted and observed BD was caused by the presence and time course of the sustained inhibition. The effect of inhibition is particularly evident when we compare responses evoked by the 1 ms and 7 ms stimuli (Fig. 3.3*A*). At 1 and 7 ms, the difference in spike timing between the onset- and offset-evoked excitatory inputs was identical (3 ms), as were the magnitudes of the summed excitations even though the order of the inputs was reversed. The reason why the model DTN did not produce an equivalent response at 1 ms and 7 ms is because of the difference in duration of the sustained inhibition. For the 1 ms stimulus, the sustained inhibition lasted for 1 ms and was easily overcome by the excitations even though they were not perfectly coincident, and this resulted in an effective excitation that typically evoked 2 spikes per stimulus (19 of 20 trials; Fig. 3.3*B,C*). For the 7 ms stimulus, the sustained inhibition lasted for 7 ms and decreased the effective strength of the summed excitations, resulting in one spike (16 of 20 trials) or no spikes per stimulus (4 of 20 trials; Fig. 3.3*B,C*). The interaction of inhibition with excitation caused the peak net excitation in the model, and thus the cell's BD, to occur in response to 1 ms stimuli even though excitatory inputs to the DTN were maximally coincident for 4 ms stimuli.

First-Spike Latency

First-spike latencies in the default model of duration tuning followed stimulus offset but exhibited a non-linear relationship with stimulus duration (Fig. 3.3*D*). At short durations (1-4 ms), the increase in FSL was smaller than the increase in stimulus duration. At intermediate durations (4-6 ms), FSL increased in proportion to stimulus duration, and at
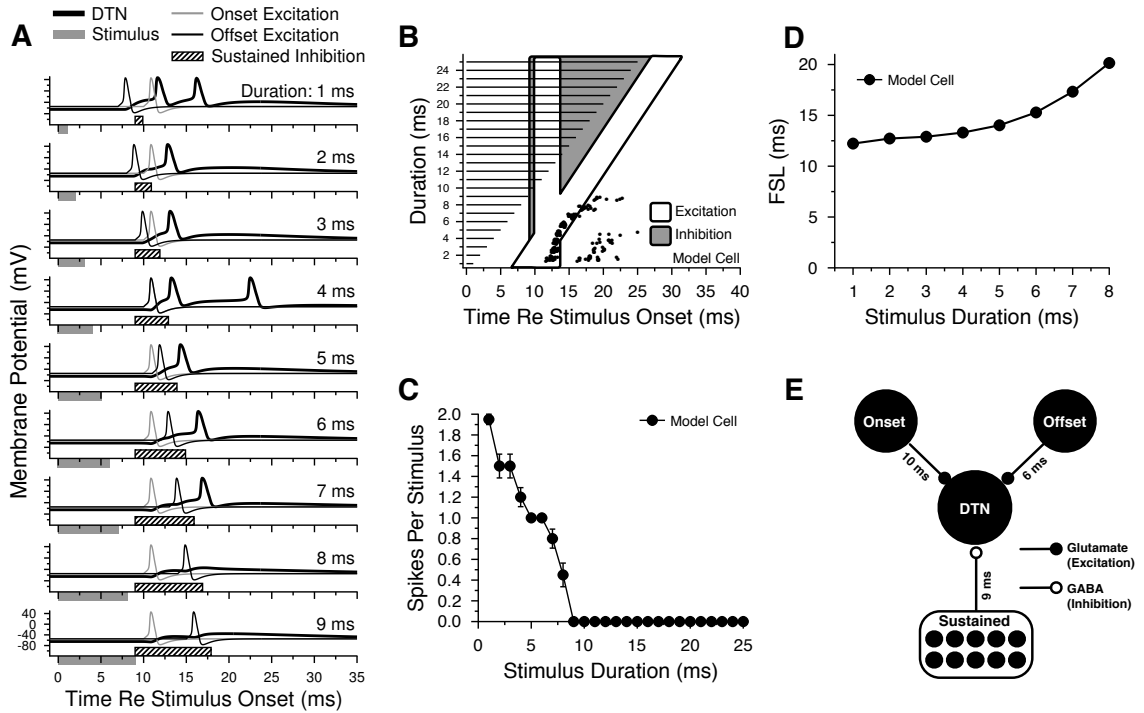
Figure 3.3: Response properties of the default model of the coincidence detection mechanism of duration tuning. *A*, Membrane potential as a function of time (re stimulus onset) of the onset-responding (*grey line*) and offset-responding *black line* pre-synaptic input neurons, and of the model shortpass DTN (*bold line*) for a single stimulus presentation at 9 different pulse durations. For clarity, the time course of spikes from the population of 10 inhibitory input neurons is represented as hatched lines above time axes. Stimuli represented by grey bars below time axes. *B*, Dot raster display of the spiking responses (*black dots*) of the shortpass model DTN over 20 repeated trials for stimuli varied in duration from 1 to 25 ms. Timing of the excitatory (*white*) and inhibitory (*grey*) inputs to the model DTN are overlaid. Stimuli represented by *black lines* on the y-axis. *C*, Duration tuning profile showing mean ± standard error (SE) spikes per stimulus as a function of stimulus duration. The default shortpass model DTN has a BD of 1 ms. *D*, Mean ± SE FSL of default model cell. *E*, Neural circuit diagram of default model. Inputs to the DTN shown with excitatory (*filled circles*) or inhibitory (*open circle*) connections, with synaptic latencies beside each connection.

longer durations ($>$6 ms) the increase in FSL was greater than the increase in stimulus duration. For comparison, a dot raster display of a shortpass DTN from the ICc of the bat exhibiting a similar non-linear increase in FSL is shown in Figure 3.4*A*. In the *in vivo* neuron, FSL was relatively stable at short stimulus durations (1-3 ms) but then increased and followed stimulus offset at longer durations. A non-linear shift in FSL was previously reported by Fuzessery and Hall (1999) and Faure et al. (2003) who hypothesized that the offset-evoked excitatory input to a DTN had a minimum response latency that did not change for stimulus durations below some minimum duration, but that increased and thus mirrored the concomitant lengthening of the stimulus offset at longer durations.

We compared FSL changes in our model with those observed from *in vivo* recordings of DTNs from the ICc of the bat (Fig. 3.4*B*). To simplify the comparison, we shifted absolute FSLs (re stimulus onset) in both *in vivo* and model responses so that the shortest (i.e. minimum duration) stimulus to evoke a response had a FSL that fell on the line $y = x - 1$. Latencies were shifted according to the equation

$$\text{FSL}_{\text{shifted}} = \text{FSL}_{\text{absolute}} - \text{FSL}_{\text{mindur}} + \text{mindur} - 1,$$

where $\text{FSL}_{\text{shifted}}$ was the resulting shifted FSL, $\text{FSL}_{\text{absolute}}$ was the observed FSL, $\text{FSL}_{\text{mindur}}$ was the observed FSL at the shortest duration to evoked spiking, and *mindur* was the minimum duration stimulus that evoked spiking. The slope of the shifted FSL function was defined as the change in FSL divided by the change in duration. In our default model DTN with a standard GABA$_\text{A}$ inhibitory conductance of 2.5 nS, the slope of the shifted FSL function was $<$1 at the shortest stimulus durations (1-5 ms) but then increased and eventually became $>$1 at longer stimulus durations (3.4*B*, *black circles*). A similar change in FSL was observed in approximately half of the *in vivo* cells recorded from the bat, with examples shown in Figure 3.4*B*.

To quantify the change in FSL observed in the *in vivo* recordings from the ICc of the bat, we computed separate linear regressions for the mean FSL data evoked at both short (1-3 ms) and longer stimulus durations ($\geq$3 ms), and plotted the distribution of the slopes for the two separate stimulus ranges at each level above threshold (Fig. 3.5). A slope of 0 indicates no change in FSL with increasing stimulus duration and corresponds to a cell with an onset response and constant FSL re stimulus onset. A slope of 1 indicates an increase in FSL equal to the increase in stimulus duration and corresponds to an offset response with a constant FSL re stimulus offset. A slope of $>$1 indicates that FSL increases more quickly
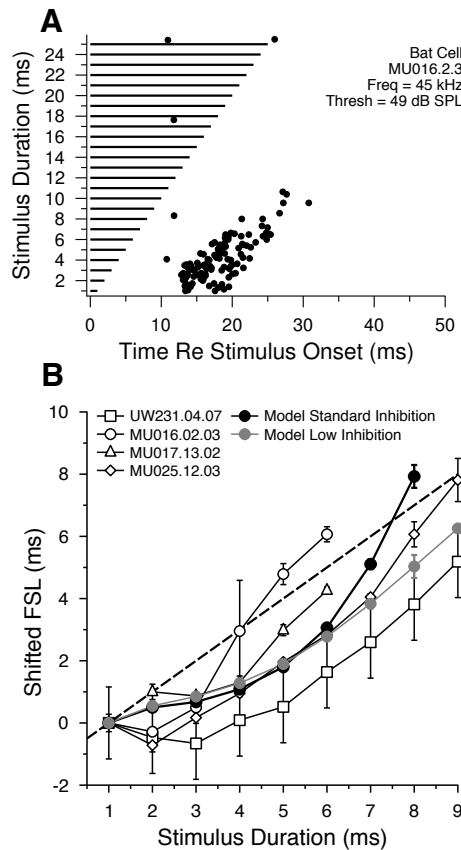
Figure 3.4: Non-linear change in first-spike latency. **A**, Dot raster display of an *in vivo* shortpass DTN from the ICc of a big brown bat showing a non-linear increase in FSL with increasing stimulus duration. The FSL remains stable at short stimulus durations (1-3 ms) but increases to follow stimulus offset at longer durations. **B**, Change in FSL in four *in vivo* DTNs from the ICc of the bat compared with FSLs generated by two versions of the coincidence detection model of duration tuning: the default model with standard and with decreased inhibition. Mean FSLs at each duration were shifted by $FSL_{shifted} = FSL_{absolute} - FSL_{mindur} + mindur - 1$ so that the shortest stimulus duration that a cell responds to is on the line $y = x - 1$, *dotted line*. First-spike latency changes in a non-linear manner in both *in vivo* and model responses. *Black filled circles* show responses of the default model using standard inhibition ($\bar{g}_{GABA_A} = 2.5$ nS), whereas *grey filled circles* are responses of the model using decreased inhibition ($\bar{g}_{GABA_A} = 1.5$ nS). UW231.04.7: BEF = 41 kHz, Threshold = 74 dB SPL, Amp = +20 dB (re threshold), 15 trials per stimulus, unpublished recording from dataset in Faure et al. (2003), Figure 6*A*; MU016.02.3: BEF = 45 kHz, Threshold = 49 dB SPL, Amp = +0 dB, 10 trials per stimulus; MU017.13.2: BEF = 39 kHz, Threshold = 59 dB SPL, Amp = +10 dB, 10 trials per stimulus; MU025.12.3: BEF = 49 kHz, Threshold = 48 dB SPL, Amp = +10 dB, 15 trials per stimulus
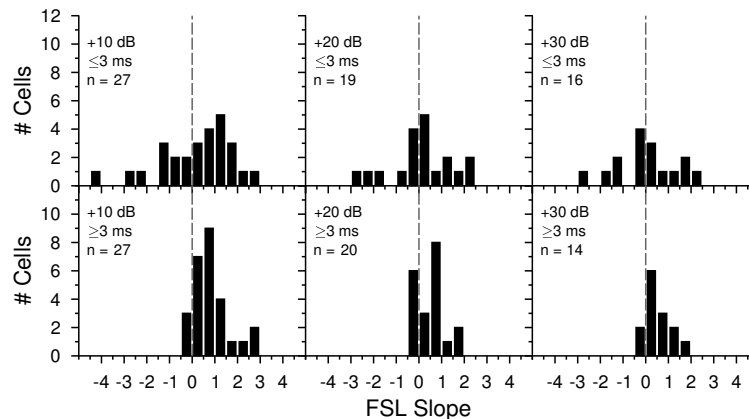
Figure 3.5: Distribution of FSL slope at short and long durations for *in vivo* DTNs from the ICc of the bat. Histograms are shown for 38 DTNs (15 shortpass and 23 bandpass) tested at +10 dB (*left column*), +20 dB (*middle column*) and/or +30 dB (*right column*) re threshold. To capture the non-linear change in FSL observed from *in vivo* recordings, we calculated separate FSL slopes for responses evoked at short (1-3 ms; *top row*) and longer stimulus durations (≥3 ms; *bottom row*). Slopes were calculated by a performing linear regression on the mean FSL data within each duration range. Responses were included only if spikes were evoked with a probability ≥ 0.25 (i.e. if the cell responded with ≥1 spike on 25% of trials). If a neuron responded only to short (1-3 ms) or only to long (≥3 ms) duration signals, its calculated slope was included in only one of the two distributions. The number of neurons appearing in both distributions at each level above threshold was: +10 dB, n = 22; +20 dB, n = 16; and +30 dB, n = 12.

than the increase in stimulus duration and also corresponds to an offset response. Finally, a slope of <0 corresponds to a decrease in FSL with an increase in stimulus duration and corresponds to a cell with paradoxical latency shift (e.g. see Covey et al., 1996; Galazyuk and Feng, 2001; Hechavarría et al., 2011). We also tested for the equality of variances and means between the distributions at each level above threshold using Levene's test and a t-test, respectively.

At +10 dB re threshold, 10 of 27 cells had negative FSL slope functions for responses evoked by short (1 to 3 ms) stimuli, and 24 of 27 cells had positive FSL slope functions for responses evoked by longer (≥3 ms) stimuli (Fig. 3.5, *left column*). Moreover, the two distributions differed significantly in both their means ($t = -2.0776$; $p = 0.0427$) and variances ($W = 7.2427$; $p = 0.0096$); however, the differences were not solely caused by having different neurons appear in each histogram as 22 cells yielded FSL slope data that appeared in both distributions; 6 neurons with a negative FSL slope at short durations

exhibited a positive FSL slope at longer durations, 13 cells with a positive FSL slope at short durations remained positive at longer durations, 2 cells stayed negative, and 1 cell switched from positive to negative. At +20 dB re threshold, 8 of 19 cells had negative FSL slope functions for responses evoked by 1 to 3 ms stimuli and 14 of 20 cells had positive FSL slope functions for responses evoked by stimuli $\geq$3 ms, and there was a statistically significant difference between the variances ($W = 5.2114$; $p = 0.0283$) but not the means ($t = -1.3929$; $p = 0.1720$) of the two distributions (Fig. 3.5, *middle column*). Notably, 16 cells yielded FSL slope data that appeared in both distributions and 6 neurons with a negative FSL slope at short durations exhibited a positive FSL slope at longer durations. At +30 dB re threshold, 8 of 16 cells had negative FSL slopes between 1 and 3 ms, 12 of 14 cells had positive FSL slope functions for responses evoked by stimuli $\geq$3 ms, and again there was a statistically significant difference between the variances ($W = 6.1296$; $p = 0.0196$) but not the means ($t = -1.3438$; $p = 0.1898$) of the two distributions (Fig. 3.5, *right column*). Twelve neurons yielded FSL slope data that appeared in both distributions and 5 neurons with a negative FSL slope at short durations exhibited a positive FSL slope at longer durations. In summary, non-linear change in FSL is a common feature of DTNs in the ICc of the bat. Many cells showed constant or decreasing FSLs in response to very short stimulus durations, and the majority of cells exhibited increasing FSLs with clear offset-following responses to longer stimulus durations.

We hypothesized that non-linear change in FSL results from the relative timings of the onset- and offset-evoked excitations in combination with the sustained inhibition. Onset-evoked, sustained inhibition is known to increase FSL in mammalian DTNs (Casseday et al., 2000; Fuzessery et al., 2002; Yin et al., 2008). At longer stimulus durations, the offset-evoked excitation occurs after the onset-evoked excitation (see Fig. 3.3*A,B*), so the depolarized membrane potential of the DTN will have more time to decay towards its resting potential before the offset-evoked excitation arrives. This decay will be accelerated by the presence of sustained inhibition that pushes the membrane potential of the DTN more negative and towards the E_{GABA_A} = -80 mV; at longer durations, the membrane potential of the DTN will be further from and take longer to reach its spike threshold, which explains why the slope of the shifted FSL function was >1 in some *in vivo* DTNs. Leary et al. (2008) also attributed increasing FSLs at longer stimulus durations to the presence of encroaching onset-evoked inhibition because offset-evoked excitation was not observed in whole-cell patch clamp recordings of frog DTNs.

To test the hypothesis that onset-evoked, sustained inhibition can increase FSLs in our computational model, we generated two versions of the model DTN: one using the default inhibition with $\bar{g}_{\text{GABA}_\text{A}} = 2.5$ nS, and another using decreased inhibition with $\bar{g}_{\text{GABA}_\text{A}} = 1.5$ nS. Despite having a 40% reduction in the maximum GABA_A inhibitory conductance, the model employing decreased GABA_A inhibition was able to render excitatory inputs to the DTN sub-threshold, hence a fundamental aspect of the coincidence detection mechanism of duration tuning remained unchanged. The model with decreased GABA_A inhibition produced slightly shorter FSLs (≤ 1 ms difference), and a small increase in spike count and width of temporal tuning for stimulus durations between 1 and 6 ms, but otherwise resulted in a shortpass tuning profile (refer to *Maximum Receptor Conductance* section and Fig. 3.8*E,F*). Most notably, the model with decreased GABA_A inhibition produced spikes that exhibited a more linear change in FSL that faithfully followed stimulus offset (FSL slope ca. 1) at longer durations (Fig. 3.4*B*, *grey circles*), thus mirroring the responses of many *in vivo* DTNs from the ICc of the bat.

3.4.4   Single Parameter Modifications

We systematically varied the onset-evoked excitatory input latency, membrane time constant, and maximum receptor conductances of the default model to determine the relative contribution and importance of these parameters on duration tuning response profiles. The results were subsequently used to tune the default model to mimic the responses of DTNs from the bat, rat, mouse and frog.

Onset-Evoked Excitatory Input Latency

We tested four onset-evoked excitatory input latencies to determine how the relative latencies of synaptic inputs can alter the duration tuning response profile of the default model; the latency of the offset-evoked excitation was held constant at 6 ms re stimulus offset. Two important findings resulted from these simulations. First, the bandwidth of duration tuning (i.e. the width of temporal selectivity) systematically increased as a function of the latency of the onset-evoked excitation (Fig. 3.6*A*). When the onset-evoked input latency was longer than the offset of the sustained inhibition, the excitation was supra-threshold and the model DTN produced spikes at a fixed latency from stimulus onset. Mean spike counts in the model cell systematically decreased when the duration of the stimulus, and thus the sustained
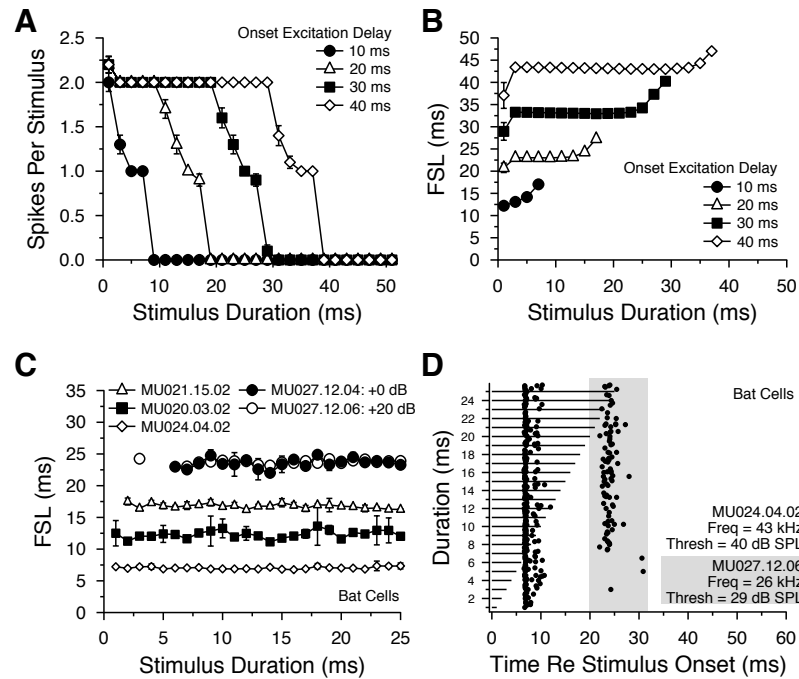
Figure 3.6: Modifying the latency of onset-evoked excitation to the model DTN. *A*, Mean ± SE spike count as a function of stimulus duration at four onset-evoked excitatory input latencies (including 10 ms as in the default model). Note how the model produced a shortpass DTN at all onset latencies; however, the temporal bandwidth of tuning widened and the model exhibited less selectivity at longer onset-evoked excitation latencies. *B*, Mean ± SE FSL of the model responses from *A*. *C*, Mean ± SE FSL of four onset responding neurons (not duration-tuned) from the ICc of the big brown bat. Responses from cell MU027.12 are shown twice: once at threshold and once at +20 dB re threshold. Notice how FSL for this cell remains stable and that the minimum duration threshold remains relatively constant over the 20 dB amplitude range. *D*, Dot raster display of two onset cells from the ICc of the bat *C*. Spikes from the second neuron appear in the grey box. The longer latency onset neuron has a minimum stimulus duration threshold of 6 ms. MU020.03.02: BEF = 59 kHz, Threshold = 56 dB SPL, Amp = +10 dB (re threshold), 10 trials per stimulus; MU021.15.02: BEF = 36 kHz, Threshold = 57 dB SPL, Amp = +10 dB, 10 trials per stimulus; MU024.04.02: BEF = 43 kHz, Threshold = 40 dB SPL, Amp = +30 dB, 10 trials per stimulus; MU027.12.04: BEF = 26 kHz, Threshold = 29 dB SPL, Amp = +0 dB, 10 trials per stimulus; MU027.12.06: BEF = 26 kHz, Threshold = 29 dB SPL, Amp = +20 dB, 10 trials per stimulus;

inhibition, was close to the latency of the onset-evoked excitation. Together, these results reinforce the notion that the onset-evoked excitation needs to be coincident with the sustained inhibition to be rendered sub-threshold.

Second, for a given onset-evoked excitation latency, FSLs of the model DTN remained

relatively constant, except at the shortest and longest stimulus durations (Fig. 3.6*B*). At the shortest stimulus durations, the offset-evoked excitation had a small non-zero probability of evoking spikes in the model DTN before the arrival of the onset-evoked excitation because the sustained inhibition at this time had a minimal impact on the membrane potential of the DTN. At intermediate durations when the latency of the onset-evoked excitation was longer than the offset of the stimulus, the onset-evoked excitation produced a constant spike count at a fixed latency re stimulus onset in the model DTN; however, at longer stimulus durations near the latency of the onset-evoked excitation, the sustained inhibition now rendered the onset-evoked excitation sub-threshold, so temporal coincidence between the offset-evoked and onset-evoked excitations was necessary to produce spikes in the model cell. Therefore, the mean FSL in the model DTN increased with stimulus duration when the offset-evoked excitation arrived after the onset-evoked excitation. First-spike latencies can also be delayed by encroaching sustained inhibition as demonstrated in Figure 3.4*B* and later in the section on *Reproducing a Frog Shortpass DTN*.

Few direct observations of excitatory synaptic input latencies to *in vivo* DTNs have been reported (e.g. whole-cell patch recording Covey et al., 1996; Tan and Borst, 2007; Leary et al., 2008). An alternative way to estimate these latencies is to characterize the FSL of neurons that exhibit purely onset response patterns. First-spike latencies of ICc neurons in the big brown bat typically range from ca. 5 ms to ≥30 ms (Haplea et al., 1994). Figure 3.6*C* shows data from four onset responding neurons from the ICc of the big brown bat, with FSLs ranging from ca. 7 ms to 23 ms. One cell (MU027.12) is shown twice, once at 0 dB (threshold) and once at +20 dB (re threshold) to illustrate its stable FSL and minimum duration threshold. Dot rasters for two neurons are shown in Figure 3.6*D*. Note how the longer latency neuron (*grey background*) requires a minimum stimulus duration of ca. 7 ms to reliably evoke spikes. Later we demonstrate that onset-evoked excitatory inputs with a minimum stimulus duration threshold could be involved in the mechanism that creates some bandpass DTNs (see *Reproducing a Bat Bandpass DTN*).

Membrane Time Constant

The membrane time constant (τ) of a neuron, defined as the product of the membrane resistance (r_m) and the membrane capacitance (c_m; $\tau_{\text{membrane}} = r_m c_m$), determines how quickly the membrane potential (voltage) will react to synaptic input currents. The membrane

time constant of an *in vivo* neuron is a complex function of multiple ion currents (e.g. K+; Rothman and Manis, 2003) and non-specific, hyperpolarization activated currents (e.g. I_h; Kopp-Scheinpflug et al., 2011); however, our simplified model allowed us to easily set the passive membrane time constant by altering the maximum conductance of passive leak channels ($\bar{g}_{\text{leak}}$). In the default model with $\bar{g}_{\text{leak}} = 0.25$ mS/cm² (i.e. $\bar{r}_{\text{leak}} = 4000 \Omega \text{cm}^2$) and $c_m = 1.0$ μF/cm², the membrane time constant was $\tau = 4$ ms.

Longer time constants in the model DTN resulted in an increased number of spikes and a wider temporal response bandwidth (Fig. 3.7*A,C*; panels separated for clarity over different timescales). Response bandwidth, defined as the range of stimulus durations with ≥0.5 spikes per trial, grew exponentially with membrane time constant because the window of effective temporal coincidence between the onset- and offset-evoked excitations broadened (Fig. 3.7*E*). Specifically, because the depolarizing effects of the first excitatory input persisted longer at longer membrane time constants, the excitation was more likely to overlap with the second excitatory input arriving later. For all time constants tested, the resulting FSL in the model DTN remained relatively unchanged. At short stimulus durations (i.e. ≤5 ms), the increase in FSL as a function of stimulus duration followed that of the default model and the slope of change in FSL was <1 (Fig. 3.7*B*). At longer stimulus durations, the slope of change in FSL was approximately 1 because the timing of spikes in the model followed the increase in latency of the offset-evoked excitatory input (Fig. 3.7*D*).

Maximum Receptor Conductance

The responses of IC neurons, including DTNs, are shaped by complex interactions of excitation and inhibition (Rose et al., 1966; Pollak and Park, 1993; McAlpine et al., 1998; Casseday et al., 2000; Gittelman and Pollak, 2011; Pollak et al., 2011). Here we vary the maximum receptor conductances ($\bar{g}$) of AMPA, NMDA and GABA$_A$ receptors to understand how these inputs contribute to duration selectivity (Fig. 3.8).

Modifying only the AMPA receptor maximum conductance provided two interesting results. First, removing the AMPA-mediated current ($\bar{g}_{\text{AMPA}} = 0$ nS) completely extinguished spiking in the model cell; without the AMPA-mediated depolarizing current, the NMDA-mediated current was stinted by the voltage-dependent Mg²⁺ block and the model neuron never reached spiking threshold (Fig. 3.8*A*; 0 nS). Second, as the maximum AMPA receptor conductance increased, the number of spikes and the bandwidth of duration tuning
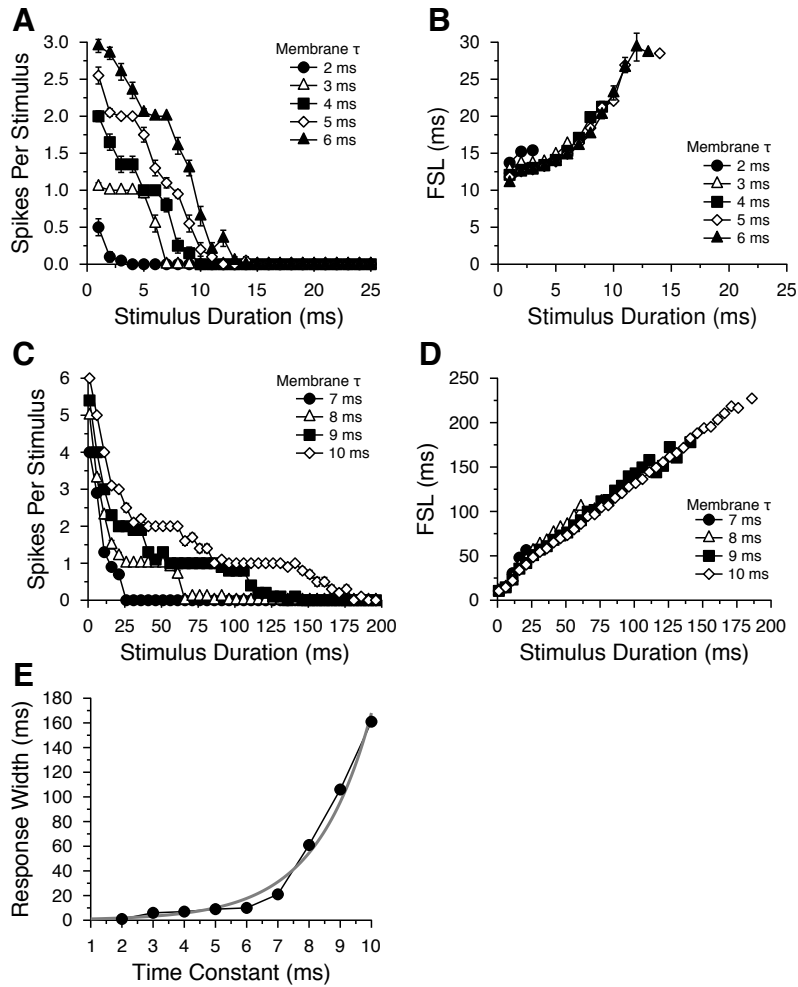
Figure 3.7: Modifying the passive membrane time constant (τ) of the model DTN. *A,C*, Mean $\pm$ SE spike count as a function of stimulus duration for nine different membrane (τ's). The model DTN produced a shortpass response profile at every τ value. Maximum spike count and temporal bandwidth of duration tuning grew with increasing τ. Stimulus durations up to 200 ms were included to illustrate that model cell spiking eventually ceased. *B,D*, Model cell FSL as a function of stimulus duration and membrane τ. *E*, Duration tuning response bandwidth as a function of membrane τ. Temporal bandwidth defined as the range of stimulus durations with $\geq$0.5 spikes per trial. *Grey line* represents best fit exponential regression $y = Ae^{Bx}$, where $A = 0.6075$ and $B = 0.5623$ ($R^2 = 0.9055$; $p = 0.000078$).
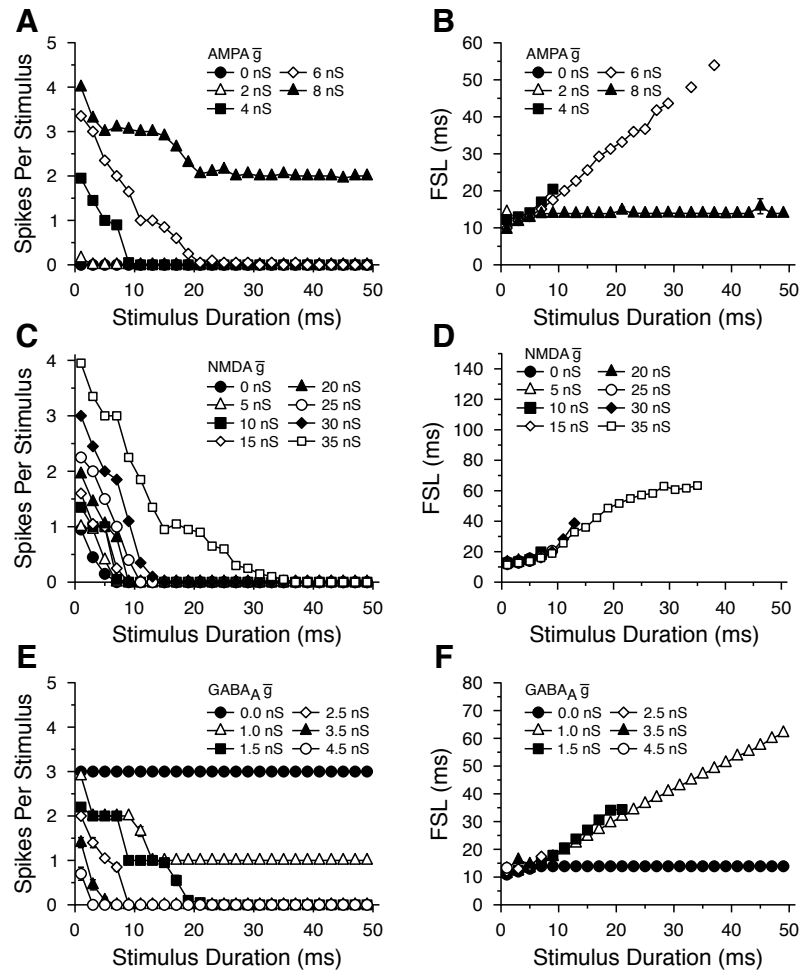
Figure 3.8: Modifying the strength of (**A,B**) AMPA, (**C,D**) NMDA and (**E,F**) GABA$_A$ receptor conductances of the model DTN. **A,C,E**, Mean $\pm$ SE spike count as a function of stimulus duration. As expected, increasing the level of excitation or decreasing the strength of GABAergic inhibition to the model DTN increased the maximum spike count and temporal bandwidth of duration tuning. **B,D,F**, The FSL of each model generally followed stimulus offset except when the excitation (inhibition) was strong (weak) enough for the onset-evoked excitation to reliably evoke spikes at a constant latency from stimulus onset.

also increased (Fig. 3.8A). Interestingly, setting $\bar{g}_{\mathrm{AMPA}} = 6$ nS permitted the model cell to have a non-zero spiking probability over a wider, but still limited, range of stimulus durations with the FSL following stimulus offset. This demonstrated that both the onset- and offset-evoked excitations were required to evoke spiking and that the temporal window of coincidence was considerably wider at higher maximum AMPA receptor conductances (Fig. 3.8B; 6 nS). When $\bar{g}_{\mathrm{AMPA}} = 8$ nS, the model cell lost temporal selectivity and produced spikes at all stimulus durations. Moreover, the FSL of the model now followed stimulus onset because the onset-evoked excitatory input was supra-threshold even with inhibition and thus no longer required temporal coincidence with the offset-evoked excitation (Fig. 3.8B; 8 nS).

Increasing only the NMDA receptor maximum conductance resulted in more spikes and a wider duration tuning response profile (Fig. 3.8C). Unlike when the AMPA conductance was abolished, spikes were still evoked in the model cell even after the NMDA-mediated current was removed ($\bar{g}_{\mathrm{NMDA}} = 0$ nS); however, the number of spikes and temporal bandwidth of tuning were greatly diminished. Even at a very high NMDA maximum conductance ($\bar{g}_{\mathrm{NMDA}} = 35$ nS), temporal coincidence between the onset- and offset-evoked excitations was still required to evoke spiking. Moreover, the model neuron maintained an offset following response pattern (Fig. 3.8D) and did not switch to an onset following response pattern until $\bar{g}_{\mathrm{NDMA}} \geq 125$ nS (data not shown). This high NMDA maximum conductance was required to overcome the strong Mg^{2+} block. Because increased AMPA-mediated depolarizing currents would further release the Mg^{2+} block from NMDA channels, a higher maximum AMPA conductance would lower the minimum NMDA conductance required to switch a neuron's spiking pattern from offset to onset following. For example, when we set the $\bar{g}_{\mathrm{AMPA}}$ to 6 nS, the model DTN switched from offset responding to onset responding when the $\bar{g}_{\mathrm{NMDA}}$ was only 55 nS (data not shown). This highlights how a neuron's spiking response pattern can be mediated by a complex interaction of solely excitatory currents (Zhang and Kelly, 2001; Sanchez et al., 2007).

Reducing the strength of the $GABA_A$-mediated current also resulted in more spikes and a wider temporal response bandwidth in the model cell (Fig. 3.8E). When the $GABA_A$ maximum conductance was reduced to 1.5 nS, the model DTN responded to durations up to 20 ms and demonstrated a wider window of temporal coincidence. When the conductance was reduced to 1.0 nS, at least 1 spike was evoked at all stimulus durations and FSL followed stimulus offset (Fig. 3.8F). In this case, the weakened sustained inhibition was strong enough

to render the onset-evoked excitation sub-threshold because it completely overlapped the excitation. In contrast, because the offset-evoked excitation only slightly overlapped the sustained inhibition it was not rendered sub-threshold so offset-evoked spikes were evoked at every duration. In the default model, the $GABA_A$-mediated inhibition was stronger and persisted long enough to render the offset-evoked excitation sub-threshold. When inhibition was removed completely, the model DTN responded at all stimulus durations (Fig. 3.8*E*; 0 nS) with a constant FSL (Fig. 3.8*F*; 0 nS). This was expected because, in the absence of inhibition, the onset-evoked excitatory input was supra-threshold on its own. Although offset-responding DTNs are common in mammals, a high proportion of onset responding DTNs have been reported in the pallid bat (Fuzessery and Hall, 1999) and least horseshoe bat (Luo et al., 2008). Offset-responding DTNs with clear onset excitation breakthrough have also been reported from the ICc of the big brown bat and were hypothesized to occur when onset-evoked excitatory input(s) overpowered inhibitory input(s) (Ehrlich et al., 1997; Faure et al., 2003). A previous computational study demonstrated that reducing the strength of inhibition relative to excitation can cause a model DTN with offset spiking responses to exhibit an "onset excitation breakthrough" spiking pattern (Aubie et al., 2009). Our present simulations reinforce the importance of balanced excitatory and inhibitory input for producing DTNs with offset responses and sharp temporal selectivity.

3.4.5   Multiple Parameter Modifications

In this section we modify the default model of duration tuning with parameters tuned to reproduce the responses of *in vivo* DTNs from the bat, rat, mouse and frog. These species were chosen to highlight how biologically plausible parameter modifications in our computational model were able to produce a range of temporal selectivities mirroring *in vivo* duration tuning response profiles. In the bat and the rat examples, we explore two modifications that we hypothesize could contribute to transforming the responses of shortpass DTNs into bandpass DTNs. In the mouse and the frog examples, we demonstrate how both the coincidence detection and anti-coincidence mechanisms can create a shortpass duration tuned response profile. The models showcase that biologically feasible instantiations of duration selectivity could by created by similar neural mechanisms in different vertebrates. Our theoretical approach provides credible support for the existence of similar plausible instantiations of temporal selectivity in different species; however, alternative mechanisms

likely exist and are not excluded by our investigation.

Reproducing a Bat Bandpass DTN

The coincidence detection mechanism is hypothesized to underlie some bandpass DTNs (e.g. Ehrlich et al., 1997; Brand et al., 2000; Faure et al., 2003; Pérez-González et al., 2006). If the onset-evoked excitatory input arrived before the offset-evoked excitatory input at short stimulus durations, but after the offset-evoked excitatory input at long stimulus durations, then theoretically such a mechanism would produce a bandpass DTN. The cell would be expected to show a symmetrical pattern of spiking for stimulus durations both shorter and longer than BD. Often, however, bandpass DTNs in bats have little to no response at the shortest stimulus duration(s), and a longer tail of diminishing spiking probability for stimuli above BD (e.g Ehrlich et al., 1997; Fuzessery and Hall, 1999; Zhou and Jen, 2001). Such a bandpass response profile can be produced using the coincidence detection mechanism if the DTN receives no excitatory input at the shortest stimulus duration(s). This mechanism is biologically feasible if the onset- and/or offset-evoked excitations have a minimum stimulus duration required for producing synaptic input to the DTN.

Our observations suggest that some bat ICc neurons have a minimum duration threshold that persists over a wide range ($\geq$20 dB) of stimulus amplitudes. The neurons, or their inputs, require a minimum integration time of stimulus energy to fire action potentials that is never or rarely met at very short stimulus durations (e.g. cell MU027.12 in Fig. 3.6*C,D; grey shading*). Therefore, removing excitatory input at the shortest stimulus duration is a plausible approach for producing a bandpass DTN. In some cases, a neuron that appears to have a minimum duration threshold may actually have a minimum energy threshold. In this case, increasing stimulus energy should recover the neuron's response at shorter durations. For example, a 1 ms tone with 0.5 ms linear onset/offset ramps has 4.77 dB less energy than a 2 ms tone with the same ramps. If a neuron with a minimum energy threshold responds to tones $\geq$2 ms at a given amplitude, then increasing the amplitude of the tone by 4.77 dB should now cause the cell to spike to 1 ms signals. Such energy integrators are not likely candidates for producing bandpass duration tuning stable over a range of stimulus amplitudes.

We implemented this strategy to reproduce a bandpass DTN from a big brown bat by removing excitatory input to the default model for 1 ms stimuli. Dot raster displays of the
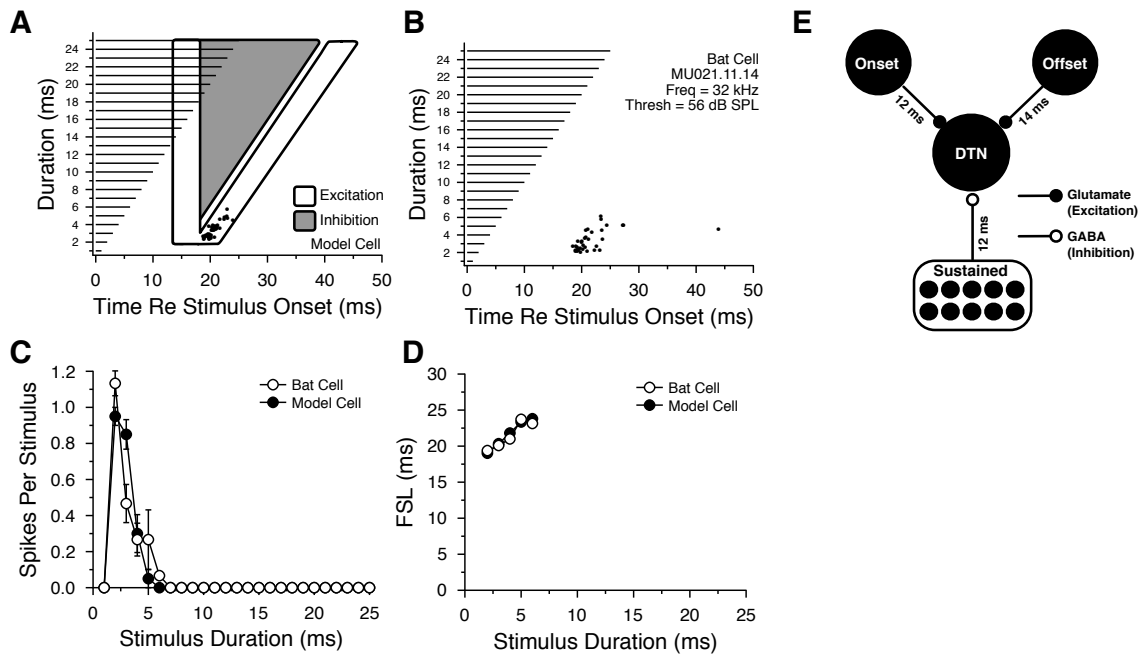
Figure 3.9: Reproduction of a bandpass DTN in a bat. **A**, Dot raster display of model responses over 20 repeated trials with excitatory (*white*) and inhibitory (*grey*) inputs overlaid. **B**, Dot raster display of an *in vivo* big brown bat DTN over 15 trials presented at +20 dB re threshold. This neuron also produced errant responses with a probability of 0.33 to 0.4 spikes per trial between 50 and 100 ms (not shown). **C**, Mean $\pm$ SE spike counts in both the model and the *in vivo* bat DTN as a function of stimulus duration. **D**, Mean $\pm$ SE FSL in both the model and *in vivo* bat DTN as a function of stimulus duration. **E**, Neural circuit diagram of model used to reproduce *in vivo* bat DTN responses.

model cell (Fig. 3.9*A*) and *in vivo* bat DTN (Fig. 3.9*B*) both show offset responding spiking patterns. The modified model reproduced both the mean spike counts (Fig. 3.9*C*) and FSLs (Fig. 3.9*D*) of the *in vivo* bat DTN. A network diagram of model inputs is shown in Figure 3.9*E* and the model parameters are listed in Table 3.5. Variation in spike timing was lower for the model cell than the *in vivo* DTN (compare Fig. 3.9*A,B*), but this was not surprising because the sole source of noise in the model was from the timing of presynaptic GABAergic spikes. Incorporating noise into the timing of excitatory inputs to the model would cause additional jitter in spike arrival times and spike probability that would lead to increased variation in FSL and spike counts per trial.

Reproducing a Rat Bandpass DTN

Rat DTNs differ from bat DTNs in their preference for longer duration acoustic signals. Pérez-González et al. (2006) reported rat DTNs with BDs up to 128 ms and presented, in detail, an *in vivo* DTN with a BD of 56 ms. The latter cell had a highly variable spiking probability with weak responses to 7.5 kHz tone durations <50 ms, a peak spike probability of 6 spikes per 10 trials in response to tones at BD, and a diminishing spiking probability for tone durations up to 159 ms.

On its own, the coincidence detection mechanism of duration tuning could produce a bandpass DTN with a BD of 56 ms; however, the duration tuning response profile of the model would be expected to show symmetrical spike counts at durations both shorter and longer than BD. The *in vivo* data show that the rat DTN had an asymmetrical spike count surrounding BD (Pérez-González et al., 2006). To account for the asymmetry in our model, we hypothesized that the onset-evoked inhibition received by the model DTN was initially strong, but then decreased and plateaued (adapted) to a weaker level for the duration of the stimulus. Whole-cell patch clamp studies in the bat (Covey et al., 1996) and frog (Leary et al., 2008), and extracelluar recordings from the bat (Faure et al., 2003) suggest that inhibition in the DTN is strongest at stimulus onset, likely as a result of both GABAergic and glycinergic inputs (Casseday et al., 2000). To simulate strong transient inhibition in our model, we added a second, stronger GABAergic input with a 15 ms latency (re stimulus onset) that persisted for the initial 35 ms of the stimulus. This modification resulted in a model rat DTN that failed to respond to short duration stimuli because its offset-evoked excitation overlapped with the early and strong transient inhibition (Fig. 3.10*A*). At stimulus durations near BD (56 ms), the onset- and offset-evoked excitations sufficiently overlapped after the early inhibition had decayed, so spikes were evoked. At durations longer than BD, decreasing temporal coincidence between the onset- and offset-evoked excitatory inputs produced a decaying trail of spikes that followed stimulus offset, resulting in a bandpass neuron with an asymmetrical response probability that mirrored the duration tuning profile of the *in vivo* rat DTN (Fig. 3.10*B*). The *in vivo* response profile was especially difficult to reproduce because of its highly variable and weaker spiking (Fig. 3.10*C*). To account for this variability, we tuned the parameter values in the model to approximate the duration tuning response profile of the *in vivo* rat neuron when averaged over 1000 simulations. We then ran the simulation 20 times with different random seeds until variability in model output was
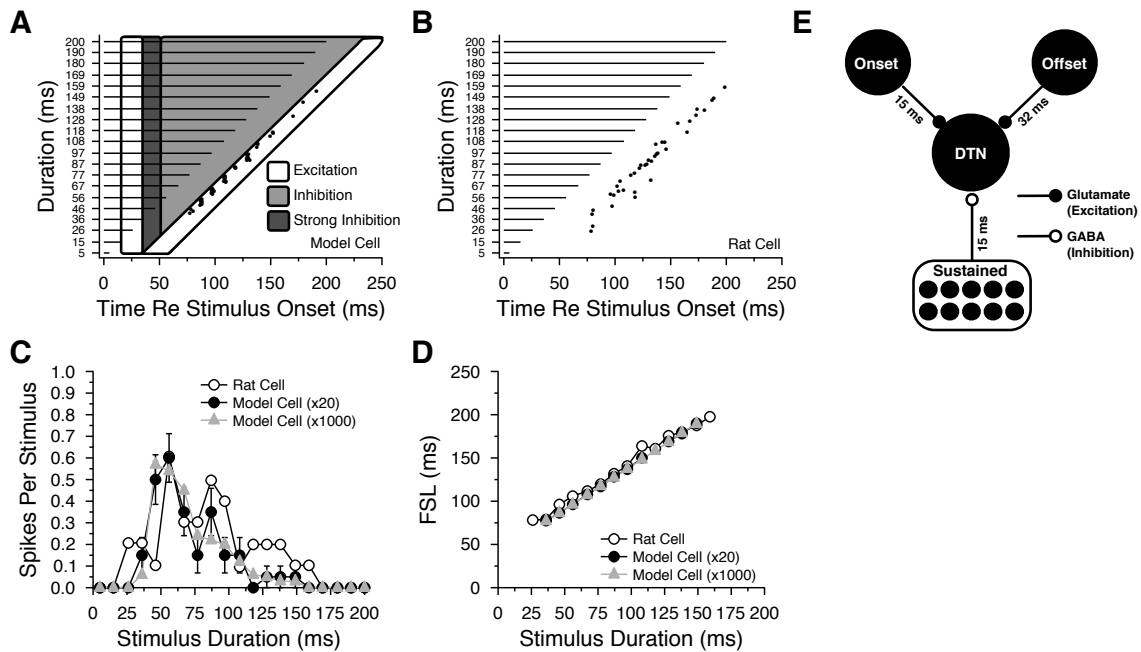
Figure 3.10: Reproduction of a bandpass DTN in a rat (Pérez-González et al., 2006, Figure 7*A,B*, unit 39.164). *A*, Dot raster display of model responses over 20 repeated trials with excitatory (*white*) and inhibitory (*grey*) inputs overlaid. *B*, Dot raster display of an *in vivo* rat DTN over 10 trials. *C*, Mean (± SE) spike count (model only) of model and *in vivo* rat DTN as a function of stimulus duration. Model spiking was highly variable across trials due to noisy inhibition, hence responses are shown after 20 and 1000 repeated trials. High response variability was also observed from the *in vivo* rat DTN. *D*, Mean (± SE) FSL (model only) of model and *in vivo* rat DTN as a function of stimulus duration. *E*, Neural circuit diagram of model used to reproduce *in vivo* rat DTN responses.

similar to the *in vivo* rat DTN. A network diagram of the inputs to the model is shown in Figure 3.10*E* with model parameters listed in Table 3.5. The tuned model reproduced the mean spike counts and FSLs of the rat *in vivo* DTN (Fig. 3.10*C-D*). Unlike the model bat DTN, excitatory inputs to the model rat DTN were present at all stimulus durations.

Reproducing a Mouse Shortpass DTN

The response profile of DTNs in mice share similarities with DTNs in bats and rats. Some mouse DTNs are tuned to short stimulus durations and have narrow temporal response bandwidths, while others have longer BDs and wider temporal bandwidths (Brand et al., 2000; Xia et al., 2000). To highlight how our computational model was able to reproduce
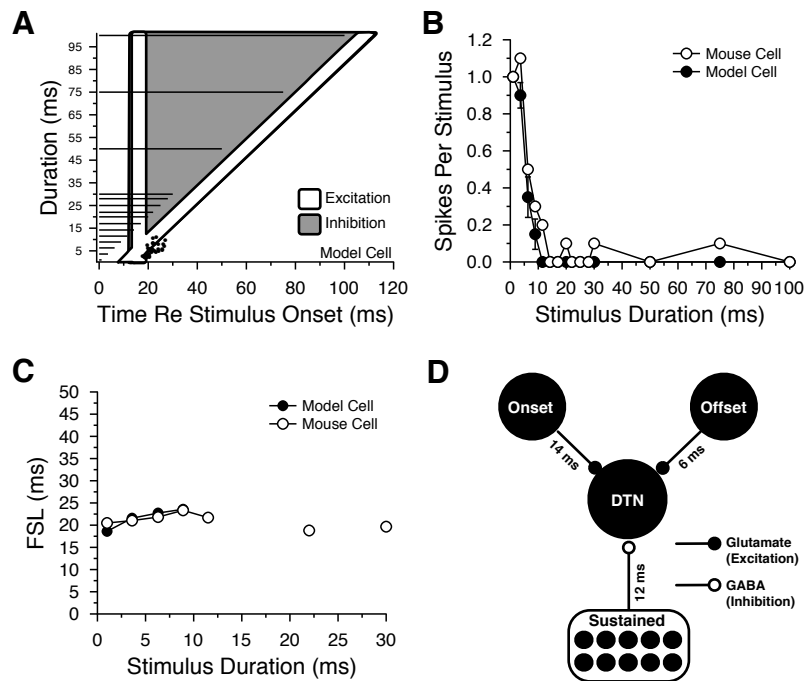
Figure 3.11: Reproduction of a shortpass DTN in a mouse (Brand et al., 2000, Figure 3, cell m-10-02-98). *A*, Dot raster display of model responses over 20 repeated trials with excitatory (*white*) and inhibitory (*grey*) inputs overlaid. *B*, Mean ($\pm$ SE) spike count (model only) of model and *in vivo* mouse DTN as a function of stimulus duration. *C*, Mean ($\pm$ SE) FSL (model only) of model and *in vivo* mouse DTN as a function of stimulus duration. *D*, Neural circuit diagram of model used to reproduce *in vivo* mouse DTN responses.

the response of a narrowly tuned DTN from the mouse, we adjusted model parameters to produce a shortpass neuron with a BD of 1-2 ms and a sharp decrease in spiking for longer stimulus durations (Brand et al., 2000).

The model DTN nicely reproduced the sharp tuning of the *in vivo* shortpass DTN, although the model failed to produce spikes at longer stimulus durations as occasionally observed in the *in vivo* DTN of the mouse (Fig. 3.11*A,B*). These additional *in vivo* spikes could have been evoked spontaneously from a source of excitatory noise not present in our model. The FSL of both the *in vivo* mouse DTN and the model DTN had a tendency to increase slightly with stimulus duration (Fig. 3.11*C*). A network diagram of the inputs to the model is shown in Figure 3.11*D* and model parameters are listed in Table 3.5.

Reproducing a Frog Shortpass DTN

Although DTNs were originally discovered and first reported from the auditory midbrain (torus semicircularis) of frogs (Potter, 1965; Straughan, 1975; Narins and Capranica, 1980), these cells have received little attention in anurans. A recent *in vivo* whole-cell patch clamp study by Leary et al. (2008) found that of 22 DTNs recorded from the torus semicircularis, 11 were shortpass, 1 was bandpass, and 10 were longpass. Intracellular recordings unveiled a short latency, onset-evoked inhibition (hyperpolarization) and a longer latency, onset-evoked excitation (depolarization). Counter to the coincidence detection mechanism of duration tuning, offset-evoked depolarizations were not observed. Therefore, we expected that the mechanism underlying duration selectivity in anurans would be more similar to the anti-coincidence mechanism originally proposed for shortpass duration selectivity in bats (Fuzessery and Hall, 1999).

We removed the offset-evoked excitatory input in our default model to reproduce the shortpass response profile of a frog DTN reported by Leary et al. (2008), including the low but non-zero spiking probability at longer stimulus durations (Fig. 3.12*A,B*). The spiking responses of our model frog DTN also mirrored the increase in FSL at longer stimulus durations (Fig. 3.12*C*) routinely observed in *in vivo* recordings. Leary et al. (2008) hypothesized that this increase was a result of encroaching inhibition delaying spikes. Spikes evoked by this example *in vivo* had a relatively weak increase in FSL compared to other frog DTNs (Leary et al., 2008). The delay of FSL in our model was caused by encroaching inhibition because only a single, fixed latency, onset-evoked excitatory input was present in the network (see Fig. 3.12*D* with model parameters listed in Table 3.5).

3.5 Discussion

Duration-tuned neurons are found in the auditory midbrain of many vertebrates: bats (Ehrlich et al., 1997; Fuzessery and Hall, 1999; Casseday et al., 2000; Faure et al., 2003; Mora and Kössl, 2004), rats (Pérez-González et al., 2006), frogs (Potter, 1965; Straughan, 1975; Narins and Capranica, 1980; Gooler and Feng, 1992; Leary et al., 2008), mice (Brand et al., 2000; Xia et al., 2000; Tan and Borst, 2007), guinea pigs (Wang et al., 2006; Yin et al., 2008), chinchillas (Chen, 1998) and cats (He et al., 1997; Qin et al., 2009). Cortical DTNs have been studied in the bat (Galazyuk and Feng, 1997; Ma and Suga, 2001) and cat (He et
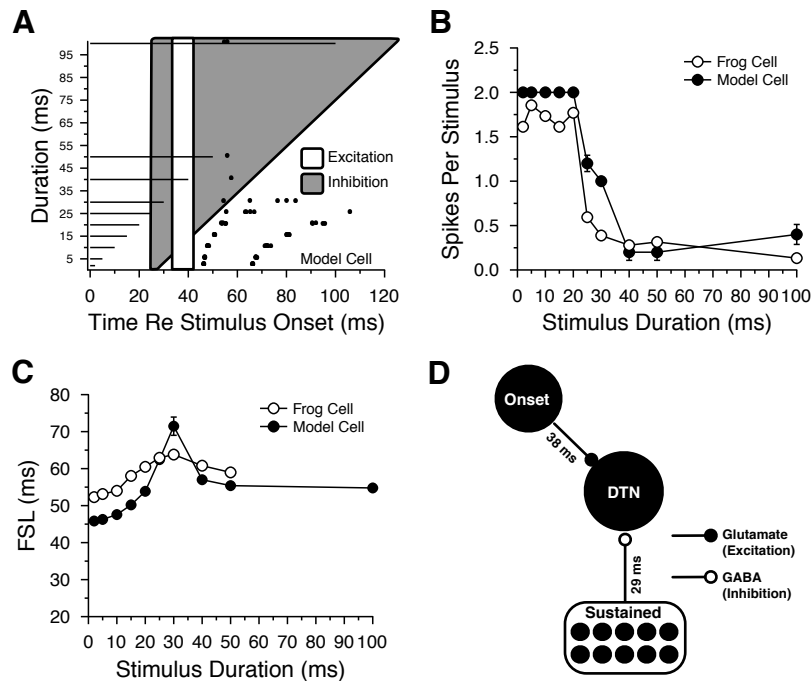
Figure 3.12: Reproductions of a shortpass DTN in a frog (Leary et al., 2008, Figure 5, open diamonds). *A*, Dot raster display of model responses over 20 repeated trials with excitatory (*white*) and inhibitory (*grey*) inputs overlaid. *B*, Mean ($\pm$ SE) spike count (model only) of model and *in vivo* frog DTN as a function of stimulus duration. *C*, Mean ($\pm$ SE) FSL (model only) of model and *in vivo* frog DTN as a function of stimulus duration. *D*, Neural circuit diagram of model used to reproduce *in vivo* frog DTN responses.

al., 1997) auditory cortex and the cat visual cortex (Duysens et al., 1996). Invertebrate duration selectivity for vibratory signals has also been found in ascending interneurons of insects (Zorović, 2011). Our results support the hypothesis that neural mechanisms of duration selectivity may be shared across vertebrates. We created neurophysiologically plausible computational models of two theoretical mechanisms, the coincidence detection and anti-coincidence mechanisms of duration tuning, that accurately reproduced the *in vivo* responses of DTNs over a wide range of temporal response profiles. We did so by modifying synaptic input latencies, synaptic input strengths, and membrane time constants of model DTNs. Here we review inherent limitations of our models and suggest future enhancements, some of which rely on yet to be obtained physiological data. We also highlight similarities between neural mechanisms of duration tuning and mechanisms underlying other stimulus feature detectors in the central nervous system.

3.5.1   Model Limitations and Future Enhancements

Intracellular recordings from DTNs have been achieved only twice: once in bats (Covey et al., 1996) and once in frogs (Leary et al., 2008). Both studies revealed the relative timing of membrane voltage changes and showed that inhibition often preceded excitation; however, the duration and strength of individual inputs were indeterminable because the individual strengths of excitation and inhibition were inseparable from their summated effect on membrane potential. Membrane time constants were not measured either. In this study we chose physiologically plausible membrane and ion channel parameters for the auditory midbrain but these parameters may be further constrained within the subclass of DTNs.

Our models incorporated only one inhibitory receptor (GABA$_A$) and two excitatory receptors (AMPA and NMDA). We employed two excitatory receptors because the long time constant of NMDA receptors was important for producing long duration membrane depolarizations from transient inputs and NMDA receptors required AMPA receptor activation due to the Mg^{2+} block. Long depolarizations increased the window of temporal coincidence for multiple inputs, a feature we believe is critical for tuning to long stimulus durations (Fig. 3.8*A,C*). Additional receptors and neurotransmitters shape IC neuron responses and may also contribute to duration tuning. GABA$_B$ receptors act presynaptically to modulate GABAergic (Ma et al., 2002a) and glutamatergic (Sun et al., 2006) inputs and are found in moderate concentration in the rat IC (Charles et al., 2001) and low concentration in the bat IC (Fubara et al., 1996). Although GABA$_B$ receptors were not explicitly modelled, their net effect is represented by the magnitude of inputs to the model.

Inhibitory glycine receptors are found in the IC of both rats (Pourcho et al., 1992) and bats (Vater et al., 1992; Fubara et al., 1996; Klug et al., 1999; Wenstrup and Leroy, 2001). Pharmacologically blocking glycine increases spike counts and reduces temporal selectivity in DTNs in a manner similar, albeit less pronounced, to blocking GABA$_A$ receptors (Casseday et al., 1994, 2000). Although glycine receptors have faster kinetics than GABA$_A$ receptors (Harty and Manis, 1998), the effect of a sustained glycinergic input to a DTN would be similar to sustained GABAergic input. That said, it is possible that glycinergic inputs differentially affect DTNs by having distinct temporal response patterns over the duration of a stimulus. Blocking glycine receptors in the IC appears to preferentially affect responses near stimulus onset, suggesting that stimulus-evoked inhibition has an early glycine component (Casseday et al., 2000). The ventral nucleus of the lateral lemniscus in

the bat is known to project transient, onset-evoked glycinergic inputs to the IC that could provide early inhibition to DTNs (Covey and Casseday, 1991; Vater et al., 1997). Some glycinergic synapses in the guinea pig ventral cochlear nucleus have fast desensitization times that could also contribute transient inhibition (Harty and Manis, 1998). We produced strong, early inhibition in our model rat DTN by incorporating additional GABAergic inputs. Additional glycine receptors would achieve a similar result.

Serotonin and dopamine have received less attention in the IC literature and were not implemented in our models; however, they likely contribute to duration selectivity. Serotonin levels in the IC are modulated by behavioural states (Hurley et al., 2002; Peruzzi and Dut, 2004), and activation of serotonin receptors can shift the FSL of IC neurons (Hurley and Pollak, 2005; Hurley, 2007) and modulate GABAergic inhibition (Hurley et al., 2008). This suggests that behavioural state may modulate the responses of DTNs. Both latency and inhibition are important parameters for determining the response profile of DTNs. Dopamine receptors are present in the IC (Charuchinda et al., 1987) but their effects on DTNs and other IC neurons are unclear at this point.

3.5.2   Duration Tuning and Other Auditory Feature Detectors

Within the central auditory system, DTNs are first observed in the IC and arise from the temporal integration of excitatory and inhibitory synaptic inputs. Our results support the hypothesis that both the timing (Fig. 3.6) and magnitude (Fig. 3.8) of inputs are important for producing the response characteristics of DTNs. Furthermore, we found that long membrane time constants produced stronger spiking and wider duration tuning bandwidths (Fig. 3.7), demonstrating that intrinsic membrane properties can provide additional response heterogeneity for cells with similar synaptic inputs.

Convergence of excitation and inhibition produces a host of response profiles in the central auditory system, including selectivity for stimulus frequency (Fuzessery and Hall, 1996; Wehr and Zador, 2003; Wu et al., 2008; Xie et al., 2008; Fukui et al., 2010), intensity (Wu et al., 2006), spatial position/sound localization (Rose et al., 1966; Fuzessery and Pollak, 1985; Zhang and Kelly, 2010; Tang et al., 2011), amplitude modulation (Grothe, 1994; Burger and Pollak, 1998), rhythm detection (Felix II et al., 2011), FM sweep direction (Gittelman et al., 2009; Gittelman and Pollak, 2011) and pulse-echo delay (Galazyuk et al., 2005; Yavuzoglu et al., 2011). Inhibition shapes and sharpens neural responses by modulating the latency,

strength and time-course of excitation. For example, we demonstrated in both the default model (Fig. 3.3) and the rat bandpass model (Fig. 3.10) that the maximum spiking response need not be evoked by the stimulus that creates the maximum temporal coincidence between excitatory inputs. In the default model DTN, weak inhibition at short stimulus durations allowed overlapping, but not perfectly coincident, excitatory inputs to maximally summate and evoke the highest spike count. In the rat bandpass model DTN, strong inhibition at short stimulus durations rendered temporally coincident excitatory inputs less effective in evoking spikes. These mechanisms share many attributes found in other auditory feature detectors.

Precisely timed excitatory and inhibitory inputs are important for improving spike timing in the auditory cortex where inhibition can lag excitation by only a few milliseconds and confine spike times for decreased response jitter (Wehr and Zador, 2003). The temporal response bandwidth of an anti-coincidence DTN also depends on the relative timing of onset-evoked inhibition and the onset-evoked excitation. As inhibition lengthens with stimulus duration, long latency onset-evoked excitation becomes blocked to produce shortpass duration selectivity (Fig. 3.2 & Fig. 3.12).

Inhibition in the bat IC can also select for FM sweep direction. Upward and downward FM sweeps evoke supra-threshold excitatory post-synaptic potentials of different magnitudes in IC neurons; however, inhibitory post-synaptic potentials raise the cell's spiking threshold to just below the largest excitatory input magnitude. This selects for only the strongest excitatory input and thus the corresponding FM sweep direction (Gittelman et al., 2009). Inhibitory inputs to DTNs are responsible for decreasing spike counts and sharpening temporal response profiles by increasing a neuron's spiking threshold (e.g. Fig. 3.8). For coincidence detection DTNs, inhibition sharpens the window of coincidence for stimulus-evoked excitatory inputs, hence sharpening temporal selectivity. Similarly, shunting inhibition in the avian nucleus laminaris (analog of mammalian medial superior olive) decreases spontaneous activity and sharpens excitatory coincidence detection important for sound localization (Tang et al., 2011).

Inhibitory frequency tuning curves for cortical auditory neurons are often broader than excitatory tuning curves. Therefore, inhibition sharpens frequency tuning by reducing net excitatory input for sounds further from the cell's BEF (Wu et al., 2008; Xie et al., 2008). Similarly, we demonstrated that the shape of inhibitory inputs to a DTN can be adjusted to produce bandpass duration tuning by selectively preventing the DTN from producing spikes to short duration stimuli (Fig. 3.10).

Complex interactions of excitation and inhibition are responsible for creating many types of feature detectors in the central nervous system. It is not surprising then that duration tuning arises from similar interactions and that the underlying neural mechanisms scale across vertebrates to produce species-specific variations in temporal selectivity. Verification of the underlying mechanisms in different species awaits additional *in vivo* physiological studies.

Table 3.2: Parameters for intrinsic membrane kinetics of the default model DTN. C_m, membrane capacitance; m, h, n, channel gating variables; α_x, β_x, gating variable dynamics functions where χ stands in for m, h, or n; V, membrane potential; $I_{Na,K,leak}$, current; $\bar{g}_{Na,K,leak}$, maximum channel conductance; $E_{Na,K,leak}$, channel reversal potential; $\dot{\chi}$, gating variable differential equation. Sodium, potassium and leak currents based on kinetics described by Traub and Miles (1991) and implemented by Destexhe et al. (1996).

DTN Model Parameters	
Soma Diameter	13 μm
C_m	1.0 μF/cm^2
Temperature	36ºC
$\dot{\chi}$	$\alpha_\chi(1 - \chi) - \beta_\chi(\chi)$
Sodium (Na) Channels	
I_{Na}	$\bar{g}_{Na}m^3h(V - E_{Na})$
α_m	$(-0.32(V + 29))/(\exp(-(V + 29)/4) - 1)$
β_m	$(0.28(V + 2))/(\exp((V + 2)/5) - 1)$
α_h	$0.128\exp(-(V + 25)/18)$
β_h	$4/(\exp((-(V + 2))/5) + 1)$
$\bar{g}_{Na}$	100 mS/cm^2
E_{Na}	50 mV
Potassium (K) Channels	
I_K	$\bar{g}_K n^4(V - E_K)$
α_n	$(-0.032(V + 27))/(\exp(-(V + 27)/5) - 1)$
β_n	$0.5\exp(-(V + 32)/40)$
$\bar{g}_K$	8 mS/cm^2
E_K	-90 mV
Passive Leak Channels	
I_{leak}	$\bar{g}_{leak}(V - E_{leak})$
$\bar{g}_{leak}$	0.25 mS/cm^2
E_{leak}	-65 mV

Table 3.3: Parameters for intrinsic membrane kinetics of the pre-synaptic excitatory model neurons. C_m, membrane capacitance; m, h, n, channel gating variables; α_x, β_x, gating variable dynamics functions where χ stands in for m, h, or n; V, membrane potential; $I_{Na,K,leak}$, current; $\bar{g}_{Na,K,leak}$, maximum channel conductance; $E_{Na,K,leak}$, channel reversal potential; $\dot{\chi}$, gating variable differential equation. Sodium, potassium and leak currents based on kinetics described by Traub and Miles (1991) and implemented by Destexhe et al. (1996).

Excitatory Pre-Synaptic Neuron Model Parameters	
Soma Diameter	10 μm
C_m	1.0 μF/cm^2
Temperature	36ºC
$\dot{\chi}$	$\alpha_\chi(1-\chi) - \beta_\chi(\chi)$
Sodium (Na) Channels	
I_{Na}	$\bar{g}_{Na}m^3h(V - E_{Na})$
α_m	$(-0.32(V+44))/(\exp(-(V+44)/4) - 1)$
β_m	$(0.28(V+17))/(\exp((V+17)/5) - 1)$
α_h	$0.128\exp(-(V+40)/18)$
β_h	$4/(\exp((-(V+17))/5) + 1)$
$\bar{g}_{Na}$	100 mS/cm^2
E_{Na}	50 mV
Potassium (K) Channels	
I_K	$\bar{g}_K n^4(V - E_K)$
α_n	$(-0.032(V+42))/(\exp(-(V+42)/5) - 1)$
β_n	$0.5\exp(-(V+47)/40)$
$\bar{g}_K$	30 mS/cm^2
E_K	-90 mV
Passive Leak Channels	
I_{leak}	$\bar{g}_{leak}(V - E_{leak})$
$\bar{g}_{leak}$	1.0 mS/cm^2
E_{leak}	-55 mV

Table 3.4: Parameters for intrinsic membrane kinetics of the pre-synaptic inhibitory model neurons. C_m, membrane capacitance; m, h, n, channel gating variables; α_x, β_x, gating variable dynamics functions where χ stands in for m, h, or n; V, membrane potential; $I_{Na,K,leak}$, current; $\bar{g}_{Na,K,leak}$, maximum channel conductance; $E_{Na,K,leak}$, channel reversal potential; $\dot{\chi}$, gating variable differential equation. Sodium, potassium and leak currents based on kinetics described by Traub and Miles (1991) and implemented by Destexhe et al. (1996).

Inhibitory Pre-Synaptic Neuron Model Parameters	
Soma Diameter	10 μm
C_m	1.0 μF/cm^2
Temperature	36°C
$\dot{\chi}$	$\alpha_\chi(1 - \chi) - \beta_\chi(\chi)$
Sodium (Na) Channels	
I_{Na}	$\bar{g}_{Na}m^3h(V - E_{Na})$
α_m	$(-0.32(V + 41))/(\exp(-(V + 41)/4) - 1)$
β_m	$(0.28(V + 14))/(\exp((V + 14)/5) - 1)$
α_h	$0.128 \exp(-(V + 37)/18)$
β_h	$4/(\exp((-(V + 14))/5) + 1)$
$\bar{g}_{Na}$	100 mS/cm^2
E_{Na}	50 mV
Potassium (K) Channels	
I_K	$\bar{g}_K n^4(V - E_K)$
α_n	$(-0.032(V + 39))/(\exp(-(V + 39)/5) - 1)$
β_n	$0.5 \exp(-(V + 44)/40)$
$\bar{g}_K$	30 mS/cm^2
E_K	-90 mV
Passive Leak Channels	
I_{leak}	$\bar{g}_{leak}(V - E_{leak})$
$\bar{g}_{leak}$	1.0 mS/cm^2
E_{leak}	-55 mV

Table 3.5: Parameters for the default, bat, rat, mouse, and frog DTN models.

DTN Model Parameters	Default	Bat[1]	Rat[2]	Mouse	Frog
Onset Excitatory Input Latency (re stimulus onset)	10 ms	12 ms	15 ms	14 ms	38 ms
Offset Excitatory Input Latency (re stimulus offset)	6 ms	14 ms	32 ms	6 ms	None
Inhibitory Input Latency (re stimulus onset)	9 ms	12 ms	15 ms / 50 ms	12 ms	29 ms
$\bar{g}_{AMPA}$	4 nS	12 nS	3 nS	1.9 nS	1.19 nS
$\bar{g}_{NMDA}$	20 nS	8 nS	12 nS	19 nS	36 nS
$\bar{g}_{GABA_A}$	2.5 nS	8 nS	3 nS / 0.8 nS	1.2 nS	0.32 nS
Membrane τ	4 ms	1.2 ms	10 ms	5 ms	9 ms

[1] Excitatory input removed for 1 ms stimuli.

[2] Short latency, strong inhibition lasting up to 35 ms; weak inhibition sustained for stimulus duration.

3.6   References

Aubie B, Becker S, Faure PA (2009) Computational models of millisecond level duration tuning in neural circuits. *J Neurosci* 29:9255–9270.

Brand A, Urban A, Grothe B (2000) Duration tuning in the mouse auditory midbrain. *J Neurophysiol* 84:1790–1799.

Brugge JF (1992) An overview of central auditory processing In Popper A, Fay R, editors, *The mammalian auditory pathway: neurophysiology*, pp. 1–33. Springer-Verlag, New York.

Burger RM, Pollak GD (1998) Analysis of the role of inhibition in shaping responses to sinusoidally amplitude-modulated signals in the inferior colliculus. *J Neurophysiol* 80:1686–1701.

Carnevale NT, Hines ML (2006) *The NEURON book* Cambridge University Press, Cambridge, UK.

Casseday JH, Ehrlich D, Covey E (1994) Neural tuning for sound duration: role of inhibitory mechanisms in the inferior colliculus. *Science* 264:847–850.

Casseday JH, Ehrlich D, Covey E (2000) Neural measurement of sound duration: control by excitatory-inhibitory interactions in the inferior colliculus. *J Neurophysiol* 84:1475–1487.

Charles K, Evans M, Robbins M, Calver A, Leslie R, Pangalos M (2001) Comparative immunohistochemical localisation of $GABA_{B1a}$, $GABA_{B1b}$ and $GABA_{B2}$ subunits in rat brain, spinal cord and dorsal root ganglion. *Neuroscience* 106:447–467.

Charuchinda C, Supavilai P, Karobath M, Palacios J (1987) Dopamine D2 receptors in the rat brain: autoradiographic visualization using a high-affinity selective agonist ligand. *J Neurosci* 7:1352–1360.

Chen GD (1998) Effects of stimulus duration on responses of neurons in the chinchilla inferior colliculus. *Hear Res* 112:142–150.

Covey E, Casseday JH (1991) The monaural nuclei of the lateral lemniscus in an echolocating bat: parallel pathways for analyzing temporal features of sound. *J Neurosci* 11:3456–3470.

Covey E, Kauer JA, Casseday JH (1996) Whole-cell patch-clamp recording reveals subthreshold sound-evoked postsynaptic currents in the inferior colliculus of awake bats. *J Neurosci* 16:3009–3018.

Destexhe A, Bal T, McCormick DA, Sejnowski TJ (1996) Ionic mechanisms underlying synchronized oscillations and propagating waves in a model of ferret thalamic slices. *J Neurophysiol* 76:2049–2070.

Destexhe A, Mainen ZF, Sejnowski TJ (1998) Kinetic models of synaptic transmission In Koch C, Segev I, editors, *Methods in neuronal modeling*, pp. 1–25. MIT Press, Cambridge, MA.

Duysens J, Schaafsma SJ, Orban GA (1996) Cortical off response tuning for stimulus duration. *Vision Res* 36:3243–3251.

Ehrlich D, Casseday JH, Covey E (1997) Neural tuning to sound duration in the inferior colliculus of the big brown bat, *Eptesicus fuscus*. *J Neurophysiol* 77:2360–2372.

Faure PA, Fremouw T, Casseday JH, Covey E (2003) Temporal masking reveals properties of sound-evoked inhibition in duration-tuned neurons of the inferior colliculus. *J Neurosci* 23:3052–3065.

Felix II RA, Fridberger A, Leijon S, Berrebi AS, Magnusson AK (2011) Sound rhythms are encoded by postinhibitory rebound spiking in the superior paraolivary nucleus. *J Neurosci* 31:12566–12578.

Frederiksen E (1977) Condenser microphones used as sound sources. *Bruël Kjær Technical Review* 3:3–23.

Fremouw T, Faure PA, Casseday JH, Covey E (2005) Duration selectivity of neurons in the inferior colliculus of the big brown bat: tolerance to changes in sound level. *J Neurophysiol* 94:1869–1878.

Fubara BM, Casseday JH, Covey E, Schwartz-Bloom RD (1996) Distribution of $GABA_A$, $GABA_B$, and glycine receptors in the central auditory system of the big brown bat, *Eptesicus fuscus*. *J Comp Neurol* 369:83–92.

Fukui I, Burger RM, Ohmori H, Rubel EW (2010) GABAergic inhibition sharpens the frequency tuning and enhances phase locking in chicken nucleus magnocellularis neurons. *J Neurosci* 30:12075–12083.

Fuzessery ZM, Hall JC (1996) Role of GABA in shaping frequency tuning and creating FM sweep selectivity in the inferior colliculus. *J Neurophysiol* 76:1059–1073.

Fuzessery ZM, Hall JC (1999) Sound duration selectivity in the pallid bat inferior colliculus. *Hear Res* 137:137–154.

Fuzessery ZM, Pollak GD (1985) Determinants of sound location selectivity in bat inferior colliculus: a combined dichotic and free-field stimulation study. *J Neurophysiol* 54:757–781.

Fuzessery ZM, Wenstrup JJ, Hall JC, Leroy S (2002) Inhibition has little effect on response latencies in the inferior colliculus. *JARO* 4:60–73.

Galazyuk AV, Feng AS (1997) Encoding of sound duration by neurons in the auditory cortex of the little brown bat, *Myotis lucifugus*. *J Comp Physiol A* 180:301–311.

Galazyuk AV, Feng AS (2001) Oscillation may play a role in time domain central auditory processing. *J Neurosci* 21:RC147 (1–5).

Galazyuk AV, Lin W, Llano D, Feng AS (2005) Leading inhibition to neural oscillation is important for time-domain processing in the auditory midbrain. *J Neurophysiol* 94:314–326.

Gittelman JX, Pollak GD (2011) It's about time: how input timing is used and not used to create emergent properties in the auditory system. *J Neurosci* 31:2576–2583.

Gittelman JX, Li N, Pollak GD (2009) Mechanisms underlying directional selectivity for frequency-modulated sweeps in the inferior colliculus revealed by *in vivo* whole-cell recordings. *J Neurosci* 29:13030–13041.

Gooler DM, Feng AS (1992) Temporal coding in the frog auditory midbrain: the influence of duration and rise-fall time on the processing of complex amplitude-modulated stimuli. *J Neurophysiol* 67:1–22.

Grothe B, Covey E, Casseday JH (2001) Medial superior olive of the big brown bat: neuronal responses to pure tones, amplitude modulations, and pulse trains. *J Neurophysiol* 86:2219–2230.

Grothe B, Park TJ, Schuller G (1997) Medial superior olive in the free-tailed bat: response to pure tones and amplitude-modulated tones. *J Neurophysiol* 77:1553–1565.

Grothe B (1994) Interaction of excitation and inhibition in processing of pure tone and amplitude-modulated stimuli in the medial superior olive of the mustached bat. *J Neurophysiol* 71:706–721.

Guinan J, Guinan S, Norris B (1972) Single auditory units in the superior olivary complex: I: responses to sounds and classifications based on physiological properties. *Int J Neurosci* 4:101–120.

Haplea S, Covey E, Casseday JH (1994) Frequency tuning and response latencies at three levels in the brainstem of the echolocating bat, *Eptesicus fuscus*. *J Comp Physiol A* 174:671–683.

Harty TP, Manis PB (1998) Kinetic analysis of glycine receptor currents in ventral cochlear nucleus. *J Neurophysiol* 79:1891–1901.

He J, Hashikawa T, Ojima H, Kinouchi Y (1997) Temporal integration and duration tuning in the dorsal zone of cat auditory cortex. *J Neurosci* 17:2615–2625.

Hechavarría JC, Cobo AT, Fernández Y, Macías S, Kössl M, Mora EC (2011) Sound-evoked oscillation and paradoxical latency shift in the inferior colliculus of the big fruit-eating bat, *Artibeus jamaicensis*. *J Comp Physiol A* 197:1159–1172.

Hines ML, Davison AP, Muller E (2009) NEURON and Python. *Front Neuroinform* 3:1–12.

Hooper SL, Buchman E, Hobbs KH (2002) A computational role for slow conductances: single-neuron models that measure duration. *Nat Neurosci* 5:552–556.

Hurley LM (2007) Activation of the serotonin 1A receptor alters the temporal characteristics of auditory responses in the inferior colliculus. *Brain Res* 1181:21–29.

Hurley LM, Pollak GD (2005) Serotonin shifts first-spike latencies of inferior colliculus neurons. *J Neurosci* 25:7876–7886.

Hurley LM, Thompson AM, Pollak GD (2002) Serotonin in the inferior colliculus. *Hear Res* 168:1–11.

Hurley LM, Tracy JA, Bohorquez A (2008) Serotonin 1B receptor modulates frequency response curves and spectral integration in the inferior colliculus by reducing GABAergic inhibition. *J Neurophysiol* 100:1656–1667.

Jahr C, Stevens C (1990) Voltage dependence of NMDA-activated macroscopic conductances predicted by single-channel kinetics. *J Neurosci* 10:3178–3182.

Jen PHS, Feng RB (1999) Bicuculline application affects discharge pattern and pulse-duration tuning characteristics of bat inferior collicular neurons. *J Comp Physiol A* 184:185–194.

Jen PHS, Kamada T (1982) Analysis of orientation signals emitted by the CF-FM bat, *Pteronotus p. parnellii* and the FM bat, *Eptesicus fuscus* during avoidance of moving and stationary obstacles. *J Comp Physiol A* 148:389–398.

Jen PHS, Schlegel PA (1982) Auditory physiological properties of the neurones in the inferior colliculus of the big brown bat, *Eptesicus fuscus*. *J Comp Physiol A* 147:351–363.

Jen PHS, Wu CH (2005) The role of GABAergic inhibition in shaping the response size and duration selectivity of bat inferior collicular neurons to sound pulses in rapid sequences. *Hear Res* 202:222–234.

Kadner A, Kulesza RJ, Berrebi AS (2006) Neurons in the medial nucleus of the trapezoid body and superior paraolivary nucleus of the rat may play a role in sound duration coding. *J Neurophysiol* 95:1499–1508.

Kiang NYS (1965) *Discharge patterns of single fibers in the cat's auditory nerve* MIT Press, Cambridge, MA.

Klug A, Bauer EE, Pollak GD (1999) Multiple components of ipsilaterally evoked inhibition in the inferior colliculus. *J Neurophysiol* 82:593–610.

Kopp-Scheinpflug C, Tozer AJB, Robinson SW, Tempel BL, Hennig MH, Forsythe ID (2011) The sound of silence: ionic mechanisms encoding sound termination. *Neuron* 71:911–925.

Kössl M, Vater M (1985) The cochlear frequency map of the mustache bat, *Pteronotus parnellii*. *J Comp Physiol A* 157:687–697.

Leary CJ, Edwards CJ, Rose GJ (2008) Midbrain auditory neurons integrate excitation and inhibition to generate duration selectivity: an *in vivo* whole-cell patch study in anurans. *J Neurosci* 28:5481–5493.

Luo F, Metzner W, Wu F, Wu FJ, Zhang S, Zhang SY, Chen Q, Chen QC (2008) Duration-sensitive neurons in the inferior colliculus of horseshoe bats: adaptations for using CF-FM echolocation pulses. *J Neurophysiol* 99:284–296.

Ma CL, Kelly JB, Wu SH (2002a) Presynaptic modulation of GABAergic inhibition by GABA$_B$ receptors in the rat's inferior colliculus. *Neuroscience* 114:207–215.

Ma CL, Kelly JB, Wu SH (2002b) AMPA and NMDA receptors mediate synaptic excitation in the rat's inferior colliculus. *Hear Res* 168:25–34.

Ma X, Suga N (2001) Corticofugal modulation of duration-tuned neurons in the midbrain auditory nucleus in bats. *PNAS* 98:14060–14065.

McAlpine D, Jiang D, Shackleton T, Palmer A (1998) Convergent input from brainstem coincidence detectors onto delay-sensitive neurons in the inferior colliculus. *J Neurosci* 18:6026–6039.

Mora EC, Kössl M (2004) Ambiguities in sound duration selectivity by neurons in the inferior colliculus of the bat *Molossus molossus* from Cuba. *J Neurophysiol* 91:2215–2226.

Narins PM, Capranica RR (1980) Neural adaptations for processing the two-note call of the Puerto Rican treefrog, *Eleutherodactylus coqui*. *Brain Behav Evol* 17:48–66.

Nayagam DAX, Clarey JC, Paolini AG (2005) Powerful, onset inhibition in the ventral nucleus of the lateral lemniscus. *J Neurophysiol* 94:1651–1654.

Oliver DL, Beckius GE, Shneiderman A (1995) Axonal projections from the lateral and medial superior olive to the inferior colliculus of the cat: a study using electron microscopic autoradiography. *J Comp Neurol* 360:17–32.

Pérez-González D, Malmierca MS, Moore JM, Hern a ndez O, Covey E (2006) Duration selective neurons in the inferior colliculus of the rat: topographic distribution and relation of duration sensitivity to other response properties. *J Neurophysiol* 95:823–836.

Peruzzi D, Dut A (2004) GABA, serotonin and serotonin receptors in the rat inferior colliculus. *Brain Res* 998:247–250.

Pfeiffer R (1966) Classification of response patterns of spike discharges for units in the cochlear nucleus: tone-burst stimulation. *Exp Brain Res* 1:220–235.

Pollak GD, Bodenhamer RD (1981) Specialized characteristics of single units in inferior colliculus of mustache bat: frequency representation, tuning, and discharge patterns. *J Neurophysiol* 46:605–620.

Pollak GD, Park TJ (1993) The effects of GABAergic inhibition on monaural response properties of neurons in the mustache bat's inferior colliculus. *Hear Res* 65:99–117.

Pollak GD, Xie R, Gittelman JX, Andoni S, Li N (2011) The dominance of inhibition in the inferior colliculus. *Hear Res* 274:27–39.

Potter HD (1965) Patterns of acoustically evoked discharges of neurons in the mesencephalon of the bullfrog. *J Neurophysiol* 28:1155–1184.

Pourcho RG, Goebel DJ, Jojich L, Hazlett JC (1992) Immunocytochemical evidence for the involvement of glycine in sensory centers of the rat brain. *Neuroscience* 46:643–656.

Qin L, Liu Y, Wang J, Li S, Sato Y (2009) Neural and behavioral discrimination of sound duration by cats. *J Neurosci* 29:15650–15659.

Rose JE, Gross N, Geisler C, Hind JE (1966) Some neural mechanisms in the inferior colliculus of the cat which may be relevant to localization of a sound source. *J Neurophysiol* 29:288–314.

Rothman JS, Manis PB (2003) The roles potassium currents play in regulating the electrical activity of ventral cochlear nucleus neurons. *J Neurophysiol* 89:3097–3113.

Sanchez JT, Gans D, Wenstrup JJ (2007) Contribution of NMDA and AMPA receptors to temporal patterning of auditory responses in the inferior colliculus. *J Neurosci* 27:1954–1963.

Sayegh R, Aubie B, Faure PA (2011) Duration tuning in the auditory midbrain of echolocating and non-echolocating vertebrates. *J Comp Physiol A* 197:571–583.

Stapells DR, Picton TW, Smith AD (1982) Normal hearing thresholds for clicks. *J Acoust Soc Am* 72:74–79.

Straughan IR (1975) An analysis of the mechanisms of mating call discrimination in the frogs *Hyla regilla* and *H. cadaverina*. *Copeia* 3:415–424.

Suga N, Simmons J, Jen PH (1975) Peripheral specialization for fine analysis of doppler-shifted echoes in the auditory system of the "CF-FM" bat *Pteronotus parnellii*. *J Exp Bio* 63:161–192.

Suga N, Jen PHS (1976) Disproportionate tonotopic representation for processing CF-FM sonar signals in the mustache bat auditory cortex. *Science* 194:542–544.

Sun H, Ma CL, Kelly JB, Wu SH (2006) GABA$_B$ receptor-mediated presynaptic inhibition of glutamatergic transmission in the inferior colliculus. *Neurosci Lett* 399:151–156.

Tan ML, Borst JGG (2007) Comparison of responses of neurons in the mouse inferior colliculus to current injections, tones of different durations, and sinusoidal amplitude-modulated tones. *J Neurophysiol* 98:454–466.

Tang ZQ, Hoang Dinh E, Shi W, Lu Y (2011) Ambient GABA-activated tonic inhibition sharpens auditory coincidence detection via a depolarizing shunting mechanism. *J Neurosci* 31:6121–6131.

Traub RD, Miles R (1991) *Neuronal networks of the hippocampus* Cambridge University Press, Cambridge, UK.

Vater M, Covey E, Casseday JH (1997) The columnar region of the ventral nucleus of the lateral lemniscus in the big brown bat (*Eptesicus fuscus*): synaptic arrangements and structural correlates of feedforward inhibitory function. *Cell Tissue Res* 289:223–233.

Vater M, Habbicht H, Kössl M, Grothe B (1992) The functional role of GABA and glycine in monaural and binaural processing in the inferior colliculus of horseshoe bats. *J Comp Physiol A* 171:541–553.

Wang J, van Wijhe R, Chen Z, Yin S (2006) Is duration tuning a transient process in the inferior colliculus of guinea pigs? *Brain Res* 1114:63–74.

Wehr M, Zador AM (2003) Balanced inhibition underlies tuning and sharpens spike timing in auditory cortex. *Nature* 426:442–446.

Wenstrup J, Leroy SA (2001) Spectral integration in the inferior colliculus: role of glycinergic inhibition in response facilitation. *J Neurosci* 21:RC124 (1–6).

Wu GK, Arbuckle R, Liu BH, Tao HW, Zhang LI (2008) Lateral sharpening of cortical frequency tuning by approximately balanced inhibition. *Neuron* 58:132–143.

Wu GK, Li P, Tao HW, Zhang LI (2006) Nonmonotonic synaptic excitation and imbalanced inhibition underlying cortical intensity tuning. *Neuron* 52:705–715.

Xia YF, Qi ZH, Shen JX (2000) Neural representation of sound duration in the inferior colliculus of the mouse. *Acta Otolaryngol* 120:638–643.

Xie R, Gittelman JX, Li N, Pollak GD (2008) Whole cell recordings of intrinsic properties and sound-evoked responses from the inferior colliculus. *Neuroscience* 154:245–256.

Yavuzoglu A, Schofield BR, Wenstrup JJ (2011) Circuitry underlying spectrotemporal integration in the auditory midbrain. *J Neurosci* 31:14424–14435.

Yin S, Chen Z, Yu D, Feng Y, Wang J (2008) Local inhibition shapes duration tuning in the inferior colliculus of guinea pigs. *Hear Res* 237:32–48.

Zhang H, Kelly JB (2001) AMPA and NMDA receptors regulate responses of neurons in the rat's inferior colliculus. *J Neurophysiol* 86:871–880.

Zhang H, Kelly JB (2010) Time dependence of binaural responses in the rat's central nucleus of the inferior colliculus. *Hear Res* 268:271–280.

Zhou X, Jen PH (2001) The effect of sound intensity on duration-tuning characteristics of bat inferior collicular neurons. *J Comp Physiol A* 187:63–73.

Zorović M (2011) Temporal processing of vibratory communication signals at the level of ascending interneurons in *Nezara viridula* (Hemiptera: Pentatomidae). *PLoS One* 6:e26843.

4

Estimating stimulus duration from neurons in the auditory midbrain of the big brown bat, *Eptesicus fuscus*

Preamble

This chapter is a preliminary version of a manuscript to be co-authored with Riziq Sayegh, Thane Fremouw, John H. Casseday, Ellen Covey and Paul A. Faure. The version included in this thesis uses data collected by all of these individuals but was written solely by Brandon Aubie.

Introduction to Manuscript

Thus far, this dissertation has been concerned with the mechanisms responsible for generating DTN responses. In this chapter, I analyze the effectiveness of those responses for encoding stimulus duration. *In vivo* responses from 97 big brown bat DTNs collected with sound pulses presented at +20 dB relative to threshold were combined from electrophysiological data collected at the University of Washington by Paul A. Faure, Thane Fremouw, John H. Casseday and Ellen Covey along with data collected at McMaster University by Brandon Aubie and Riziq Sayegh. SpikeDB (Written by Brandon Aubie; see Appendix D) was used extensively for individual and population level DTN response analyses. This study originated with the question of whether or not DTNs in the bat followed Weber's Law but has since become a more in depth analysis of the encoding performance of DTNs both individually and as a population.

4.1 Introduction

Duration-tuned neurons (DTNs) respond selectivity to only particular stimulus durations and may be used by the brain to encode temporal information about a stimulus. Duration-tuned neurons were first observed along the auditory midbrain of frogs subsequently found in many vertebrate species (see Sayegh et al., 2011, for review) and have been especially well characterized in echolocating bats. While the physiological response properties and mechanisms of DTNs are beginning to be understood, what remains to be understood is how the responses of DTNs are used within the nervous system.

Historically, DTNs have been characterized by their duration tuning response profile and best duration (BD), defined as the duration that evokes the highest mean spike count (Casseday et al., 1994, 2000; Ehrlich et al., 1997; Faure et al., 2003; Aubie et al., 2009; Sayegh et al., 2011; Aubie et al., 2012), however; it is not obvious that peak spike count best describes the encoding characteristics of the neuron.

In this study we measure the information content and the response sensitivity of DTNs from the central nucleus of the inferior colliculus (IC) of the big brown bat, *Eptesicus fuscus*. We apply optimal and non-optimal Bayesian decoding methods to both spike counts and first-spike latencies (FSLs) of individual DTNs and a population of DTNs to characterize the robustness and sensitivity of duration encoding. Finally, we use population responses to model a two-alternative forced choice classification task to estimate the Weber fraction of population level encoding of duration. We find that DTNs robustly encode stimulus duration in both spike counts and spike latency and that the Weber fractions we calculate from neural responses are within the range of expected values based on behavioural data available from other species.

4.2 Methods

4.2.1 Electrophysiology

Extracellular recordings of 97 DTNs (51 at McMaster University, 46 at the University of Washington) from the central nucleus of the big brown bat, *Eptesicus fuscus*, were were obtained from 47 adult animals of either sex (27 at McMaster University, 20 at the University of Washington). Procedures for single unit, extracellular recordings from the central nucleus

of the awake big brown bat IC are reported in detail elsewhere (Faure et al., 2003; Aubie et al., 2012). Briefly, a steel post was affixed to the dorsal surface of the skull with cyanoacrylate superglue 24 to 48 hours prior to the first recording session. A chlorided silver wire glued to the steel post was place beneath the right temporal muscle to serve as a reference electrode. For the first recording session, a scalpel was used to cut a small hole in the skull and dura matter over the dorsal surface of the IC. Thin-wall borosilicate glass microelectrodes with resistances ranging from 10 to 30 MΩ were advanced into the brain at 1 μm intervals by a hydraulic micropositioner. Action potential times relative to stimulus presentations were recorded on a PC for offline analysis. Recordings lasting 4 to 6 hours were performed over 1 to 6 days for each bat. All procedures performed at the University of Washington were approved by the University of Washington Laboratory Animal Care and Use Committee. All procedures performed at McMaster University were approved by the McMaster University Animal Research Ethics Board and were in accordance with the Canadian Council on Animal Care.

Stimulus generation and online data collection were controlled with custom software. Pure tone sound pulses were digitally generated, fed through a digital-to-analog converter, low-pass filtered for anti-aliasing, amplified, and presented either monaurally ca. 1 mm in front of the contralateral ear with a 1/4 inch condenser microphone modified for use as a loudspeaker (88 / 97 DTNs), or in free space with a free-field electrostatic speaker (TDT ES1) positioned 30 cm from the bat's head at 30º from midline contralateral to the recording site (9 / 97 DTNs). All stimuli had square cosine shaped rise/fall times of 0.4 - 0.5 ms and were presented at a rate of 3 Hz.

Single units were isolated by searching with a variety of stimulus frequencies, durations and amplitudes until action potentials were observed. Once a cell was located, the best excitatory frequency, amplitude threshold, and duration tuning characteristics were determined. Duration tuning profiles were determined with best excitatory frequency tones at several stimulus amplitudes. When possible, responses were obtained at threshold and at +10 dB, +20 dB and +30 dB relative to threshold; however, only a subset of amplitudes were recorded for many DTNs. Each stimulus duration from 1 to 25 ms (1 ms steps) was tested in random order and was presented 10 to 20 times.

4.2.2 Single Neuron Analysis

Spike times were windowed to include spikes occurring after stimulus onset and up to 50 ms from stimulus offset. Separate analyses were performed on stimuli presented at different sound pressure levels (SPLs) relative to threshold. When none of those four amplitudes re threshold were available, but recordings within 10 dB of a bin was available, files were binned to the nearest amplitude rounding down to the nearest 10 dB. There was little to no difference in results across stimulus amplitudes and thus we only present responses collected at +20 dB re threshold[1]. In previous DTN studies, a DTN's response was required to drop to 50% of maximum at shorter and/or longer stimulus durations from BD to be classified as a DTN (Faure et al., 2003); however, we included some cells that appeared duration-tuned but did not meet this criteria. Furthermore, the peak spike count at BD must have been at least an average of 0.6 spikes per trial. The BD was defined as the midpoint (average) of the longer and shorter values of the durations with $\geq 90\%$ of the maximum spike count (Fremouw et al., 2005). This permitted the calculated BD to occur between tested stimulus durations when peak spiking responses at multiple durations were similar. All analyses were performed with SpikeDB[2] (http://spikedb.aubie.ca) and the Python programming language (http://www.python.org).

Characterizing Spontaneous Activity

To measure spontaneous activity, we counted spikes occurring at least 100 ms from stimulus offset (well after typical stimulus evoked spiking responses) to the end of a recording trial and divided by the total amount of observed time. Spike counts were performed on recordings done at least 2 minutes before cell death to ensure an accurate estimation of spontaneous activity. Spontaneous activity in DTNs and non-DTNs were compared with a Mann-Whitney U non-parametric statistical hypothesis test (Zar, 1984).

Spike Count Distribution

Reporting the mean spike counts implicitly presumes that the mean accurately represents the distribution of all observed spike counts. We applied the Shapiro-Wilk test for normality to the distribution of spike counts evoked across stimulus durations to our population of

---

[1]Additional analyses across all stimulus amplitudes are presented in Appendix C
[2]Additional details on SpikeDB are available in Appendix D

DTNs and found non-normally distributed spike counts in the majority of cases. Therefore, our analysis uses the explicitly observed spiking probability, $\Pr(s|\mathbf{d})$, where s denotes the number of spikes evoked by a stimulus of duration $\mathbf{d}$.

Information and Sensitivity Measures

The response distribution of a DTN was first characterized by the stimulus-specific information (SSI) measure (Butts, 2003) as implemented by Montgomery and Wehr (2010),

$$SSI(\mathbf{d}) = \sum_{i \in S} \Pr(s_i|\mathbf{d})i(s_i)$$

$$i(s) = -\sum_{\mathbf{d} \in D} \Pr(\mathbf{d}) \log_2 \Pr(\mathbf{d}) + \sum_{\mathbf{d} \in D} \Pr(\mathbf{d}|s) \log_2 \Pr(\mathbf{d}|s)$$

where $i(s_i)$ is the specific information conveyed by spike count s_i (DeWeese and Meister, 1999), D is the set of all tested durations and S is the set of all spike counts. Stimulus-specific information can be understand in relation to mutual information; the reduction of uncertainty of a random variable (stimulus) given the knowledge of another random variable (response). Unlike mutual information that operates under the knowledge of the entire response distribution, specific information quantifies the reduction in uncertainty given a *specific* response value. Stimulus-specific information is then a measure of the expected specific information for a particular stimulus presentation. Intuitively, SSI is a measure of the expected reduction in uncertainty about a stimulus after observing a response evoked by that stimulus. Alternatively, SSI can be thought of as a measure of representation uniqueness within a system. A stimulus with high SSI will have a relatively unique encoding across the entire stimulus domain, allowing one to gain high informartion about the stimulus given a response evoked by that stimulus. A stimulus with low SSI will have a relatively common representation relative to other stimuli resulting in high levels of stimulus uncertainty even after observing a typical response.

In addition to calculating the SSI for each stimulus duration, we also estimated the observed Fisher information (FI), $\mathcal{I}_{\text{est}}(\mathbf{d})$, defined as[3]

$$\mathcal{I}_{\text{est}}(\mathbf{d}) = -\mathrm{E}\left[\frac{\partial^2}{\partial \mathbf{d}^2} \ln \Pr(\mathbf{S}|\mathbf{d}) \Big| \mathbf{d}\right] = \mathrm{E}\left[\left(\frac{\partial}{\partial \mathbf{d}} \ln(\Pr(\mathbf{S}|\mathbf{d}))\right)^2 \Big| \mathbf{d}\right]$$

---

[3]For further details on this equivalency, see Equation C.1 in Appendix C.

where $\ln$ denotes the natural logarithm, base e (Kay, 1993). Fisher information is a measure of the average slope of the log response distribution (spike count probability distribution) along the stimulus domain. The Cramér-Rao bound is a lower bound of the variance of an unbiased estimator of a stimulus (Kay, 1993), which in the context of this study can be written as

$$\mathrm{Var}[\hat{\mathbf{d}}] \geq 1/\mathcal{I}_{\mathrm{est}}(\mathbf{d}).$$

Fisher information is therefore the inverse of the minimum variance of an optimal stimulus estimator. A stimulus with high FI will be decoded with low variance along the stimulus domain. In other words, high FI implies that the response distributions of immediately nearby stimuli are significantly different. Unlike SSI that measures the uniqueness of stimulus encoding across the entire stimulus domain (i.e. globally), FI is a measure of the uniqueness of stimulus encoding relative to immediately adjacent stimuli (i.e. locally). Therefore, FI can be used as a measure of a system's ability to robustly encode a gradually changing stimulus. As a stimulus value changes, high FI implies that the response distribution will change sharply and thus precisely represent the stimulus with relatively unique representations. Low FI and the associated higher minimum decoding variance means that nearby stimulus values would be less distinguishable within the variance of the decoder's estimate of the stimulus.

Because our data provides only discrete values of $\Pr(s|\mathbf{d})$ for all spike counts s and stimulus durations $\mathbf{d}$, we could not compute the first (or second) derivative of this distribution as required for calculating the actual observed FI. Instead, we estimated the slope of the probability distribution for durations in-between recorded stimulus durations ($\mathbf{d}_{\mathrm{mid}} = \mathbf{d} + 0.5$ ms) where we can approximate the derivative of $\ln(\Pr(s|\mathbf{d}))$ from the difference of adjacent stimulus duration spiking probabilities. Using this formulation, the estimated FI can be written as the expected value of the square of the first derivative of the natural logarithm of the probability density function (Dayan and Abbott, 2001). Therefore, the FI becomes a function of the change in the probability distribution over duration, $\mathbf{d}$.

$$
\begin{aligned}
&\mathcal{I}_{\text{est}}(\mathbf{d}_{\text{mid}} = \mathbf{d} + 0.5) \\
&= \mathrm{E}\left[\left(\tfrac{\partial}{\partial \mathbf{d}} \ln(\Pr(\mathbf{S}|\mathbf{d}_{\text{mid}}))\right)^2 \Big| \mathbf{d}_{\text{mid}}\right] \\
&= \sum_{i \in \mathbf{S}} \tfrac{1}{2}\left(\Pr(s_i|\mathbf{d}+1) + \Pr(s_i|\mathbf{d})\right)\left[\left(\tfrac{d}{d\mathbf{d}} \ln(\Pr(s_i|\mathbf{d}_{\text{mid}}))\right)^2 \Big| \mathbf{d}_{\text{mid}}\right] \\
&= \tfrac{1}{2}\sum_{i \in \mathbf{S}}\left(\Pr(s_i|\mathbf{d}+1) + \Pr(s_i|\mathbf{d})\right)\left[\left(\ln(\Pr(s_i|\mathbf{d}+1)) - \ln(\Pr(s_i|\mathbf{d}))\right)^2 \Big| \mathbf{d}\right]
\end{aligned}
$$

where $\mathbf{S}$ is a vector of all spike counts, s_i is the ith spike count and $\mathbf{d}+1$ is the stimulus duration 1 ms longer than $\mathbf{d}$. Fisher information can take any value between 0 and ∞, where 0 represents no change in response probabilities and ∞ represents a change from nonzero to zero probabilities, or vice versa. To avoid infinite FI values, we limited the maximum FI value by setting zero spiking probability values to $1/10^{100}$. This limiting could decrease the absolute difference in FI values across stimulus durations but would not change the ordering. As a result of these approximations, the absolute FI values we calculated were not particularly meaningful; however, relative FI values across stimulus durations were relevant to quantify changes in response sensitivity. Therefore, only FI values normalized to 1 are reported. We estimated FI values with spike first-spike latencies in a similar manner to spike counts except with $\Pr(s_i|\mathbf{d}_{\text{mid}})$ replaced with $\Pr(l_i|\mathbf{d}_{\text{mid}})$, where l_i is the FSL of the ith as defined in *Decoding Stimulus Duration from First-Spike Latency*.

Decoding Stimulus Duration from Spike Counts

For each DTN, a spike count probability given a stimulus duration, $\Pr(s|\mathbf{d})$, was calculated that represents the probability of producing s spikes when presented with a stimulus of duration, $\mathbf{d} \in [1, 2, 3, \ldots, 25\text{ ms}]$. Our population of neurons included 10 DTNs tested with stimulus durations from 1 to 15 ms. Because these cells had a zero or nearly zero spiking probability at the longest stimulus durations tested, they were arbitrarily assigned a zero spiking probability for durations longer than 15 ms.

We also calculated alternative spike count probabilities that ignored zero spike counts by forcing $\Pr(s = 0|\mathbf{d}) = 0$ for all stimulus durations. We did so to characterize the responses when no external cue for a stimulus is available. Therefore, a zero spike response was equivalent to no stimulus being presented.

To calculate the posterior probability distribution, $\Pr(\mathbf{d}|s)$, we applied Bayes' formula. We chose a naïve prior, $\Pr(\mathbf{d}) = 1/25$ for all $\mathbf{d}$, to produce a conservative posterior probability estimation. The posterior probability represents the probability of a particular stimulus duration given the observation of a particular spike count.

$$\Pr(\mathbf{d}|s) = \frac{\Pr(s|\mathbf{d})\,\Pr(\mathbf{d})}{\sum_{i=1}^{25}\Pr(s|\mathbf{d}_i)\,\Pr(\mathbf{d}_i)}$$

The posterior probability, $\Pr(\mathbf{d}|s)$, which is the probability of a stimulus duration $\mathbf{d}$ given a spike count s, characterizes a DTN by both spike counts and spike count variability. From the response probabilities and the posterior probabilities, we computed the decoded duration probability distribution matrix, $\mathbf{DUR}$, over all stimulus durations where the probability of duration $\mathbf{d}$ given the presentation of duration $\mathbf{d}_{\text{pres}}$ by

$$\mathbf{DUR}_{\mathbf{d}_{\text{pres}},\mathbf{d}} = \Pr(\mathbf{d}|\mathbf{d}_{\text{pres}}) = \sum_i \Pr(\mathbf{d}|s_i)\,\Pr(s_i|\mathbf{d}_{\text{pres}}).$$

Decoding Stimulus Duration from First-Spike Latency

Decoding stimulus duration from FSL (relative to stimulus onset) was similar to decoding stimulus duration from spike counts, except that we replaced $\Pr(s|\mathbf{d})$ with $\Pr(l|\mathbf{d})$, where l is FSL. The distribution of FSLs for a given stimulus duration was approximately normal (Shapiro-Wilks tests; data not shown). Therefore, we calculated the probability of a spike latency l from a normal distribution fitted to the FSLs of each stimulus duration. In cases where only 1 spike was produced over all trials at a particular duration (and thus the variance in spike time was 0), we set the variance to 1 ms. To mirror the methods of the spike count analysis, we discretized the normal distributions into 0.5 ms bins and integrated the normal curve within each 0.5 ms bin to calculate the probability of a spike occurring within each interval. Therefore, the probability of a spike with latency l was calculated as the probability of a spike occurring in the ith 0.5 ms window, $[l_i, l_i + 0.5]$, where $l_i \leq l \leq l_i + 0.5$.

$$\Pr(\mathbf{d}|l) = \frac{\Pr(l|\mathbf{d})\,\Pr(\mathbf{d})}{\sum_{i=1}^{25}\Pr(l|\mathbf{d}_i)\,\Pr(\mathbf{d}_i)}$$

$$\Pr(l|\mathbf{d}) = \Pr(s \geq 1|\mathbf{d})\int_{l_i}^{l_i+0.5} \mathcal{N}(x; \mu_{\mathbf{d}}, \sigma_{\mathbf{d}})\,\mathrm{d}x$$

where $\mu_{\mathbf{d}}$ is the mean FSL for duration $\mathbf{d}$, $\sigma_{\mathbf{d}}$ is the standard deviation of the FSL for duration $\mathbf{d}$ and $\mathcal{N}$ represents the normal distribution probability density function. Producing the decoded duration probability distribution matrix with FSLs then proceeded exactly the same way as with the spike count method.

4.2.3 Population Analysis

Decoding Stimulus Duration

Computing the expected optimal duration decoding matrix from population responses requires determining the joint response probabilities over all possible population responses. Due to the infeasibility of this calculation we could not calculate it directly. For example, if N DTNs each produced x different spike counts with non-zero probability, calculating the expected optimal population duration decoding matrix would require x^N joint probability calculations. To approximate the optimal duration decoding matrix, we applied a Monte Carlo procedure and took advantage of the fact that posterior probability distributions with naïve priors are proportional to the response probability distributions (i.e. $\Pr(\mathbf{d}|S) \propto \Pr(S|\mathbf{d})$). In other words, we performed maximum likelihood optimization since no prior information was not taken into account. First, spike counts were randomly selected from $\Pr(s|\mathbf{d}_{\mathrm{pres}})$ for $T = 100{,}000$ trials. The posterior probability was then estimated by averaging the responses from all trials.

$$\Pr(\mathbf{d}|S_{\mathrm{sample}}) \propto \frac{\sum_{i=1}^{T}\left(\prod_{j \in \mathrm{DTNs}} \Pr(s_i|\mathbf{d}_{\mathrm{pres}}, \mathrm{DTN}_j)\right)}{T}$$

$$\Pr(\mathbf{d}|\mathbf{d}_{\mathrm{pres}}) \approx \frac{\Pr(\mathbf{d}|S_{\mathrm{sample}})}{\sum_{\mathbf{d}_i=1}^{25} \Pr(\mathbf{d}_i|S_{\mathrm{sample}})}$$

where S_{sample} represents the averaged spiking response over all trials and s_i is the ith randomly selected spike count from the jth DTN's spike probability distribution, $\Pr(s|\mathbf{d}_{\mathrm{pres}}, \mathrm{DTN}_j)$.

A non-optimal alternative that is computationally more efficient to calculate is the average duration decoding matrix over all DTNs,

$$\mathbf{DUR}_{\mathrm{pop}} = \mathbf{Avg}_{i \in \mathrm{DTNs}} (\mathbf{DUR}_i)$$

where $\mathbf{Avg}_i(\mathbf{X_i})$ calculates the average of each entry across all matrices as indexed by i.

To visualize the relative probabilities of decoded durations, we also produced an alternative duration decoding matrix with rows scaled to the maximum value within that row,

$$\mathbf{DUR}_{\text{pop,max}} = \mathbf{ScaleMax}\left(\underset{i \in \text{DTNs}}{\mathbf{Avg}}\left(\mathbf{DUR}_i\right)\right)$$

where $\mathbf{ScaleMax}(\mathbf{X})$ divides each matrix row by the maximum value in that row.

Just-Noticeable Difference

The just-noticeable difference (JND) is defined as the smallest non-zero duration increase, $\Delta \mathbf{d}$, between a reference duration, $\mathbf{d}_{\text{ref}}$, and a probe duration, $\mathbf{d}_{\text{probe}}$, such that the two stimuli are perceived as different. To determine the JND of the population of DTNs across all stimulus durations, we performed a two-alternative forced choice experiment over all unique pairs of presented stimulus durations, repeated 100 times. For each trial, spike counts were randomly chosen for each stimulus duration from the spike count probability distribution of each DTN. A summated posterior probability distribution vector, $\overline{\mathbf{D}_{\mathbf{d}}}$, was calculated over all DTNs to represent the population's average posterior probability distribution for that particular stimulus duration $\mathbf{d}$ and the particular spike counts that were randomly chosen for each DTN.

$$\overline{\mathbf{D}_{\mathbf{d}}} = \sum_{i \in \text{DTNs}} \left[\frac{\Pr(\mathbf{d}_1|s_i, \mathbf{DTN}_i)}{\#\text{DTNs}}, \frac{\Pr(\mathbf{d}_2|s_i, \mathbf{DTN}_i)}{\#\text{DTNs}}, \cdots \right]$$

If the posterior probability vectors were determined to be different (see below) and the two stimulus durations were in fact different, a point was scored. Similarly, if the vectors were decided to be within the threshold of similarity, and the two stimulus durations were also equivalent, then a point was scored. Otherwise, no point was scored for the trial. The JND for a particular reference duration was defined as the smallest $\Delta \mathbf{d} > 0$ such that $\geq 75\%$ of trials were accurately determined as different.

To determine if $\mathbf{d}_{\text{ref}}$ and $\mathbf{d}_{\text{probe}} = \mathbf{d}_{\text{ref}} + \Delta \mathbf{d}$ constituted a "noticeable difference" on any given trial, we determined the similarity of the posterior probability distribution vectors with a similarity index, $S(\overline{\mathbf{D}_{\mathbf{d}_{\text{ref}}}}, \overline{\mathbf{D}_{\mathbf{d}_{\text{probe}}}})$, based on the angle between the posterior probability distribution vectors. First, the inverse cosine of the normalized dot product of the vectors was used to calculate the absolute angle between the vectors. Then, the angle was doubled,

divided by π and subtracted from 1 so that equivalent vectors with an angle of 0 had a similarity index of 1 and orthogonal vectors with an angle of $\frac{\pi}{2}$ had a similarity index of 0.

$$S(\overline{\mathbf{D}}_{\mathbf{d}_{\text{ref}}}, \overline{\mathbf{D}}_{\mathbf{d}_{\text{probe}}}) = 1 - \frac{2\cos^{-1}\left(\overline{\mathbf{D}}_{\mathbf{d}_{\text{ref}}} \cdot \overline{\mathbf{D}}_{\mathbf{d}_{\text{probe}}} / |\overline{\mathbf{D}}_{\mathbf{d}_{\text{ref}}}||\overline{\mathbf{D}}_{\mathbf{d}_{\text{probe}}}|\right)}{\pi}$$

To decide on an appropriate threshold, S_{thresh}, for classifying stimulus durations as being the same or different, we plotted the proportional distributions of similarity indices for each $(\mathbf{d}_{\text{ref}}, \mathbf{d}_{\text{probe}})$ pair over 250 trials, separated into same duration trials and different duration trials (Fig. 4.9a,b). We chose a similarity index threshold $S_{\text{thresh}} = 0.9$ for our analysis. We did this for practical reasons since smaller threshold values resulted in more stimulus pairs being incorrectly classified as "same" and larger values resulted in more pairs incorrectly classified as "different".

The procedure for determining JNDs from FSL was equivalent to that using spike counts except that $\Pr(\mathbf{d}|s)$ was replaced with $\Pr(\mathbf{d}|l)$ in all cases. Again we plotted each $(\mathbf{d}_{\text{ref}}, \mathbf{d}_{\text{probe}})$ pair over 250 trials, separated into same duration trials and different duration trials (Fig. 4.9c) and used the same similarity index threshold $S_{\text{thresh}} = 0.9$ for classifying stimulus duration pairs as being "same" or "different".

4.3 Results

4.3.1 Single Neuron Analysis

Neurons in the IC of the big brown bat tend to show little to no spontaneous activity with DTNs being especially quiet in the absence of excitatory acoustic stimuli (mean DTN spontaneous rate: 0.620 Hz, 207 cells; mean non-DTN spontaneous rate: 2.039 Hz, 424 cells ; Mann-Whitney U non-parametric test: U = 34540.0; $p_{\text{2-tailed}} = 9.757 \times 10^{-6}$; Fig. 4.1). The results suggest that the response of DTNs are especially reliable for signaling the presence of an external stimulus.

Within the population of DTNs tested at +20 dB relative to threshold, population average spike counts peaked for 1 and 2 ms stimulus durations and decreased with longer stimulus durations (Fig. 4.2a,c). Population wide FSLs had a minimum value of ca. 8 ms and tended to increase with stimulus duration; however, owing to a large number of cells with more-or-less constant spike latencies resulted in the population mean FSL to increase only minimally (Fig. 4.2b).
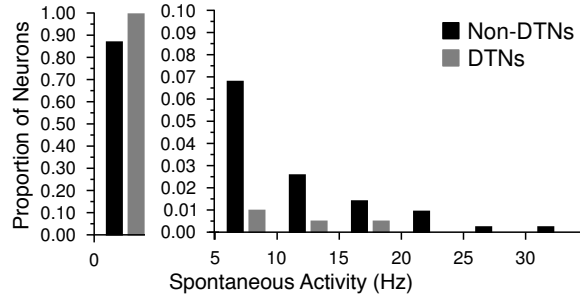
Figure 4.1: Spontaneous activity in duration-tuned ($N = 204$) and non-duration-tuned ($N = 427$) neurons in the IC of the big brown bat. The majority of IC neurons exhibit little to no spontaneous activity (<5 Hz). Non-duration-tuned neurons exhibited significantly higher levels of spontaneous activity than DTNs. Bin width = 5 Hz.
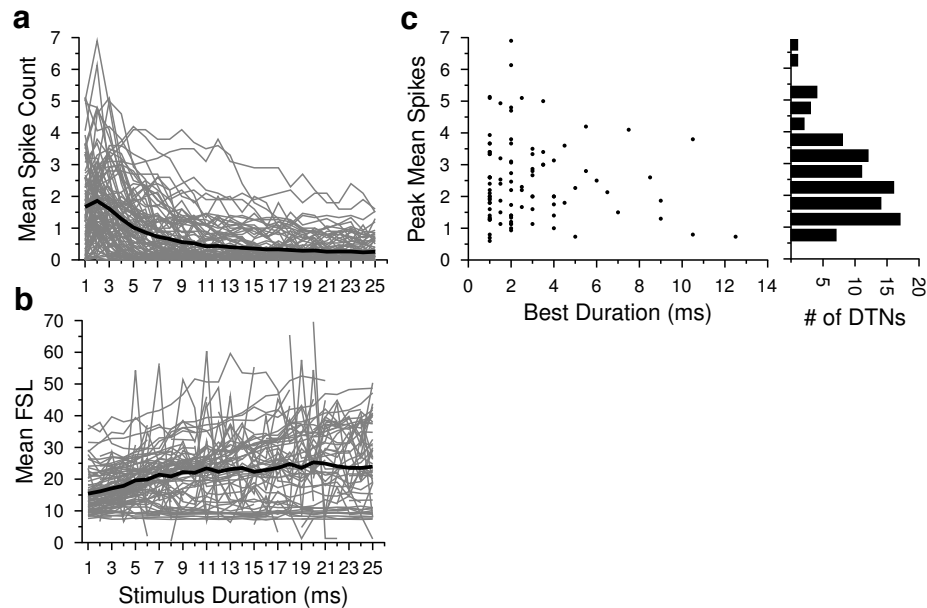
Figure 4.2: Mean spike counts, *a*, mean first-spike latencies, *b*, and peak mean spike count as a function of best duration, *c*, for all DTNs over all stimulus durations from 1 to 25 ms. *a,b* Individual DTN responses are shown as *gray lines* and mean values are shown as *bold black lines*. *c, right* Distribution of peak spike counts from all BDs. Histogram bin width = 0.5 spikes.

Information Characterization

Previous studies characterized the temporal tuning response profiles of DTNs by the stimulus duration that evoked the highest mean spike count (best duration, BD; Casseday et al., 1994) and each cell's 50% response bandwidth (Fremouw et al., 2005). Here we determined whether the BD of a DTN was actually the stimulus duration that was "best encoded". To do this, we calculated the stimulus-specific information (SSI) from the responses evoked at each stimulus duration, d. Stimulus-specific information conveys the average reduction of stimulus uncertainty gained from a single neural response and thus provides a metric for determining the stimuli that are best encoded by a neuron (Butts, 2003).

Another measure of a cell's encoding performance can be obtained by calculating the observed Fisher information (FI) across the stimulus domain (e.g. duration). Fisher information offers a measure of the encoding sensitivity because FI is highest for stimuli encoded uniquely relative to similar stimuli (Dayan and Abbott, 2001). Calculating FI requires the conditional probability distribution to be differentiable; however, *in vivo* data for DTNs provides only discrete probability values for each spike count conditional on duration. Therefore, we estimated the FI for stimulus durations that fell in-between stimulus durations that were presented to cells (d_{mid}) so that the derivative could be estimated by the difference in neighbouring probability values. The peak FI need not be related to the peak spike count or peak SSI, but is usually highest where response probabilities are changing quickly (Dayan and Abbott, 2001). Therefore, small changes in stimulus duration near durations with high FI values will be more uniquely encoded than durations near areas of low FI values.

To illustrate the responses and corresponding SSI and FI values for the population of DTNs tested, we present two example DTNs with tuning selectivity for short (shortpass; Fig. 4.3a,d) and intermediate durations (bandpass; Fig. 4.3b,e), and one example non-DTN that responded similarly to all stimulus durations (Fig. 4.3c,f). Dot raster displays (Fig. 4.3a,b,c) illustrate the spiking responses of each cell to multiple stimulus presentations. For both DTNs, the SSI was proportional to spike count (Fig. 4.3d,e), suggesting that spike counts are appropriate for characterizing the best durations encoded by DTNs. The shortpass neuron (Fig. 4.3a,d) had low FI values between the durations with maximum spike counts (1 and 2 ms). Instead, the FI was maximized at 2.5 ms where the change in spike count was greatest. Therefore, this shortpass DTN was most sensitive to changes in stimulus duration around 2 to 3 ms. Fisher information for the bandpass DTN (Fig. 4.3b,e) was greatest at 1.5 ms
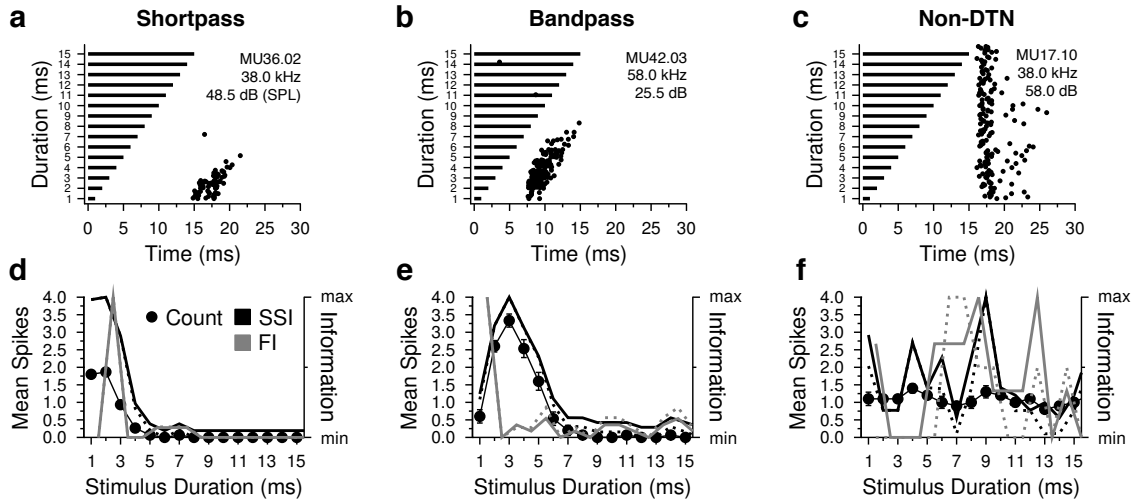
Figure 4.3: Example responses and calculated information content from three neurons from the IC of the big brown bat. *Left column*, shortpass DTN, 15 trials; ***Middle column***, bandpass DTN, 15 trials per stimulus duration; ***Right column***, non-duration-tuned neuron with an onset response, 10 trials. ***a,b,c***, Dot raster display of spike times (*black dots*) relative to stimulus onset of varying signal duration (*black bars*). Best excitatory frequency (kHz) and amplitude threshold (dB SPL) are reported for each neuron. ***d,e,f***, Mean spike count $\pm$ standard error (SE) (*filled circles*), normalized SSI where $\Pr(s = 0|\mathbf{d}) \geq 0$ (*black line*; ***d***, peak SSI = 3.52 bits, ***e***, peak SSI = 3.04 bits, ***f***, peak SSI = 0.57 bits), normalized SSI where $\Pr(s = 0|\mathbf{d}) = 0$ (*dashed black line*; ***d***, peak SSI = 3.52, ***e***, peak SSI = 3.04, ***f***, peak SSI=0.57 bits), normalized estimated FI where $\Pr(s = 0|\mathbf{d}) \geq 0$ (*solid gray line*) and normalized estimated FI where $\Pr(s = 0|\mathbf{d}) = 0$ (*dashed gray line*) as a function of stimulus duration. Notice that the peak FI, a measure of sensitivity, need not align with peak spike count or peak SSI as in ***d*** and ***e***. The FI values were similar in both DTNs regardless of whether zero spike responses were included. With the non-DTN, both SSI and FI fluctuated randomly and were essentially a function of the trial to trial variance in spiking responses. All stimuli presented at the neuron's BEF, +20 dB above threshold.

where the increase in spike count was greatest. The FI and SSI for the non-DTN (Fig. 4.3c,f) was, as expected, low across all stimulus durations. We also examined the SSI and FI when forcing $\Pr(s = 0|\mathbf{d}) = 0$ for all stimulus durations and found that the relative ordering of the values was approximately the same as when zero spike responses were included in the analysis (Fig. 4.3d,e,f *dashed lines*).

The trends observed in the three example neurons were mirrored throughout the population of DTNs studied. The SSI for most DTNs peaked near the neuron's BD (Fig. 4.4a,c). The FI also tended to peak near BD; however, a large proportion of DTNs had peak FI values
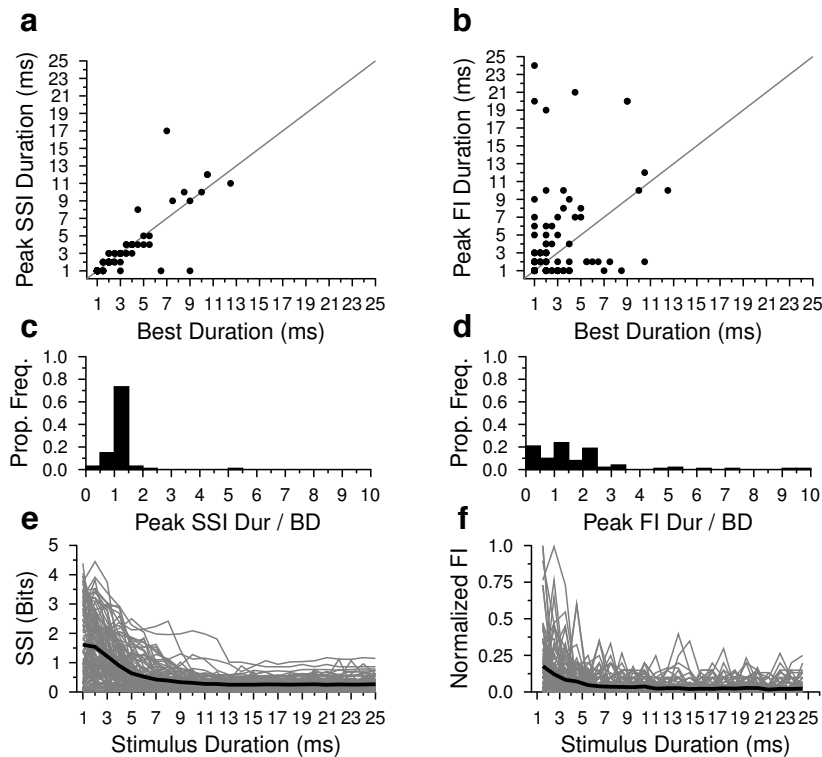
Figure 4.4: Peak SSI and FI versus neuronal BD calculated with spike counts. *a*, Stimulus duration evoking the peak SSI versus BD. Peak SSI tends to align directly with BD as shown in *c* by the proportional frequency of DTNs with a peak SSI to BD ratio near 1. *b*, Stimulus duration evoking the peak estimated FI versus BD. Peak FI tends to be evenly spread across stimulus durations both shorter than and longer than BD. This is also reflected in *d*. The line $y = x$ is drawn in gray. Histogram bin widths = 0.5. *e,f* both SSI and FI values across all DTNs (*gray lines*) tended to peak at the shortest stimulus durations and decrease monotonically with increasing stimulus duration (mean shown as *bold black line*).

away from a BD stimulus (Fig. 4.4b,d). These results suggest that DTNs most accurately encode the stimulus duration that evokes the strongest spiking response; however, a neuron's sensitivity to change in stimulus duration is not necessarily that same duration. On average, SSI and FI were highest for 1 ms stimuli and monotonically decreased with increasing stimulus duration (Fig. 4.4e,f). Moreover, population trends when $\Pr(s = 0|\mathbf{d}) = 0$ for all stimulus durations were vastly similar (data not shown).

Decoding Stimulus Duration from Spike Counts

Assuming DTNs are used to encode stimulus duration then there must be a procedure for decoding stimulus duration from the response of a DTN (or, as shown later, from a population of DTNs). Response variability prohibits the existence of a function that maps spike counts onto stimulus duration. Therefore, the best decoding function, given spike count, s, will rely on the posterior probability distribution, $\Pr(\mathbf{d}|s)$, over all stimulus durations, $\mathbf{d}$. A straight forward method of determining the posterior probability distribution is to apply Bayes' formula:

$$\Pr(\mathbf{d}|s) = \frac{\Pr(s|\mathbf{d})\Pr(\mathbf{d})}{\sum_i \Pr(s|\mathbf{d}_i)\Pr(\mathbf{d}_i)}.$$

For this analysis, we chose naïve priors, $\Pr(\mathbf{d}) = 1/25$, for all 25 stimulus durations tested. Spiking probabilities were obtained directly from *in vivo* responses. The spike count probability distributions for the three example neurons are shown in Figure 4.5a,b,c and their corresponding posterior probability distributions are shown in Figure 4.5d,e,f (same neurons as Figure 4.3). Notice that the stimulus durations with high posterior probabilities tend to correspond with high SSI (compare Fig. 4.5d,e,f with Fig. 4.3d,e,f). The non-DTN assigns a probability of 100% to $\Pr(\mathbf{d} = 9|s = 3)$ because the neuron produced 3 spikes for one of the trials with a 9 ms stimulus but did not produce 3 spikes for any other stimulus duration tested. Therefore, the numerator and denominator in Bayes' formula are equal and thus $\Pr(\mathbf{d} = 9|s = 3) = 1$.

Given the spike count and posterior probability distributions we can estimate the expected posterior probabilities for each stimulus duration, $\mathbf{d}$, given the presentation of a stimulus with duration $\mathbf{d}_{\mathrm{pres}}$ by

$$\Pr(\mathbf{d}|\mathbf{d}_{\mathrm{pres}}) = \sum_i \Pr(\mathbf{d}|s_i)\Pr(s_i|\mathbf{d}_{\mathrm{pres}})$$

where i iterates over all spike counts. The corresponding duration decoding matrices in Figure 4.5g,h,i ($\mathrm{DUR}_{\mathbf{d}_{\mathrm{pres}},\mathbf{d}}$) show that stimulus durations with high SSI tends to be decoded with high probability and that stimulus durations encoded with similar spiking probabilities, and thus low FI, are ambiguous (e.g. compare 1 and 2 ms for the shortpass DTN in Figure 4.5g). As expected, the non-DTN fails to assign substantial probabilities to any stimulus
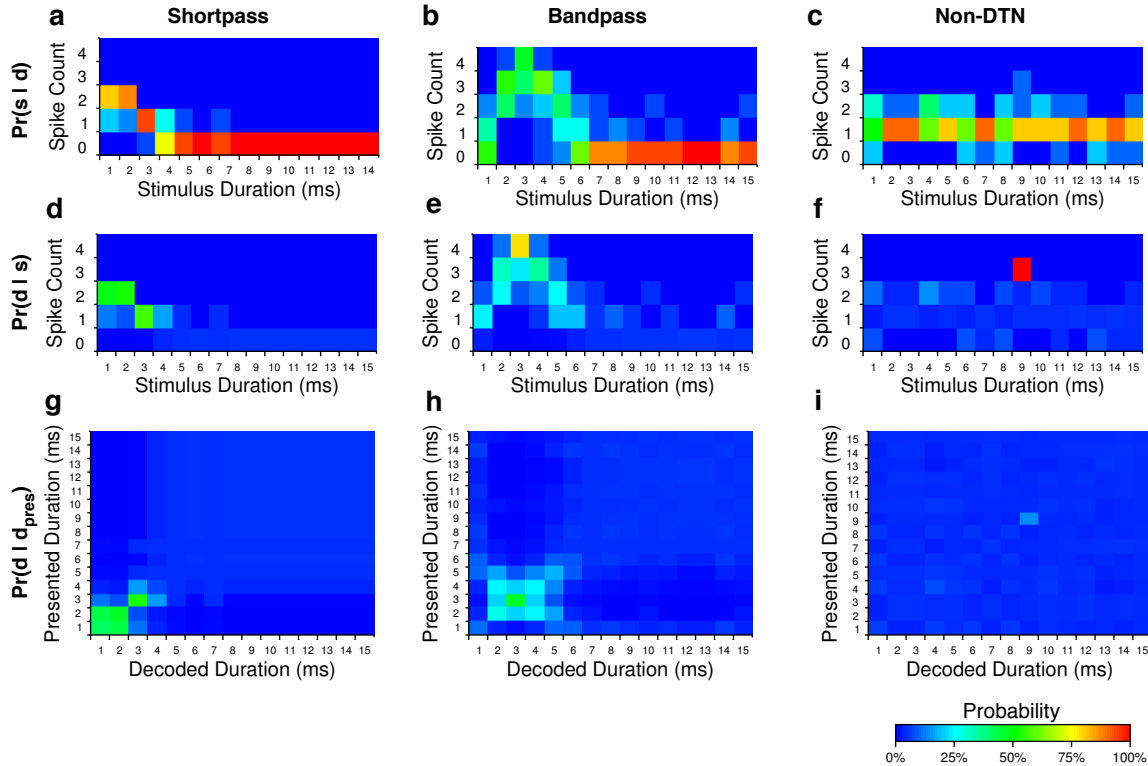
Figure 4.5: Example response and posterior probability distributions from three neurons in the bat IC. Neurons are the same as shown in Figure 4.3. *a,b,c*, $\Pr(s|\mathbf{d})$ for $s \in [0,1,2,3,4]$ spikes per trial and stimulus durations $\mathbf{d} \in [1,2,\ldots,25]$ ms. *d,e,f*, $\Pr(\mathbf{d}|s)$ for the same spike counts and stimulus durations as above. *g,h,i*, duration decoding matrices, $\Pr(\mathbf{d}|\mathbf{d}_{\text{pres}})$, for all stimulus durations $\mathbf{d}$ and presented stimulus durations $\mathbf{d}_{\text{pres}}$.

duration regardless of the duration presented due to the non-specific response probabilities across stimulus durations.

4.3.2 Population Analysis

Optimally Decoding Duration with Spike Counts

Computing the expected optimal duration decoding probabilities given a presented stimulus duration requires computing the joint posterior probabilities over the entire N neuron response space. We collected responses from 97 DTNs that produced up to an average of 7 spikes per stimulus presentation, making such a computation infeasible ($7^{97} \approx 9.43 \times 10^{81}$). Therefore, the optimal decoding probabilities were estimated with a Monte Carlo procedure

by selecting 100,000 random population responses (determined by the spiking response probabilities of each neuron) for each presented stimulus duration and calculating the joint spiking probability, $\Pr(S|\mathbf{d}) = \prod_i (\Pr(s_i|\mathbf{d})$ where S is the set of spiking responses from all DTNs in the population. This provides a proportional estimation for the posterior probability distribution by the fact that $\Pr(\mathbf{d}|S) \propto \Pr(S|\mathbf{d})$ for a population spiking response, S and duration $\mathbf{d}$. The final duration decoding matrix was produced by averaging all 100,000 duration decoding matrices and scaling the probabilities to sum to 1.

It is not obvious whether the brain can use the absence of a response from a DTN (zero spikes) or if it requires at least 1 spike to gain information. For example, a neuron's silence could be detected if a stimulus evokes responses from one neuron but not another. This might produce half of the input strength to another neuron as would otherwise be produce if both neurons were evoked. To assess the impact of ignoring zero spike responses, we performed two decoding procedures. First, we allowed $\Pr(s = 0|\mathbf{d}) \leq 1$ (Fig. 4.6a) and second, we forced $\Pr(s = 0|\mathbf{d}) = 1$ (i.e. zero spikes will have no effect on the joint probability distribution) for all durations (Fig. 4.6b). Both estimates of the optimal duration decoding matrix performed well with perfect decodings at the shortest stimulus durations. Later we investigated the consequences of including or excluding zero spike count responses further when we performed non-optimal duration decoding.

Non-Optimally Decoding Duration with Spike Counts

We calculated non-optimal population duration decoding matrices by averaging the duration decoding matrices of all individual DTNs. This method is more computationally feasible than producing an optimal duration decoding matrix. Additional optimization of this method could be made by using a weighted average based on the reliability of a particular DTN; however, for this analysis all DTNs were weighted equally.

When computing the average duration decoding matrix over all *in vivo* DTNs, the highest peaks were for 1 - 4 ms (Fig. 4.6a), an unsurprising result given that the majority of DTNs had a BD and peak SSI at short stimulus durations (Fig. 4.4). One consequence of naïvely weighting all DTNs equally is that peak duration decoding probabilities tend to be lower than the peaks of individual DTN decoding probabilities (e.g. the peak probability in Fig. 4.6a is only $\Pr(\mathbf{d} = 1|\mathbf{d}_{\text{pres}} = 1) = 0.254$). This occurs because the posterior probability distributions for individual DTNs tend to be very low for the majority of spike counts and

stimulus durations and high only for those stimulus durations encoded by the non-zero spiking response. Therefore, the average across all DTNs is pushed towards zero.

We investigated two methods to overcome the low population level decoding probabilities. First, the majority of neurons had little to no selectivity to stimulus durations >10 ms, making the corresponding posterior probabilities, $\Pr(\mathbf{d} > 10|s)$, uniformly low. Any neurons that spike in response to longer stimulus durations would be "washed out" in the average by all other responses. Therefore, we recomputed the population duration decoding matrix under the assumption that no knowledge was gained from a DTN producing zero spikes. In other words, we forced $\Pr(\mathbf{d}|s = 0) = 0$ for all stimulus durations, which is mathematically equivalent to setting $\Pr(s = 0|\mathbf{d}) = 1$ in the optimal decoding procedure described above. Overall, this produced higher decoding probabilities at all stimulus durations (Fig. 4.6d). This result suggests that some information, even if valid, can be detrimental to this non-optimal decoding procedure and should thus be discarded when the information provided is too vague.

Alternatively, the decoding procedure may care only about relative probabilities instead of absolute probabilities. For example, once a particular stimulus was decided to be the most likely duration presented then selecting the duration with the highest posterior probability is an obvious solution (Beck et al., 2008). We calculated the normalized duration decoding matrix by dividing the posterior probabilities for each duration, given a particular presented duration, by the probability of the most likely duration (Fig. 4.6e). The stimulus duration with the highest posterior probability was always equal to the presented duration; however, the normalized probabilities of nearby durations, especially at longer durations, was also very close to 1. For example, when the presented stimulus duration was 24 ms, the normalized estimated probability of a 23 ms duration was $\Pr_{\text{Norm}}(\mathbf{d} = 23|\mathbf{d}_{\text{pres}} = 24) = 0.94$, a difference of only 6%. The non-normalized probabilities of these probabilities differed by only 0.0035. Accurately decoding such responses would require a very selective decoder with highly accurate representations of the posterior probability distributions, a feat likely challenging for *in vivo* neural networks.

Combining both methodologies resulted in the greatest disambiguation of decoded stimulus durations (Fig. 4.6f). After discarding information gained from zero spike counts and normalizing the decoded duration probabilities, the presented stimulus durations were clearly delineated from all other stimulus durations. For example, in the combined decoding procedure, $\Pr_{\text{Norm}}(\mathbf{d} = 23|\mathbf{d}_{\text{pres}} = 24) = 0.87$, creating a probability difference from the

Figure 4.6: Duration estimation from population spike count responses. $\boldsymbol{a}$, Estimated optimal decoding probabilities across all decoded stimulus durations given the presentation of all stimulus durations (i.e. $\Pr(\mathbf{d}|\mathbf{d}_{\mathrm{pres}})$) when allowing $\Pr(s=0|\mathbf{d}) \leq 1$. $\boldsymbol{b}$, Estimated optimal decoding probabilities across all decoded stimulus durations given the presentation of all stimulus durations when forcing $\Pr(s=0|\mathbf{d}) = 1$. $\boldsymbol{c}$, Non-optimal average of duration decoding matrices over all DTNs when allowing $\Pr(\mathbf{d}|s=0) \geq 0$. $\boldsymbol{d}$, Non-optimal average of duration decoding matrices over all DTNs when forcing $\Pr(\mathbf{d}|s=0) = 0$. Note that the probability scale in $\boldsymbol{c}$ and $\boldsymbol{d}$ is from 0 to 0.4 for improved visual discrimination. $\boldsymbol{e},\boldsymbol{f}$, same data as shown in panels $\boldsymbol{c}$ and $\boldsymbol{d}$ scaled to the maximum probability value across all decoded stimulus durations.

correct stimulus duration of 13%, more than double the difference when information from zero spikes was included. Although the most probable decoded stimulus durations were always the presented stimulus duration, durations shorter than this also received high decoding probabilities. This suggests that decoding errors would likely result in underestimating stimulus duration.

Remarkably, both non-optimal methods of decoding assigned the most likely stimulus duration correctly even though the range of BDs and peak SSI durations did not cover all presented durations (Fig. 4.4). This indicates that the range of stimulus durations encoded by a population of DTNs is not simply characterized by just the range of BDs but encompasses the entire response profile of the cells.

Optimal and Non-Optimal Duration Decoding with Spike Latencies

Thus far, our analysis has been based on the number of spikes produced by DTNs; however, duration can also be encoded by the latency of spikes relative to stimulus onset. We calculated the posterior probability distributions of DTNs by FSL in the same fashion as spike counts (see *Methods*). First-spike latencies were generally normally distributed so we estimated the FSL distributions with normal distributions fitted to the sampled data. Spike latency information is only available when at least 1 spike is produced; therefore, the probability of a spike occurring within a particular interval, $[a, b]$, is a product of the FSL probability multiplied by the probability of producing at least 1 spike for that stimulus duration. For our analysis, we chose interval widths of 0.5 ms. In particular,

$$\Pr(a \leq l \leq b|\mathbf{d}) = \Pr(s \geq 1|\mathbf{d}) \int_a^b \mathcal{N}(x; \mu_{\mathbf{d}}, \sigma_{\mathbf{d}}) \, \mathrm{d}x.$$

Estimating the optimal duration decoding matrix with FSL with a Monte Carlo estimation procedure was performed in the same manner as with spike counts. Spike latencies were randomly selected from a normal distribution describing spike latencies for that neuron and stimulus duration. For each Monte Carlo trial, only spikes occurring with probability $\Pr(s \geq 1|\mathbf{d})$ were used for computing the joint probability distribution. The optimal FSL decoding estimation produced a nearly perfect decoding where $\Pr(\mathbf{d} = \mathbf{d}_{\text{pres}}|\mathbf{d}_{\text{pres}}) \approx 1$ (within 5×10^{-55} of 1) for all presented stimulus durations (Fig. 4.7a). This result is not surprising because many DTNs have offset following responses that produced spikes at

stimulus offset for all stimulus durations (Fig. 4.2b) and thus would accurately encode stimulus duration in FSL.

Using the non-optimal decoding method, FSL performed better than spike counts with both the absolute (Fig. 4.7b) and normalized probability (Fig. 4.7c). First-spike latency analysis necessarily ignores spike counts of zero so it is not surprising that the performance is similar to spike count decoding that forces $\Pr(\mathbf{d}|s=0)=0$. Furthermore, several DTNs responded to the offset of all stimulus durations with at least 1 spike and thus could accurately encode stimulus duration by spike latency (Fig. 4.2b). When the presented stimulus duration was short ($\leq$12 ms), slightly shorter durations tended to receive high relative posterior probabilities. This result is consistent with the observation that, at least for some DTNs, spike latency less reliably tracks stimulus offset for short durations and instead has a more stable latency relative to stimulus onset (Fuzessery and Hall, 1999; Faure et al., 2003; Aubie et al., 2012).

To assess the information content of FSLs, we calculated the SSI and FI using FSL instead of spike counts. Because BD is based on a maximum spike count and not spike latency, BD and FSL are not necessarily related. Despite this, the majority of DTNs peaked in FSL SSI at or near BD (Fig. 4.8a,c), whereas peak FSL FI tended to occur at durations higher than BD (Fig. 4.8b,d). On average, FSL SSI was highest for 1 - 2 ms stimuli and monotonically decreased with stimulus duration (Fig. 4.4e). In contrast, FSL FI had wide variance with no clear relation to stimulus duration.

4.3.3   Just-Noticeable Difference

The just-noticeable difference (JND) for a stimulus is the minimum change required to perceive a difference in the quality of the stimulus perceived. The JND for stimulus duration, then, is the minimum duration change required to perceive a different duration. To determine the JND for each stimulus duration, as perceived by the responses of a population of *in vivo* DTNs, we implemented a two-alternative forced choice task. We used the non-optimal decoding procedure to determine posterior probability distributions because the optimal procedure yielded a perfect ability to discriminate between all stimulus durations. First, a population response was chosen from the response probability distributions of each DTN for a presented stimulus duration, and then an average posterior probability distribution over all stimulus durations was calculated. Next, a population response was chosen from the
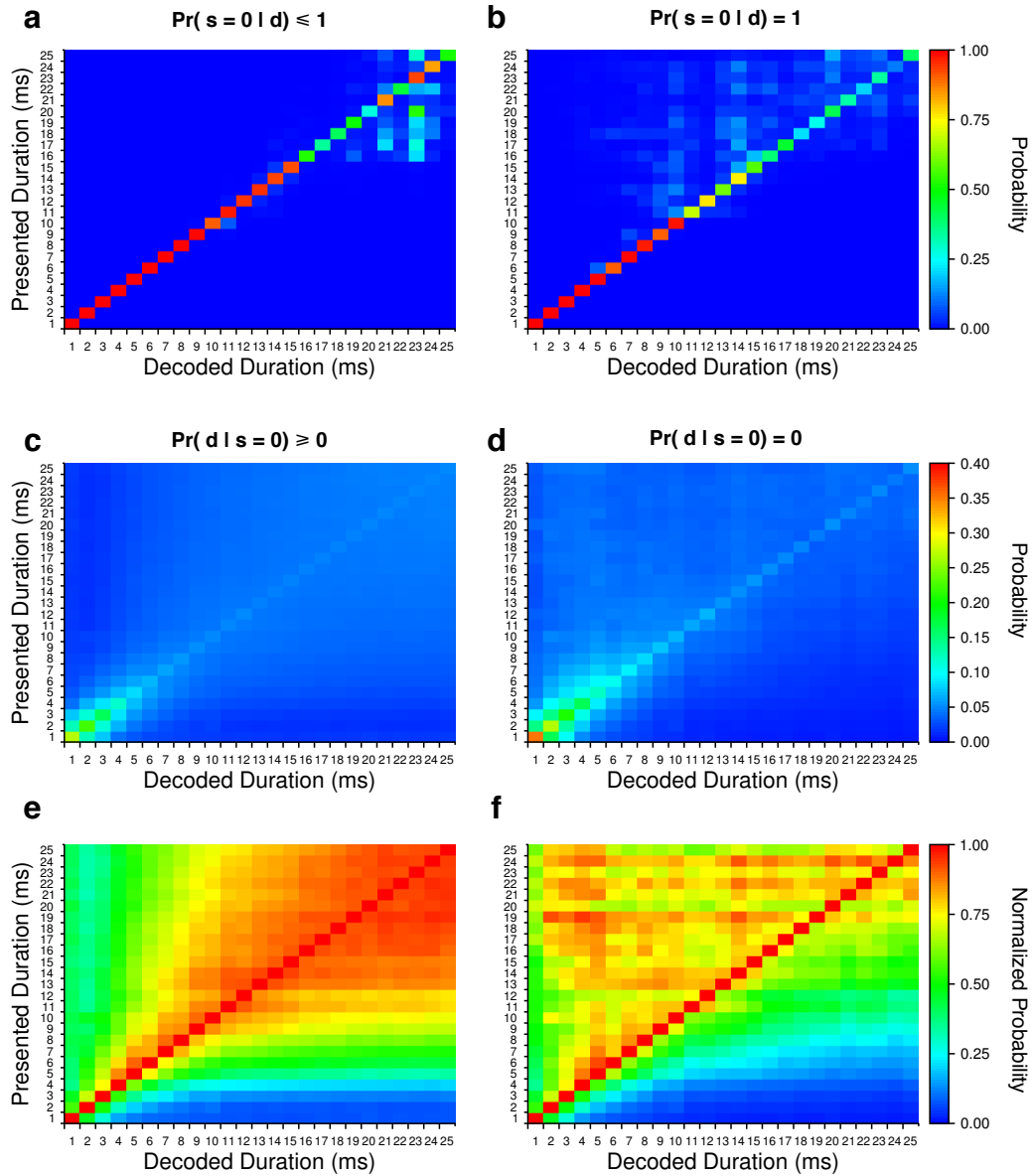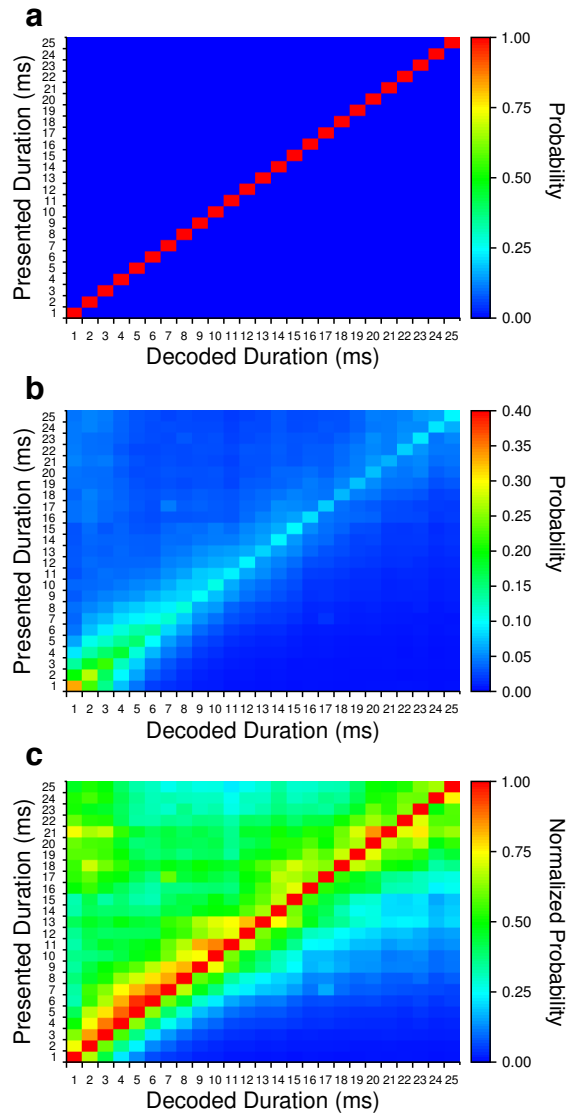
Figure 4.7: Duration estimation from population FSL probabilities. *a*, Estimated optimal decoding probabilities across all decoded stimulus durations given the presentation of all stimulus durations (i.e. $\Pr(\mathbf{d}|\mathbf{d}_{\mathrm{pres}})$). *b*, Probabilities across all decoded stimulus durations given the presentation of all stimulus durations. Note that the probability scale in *b* is from 0 to 0.4 for improved visual discrimination. *c*, same data as shown in panel *b* scaled to the maximum probability value across all decoded stimulus durations.
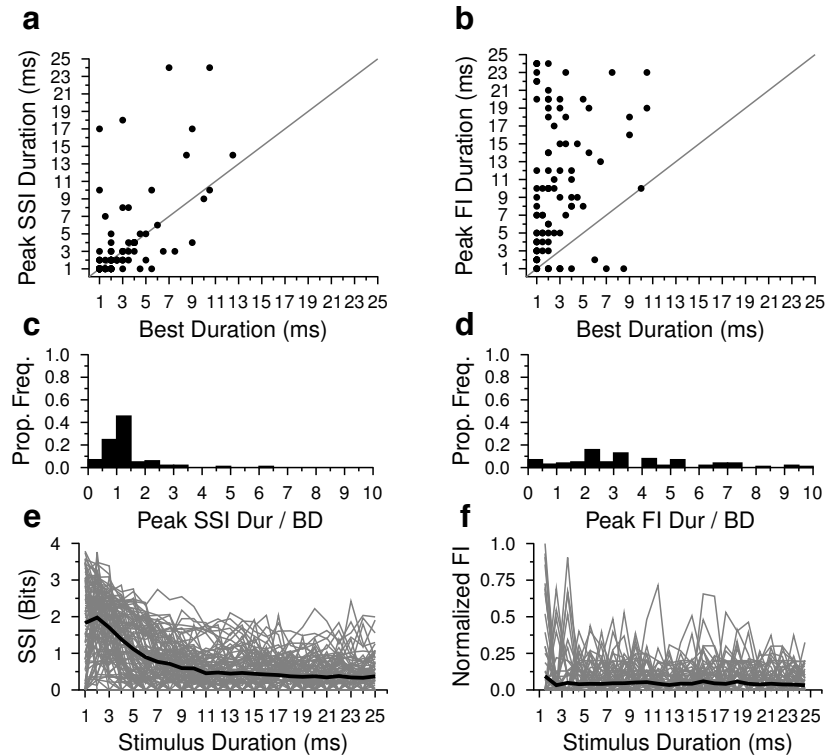
Figure 4.8: Peak FSL SSI and FSL FI versus BD. *a*, Stimulus duration evoking the peak FSL SSI versus BD. Peak FSL SSI tends to align with the BD as shown in *c*. *b*, Stimulus duration evoking the peak estimated FSL FI as a function of BD. Peak FI tends to be greater than BD as shown in *d*. The line $y = x$ is drawn in gray. Histogram bin widths = 0.5. *e*, FSL SSI for all DTNs (*gray lines*) and the mean (*black line*). *f*, FSL FI for all DTNs (*gray lines*) and the mean (*black line*).

response probability distributions of each DTN for a stimulus duration that was either the same as the first duration or longer and the average posterior probability distribution was determined. A similarity index between the two posterior probability distributions was then calculated. A guess of "same" was made if the similarity index was above some threshold, θ_{thresh}, otherwise, a guess of "different" was made. If the guess was correct, a point was scored. This procedure was repeated 100 times per stimulus duration pair and the average score is reported. A pair of stimulus durations were considered to be "noticeably different" if the average task score was ≥ 0.75 (i.e. a correct same/difference decision was made at least 75% of the time).

A similarity index between 0 and 1 was computed, where 0 was perfectly dissimilar (orthogonal) and 1 was perfectly similar (parallel) (see *Methods* for details). To determine

an appropriate threshold value, the two-alternative forced choice task was performed 250 times for each stimulus duration pair and the similarity indices were recorded. The majority of trials with the same stimulus duration had similarity indices ≥ 0.9 for both the spike count ($\Pr(\mathbf{d}|s = 0) \geq 0$) and the FSL analysis (Fig. 4.9a,c) and thus we set $\theta_{\text{thresh}} = 0.9$. In contrast, spike count decoding with $\Pr(\mathbf{d}|s = 0) = 0$ resulted in much lower similarity indices for same duration pairs, so we lowered the threshold to $\theta_{\text{thresh}} = 0.82$. Similar performance was obtained when θ_{thresh} was within ± 0.03 of these thresholds (data not shown). The similarity index when using the optimal decoding method was always 0 for different stimulus durations (i.e. orthogonal posterior probability distributions) and nearly always 1 for equivalent stimulus durations (Fig. 4.9d).

We performed the JND task with spike counts while setting $\Pr(\mathbf{d}|s = 0) \geq 0$ (Fig. 4.10a) and forcing $\Pr(\mathbf{d}|s = 0) = 0$ (Fig. 4.10b). The similarity index operates on only the angle between posterior probability distributions, not the magnitude of the probabilities, thus the normalized probability decoding method yielded equivalent results to the non-normalized probability method. When decoding with spike counts, the JND was 1 ms for 1 to 4 ms reference durations, but increased as the reference duration was lengthened. When $\Pr(\mathbf{d}|s = 0) = 0$, performance was slightly better than when allowing zero spike responses, but not greatly so (compare Fig. 4.10a and b). When decoding with FSL responses, the JND was 1 ms for all reference durations tested; however, pairs of equal duration stimuli were often incorrectly perceived as being different, especially at the longer reference durations (Fig. 4.10c). This was due to the majority of DTNs having low response probabilities to long stimulus durations. Therefore, trial to trial responses yielded vastly dissimilar response profiles and thus produced low similarity indices.

From these responses, we calculated the Weber fraction, $\frac{JND}{\mathbf{d}_{\text{ref}}}$, for each reference duration, $\mathbf{d}_{\text{ref}}$, as the minimum JND ≥ 1 ms with a score of at least 0.75 (Fig. 4.10d). The Weber fraction for FSL decoding was simply $\frac{1}{\mathbf{d}_{\text{ref}}}$; however, the Weber fraction for both types of spike count decoding had a lower bound of 0.25 with a reference duration of $\mathbf{d}_{\text{ref}} = 4$ ms and then grew with increasing stimulus duration. For comparison, known Weber fractions for auditory duration discrimination tasks are shown for starlings, parakeets, macaques and humans (Maier and Klump, 1990). Although animal performance data was determined with stimulus durations at least one order of magnitude larger, the Weber fractions computed from our population of bat DTNs tended to match the behavioural Weber fractions by virtue of consistently being ≤ 1 (i.e. the JND was smaller than the duration of the reference stimulus
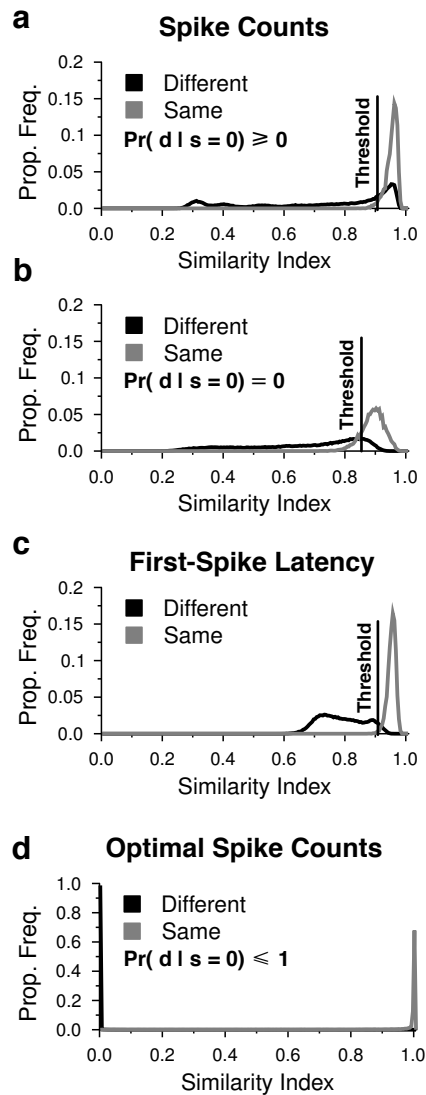
Figure 4.9: Distribution of similarity index scores from decoding with spike counts (**a**,**b**) and spike latencies (**c**). The nearly perfect similarity index scores when using optimal spike count decoding methods (including zero spike responses) is shown in **d**. Each stimulus duration pair was tested 250 times.
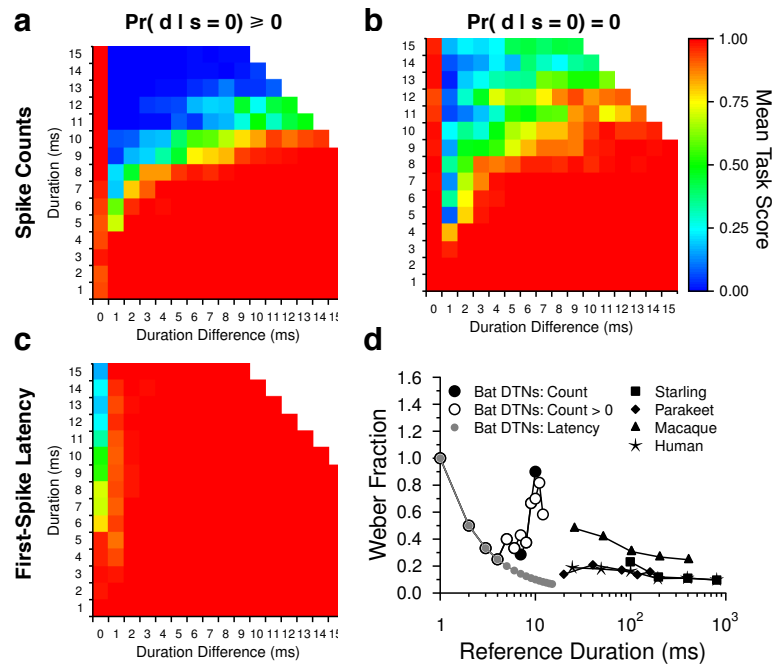
Figure 4.10: Two-alternative forced choice duration discrimination performance and calculated Weber fractions. ***a,b,c*** Mean two-alternative forced choice task scores calculated with spike count probabilities (***a,b***) and FSL probabilities (***c***). ***d***, Computed Weber fractions for both spike count and FSL decoding methods. Also plotted are known Weber fractions for auditory duration discrimination tasks for the starling, parakeet, macaque and human (Maier and Klump, 1990).

duration).

4.4 Discussion

The responses of auditory DTNs have been studied extensively in a variety of species and especially in echolocating bats (for review, see Sayegh et al., 2011) but a theoretic analysis of the encoding properties and efficiency of DTNs has not previously been done. In this study, we analyzed extracellular electrophysiological data of DTNs from the big brown bat, *E. fuscus*, to characterize the ability of individual DTNs and a population of DTNs to encode information about stimulus duration.

4.4.1 Decoding stimulus duration with neural networks

We analyzed how spike counts and first-spike latency responses of DTNs could encode stimulus duration. Analysis of human and non-human animal data suggests that perceptual information is processed probabilistically and often in a "Bayes optimal" manner (Geisler and Albrecht, 1995; Knill and Pouget, 2004; Nelken et al., 2005; Goldreich, 2007; Yang and Shadlen, 2007). Methods for computing posterior probability distributions with neural networks have been demonstrated on many occasions and are often computed with the logarithm of posterior probabilities or posterior probability ratios (Rao, 2004; Jazayeri and Movshon, 2006; Ma et al., 2006; Beck et al., 2008; Deneve, 2008). Direct calculation of joint probabilities and posterior probabilities requires multiplication; however, the logarithmic equivalent is additive, a computation that seems more feasible for neural circuits (Deneve, 2005). Although the analysis presented here is not logarithmic, the monotonicity of logarithms means the relative ordering of probabilities would remain the same.

We calculated both optimal decoding estimations and non-optimal estimations of duration using Bayes' formula. The optimal decoding procedure produced very good results with nearly perfect decoding ability with spike counts and absolutely perfect decoding ability with spike latencies. While the true decoding ability of the bat is not known, it is unlikely to be as good as this optimal decoding procedure due to the unlikely ability of the brain to perfectly represent all required information.

We performed non-optimal decoding via the averaged population posterior probability distributions for stimulus duration from spike counts under two conditions. First, we allowed information to be gained from the absence of spikes; and second, we ignored neurons that did not respond (spikes) to a particular stimulus duration. In general, DTNs have low levels of spontaneous activity and low spiking probabilities to non-preferred durations. Including information gained from the absence of spikes tended to "wash out" the posterior probabilities, particularly near long durations that had fewer representative neurons (compare Fig. 4.6 *left column* to Fig. 4.6 *right column*). Therefore, including only actual spiking responses responses appears beneficial for decoding in this non-optimal strategy. Furthermore, learning probability distributions with neural networks may be easier if the determination of synaptic weights depends only on spiking activity.

We also calculated non-optimal posterior probability distributions for stimulus duration from FSLs. Duration-tuned neurons often have spike latencies that follow stimulus offset

(Casseday et al., 1994; Faure et al., 2003); however, spike latencies less reliably follow stimulus offset at shorter stimulus durations (Fuzessery and Hall, 1999; Aubie et al., 2012) which suggests that spike latency may be less robust at encoding stimulus duration at short durations. Our population of DTNs had a mixture of onset and offset following spike latencies (Fig. 4.2b). Stimulus duration was accurately decoded from spike latencies; however, decoding was more ambiguous at the shortest stimulus durations, as predicted (Fig. 4.7*b*,*c*).

Two potential obstacles exist for using spike latency to decode stimulus duration. First, latency is only meaningful relative to an other (earlier) event. An outside observer can perceive the spike latency relative to stimulus onset, but the brain can not (VanRullen et al., 2005). One solution is the existence of precisely timed onset-evoked responses in the auditory cortex that could provide a reference signal for measuring the temporal difference between onset-evoked and DTN responses (Brasselet et al., 2012).

A second obstacle to consider is how accurately spike latencies with small relative differences can be discriminated. For example, our analysis used spike latencies to accurately discriminate between 24 and 25 ms stimulus durations (Fig. 4.7). Discriminating absolute spike latencies on the order of milliseconds has been well characterized in the auditory pathway (Carr and Konishi, 1990; Howard and Rubel, 2010); however, it is unclear if spike latency differences on the order of tens of milliseconds can also be discriminated with millisecond level resolution.

An alternative solution to both obstacles of using spike latency is to combine spike count and spike latency information. If a subset of neurons are known to produce spikes for only a specific range of stimulus durations then spike counts could provide a rough estimate of stimulus duration and then relative spike latencies within those responses could sharpen the decoded duration probabilities. This alleviates the need for the brain to mark stimulus onset absolutely and instead rely on relative spike times within the population of responding DTNs (Jenison, 2001). If the majority of a subpopulation of DTNs evoked early spikes, relative to the entire spiking response, then a shorter stimulus duration would be decoded. If the majority of DTNs evoke longer latency spikes, then a longer stimulus duration would be decoded.

A class of neural responses not considered in this study were the sustained responses of long-pass neurons that produce spike trains with increasing spike counts as a function of stimulus duration. Some neurons with sustained responses in the IC require minimum

146

stimulus durations before producing spikes, and these cells maintain or increase this minimum duration across stimulus amplitudes. Such neurons have previously been classified as longpass DTNs (Faure et al., 2003; Aubie et al., 2009). Theoretically, stimulus duration could be decoded from these responses as a linear function of spike count; however, similar issues to measuring spike latencies arise. For example, if a 24 ms stimulus evoked 20 spikes and a 25 ms stimulus evoked 21 spikes, the brain may be unable to differentiate between these two spike trains as accurately as the responses of shortpass and/or bandpass DTNs tuned to shorter durations and producing only 1 or 2 spikes.

4.4.2   Encoding Efficiency and Just-Noticeable Differences

A neuron's ability to encode information can be characterized in terms of encoding accuracy and sensitivity. For measuring accuracy, we computed the SSI for each stimulus duration across all DTNs. Stimulus-specific information is a measure of the average reduction of stimulus uncertainty gained from a single neural response (Butts, 2003). All previous reports of DTNs have characterized the stimulus duration evoking maximum spiking as the DTN's BD. The SSI aligned with peak spiking responses, thus BD as a method of characterization. But it is not the case that a population of DTNs must contain neurons with BDs at all stimulus durations. Our decoding methods were able to accurately decode stimulus durations between 1 and 25 ms even though many DTNs did not have corresponding BDs >10 ms (4.4).

For measuring encoding sensitivity, estimated the observed FI of hypothetical stimulus durations in between the durations tested *in vivo*. Fisher information is a measure of change in the response distribution of stimulus duration changes, thus it measures encoding sensitivity. High FI values occur where response curves have steep slopes and indicate the ability to discriminate very similar stimulus durations. Contrary to SSI, peak FI values were often located at stimulus durations off of BD. For example, a neuron that most accurately encoded a 1 ms stimulus may also be able to discriminate between 3 and 4 ms stimuli. Optimized FI over physiologically relevant stimulus values instead of maximum response magnitudes is common in auditory neurons (Fitzpatrick et al., 1997; Harper and McAlpine, 2004) and thus may be similarly employed in the encoding scheme of stimulus duration.

Duration-tuned neurons in the bat generally have increased duration tuning bandwidths with BD (Ehrlich et al., 1997); however, no behavioural studies of bat duration discrimination have been performed. The tuning of individual DTNs could predict that a population of

DTNs would discriminate the same absolute difference in stimulus duration between two short sounds with greater accuracy than for two long duration sounds. The Weber-Fechner law of psychophysics states that the JND in stimulus magnitude scales in proportion to the absolute stimulus magnitude ($|s|$). In other words,

$$\text{JND} \propto |s|.$$

This perceptual feature is observed in the fringe-lipped bat (*Trachops cirrhosus*) that preys on túngara frogs (*Physalaemus pustulosus*) with preference towards frogs that emit mating calls with a greater number of chucks (broadband pulses). As predicted by the Weber-Fechner law, the bat's preference between two frog mating calls varied not with the absolute difference in chuck number but with chuck ratio (Akre et al., 2011).

When we calculated the JND of a population of DTNs with spike count information using a non-optimal decoding procedure, the JND increased with stimulus duration, a feature consistent with the Weber-Fechner law of psychophysics (Fechner, 1966). This suggests that if bats do, in fact, obey the Weber-Fechner law for duration discrimination, then their method of decoding stimulus duration from DTNs is non-optimal. Optimal decoding of duration yielded nearly perfect duration decoding that results in a constant JND independent of the reference duration.

4.4.3 Conclusions

Three primary conclusions can be drawn from this analysis. First, the common method of characterizing DTNs by their BD is valid from an encoding perspective because SSI also peaks at BD; however, the greatest sensitivity to change in stimulus duration often occurred at durations away from BD. Second, the range of neuronal BDs in a population of DTNs by itself does not predict the range of encodable durations. Instead, the full response profiles of DTNs must be taken into account. Third, both spike counts and latencies from can reliably encode stimulus duration. Behavioural studies are required to ascertain the behavioural accuracy of duration decoding in bats to determine which decoding methods are most likely performed *in vivo*.

4.5 References

Akre KL, Farris HE, Lea AM, Page RA, Ryan MJ (2011) Signal perception in frogs and bats and the evolution of mating signals. *Science* 333:751–752.

Aubie B, Becker S, Faure PA (2009) Computational models of millisecond level duration tuning in neural circuits. *J Neurosci* 29:9255–9270.

Aubie B, Sayegh R, Faure PA (2012) Duration Tuning across Vertebrates. *J Neurosci* 32:6373–6390.

Beck JM, Ma WJ, Kiani R, Hanks T, Churchland AK, Roitman J, Shadlen MN, Latham PE, Pouget A (2008) Probabilistic population codes for Bayesian decision making. *Neuron* 60:1142–1152.

Brasselet R, Panzeri S, Logothetis NK, Kayser C (2012) Neurons with stereotyped and rapid responses provide a reference frame for relative temporal coding in primate auditory cortex. *J Neurosci* 32:2998–3008.

Butts DA (2003) How much information is associated with a particular stimulus? *Network: Comput Neural Syst* 14:177–187.

Carr CE, Konishi M (1990) A circuit for detection of interaural time differences in the brain stem of the barn owl. *J Neurosci* 10:3227–3246.

Casseday JH, Ehrlich D, Covey E (1994) Neural tuning for sound duration: role of inhibitory mechanisms in the inferior colliculus. *Science* 264:847–850.

Casseday JH, Ehrlich D, Covey E (2000) Neural measurement of sound duration: control by excitatory-inhibitory interactions in the inferior colliculus. *J Neurophysiol* 84:1475–1487.

Dayan P, Abbott LF (2001) *Theoretical Neuroscience: Computational and Mathematical Modeling of Neural Systems* MIT Press, Cambridge, MA.

Deneve S (2005) Bayesian inference in spiking neurons In Saul LK, Weiss Y, Bottou L, editors, *Advances in neural information processing systems, 17*. MIT Press, Cambridge, MA.

Deneve S (2008) Bayesian spiking neurons I: inference. *Neural Comput* 20:91–117.

DeWeese MR, Meister M (1999) How to measure the information gained from one symbol. *Network: Comput Neural Syst* 10:325–340.

Ehrlich D, Casseday JH, Covey E (1997) Neural tuning to sound duration in the inferior colliculus of the big brown bat, *Eptesicus fuscus*. *J Neurophysiol* 77:2360–2372.

Faure PA, Fremouw T, Casseday JH, Covey E (2003) Temporal masking reveals properties of sound-evoked inhibition in duration-tuned neurons of the inferior colliculus. *J Neurosci* 23:3052–3065.

Fechner GT (1966) *Elements of psychophysics* Holt, Rinehart and Winston, New York, NY.

Fitzpatrick D, Batra R, Stanford TR, Kuwada S (1997) A neuronal population code for sound localization. *Nature* 388:871–874.

Fremouw T, Faure PA, Casseday JH, Covey E (2005) Duration selectivity of neurons in the inferior colliculus of the big brown bat: tolerance to changes in sound level. *J Neurophysiol* 94:1869–1878.

Fuzessery ZM, Hall JC (1999) Sound duration selectivity in the pallid bat inferior colliculus. *Hear Res* 137:137–154.

Geisler WS, Albrecht DG (1995) Bayesian analysis of identification performance in monkey visual cortex: nonlinear mechanisms and stimulus certainty. *Vision Res* 35:2723–2730.

Goldreich D (2007) A Bayesian perceptual model replicates the cutaneous rabbit and other tactile spatiotemporal illusions. *PLoS One* 2:e333.

Harper NS, McAlpine D (2004) Optimal neural population coding of an auditory spatial cue. *Nature* 430:682–686.

Howard MA, Rubel EW (2010) Dynamic spike thresholds during synaptic integration preserve and enhance temporal response properties in the avian cochlear nucleus. *J Neurosci* 30:12063–12074.

Jazayeri M, Movshon JA (2006) Optimal representation of sensory information by neural populations. *Nat Neurosci* 9:690–696.

Jenison R (2001) Decoding first-spike latency: a likelihood approach. *Neurocomputing* 38:239–248.

Kay SM (1993) *Fundamentals of statistical signal processing: Estimation Theory*, Vol. 1 Prentice-Hall PTR (New Jersey, NY).

Knill DC, Pouget A (2004) The Bayesian brain: the role of uncertainty in neural coding and computation. *Trends Neurosci* 27:712–719.

Ma WJ, Beck JM, Latham PE, Pouget A (2006) Bayesian inference with probabilistic population codes. *Nat Neurosci* 9:1432–1438.

Maier E, Klump G (1990) Auditory duration discrimination in the European starling (*Sturnus vulgaris*). *J Acoust Soc Am* 88:616.

Montgomery N, Wehr M (2010) Auditory Cortical Neurons Convey Maximal Stimulus-Specific Information at Their Best Frequency. *J Neurosci* 30:13362–13366.

Nelken I, Chechik G, Mrsic-Flogel TD, King AJ, Schnupp JWH (2005) Encoding stimulus information by spike numbers and mean response time in primary auditory cortex. *J Comput Neurosci* 19:199–221.

Rao RPN (2004) Bayesian computation in recurrent neural circuits. *Neural Comput* 16:1–38.

Sayegh R, Aubie B, Faure PA (2011) Duration tuning in the auditory midbrain of echolocating and non-echolocating vertebrates. *J Comp Physiol A* 197:571–583.

VanRullen R, Guyonneau R, Thorpe SJ (2005) Spike times make sense. *Trends Neurosci* 28:1–4.

Yang T, Shadlen MN (2007) Probabilistic reasoning by neurons. *Nature* 447:1075–1080.

Zar JH (1984) *Biostatistical analysis* Englewood Cliffs, N.J.: Prentice-Hall, 2nd edition.

Discussion

5

5.1 Significance of Work

Prior to research performed for this dissertation, several mechanisms had been proposed to explain the response characteristics of DTNs. *In vivo* electrophysiological experiments revealed clues about the underlying neural circuitry and provided a framework for building hypothetical conceptual models of neural tuning to stimulus duration. These models were constructed to fit the observed data and were well supported by research of the time. This dissertation contributes a deeper understanding of the mechanisms inherent in these models by instantiating them computationally. A computational model provides a malleable parameter space that permits in-depth exploration of a mechanism's biological plausibility, response characteristics, and relationship to other mechanisms. A valid computational model can also be used to predict responses in novel experimental tests.

A computational model cannot prove the existence of a biological mechanism nor is that the purpose of producing a model. In Chapters 2 and 3, we explored the consequences of implementing purely theoretical models of duration tuning with actual spiking neurons. First we demonstrated that spiking neuron implementations of the mechanisms offered no immediate existential barriers. Next, we demonstrated by modifications of the parameters that the models could reproduce responses observed *in vivo* under both standard and modified (e.g. pharmacological manipulation) conditions. The results of experiments performed *in vivo* allow one to infer, or at least narrow down, the underlying mechanisms from the observable outcomes (e.g. response profiles). Performing the equivalent experiments with computational models admits one full access to the mechanisms responsible for the output. If the computational model is able to reproduce, and predict, observable data then it is evidence that the biological and computational mechanisms might be similar.

Our computational models reproduced non-manipulated responses of *in vivo* DTNs but also, unintentionally, reproduced manipulated responses. This provides additional evidence that the implemented mechanisms were plausible and increases the likelihood that the mechanisms are, at least partially, correct. Furthermore, we are able to make predictions about *in vivo* responses from subtleties in the computational models. For example, in Chapter 3 we predicted that the stimulus duration evoking a maximum response need not be the duration that produces the maximum coincidence of onset- and offset-evoked excitatory inputs; a previous tenet of the coincidence detection mechanism. This result and other response predictions provide further evidence, testable *in vivo*, in support of the proposed

mechanisms. Together, the computational modelling studies in this dissertation provide a framework for studying the neural mechanisms of DTNs both by revealing testable subtleties in the mechanisms and by demonstrating the interconnectedness of an entire family of mechanisms hypothesized to produce their responses.

Researchers studying DTNs have typically worked under the hypothesis that DTNs were used to encode stimulus duration. In Chapter 4, I applied information theoretic approaches to the responses of *in vivo* DTNs to evaluate how robust and sensitive their encoding of duration was. I validated the prior assumption that durations evoking the most spikes (best duration) from a DTN often have the most robust encoding; however, a DTN's peak sensitivity to changing stimulus duration is often at non-best durations. Furthermore, I used responses from a population of 97 DTNs to demonstrate how stimulus durations from 1 to 25 ms could reliably be decoded from spiking responses even though the span of best durations did not cover all such durations. These results are important for future studies that aim to characterize DTN responses within a species. It is not just the best duration that is important but the entire response profile over all stimulus durations that matters. Furthermore, the information theory analysis used in this study provides a tool set for researchers to gain a deeper understanding of DTN responses beyond the classically reported response probability functions.

5.2   How the Nervous System Tells Time

Time is a fundamental component of all perception. Even the perception of a static visual scene must be integrated over time and specific neural mechanisms have evolved to encode time absolutely. Duration-tuned neurons are examples of such a mechanism. A general principle that underlies all mechanisms of temporal perception is a change of state over time. By learning the correlation between changes in neural states and temporal intervals, the nervous system can encode temporal information (Buonomano and Maass, 2009). The state of a neural system can be characterized by a host of kinetic variables operating on multiple levels such spiking responses, synaptic plasticity, membrane voltage, receptor sensitivity, etc. The key is that each of these variables can have well defined and stable kinetics that can be used as markers for the passage of time. For example, in the coincidence detection mechanism of DTNs, a neuron's temporal tuning is partially determined by the latency of

onset-evoked excitatory inputs to the neuron. In order for a DTN to reliably encode a specific duration, it must rely on these latencies to be stable across multiple presentations of the same stimulus. Therefore, DTNs are essentially mapping external temporal events onto the kinetics of inter-neuron projection latencies.

In general, suppose S_0 is the state of the nervous system at time 0 and that a function, $\hat{K}(S, t)$, determines the state at time t, S_t, as a function of the system's kinetics. An observer could compute the passage of time from these neural states if the observer was able to compute an inverse of $\hat{K}$ that solves for t. That is,

$$\hat{K}^{-1}(S_0, S_t) = t.$$

For example, consider the pacemaker-accumulator model described in Chapter 2. The relevant state variable in this case is the number of events that have occurred (e.g. spikes). Given two states, the passage of time can be computed with

$$t = \hat{K}^{-1}(S_0, S_t) = (S_t - S_0)\Delta e$$

where S_0 and S_t represent the number of events at time 0 and time t and Δe represents the time difference between successive events.

A DTN's ability to encode duration can be formulated in a similar manner. At any given time, the state of a duration-tuned neural network includes the state of inputs (excitatory and inhibitory) as well as the state of the DTN itself. Consider a simplified example of the coincidence detection mechanism where the onset- and offset-evoked excitatory inputs are perfectly coincident for stimuli with duration d_0 and a single spike is produced if and only if this duration is presented. For all other stimulus durations, no spikes are produced. The temporal decoding function could be formulated as

$$t = \hat{K}^{-1}(S_0, S_t) = \begin{cases} d_0 & : \text{ON}_{\text{Arrive}} \text{ AND OFF}_{\text{Arrive}} \\ unknown & : otherwise \end{cases}$$

where $\text{ON}_{\text{Arrive}}$ stands for the arrival of a spike from the onset-evoked excitatory input and $\text{OFF}_{\text{Arrive}}$ stands for the arrival of a spike from the offset-evoked excitatory input. In other words, if the state of the system at time t is such that both the onset- and offset-evoked excitatory inputs arrive at the DTN, then we can compute that time t is equal to the duration d_0. The starting state, S_0, is assumed to always be the onset of a stimulus. A system would have to understand how the latencies of the onset- and offset-evoked events corresponded

to the duration d_0 in order to learn that the response of this DTN corresponds to external temporal events of that duration. That is, d_0 becomes encoded as a function of input latencies. In reality, the state of a DTN and its inputs at any given time will have additional noise (e.g. membrane potential fluctuations, input spike time jitter) and thus only be an approximation of the duration (i.e. $t \approx \hat{K}^{-1}(S_0, S_t)$); however, as demonstrated in Chapter 4, combining such responses across a population can create far more robust determinations of duration.

The passage of time is measured, by any system, relative to the kinetics of a reference system (Falk, 2008). The only reference available to the nervous system is its own internal kinetics. Several different internal kinetics are available such as spike latencies, spike counts, membrane integration times, receptor activation times, receptor deactivation times, just to name a few. One could suggest that the environment can also act as a reference for the passage of time, such as watching the seconds hand on a clock. However, in order to perceive that a second has passed, a memory of each successive tick of the clock must be stored by the nervous system and the distance between percepts of the second hand moving can only be measured relative to the kinetics of the internal memory trace of the previous tick. In fact, the state of the nervous system, such as during or after a saccade, can distort this temporal perception and produce the "stopped clock" illusion (Eagleman, 2008). The next section describes different factors that could lead to changes in the kinetics of neural circuits underlying DTNs and thus distort their ability to encode time.

5.3 Future Avenues of Research

5.3.1 Duration-Tuned Neurons and Behaviour

Response properties of DTNs have been documented in a variety of vertebrates. Unfortunately, those results do not demonstrate how DTNs relate to the behaviour of an animal. It is tempting to suggest that vocalization durations relevant to a particular species are selected for in the response distributions of DTNs and that vocal behaviour can be, at least in part, a function of the duration decoded from the responses of DTNs. The mechanisms that produce these responses are becoming better understood, but until now, information contained within those responses has not been characterized. Narins and Capranica (1980) suggested a simple filtering mechanism within the frog auditory midbrain (torus semicircularis) that includes DTNs to filter the duration of auditory signals. If a "CO-QUI" vocalization from another

frog is heard then it will pass through a series of filters, including a duration tuning filter. If the sound passes through all filters then the frog will evoke a response of "CO". It appears that the typical range of duration tuning within a species is somewhat correlated with the durations of typical species-specific vocalizations (Sayegh et al. (2011), Table 5.1). This suggests that DTNs may be used for filtering and detecting import acoustic signals for that species; however, a study comparing the responses of DTNs with simple acoustic stimuli (e.g. pure tones or noise stimuli) and also species-specific vocalizations, has yet to be done in non-bat species. In bats, DTNs appear especially suited for processing echolocation calls (Mora and Kössl, 2004; Jen and Wu, 2008; Luo et al., 2008; Wu and Jen, 2008); however, the difficulty of recording from neurons in actively behaving animals makes it extremely difficult to properly test the responses of DTNs to real outgoing biosonar pulses and their echo reflected during echolocation.

We must also consider potential differences between neural responses recorded in a quiet laboratory versus responses from the same neuron in the animal's a natural setting. Duration-tuned neuron responses in most species were recorded while the animal was anaesthetized with drugs such as urethane (e.g. Yin et al., 2008; Pérez-González et al., 2006) or ketamine (e.g. Brand et al., 2000). Both anaesthetics are known to affect excitatory and inhibitory receptor channels to different degrees (urethane: Hara and Harris (2002), ketamine: Yamakura et al. (2000)), hence they would likely affect the response characteristics of DTNs. Even though recordings of DTNs in bats have nearly always[1] been obtained from awake animals, the conditions in a laboratory are not the same as an animal in its natural setting.

For example, Hall et al. (2010) demonstrated that serotonin levels (5-hydroxytryptamine; 5-HT) in the IC of the mouse are modulated by both internal state and behavioural conditions. Awake mice had higher 5-HT levels in the IC than anaesthetized mice and mice exposed to noise or physical restraint had higher IC 5-HT levels than freely behaving mice. Serotonin has not explicitly been studied in the context of duration tuning; however, it likely modulates the response characteristics of DTNs when animals are in different behavioural states. The metabotropic 5-HT_{1A} receptor tends to depress the response of bat IC neurons with long FSLs (Hurley, 2007), and the metabotropic 5-HT_{1B} receptor reduces the effectiveness of GABA_A mediated inhibition in the IC (Hurley et al., 2008). The only ionotropic serotonin receptor, 5-HT_3, produces complex, neuron dependent, effects in the IC that can increase

---

[1]Fuzessery and Hall (1999) kept the pallid bat lightly sedated with sodium pentobarbital.

Table 5.1: Neuronal best duration (BD) tuning in amphibians and mammals compared with typical species-specific acoustic vocalization durations. Neuronal BD data reported as the range of BDs of shortpass and bandpass DTNs. Overlap between neural BD and vocalization duration is likely greater than reported because the range of a DTN's temporal tuning is generally wider than its BD. Table adapted from Sayegh et al. (2011).

Species	Region	Neuronal BD	Vocalization Duration
Frog			
R. pipiens & H. Regilla	TS	4 – 50 ms (PT)[1]	8 – 17 ms,32–39.9 pulses/s
R. pipiens	TS	25 – 280 ms (PT)[3]	(*R. pipiens*)[2]
R. catesbeiana	TS	25 – 40 ms (PT)[4]	800 ms[5]
Mouse			
M. musculus	IC	6 – 80 ms (PT)[6]	ca. 8 – 75 ms
		3 – 300 ms (PT)[7]	Pups: ca. 8 – 100ms[8]
Rat			
R. norvegicus	IC	4 – 128 ms (PT)[9]	ca. 20 – 80 ms & >300 ms
			Pups: ca. 80 – 140 ms [10]
Chinchilla	IC	20 – 60 ms (PT) [11]	ca. 15 – >400 ms[12]
Guinea pig	IC	<8 – 128 ms (PT) [13]	ca. 100+ ms[13]
	MGB	200 ms (PT) [14,a]	
Cat			
F. domesticus	AC	50 – 200 ms (PT)[15]	400 – 1600 ms[16]
Bat			
E. fuscus	IC	1 – 8 ms (PT)[17]	<1 – 20 ms (echolocation)
	IC	1 – 7 ms (PT)	Primarily ca. 1 ms[18]
		2 – 20 ms (FM)[19]	
	IC	1 – 20 ms (PT)[20]	
A. pallidus	IC	0.5 – 7 ms (PT & FM)[21]	<1.5 – 6 ms (echolocation)[21]
M. lucifugus	AC	<10 ms (PT)[22]	<0.5 – 20 ms (echolocation)[22]
			40 – 120 ms (social)[23]
M. molossus	IC	1 – 25 ms (PT & noise)[24,b]	ca. 10 (echolocation)[25]
R. pusillus	IC	ca. 5 – 40 ms (PT)	16.8 – 58 ms[26]
		ca. 5 – 60 ms (PT+FM)[26]	

AC: auditory cortex; *FM*: frequency modulated; *IC*: inferior colliculus; *MGB*: medial geniculate body; *PT*: pure tone; *TS*: torus semicircularis.

[a] He (2002) found only 1 DTN (bandpass) out of 20 cells tested for duration selectivity.

[b] Mora and Kössl (2004) report offset responding DTNs with two distinct best durations, a feature thus far unique to *M. molossus*.

[1] Leary et al. (2008)   [2] Mecham (1971)   [3] Gooler and Feng (1992)   [4] Potter (1965)   [5] Capranica (1968)   [6] Brand et al. (2000)   [7] Xia et al. (2000)   [8] Liu et al. (2003)   [9] Pérez-González et al. (2006)   [10] Knutson et al. (2002)   [11] Chen (1998)   [12] Hunyady (2008)   [13] Wang et al. (2006)   [14] He (2002)   [15] He et al. (1997)   [16] Brown et al. (1978)   [17] Faure et al. (2003)   [18] Simmons (1989)   [19] Ehrlich et al. (1997)   [20] Pinheiro et al. (1991)   [21] Fuzessery and Hall (1999)   [22] Galazyuk and Feng (1997)   [23] Melendez et al. (2006)   [24] Mora and Kössl (2004)   [25] Kössl et al. (1999)   [26] Luo et al. (2008)

or decrease spike rates (Bohorquez and Hurley, 2009; Miko and Sanes, 2009). Increased levels of 5-HT in the IC during active or stressful behavioural situations could therefore dramatically change the temporal selectivity of DTNs. Inhibition, in particular, seems critical for shaping the responses of DTNs (Jen and Feng, 1999; Fuzessery and Hall, 1999; Casseday et al., 2000; Jen and Wu, 2005; Yin et al., 2008) and thus increased depression via 5-HT$_{1A}$ receptors or decreased GABA$_A$ effectiveness could either sharpen or broaden the duration tuning profile of a DTN. Studies that combine *in vivo* recordings of DTNs with 5-HT receptor agonists and antagonists would help to decipher how behavioural context could change neural tuning to stimulus duration tuning in the IC.

5.3.2 Duration-Tuned Neurons and Presbycusis

Presbycusis, or age-related hearing loss, is the natural onset of hearing deficiencies with age and affects both spectral and temporal processing (Pichora-Fuller and MacDonald, 2008). For example, older humans have shown a decreased ability to detect stimulus duration differences (higher Weber fractions) even when their spectral hearing sensitivity was as good as younger listeners (Fitzgibbons et al., 2007). This suggests that auditory mechanisms of temporal processing can lose efficiency with age and unlike spectral hearing loss, they cannot be recovered with current hearing aid technologies. A potential source of temporal sensitivity degradation could be age related changes in neural inhibition mechanisms in the IC. With age, the level of GABA release in the IC decreases, but at the same time GABA$_A$ receptor affinity increases (Milbrandt et al., 1996; Caspary et al., 2008). Other age related receptor changes in the IC, such as deceased GABA$_B$ receptor binding (Milbrandt et al., 1994), upregulation of 5-HT$_{2B}$ receptors (Tadros et al., 2007) and overall attrition of dendrites and synapses (Helfert et al., 1999) will also likely change the temporal response patterns of auditory neurons, including DTNs.

A study of DTN population response characteristics across young and aged animals, similar to that presented in Chapter 4, could be valuable for understanding mechanisms responsible for temporal processing deficiencies associated with presbycusis. Although the response properties are hard to predict, behavioural data suggests that DTN responses would become less robust to encoding duration and may exhibit decreased stimulus-specific information and Fisher information as a result of increased response variance and decreased response specificity. Understanding neural mechanisms underlying or associated with

presbycusis in the temporal domain is an important step towards the development of effective treatments.

References

Aubie B, Becker S, Faure PA (2009) Computational models of millisecond level duration tuning in neural circuits. *J Neurosci* 29:9255–9270.

Aubie B, Sayegh R, Faure PA (2012) Duration Tuning across Vertebrates. *J Neurosci* 32:6373–6390.

Bandyopadhyay S, Shamma SA, Kanold PO (2010) Dichotomy of functional organization in the mouse auditory cortex. *Nat Neurosci* 13:361–368.

Behrend O, Brand A, Kapfer C, Grothe B (2002) Auditory response properties in the superior paraolivary nucleus of the gerbil. *J Neurophysiol* 87:2915–2928.

Bohorquez A, Hurley LM (2009) Activation of serotonin 3 receptors changes *in vivo* auditory responses in the mouse inferior colliculus. *Hear Res* 251:29–38.

Brand A, Urban A, Grothe B (2000) Duration tuning in the mouse auditory midbrain. *J Neurophysiol* 84:1790–1799.

Brette R, Gerstner W (2005) Adaptive exponential integrate-and-fire model as an effective description of neuronal activity. *J Neurophysiol* 94:3637–3642.

Brown KA, Buchwald JS, Johnson JR, Mikolich DJ (1978) Vocalization in the cat and kitten. *Dev Psychobiol* 11:559–570.

Buonomano DV, Maass W (2009) State-dependent computations: spatiotemporal processing in cortical networks. *Nature Rev Neurosci* 10:113–125.

Busch KE, Laurent P, Soltesz Z, Murphy RJ, Faivre O, Hedwig B, Thomas M, Smith HL, de Bono M (2012) Tonic signaling from O2 sensors sets neural circuit activity and behavioral state. *Nat Neurosci* 15:581–591.

Capranica RR (1968) The vocal repertoire of the bullfrog (*Rana catesbeiana*). *Behaviour* 31:302–325.

Carnevale NT, Hines ML (2006) *The NEURON book* Cambridge University Press, Cambridge, UK.

Caspary DM, Ling L, Turner JG, Hughes LF (2008) Inhibitory neurotransmission, plasticity and aging in the mammalian central auditory system. *J Exp Biol* 211:1781–1791.

Casseday JH, Ehrlich D, Covey E (1994) Neural tuning for sound duration: role of inhibitory mechanisms in the inferior colliculus. *Science* 264:847–850.

Casseday JH, Ehrlich D, Covey E (2000) Neural measurement of sound duration: control by excitatory-inhibitory interactions in the inferior colliculus. *J Neurophysiol* 84:1475–1487.

Chen GD (1998) Effects of stimulus duration on responses of neurons in the chinchilla inferior colliculus. *Hear Res* 112:142–150.

Chen X, Leischner U, Rochefort NL, Nelken I, Konnerth A (2011) Functional mapping of single spines in cortical neurons in vivo. *Nature* 475:501–505.

Courant R (1961) *Differential and Integral Calculus* Blackie & Son Limited, London and Glasgow.

Covey E, Casseday JH (1991) The monaural nuclei of the lateral lemniscus in an echolocating bat: parallel pathways for analyzing temporal features of sound. *J Neurosci* 11:3456–3470.

Dallos P (1992) The active cochlea. *J Neurosci* 12:4575–4585.

Dallos P, Harris D (1978) Properties of auditory nerve responses in absence of outer hair cells. *J Neurophysiol* 41:365–383.

Dallos P (2008) Cochlear amplification, outer hair cells and prestin. *Curr Opin Neurobiol* 18:370–376.

Eagleman DM (2008) Human time perception and its illusions. *Curr Opin Neurobiol* 18:131–136.

Ehrlich D, Casseday JH, Covey E (1997) Neural tuning to sound duration in the inferior colliculus of the big brown bat, *Eptesicus fuscus. J Neurophysiol* 77:2360–2372.

Faingold CL, Boersma Anderson CA, Caspary DM (1991) Involvement of GABA in acoustically-evoked inhibition in inferior colliculus neurons. *Hear Res* 52:201–216.

Falk D (2008) *In Search of Time: Journeys Along a Curious Dimension* McClelland & Stewart, Toronto.

Faure PA, Fremouw T, Casseday JH, Covey E (2003) Temporal masking reveals properties of sound-evoked inhibition in duration-tuned neurons of the inferior colliculus. *J Neurosci* 23:3052–3065.

Fitzgibbons PJ, Gordon-Salant S, Barrett J (2007) Age-related differences in discrimination of an interval separating onsets of successive tone bursts as a function of interval duration. *J Acoust Soc Am* 122:458.

Fuzessery ZM, Hall JC (1999) Sound duration selectivity in the pallid bat inferior colliculus. *Hear Res* 137:137–154.

Galazyuk AV, Feng AS (1997) Encoding of sound duration by neurons in the auditory cortex of the little brown bat, *Myotis lucifugus. J Comp Physiol A* 180:301–311.

Gold T (1948) Hearing. II. The physical basis of the action of the cochlea. *Proc. Biol. Sci.* 135:492–498.

Gooler DM, Feng AS (1992) Temporal coding in the frog auditory midbrain: the influence of duration and rise-fall time on the processing of complex amplitude-modulated stimuli. *J Neurophysiol* 67:1–22.

Grothe B, Covey E, Casseday JH (2001) Medial superior olive of the big brown bat: neuronal responses to pure tones, amplitude modulations, and pulse trains. *J Neurophysiol* 86:2219–2230.

Grothe B, Park TJ, Schuller G (1997) Medial superior olive in the free-tailed bat: response to pure tones and amplitude-modulated tones. *J Neurophysiol* 77:1553–1565.

Guinan J, Guinan S, Norris B (1972) Single auditory units in the superior olivary complex: I: responses to sounds and classifications based on physiological properties. *Int J Neurosci* 4:101–120.

Hall IC, Rebec GV, Hurley LM (2010) Serotonin in the inferior colliculus fluctuates with behavioral state and environmental stimuli. *J Exp Bio* 213:1009–1017.

Hara K, Harris RA (2002) The anesthetic mechanism of urethane: the effects on neurotransmitter-gated ion channels. *Anesth. Analg.* 94:313–8– table of contents.

He J (2002) OFF responses in the auditory thalamus of the guinea pig. *J Neurophysiol* 88:2377–2386.

He J, Hashikawa T, Ojima H, Kinouchi Y (1997) Temporal integration and duration tuning in the dorsal zone of cat auditory cortex. *J Neurosci* 17:2615–2625.

Helfert RH, Sommer TJ, Meeks J, Hofstetter P, Hughes LF (1999) Age-related synaptic changes in the central nucleus of the inferior colliculus of Fischer-344 rats. *J Comp Neurol* 406:285–298.

Hines ML, Davison AP, Muller E (2009) NEURON and Python. *Front Neuroinform* 3:1–12.

Hooper SL, Buchman E, Hobbs KH (2002) A computational role for slow conductances: single-neuron models that measure duration. *Nat Neurosci* 5:552–556.

Hunyady H (2008) Vocal sounds of the chinchilla Ph.D. diss., Bowling Green State University.

Hurley LM (2007) Activation of the serotonin 1A receptor alters the temporal characteristics of auditory responses in the inferior colliculus. *Brain Res* 1181:21–29.

Hurley LM, Tracy JA, Bohorquez A (2008) Serotonin 1B receptor modulates frequency response curves and spectral integration in the inferior colliculus by reducing GABAergic inhibition. *J Neurophysiol* 100:1656–1667.

Jen PHS, Feng RB (1999) Bicuculline application affects discharge pattern and pulse-duration tuning characteristics of bat inferior collicular neurons. *J Comp Physiol A* 184:185–194.

Jen PHS, Schlegel PA (1982) Auditory physiological properties of the neurones in the inferior colliculus of the big brown bat, *Eptesicus fuscus*. *J Comp Physiol A* 147:351–363.

Jen PHS, Wu CH (2005) The role of GABAergic inhibition in shaping the response size and duration selectivity of bat inferior collicular neurons to sound pulses in rapid sequences. *Hear Res* 202:222–234.

Jen PHS, Wu CH (2008) Echo duration selectivity of the bat varies with pulse-echo amplitude difference. *NeuroReport* 19:373–377.

Kelly JB, van Adel BA, Ito M (2009) Anatomical projections of the nuclei of the lateral lemniscus in the albino rat (*Rattus norvegicus*). *J Comp Neurol* 512:573–593.

Kiang NYS (1965) *Discharge patterns of single fibers in the cat's auditory nerve* MIT Press, Cambridge, MA.

Knutson B, Burgdorf J, Panksepp J (2002) Ultrasonic vocalizations as indices of affective states in rats. *Psychol Bull* 128:961–977.

Kössl M, Mora E, Coro F, Vater M (1999) Two–toned echolocation calls from *Molossus molossus* in Cuba. *J Mammal* 80:929–932.

Kulesza RJ, Spirou GA, Berrebi AS (2003) Physiological response properties of neurons in the superior paraolivary nucleus of the rat. *J Neurophysiol* 89:2299–2312.

Leary CJ, Edwards CJ, Rose GJ (2008) Midbrain auditory neurons integrate excitation and inhibition to generate duration selectivity: an *in vivo* whole-cell patch study in anurans. *J Neurosci* 28:5481–5493.

Liberman MC, Gao J, He DZZ, Wu X, Jia S, Zuo J (2002) Prestin is required for electromotility of the outer hair cell and for the cochlear amplifier. *Nature* 419:300–304.

Liu RC, Miller KD, Merzenich MM, Schreiner CE (2003) Acoustic variability and distinguishability among mouse ultrasound vocalizations. *J Acoust Soc Am* 114:3412–3422.

Llinás RR, Steriade M (2006) Bursting of thalamic neurons and states of vigilance. *J Neurophysiol* 95:3297–3308.

Loftus WC, Bishop DC, Saint Marie RL, Oliver DL (2004) Organization of binaural excitatory and inhibitory inputs to the inferior colliculus from the superior olive. *J Comp Neurol* 472:330–344.

Luo F, Metzner W, Wu F, Wu FJ, Zhang S, Zhang SY, Chen Q, Chen QC (2008) Duration-sensitive neurons in the inferior colliculus of horseshoe bats: adaptations for using CF-FM echolocation pulses. *J Neurophysiol* 99:284–296.

Malmierca MS, Izquierdo MA, Cristaudo S, Hernandez O, Pérez-González D, Covey E, Oliver DL (2008) A Discontinuous Tonotopic Organization in the Inferior Colliculus of the Rat. *J Neurosci* 28:4767–4776.

Mecham J (1971) Vocalizations of the leopard frog, *Rana pipiens*, and three related Mexican species. *Copeia* 1971:505–516.

Melendez KV, Jones DL, Feng AS (2006) Classification of communication signals of the little brown bat. *J Acoust Soc Am* 120:1095.

Miko IJ, Sanes DH (2009) Transient gain adjustment in the inferior colliculus is serotonin- and calcium-dependent. *Hear Res* 251:39–50.

Milbrandt JC, Albin RL, Caspary DM (1994) Age-related decrease in $GABA_B$ receptor binding in the Fischer 344 rat inferior colliculus. *Neurobiol Aging* 15:699–703.

Milbrandt JC, Albin RL, Turgeon SM, Caspary DM (1996) $GABA_A$ receptor binding in the aging rat inferior colliculus. *Neuroscience* 73:449–458.

Møller AR (2000) *Hearing: its physiology and pathophysiology* Academic Press.

Moore D, Kotak V, Sanes D (1998) Commissural and lemniscal synaptic input to the gerbil inferior colliculus. *J Neurophysiol* 80:2229.

Mora EC, Kössl M (2004) Ambiguities in sound duration selectivity by neurons in the inferior colliculus of the bat *Molossus molossus* from Cuba. *J Neurophysiol* 91:2215–2226.

Moser T, Neef A, Khimich D (2006) Mechanisms underlying the temporal precision of sound coding at the inner hair cell ribbon synapse. *J Physiol* 576:55–62.

Narins PM, Capranica RR (1980) Neural adaptations for processing the two-note call of the Puerto Rican treefrog, *Eleutherodactylus coqui. Brain Behav Evol* 17:48–66.

Nayagam DAX, Clarey JC, Paolini AG (2005) Powerful, onset inhibition in the ventral nucleus of the lateral lemniscus. *J Neurophysiol* 94:1651–1654.

Oliver DL, Beckius GE, Shneiderman A (1995) Axonal projections from the lateral and medial superior olive to the inferior colliculus of the cat: a study using electron microscopic autoradiography. *J Comp Neurol* 360:17–32.

Pérez-González D, Malmierca MS, Moore JM, Hern a ndez O, Covey E (2006) Duration selective neurons in the inferior colliculus of the rat: topographic distribution and relation of duration sensitivity to other response properties. *J Neurophysiol* 95:823–836.

Pichora-Fuller K, MacDonald E (2008) Auditory temporal processing deficits in older listeners: From a review to a future view of presbycusis. *1st International Symposium on Auditory and Audiological Research* .

Pickles JO (1988) *An introduction to the physiology of hearing* Academic Press, London, 2nd edition.

Pinheiro AD, Wu M, Jen PH (1991) Encoding repetition rate and duration in the inferior colliculus of the big brown bat, *Eptesicus fuscus. J Comp Physiol A* 169:69–85.

Pollak GD, Gittelman JX, Li N, Xie R (2011) Inhibitory projections from the ventral nucleus of the lateral lemniscus and superior paraolivary nucleus create directional selectivity of frequency modulations in the inferior colliculus: a comparison of bats with other mammals. *Hear Res* 273:134–144.

Potter HD (1965) Patterns of acoustically evoked discharges of neurons in the mesencephalon of the bullfrog. *J Neurophysiol* 28:1155–1184.

Rhode WS, Greenberg S (1992) Physiology of the cochlear nuclei In N PA, Fay RR, editors, *The mammalian auditory pathway: neurophysiology*, pp. 94–152. Springer-Verlag, New York.

Rhode WS, Roth GL, Recio-Spinoso A (2010) Response properties of cochlear nucleus neurons in monkeys. *Hear Res* 259:1–15.

Rothschild G, Nelken I, Mizrahi A (2010) Functional organization and population dynamics in the mouse primary auditory cortex. *Nat Neurosci* 13:353–360.

Saldaña E, Merchán MA (1992) Intrinsic and commissural connections of the rat inferior colliculus. *J Comp Neurol* 319:417–437.

Sayegh R, Aubie B, Faure PA (2011) Duration tuning in the auditory midbrain of echolocating and non-echolocating vertebrates. *J Comp Physiol A* 197:571–583.

Schreiner CE, Langner G (1997) Laminar fine structure of frequency organization in auditory midbrain. *Nature* 388:383–386.

Shneiderman A, Chase MB, Rockwood JM, Benson CG, Potashner SJ (1993) Evidence for a GABAergic projection from the dorsal nucleus of the lateral lemniscus to the inferior colliculus. *J Neurochem* 60:72–82.

Simmons JA (1989) A view of the world through the bat's ear: the formation of acoustic images in echolocation. *Cognition* 33:155–199.

Singh S, Mountain DC (1997) A model for duration coding in the inferior colliculus In *Proceedings of the annual conference on Computational neuroscience: Trends in research*, pp. 497–503. New York: Plenum.

Straughan IR (1975) An analysis of the mechanisms of mating call discrimination in the frogs *Hyla regilla* and *H. cadaverina*. *Copeia* 3:415–424.

Tadros SF, D'Souza M, Zettel ML, Zhu X, Lynch-Erhardt M, Frisina RD (2007) Serotonin 2B receptor: upregulated with age and hearing loss in mouse auditory system. *Neurobiol Aging* 28:1112–1123.

Tan ML, Borst JGG (2007) Comparison of responses of neurons in the mouse inferior colliculus to current injections, tones of different durations, and sinusoidal amplitude-modulated tones. *J Neurophysiol* 98:454–466.

Vater M, Covey E, Casseday JH (1997) The columnar region of the ventral nucleus of the lateral lemniscus in the big brown bat (*Eptesicus fuscus*): synaptic arrangements and structural correlates of feedforward inhibitory function. *Cell Tissue Res* 289:223–233.

von Békésy G (1960) *Experiments in hearing.* McGraw Hill.

Wagner TT (1996) Lemniscal input to identified neurons of the central nucleus of mouse inferior colliculus: an intracellular brain slice study. *Eur J Neurosci* 8:1231–1239.

Wang J, van Wijhe R, Chen Z, Yin S (2006) Is duration tuning a transient process in the inferior colliculus of guinea pigs? *Brain Res* 1114:63–74.

Wu CH, Jen PHS (2008) Echo frequency selectivity of duration-tuned inferior collicular neurons of the big brown bat, *Eptesicus fuscus*, determined with pulse-echo pairs. *Neuroscience* 156:1028–1038.

Xia YF, Qi ZH, Shen JX (2000) Neural representation of sound duration in the inferior colliculus of the mouse. *Acta Otolaryngol* 120:638–643.

Yamakura T, Chavez-Noriega L, Harris R (2000) Subunit-dependent inhibition of human neuronal nicotinic acetylcholine receptors and other ligand-gated ion channels by dissociative anesthetics ketamine and dizocilpine. *Anesthesiology* 92:1144.

Yin S, Chen Z, Yu D, Feng Y, Wang J (2008) Local inhibition shapes duration tuning in the inferior colliculus of guinea pigs. *Hear Res* 237:32–48.

Yost WA (2007) *Fundamentals of hearing: an introduction* Academic Press, 5th edition.

Zheng J, Shen W, He DZ, Long KB, Madison LD, Dallos P (2000) Prestin is the motor protein of cochlear outer hair cells. *Nature* 405:149–155.

Zorović M (2011) Temporal processing of vibratory communication signals at the level of ascending interneurons in *Nezara viridula* (Hemiptera: Pentatomidae). *PLoS One* 6:e26843.

`dtnet` **Modelling Software** **A**
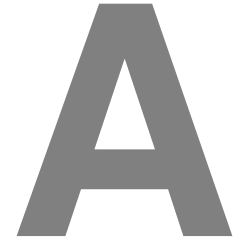
A.1   Availability

Custom written neural network simulation software named `dtnet` was used to run the simulations in Aubie et al. (2009) (Chapter 2). The current version of `dtnet` is available online at `http://www.github.com/baubie/dtnet` and can be compiled on most computers running Linux. In order to compile `dtnet`, the open source Boost C++ libraries (`http://www.boost.org`) are required. Results are outputted as human readable text files, however, built-in graphing capability can be taken advantage of by installing the open source GLE software package available at `http://glx.sourceforge.net`.

A.2   Overview

`dtnet` was designed to run simulations of neural networks and easily search parameter spaces by allowing the user to specify multiple parameter ranges and then running simulations of all possible parameter combinations. Due to the high computational demand, `dtnet` has multi-threading capability built in to run an arbitrary number of simulations in parallel and then aggregate the results after all simulations are complete.

A.2.1 Simple Example

Networks are created using the `dtnet` markup language, an XML schema. First, a user can create a list of neural populations and specify the parameters for neurons within that population. These parameters can also be randomly chosen from a normal distribution at the beginning of each simulation by specifying a non-zero sigma value in the parameter definition tag. Next, a user can specify connections between populations along with a connection weight and response delay. Any parameter values can be replaced with a range of values to have `dtnet` automatically create simulations for each value. For example, Listing A.1 snippet defines two neural populations composed of single neurons as well as a Poisson spiking process. The Poisson spiking process excites the first neuron which then excites the second neuron.

Listing A.2 is a similar XML file that defines the stimuli that will be used to drive any population of neurons with the `accept_input` value set to `true`. In this case, a single pure stimulus is created with durations 0 ms through 25 ms. All populations that accept input will receive all inputs that are defined.

Finally, to define and run simulations, a script file can be written in the `dtlang` script language. Scripts are run with the command `dtnet -s scriptname`. For more information on the `dtnet` command, run `dtnet --help`. Alternatively, running the `dtnet` command on its own will present one with a `dtnet>` prompt that allows script commands to be entered manually one-by-one. Listings A.3 shows an example script file that runs our example simulation and produces a series of figures via GLE.

A.2.2 Implementation Details

`dtnet` is separated into three interacting components as illustrated in Figure A.1. `libdtnet` contains all of core code that runs network simulations and saves the data. Neuron model definitions are separate libraries loaded dynamically, as needed, by `libdtnet` so that additional neuron models could be created without the need to recompile `libdtnet`. Simulations are defined by the user and initiated via the `dtlang` module where the `dtnet` script language is defined and parsed.

Simulations published in Aubie et al. (2009) implemented the Adaptive Exponential Integrate-and-Fire (aEIF) model neuron (Brette and Gerstner, 2005) and use the fourth order Runge-Kutta differential equation solving algorithm as implemented in Listing A.4. The

174

Listing A.1: pair.xml

```xml
 1 <?xml version="1.0" encoding="UTF-8" standalone="no"?>
 2
 3 <network title="Pair of Neurons">
 4     <population id="INPUT" title="Input" type="Poisson">
 5         <param name="size">1</param>
 6         <param name="mu">400</param>
 7         <param name="accept_input">true</param>
 8     </population>
 9
10     <population id="N1" title="Neuron 1" type="aEIF">
11         <param name="size">1</param>
12         <param name="C" sigma="1">220</param>
13         <param name="a" sigma="0">40</param>
14         <param name="b" sigma="0">10</param>
15         <param name="tauw" sigma="0">250</param>
16         <param name="EL" sigma="0">-65</param>
17         <param name="VR" sigma="0">-63</param>
18         <param name="VT" sigma="0">-52</param>
19     </population>
20
21     <population id="N2" title="Neuron 2" type="aEIF">
22         <param name="size">1</param>
23         <param name="C" sigma="5">220</param>
24         <param name="a" sigma="0">40</param>
25         <param name="b" sigma="2">10</param>
26         <param name="tauw" sigma="0">250</param>
27         <param name="EL" sigma="0">-65</param>
28         <param name="VR" sigma="0">-63</param>
29         <param name="VT" sigma="1">-52</param>
30     </population>
31
32     <connection>
33         <param name="from">INPUT</param>
34         <param name="to">N1</param>
35         <param name="weight">5</param>
36         <param name="delay">1</param>
37         <param name="density">1</param>
38         <param name="symmetric">false</param>
39     </connection>
40     <connection>
41         <param name="from">N1</param>
42         <param name="to">N2</param>
43         <param name="weight">3</param>
44         <param name="delay">1</param>
45         <param name="density">1</param>
46         <param name="symmetric">false</param>
47     </connection>
48 </network>
```

Listing A.2: durations.xml

```xml
 1 <?xml version="1.0" ?>
 2
 3 <trial>
 4     <input type="pure" ID="main">
 5         <param name="delay">0</param>
 6         <param name="amplitude">1</param>
 7         <param name="duration"><range start="0" end="25" step="1" /></param>
 8     </input>
 9 </trial>
```

Listing A.3: pair.dtnet

```
 1 set("T", 40)
 2 set("graph.width", 8.5)
 3 set("graph.height", 8.5)
 4 sim = simulation("networks/pair.xml", "inputs/durations.xml")
 5 results = run(sim,"",100,5)
 6 print(results)
 7
 8 graphspiketrains(results, "N1", "pair_N1_spikes.eps")
 9
10 short  = constrain(results, "trial.main.duration", 1)
11 medium = constrain(results, "trial.main.duration", 5)
12 long   = constrain(results, "trial.main.duration", 10)
13 graphtrial_voltage(short,0,"pair_1ms.eps")
14 graphtrial_voltage(medium,0,"pair_8ms.eps")
15 graphtrial_voltage(long,0,"pair_25ms.eps")
16 quit()
```

Listing A.4: src/libdtnet/neuron.cpp

```
 1 double Neuron::RungeKutta(double (*func)(double,double&,unsigned int&,Neuron*), double val, double
       &current, unsigned int &position, double &dt, Neuron *n) {
 2     double r;
 3     double k1,k2,k3,k4;
 4     k1 = (*func)(val, current, position, n)*dt;
 5     k2 = (*func)(val+0.5*k1, current, position, n)*dt;
 6     k3 = (*func)(val+0.5*k2, current, position, n)*dt;
 7     k4 = (*func)(val+k3, current, position, n)*dt;
 8     r = (k1+2*k2+2*k3+k4)/6;
 9     return r;
10 }
```

`Neuron::RungeKutta` method takes a function reference to a function that calculates dV for an arbitrary neuron model and then returns the computed value of $\frac{dV}{dt}$. In particular, the aEIF model calculates dV and dw in the `V_Update` and `w_update` functions shown in Listing A.5.

A Poisson spiking process was used in Aubie et al. (2009) to drive duration tuned neural networks. The Poisson spiking process neural model simulates a real neuron by setting the voltage to -65 mV when no spikes occur and +40 mV when a spike occurs. The Poisson spiking rates were increased for the first 2 ms to mimic the initial response burst observed in the auditory nerve (Kiang, 1965) and cochlear nucleus neurons (Rhode and Greenberg, 1992). The particular equations are fully documented in Aubie et al. (2009) and the function for determining whether or not a spike is produced in a given time step is shown in Listing A.6.
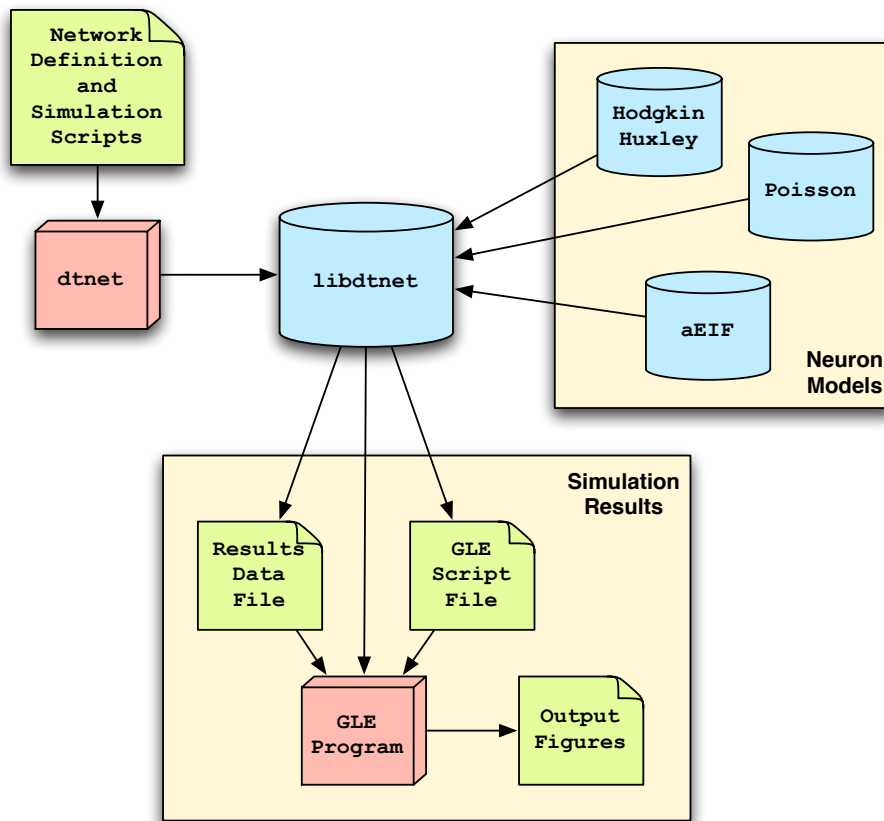
Figure A.1: Schematic diagram of the `dtnet` application program. Arrows represent the information flow direction, cubes represent executable programs and cylinders represent dynamically loaded libraries.

Listing A.5: src/models/aEIF.cpp

```cpp
void aEIF::update(double& current, unsigned int& position, double& dt) {

  // diffsolve resolves to the RungeKutta algorithm
    this->V += this->diffsolve(&V_update, this->V, current, position, dt, this);
    this->w += this->diffsolve(&w_update, this->w, current, position, dt, this);

    voltage[position] = this->V;
    this->spike(position, dt);
}

double V_update(double V, double& current, unsigned int& position, Neuron *n) {
    aEIF* a = static_cast<aEIF*>(n);
    double IL = a->gL * (V - a->EL);
    double ILd = -a->gL * a->deltaT * exp((V - a->VT) / a->deltaT);
    double r = (current - IL - ILd - a->w) / a->C;
    if (r > 10000) r = 10000; // Prevent overflows
    return r;
}

double w_update(double w, double& current, unsigned int& position, Neuron *n) {
    aEIF* a = static_cast<aEIF*>(n);
    return (a->a * (n->V - a->EL) - w) / a->tauw;
}

void aEIF::spike(unsigned int &position, double &dt) {

    if (this->V >= 20) {
        this->V = this->VR;
        this->w += this->b;
        voltage[position] = spike_height; // Artificial spike

      // this->delay offsets spike times relative to global 0 time
        spikes.push_back(position * dt - this->delay); // Save the spike time
    }
}
```

Listing A.6: src/models/poisson.cpp

```cpp
void Poisson::update(double& current, unsigned int& position, double& dt) {

    if (current == 0) {
        voltage[position] = -65;
        this->active = 0;
        return;
    }

    this->active += dt;

    // Initial faster spiking rate
    double maximum = 1000;
    double initial_spike_length = 1.0;
    double half_initial_length = 1.0;
    double initial_spike_height = (double) maximum / (double) mu;
    double half_initial_spike_height = 1.0 + (initial_spike_height - 1.0) / 2.0;
    double currentMult = 1;

    if (this->active < initial_spike_length) {
        if (mu < 100) {
            currentMult = 1;
        } else if (mu > 500) {
            currentMult = initial_spike_height;
        } else {
            currentMult = 1.0 + (initial_spike_height - 1.0) * sqrt((mu - 100.0) / 400.0);
        }
    } else if (this->active < initial_spike_length + half_initial_length) {
        if (mu < 100) {
            currentMult = 1;
        } else if (mu > 500) {
            currentMult = half_initial_spike_height;
        } else {
            currentMult = 1.0 + (half_initial_spike_height - 1.0) * sqrt((mu - 100.0) / 400.0);
        }
    }

    // Use rand() to determine if we have a spike
    // We expect to spike at mu Hz.
    double r = (double) (rand() % 10001); // Random number in [0,10000]
    // Finds mu in ms^-1 (mu is given in Hz)
    // Then multiplies by the time step to find mu in terms of per time step.
    // This gives a probability of firing in this time step.
    // When dt = 0.05, this means that mu is limited to <= 20,000Hz
    double p = (mu * 10 * dt) * current * currentMult; /**< Probability of firing. */

    if (r < p) spike(position, dt);
    else voltage[position] = -65;

}
```

B

NEURON Simulations and Additional Data for Chapter 3

B.1 Software Availability

Simulations for Aubie et al. (2012) (Chapter 3) were conducted with NEURON 7.2 (Carnevale and Hines, 2006) (software available at `http://www.neuron.yale.edu`) using the Python scripting interface (Hines et al., 2009). Simulation source code is available online at `http://www.github.com/baubie/DTNSpecies`.

B.2 Details of FSL analysis

Table B.1: Cells included in FSL analysis (Fig. 3.5). For each cell listed, the file number for each amplitude re threshold is listed (#F), the FSL slope for short stimulus durations ≤ 3 ms (S) and long stimulus durations ≥ 3 ms (L).

Cell	+10 dB			+20 dB			+30 dB		
	F#	S	L	F#	S	L	F#	S	L
MU10.01	41	-0.899	0.025	42	-0.049	0.168	2	-1.166	0.432
MU12.02	9	1.285	0.473		-			-	
MU14.04		-		2	0.059	-0.133		-	
MU14.07	2	1.955	-		-			-	
MU15.03	12	-4.339	2.543	13	-2.427	1.888	14	-1.346	1.200
MU15.06		-			-		2	-0.308	-
MU15.07	14	1.197	2.148	15	0.438	0.845	16	0.136	0.508

continued

Cell	+10 dB			+20 dB			+30 dB		
	F#	S	L	F#	S	L	F#	S	L
MU16.02		-		8	-0.984	-0.411		-	
MU17.11	2	2.061	0.992		-			-	
MU17.13	2	-0.132	1.185		-			-	
MU20.09	9	1.314	-		-			-	
MU20.14	19	-	0.958		-			-	
MU21.01	2	-1.240	-0.031		-			-	
MU21.11	13	0.638	2.747	14	0.709	-		-	
MU22.04	4	-2.921	-	5	-0.370	-	6	-2.648	-
MU22.10	4	2.689	0.102	5	2.032	0.666	6	2.267	0.450
MU22.16	5	-	1.383	6	-	1.269	7	-	1.096
MU23.05	2	-2.073	-0.028	14	-	-0.002		-	
MU23.06	6	-0.655	1.302	7	0.203	1.536	8	-0.057	0.125
MU24.02	13	1.628	1.798	14	2.360	0.582	15	1.611	-
MU25.05	2	0.488	1.237	4	1.190	0.811	9	1.290	0.408
MU25.12	3	0.085	0.768		-			-	
MU25.13	4	-	0.937	14	-	0.640		-	
MU27.11	31	-	0.597	32	-1.974	0.276		-	
MU27.13	2	-1.316	-		-			-	
MU30.06	7	0.320	-0.041	8	0.051	-0.012	9	-0.144	-0.002
MU31.04		-			-		10	0.744	-
MU33.11		-			-		2	1.773	0.019
MU34.02	4	0.611	0.222		-		2	0.260	-0.016
MU36.01	5	-1.353	0.829	6	-0.259	0.768	22	-1.812	0.625
MU36.02	5	1.150	-	25	1.484	-	10	0.228	0.803
MU36.07	5	-0.189	0.437	6	-2.845	0.008		-	
MU36.13		-			-		2	-0.066	1.858
MU36.14	21	0.617	0.814	6	0.064	-0.004		-	
MU36.16	3	0.527	0.209		-			-	
MU37.06	12	-	0.870	13	-	0.847		-	
MU39.05	11	1.857	0.290	12	1.837	-0.239	13	-	0.341
MU39.14	5	1.102	0.874	6	-0.446	0.948		-	

Additional Data and Figures from Chapter 4

C
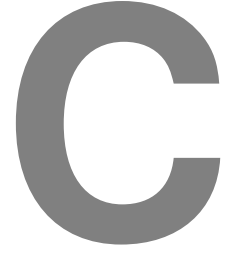
Analysis in chapter 4 was performed only on data presented at +20 dB (or between +21 dB and +29 dB if no +20 dB file was available). This appendix presents additional figures and data across all amplitudes for comparison. On a population level, there is little to no difference as a function of amplitude relative to threshold.

For our estimation of the Fisher information, we performed the following derivation to write the FI in terms of the square of the first derivative of the natural logarithm of the probability density function. The derivative of the natural logarithm of the probability density function was estimated with a linear interpolation between data points and thus the second derivative of $\Pr(\mathbf{S}|\mathbf{d}) = 0$.

$$
\begin{aligned}
\mathcal{I}(\mathbf{d}) &= -\mathrm{E}\left[\frac{\partial^2}{\partial \mathbf{d}^2} \ln \Pr(\mathbf{S}|\mathbf{d}) \Big| \mathbf{d}\right] \\
&= -\mathrm{E}\left[\frac{\Pr'(\mathbf{S}|\mathbf{d})\Pr''(\mathbf{S}|\mathbf{d}) - \Pr'(\mathbf{S}|\mathbf{d})^2}{\Pr(\mathbf{S}|\mathbf{d})^2} \Big| \mathbf{d}\right] \\
&= -\mathrm{E}\left[\frac{\Pr'(\mathbf{S}|\mathbf{d}) \times 0 - \Pr'(\mathbf{S}|\mathbf{d})^2}{\Pr(\mathbf{S}|\mathbf{d})^2} \Big| \mathbf{d}\right] \\
&= -\mathrm{E}\left[\frac{-\Pr'(\mathbf{S}|\mathbf{d})^2}{\Pr(\mathbf{S}|\mathbf{d})^2} \Big| \mathbf{d}\right] \\
&= \mathrm{E}\left[\frac{\Pr'(\mathbf{S}|\mathbf{d})^2}{\Pr(\mathbf{S}|\mathbf{d})^2} \Big| \mathbf{d}\right] \\
&= \mathrm{E}\left[\left(\frac{\Pr'(\mathbf{S}|\mathbf{d})}{\Pr(\mathbf{S}|\mathbf{d})}\right)^2 \Big| \mathbf{d}\right] \\
&= \mathrm{E}\left[\left(\frac{\partial}{\partial \mathbf{d}} \ln \Pr(\mathbf{S}|\mathbf{d})\right)^2 \Big| \mathbf{d}\right]
\end{aligned}
\tag{C.1}
$$
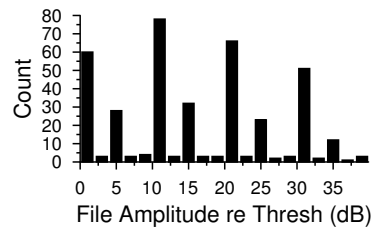
Figure C.1: Distribution of tested amplitudes. Most files were tested at threshold, +10 dB, +20 dB or +30 dB, however; many were also tested in between these amplitudes. In those cases, files were analyzed with the next lowest 10 dB multiple stimulus amplitude re threshold. Bin size = 2 dB.
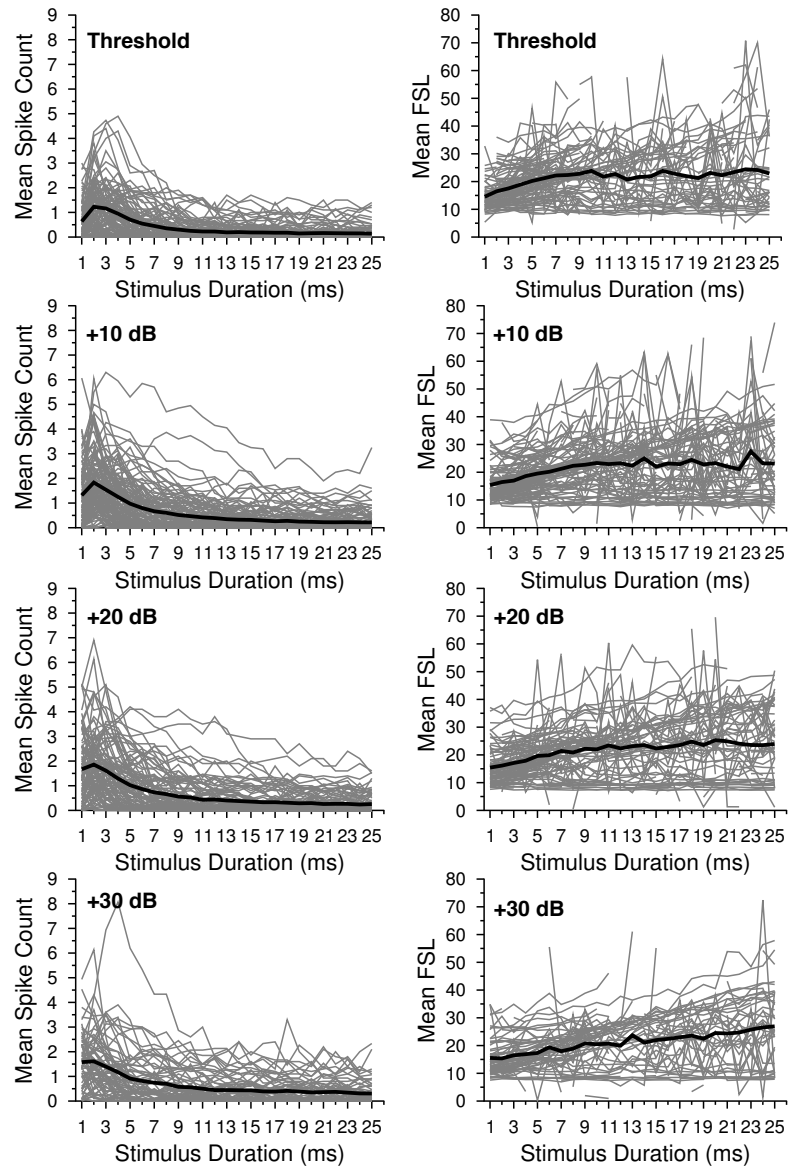
Figure C.2: Mean spike counts and first-spike latencies across all stimulus durations. See Figure 4.2 for details.
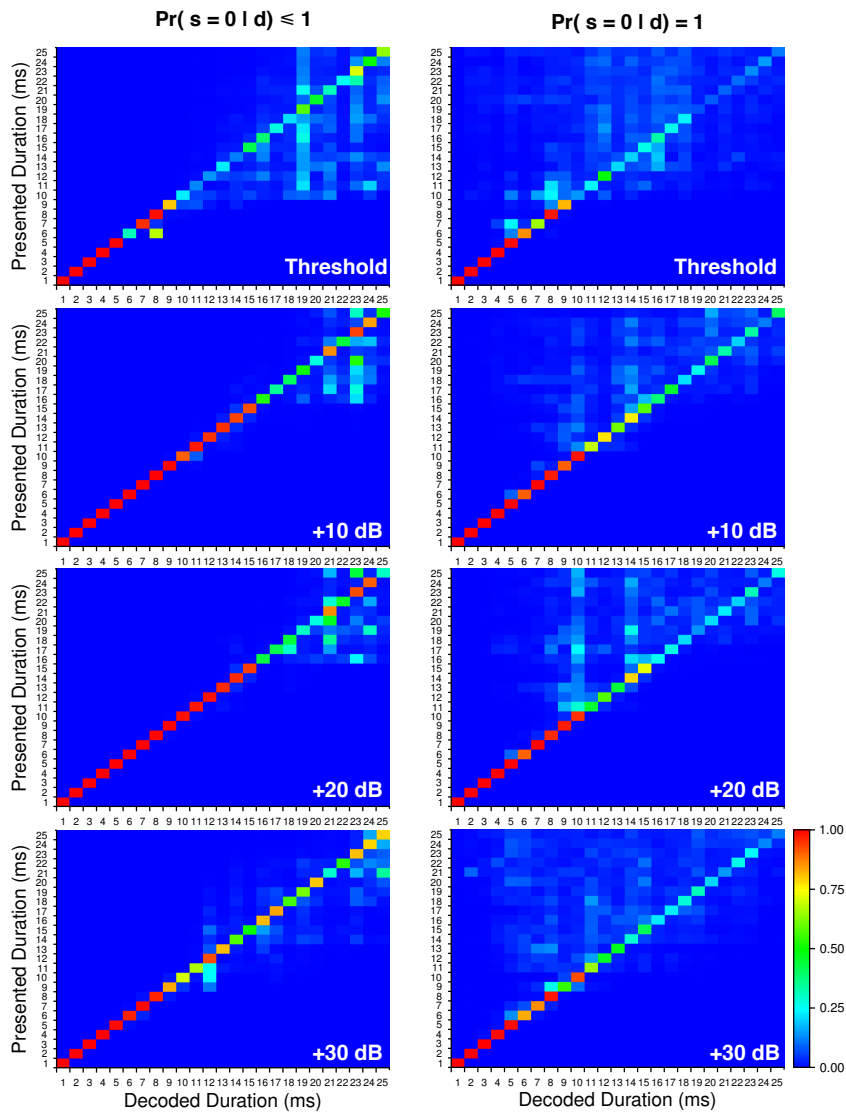
Figure C.3: Estimated optimal population count decoding across all stimulus durations (10,000 trials per stimulus duration). See Figure 4.6 for details.
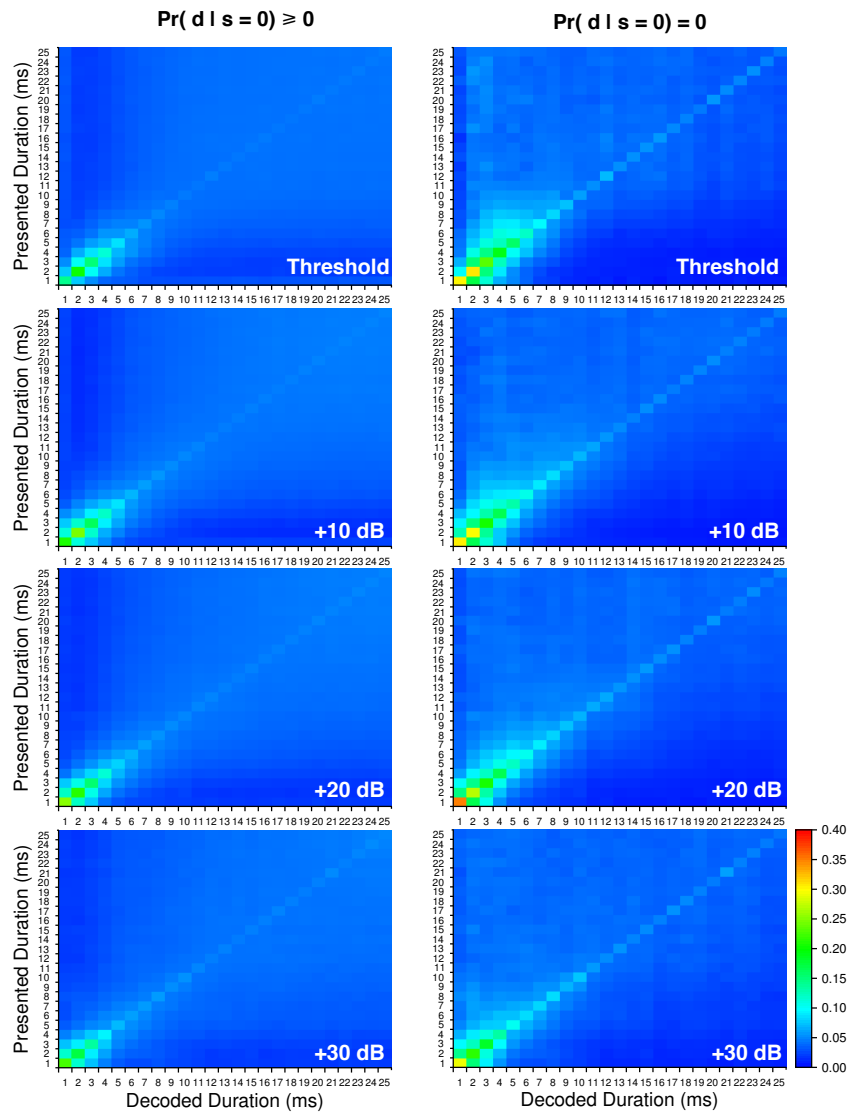
Figure C.4: Non-optimal population count decoding across all stimulus durations. See Figure 4.6 for details.
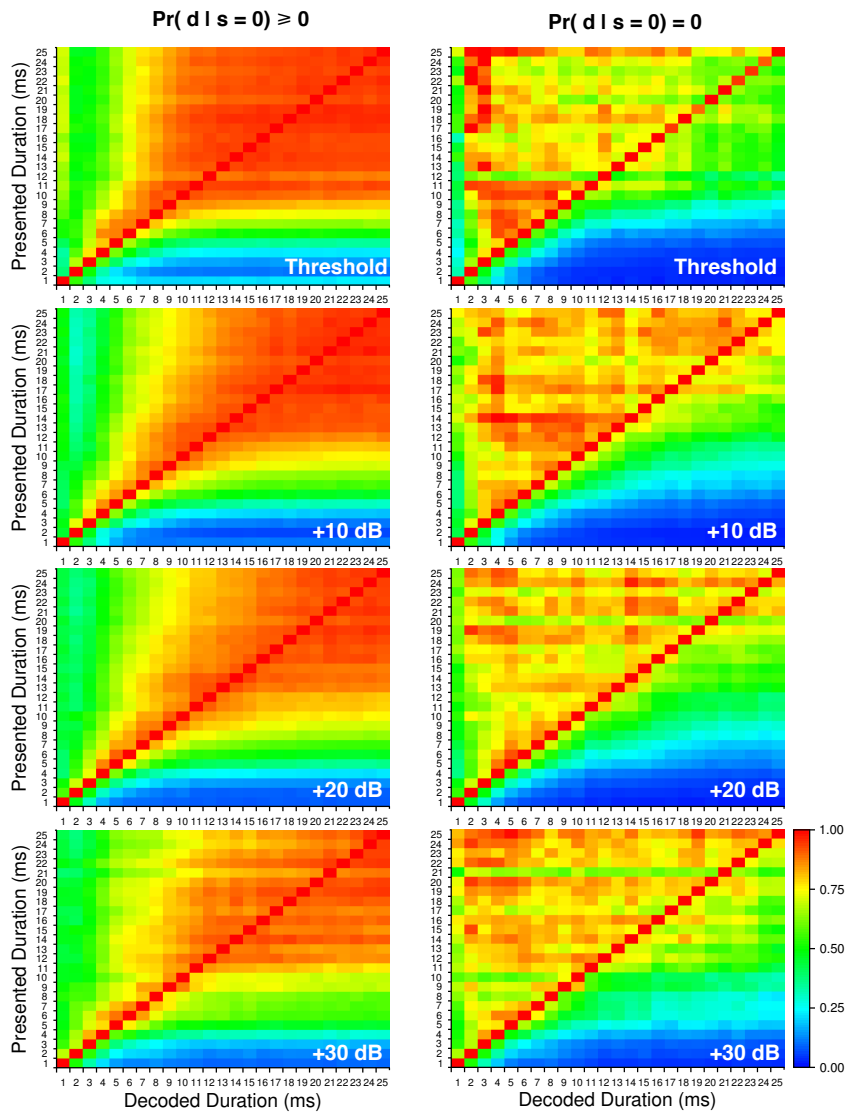
Figure C.5: Non-optimal normalized population count decoding across all stimulus durations. See Figure 4.6 for details.
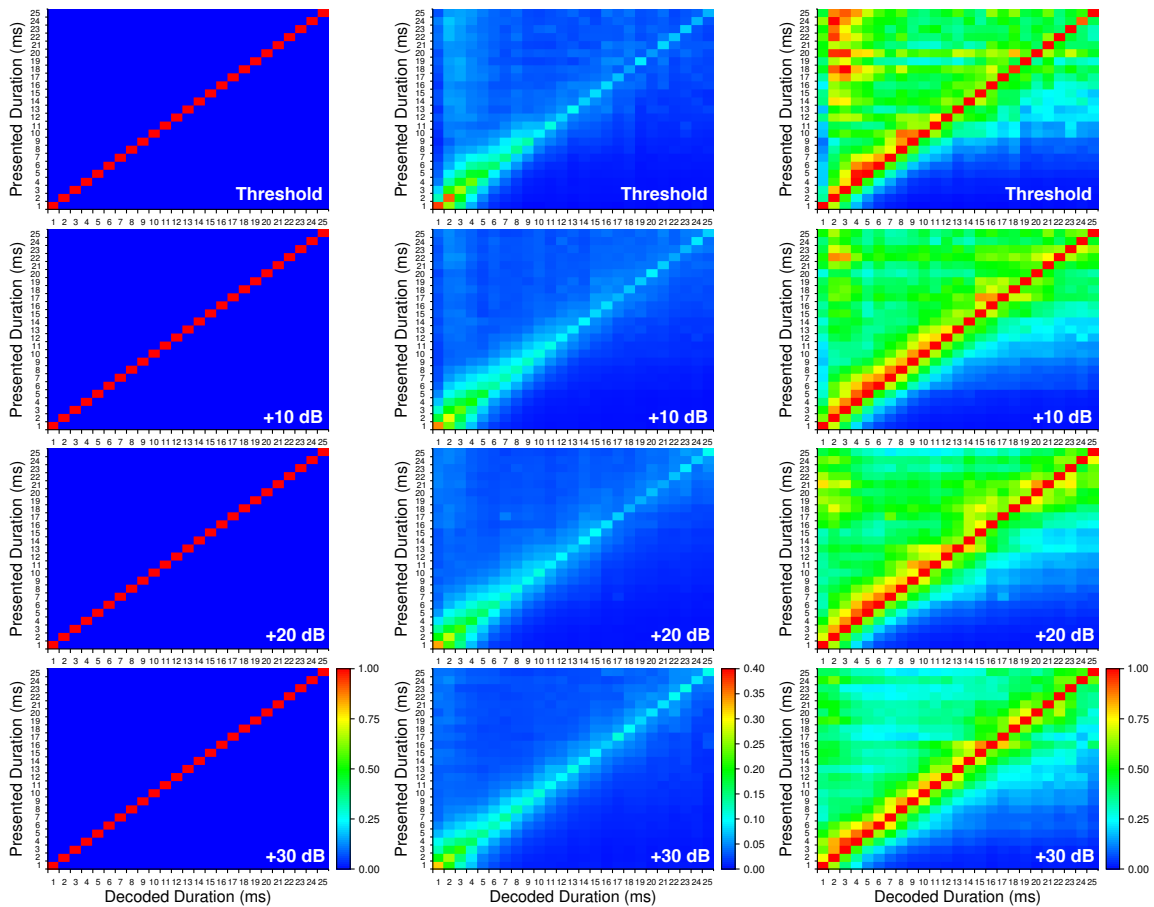
Figure C.6: Left Column: Estimated optimal duration decoding (100 trials per stimulus duration). Middle Column: Non-optimal average duration decoding. Right Column: Normalized non-optimal average duration decoding. See Figure 4.7 for details.
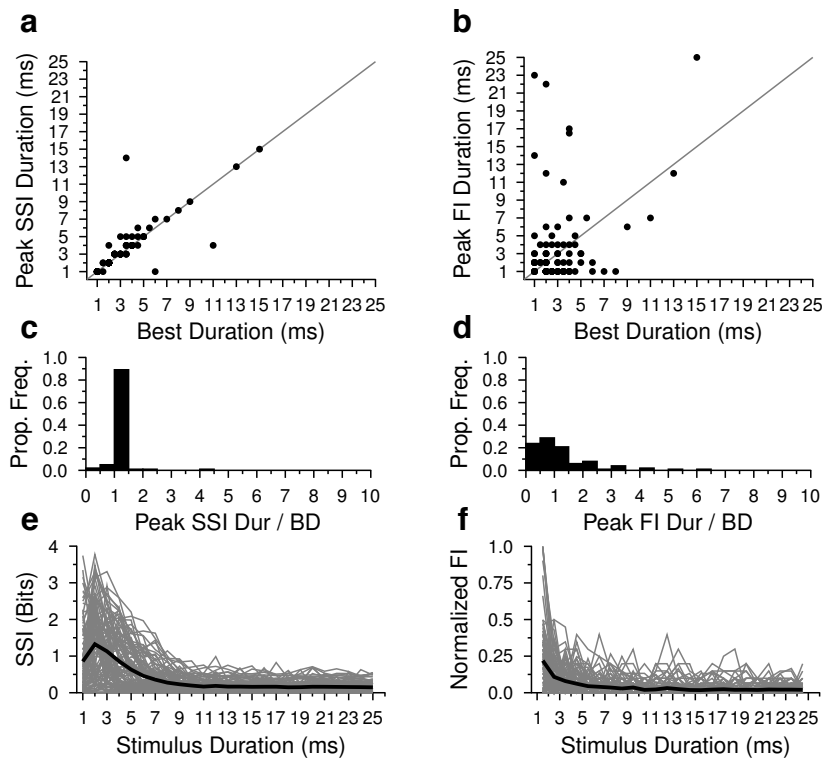
Figure C.7: Information analysis from Spike Counts at 0 dB re threshold (with zero spike counts). See Figure 4.4 for details.
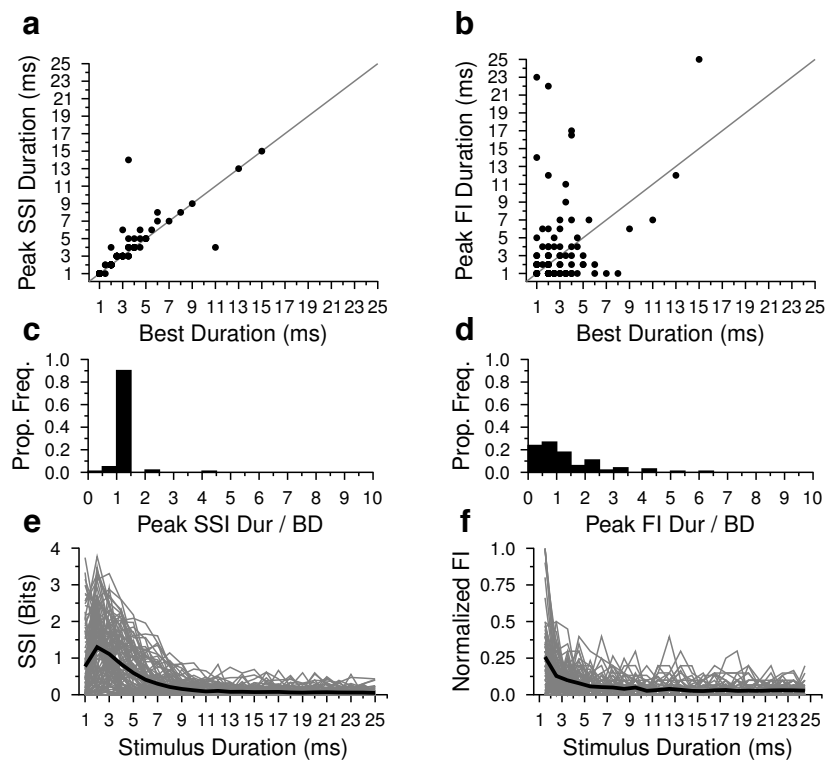
Figure C.8: Information analysis from Spike Counts at 0 dB re threshold (without zero spike counts). See Figure 4.4 for details.
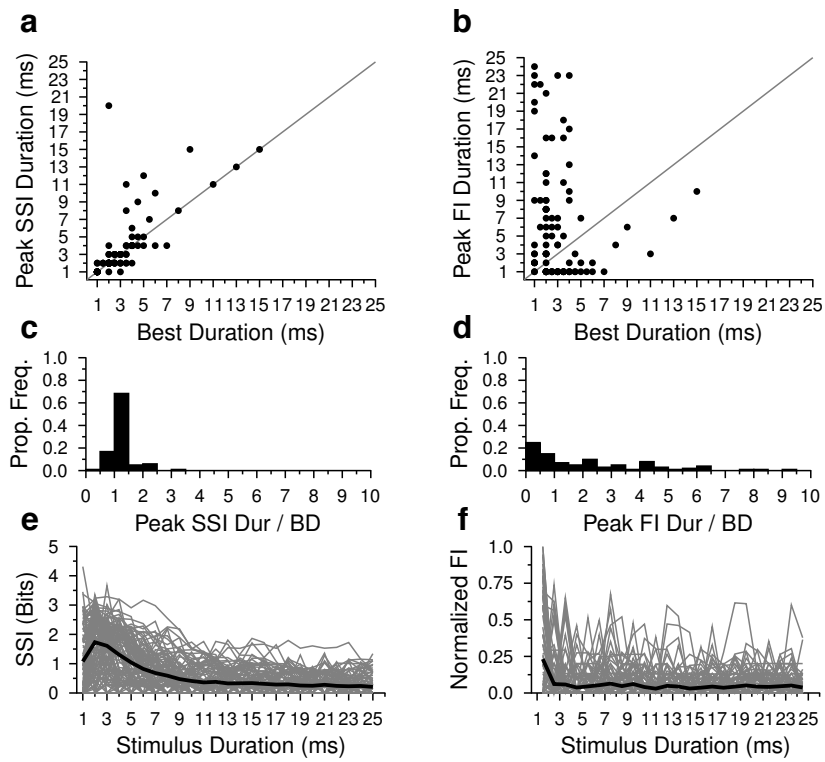
Figure C.9: Information analysis from FSL at 0 dB re threshold. See Figure 4.8 for details.
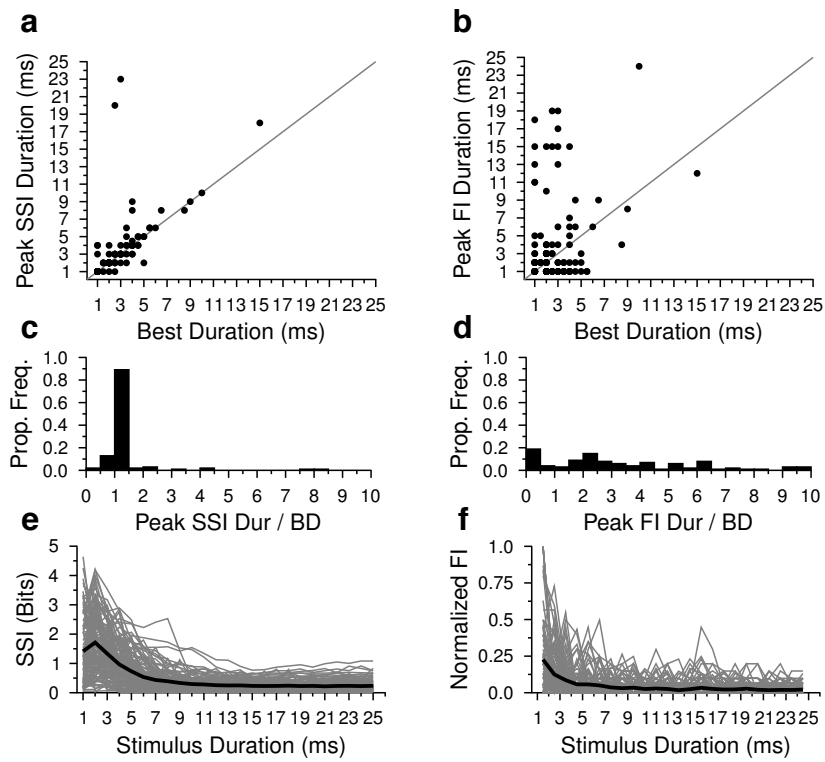
Figure C.10: Information analysis from Spike Counts at +10 dB re threshold (with zero spike counts). See Figure 4.4 for details.
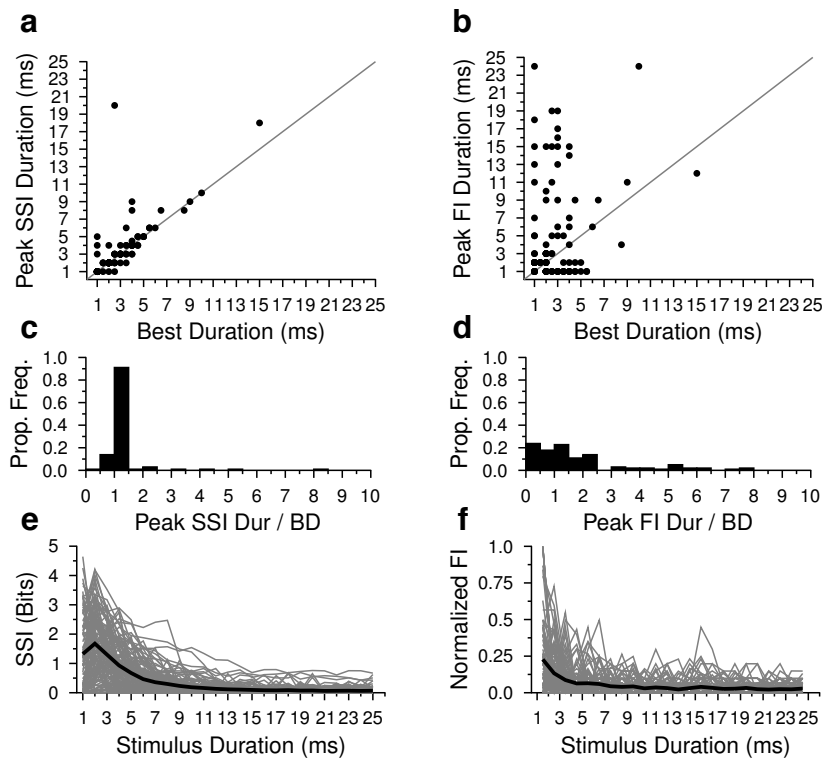
Figure C.11: Information analysis from Spike Counts at +10 dB re threshold (without zero spike counts). See Figure 4.4 for details.
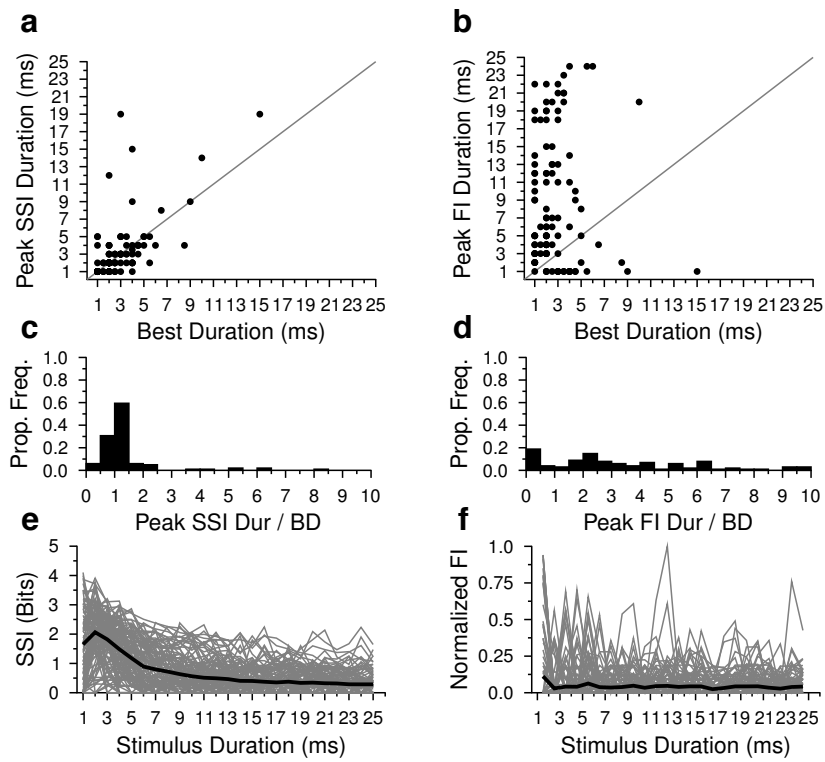
Figure C.12: Information analysis from FSL at +10 dB re threshold. See Figure 4.8 for details.
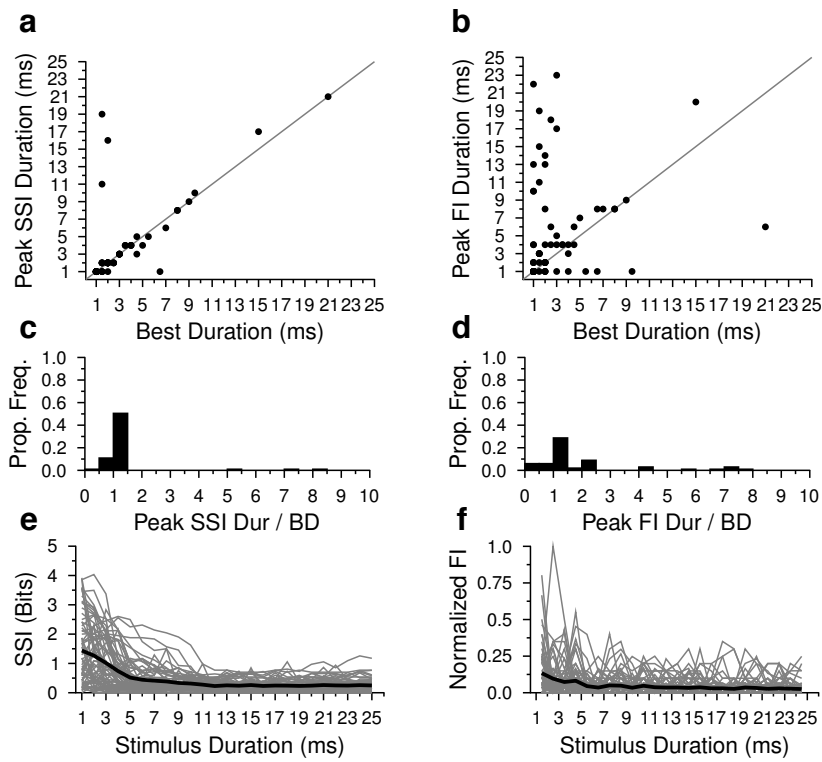
Figure C.13: Information analysis from Spike Counts at +30 dB re threshold (with zero spike counts). See Figure 4.4 for details.
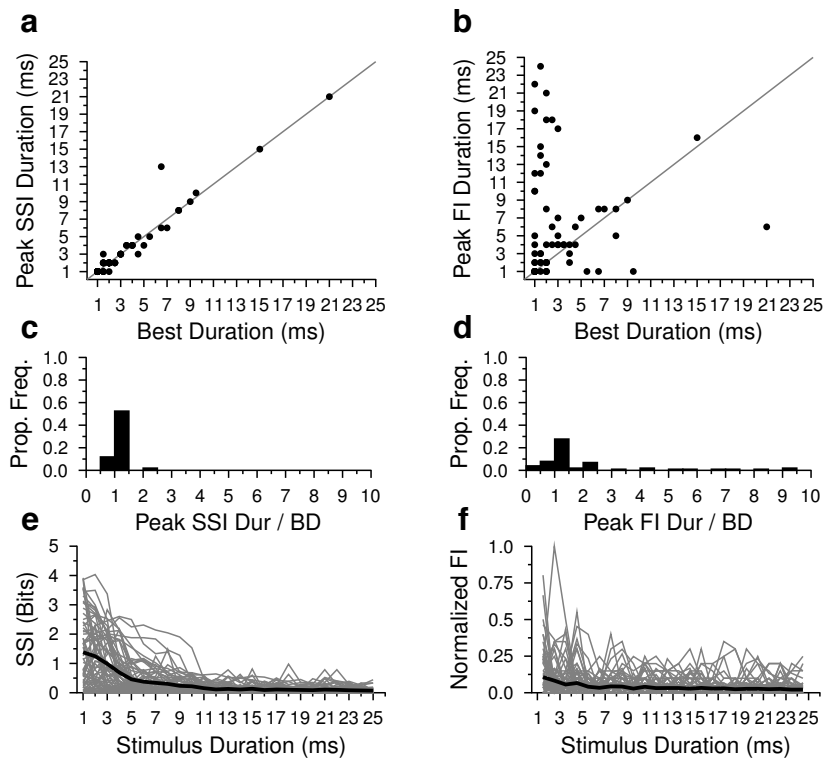
Figure C.14: Information analysis from Spike Counts at +30 dB re threshold (without zero spike counts). See Figure 4.4 for details.
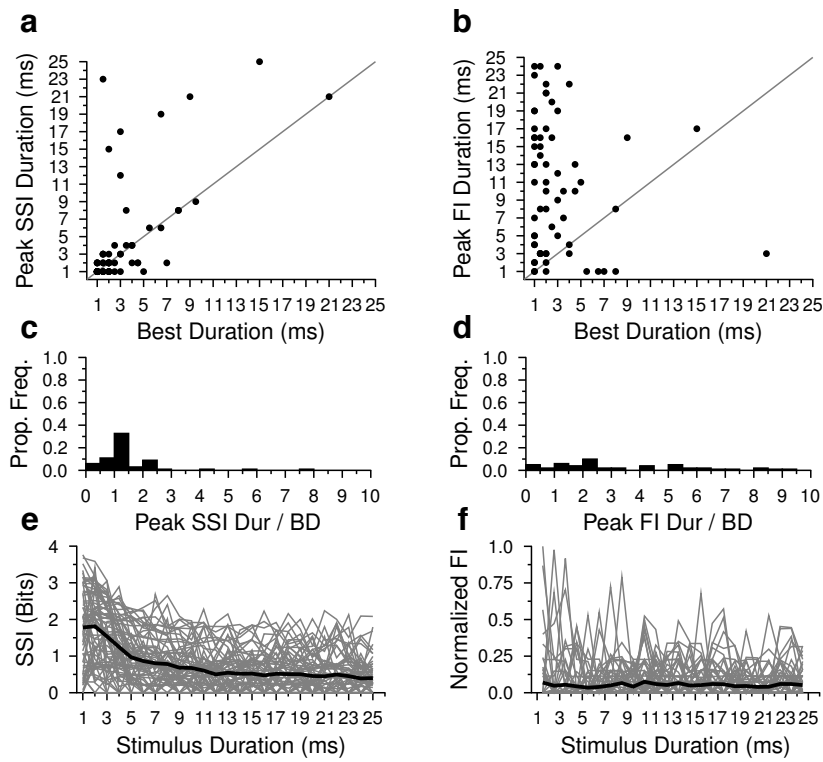
Figure C.15: Information analysis from FSL at +30 dB re threshold. See Figure 4.8 for details.

Table C.1: All cells included in analysis. Columns are the analysis sections each cell was included in and the actual stimulus amplitude re threshold (dB), the file number from that cell (F#) and the number of trials (T) is listed.

| Cell	Threshold			+10 dB			+20 dB			+30 dB		
	dB	F#	T	dB	F#	T	dB	F#	T	db	F#	T
MU07.12		-			-		+26	2	10		-	
MU09.02	+0	25	10	+10	26	10	+20	27	10	+30	28	10
MU09.05	+0	12	10	+10	2	10	+20	14	10		-	
MU09.09		-		+10	2	10		-			-	
MU10.01		-		+10	21	15	+20	22	15	+30	23	15
MU10.09	+0	2	10		-			-			-	
MU12.02	+0	9	10		-						-	
MU14.07		-		+10	2	10		-			-	
MU15.03	+0	11	10	+10	12	10	+20	13	10	+30	14	10
MU15.06		-			-			-		+30	2	10
MU16.02		-			-		+20	3	10		-	
MU17.04	+0	2	10		-			-			-	
MU17.11	+0	6	10	+10	2	10		-			-	
MU17.12	+0	13	10	+10	2	10	+20	15	10	+30	16	10
MU17.13		-		+10	2	10		-			-	
MU17.14	+0	2	10		-			-			-	
MU19.01		-			-		+20	4	10		-	
MU19.06		-			-		+20	2	10		-	
MU19.07		-		+10	10	10		-		+30	2	10
MU20.14	+0	8	10	+10	19	15		-			-	
MU20.17		-			-		+20	2	10	+30	5	10
MU21.01		-		+10	2	10		-			-	
MU21.02		-		+10	2	10		-			-	
MU21.07	+0	2	10		-			-			-	
MU21.11	+0	12	15	+10	13	15	+20	14	15	+30	15	15
MU22.04	+0	7	10	+10	4	10	+20	5	10	+30	6	10
MU22.10	+0	7	15	+10	4	15	+20	5	15	+30	6	15
MU22.17	+0	7	15	+10	8	15	+20	9	15	+30	10	15
MU23.05	+0	9	15	+15	2	10		-			-	
MU23.06	+5	6	15	+15	7	15		-			-	
MU23.10	+0	2	10		-			-			-	
MU24.02		-		+10	13	15	+20	14	15	+30	15	15
MU24.07		-			-			-		+30	2	10
MU25.05		-		+10	2	10	+20	4	10	+30	9	15
MU25.12	+0	4	15	+10	3	15		-			-	
MU25.13	+0	2	10	+10	4	15	+20	5	15		-	
MU26.04	+0	5	10		-			-			-	
MU27.08		-			-		+20	2	10		-	
MU27.11	+0	2	10	+10	9	15	+20	10	15		-	
MU27.13	+0	4	10	+10	2	10		-			-	

continued

Cell	Threshold			+10 dB			+20 dB			+30 dB		
	dB	F#	T	dB	F#	T	dB	F#	T	db	F#	T
MU28.04		-			-			-			-	
MU28.06	+0	4	15	+10	5	15		-		+30	2	10
MU30.02		-			-			-			-	
MU30.06	+0	6	15	+10	7	15	+20	8	15	+30	9	15
MU31.03		-			-		+20	2	10		-	
MU31.04	+0	4	15	+10	7	15	+20	6	15	+30	2	10
MU32.01	+0	4	10	+10	5	10	+20	6	10	+30	7	10
MU32.07		-			-			-			-	
MU33.08		-			-			-			-	
MU33.11		-			-			-		+30	2	10
MU34.02		-		+10	4	10		-		+30	2	10
MU35.04	+0	2	10		-			-			-	
MU36.01	+0	4	15	+10	5	15	+20	6	15	+30	14	15
MU36.02	+0	4	15	+10	5	15	+20	6	15	+30	7	15
MU36.07	+0	4	15	+10	5	15	+20	2	10		-	
MU36.12	+0	44	15	+10	45	15	+20	46	15	+30	47	15
MU36.13		-			-			-		+30	2	10
MU36.14	+5	4	15	+15	5	15	+25	6	15		-	
MU36.16		-			-			-			-	
MU37.01		-			-		+20	2	10		-	
MU37.06	+0	11	15	+10	12	15	+20	13	15		-	
MU38.04		-		+10	22	10	+25	23	10		-	
MU39.05	+5	10	10	+15	11	10	+25	12	10	+35	13	10
MU39.07	+5	21	10	+15	22	10	+25	1	10	+35	24	10
MU39.11	+5	21	10	+15	22	10	+25	23	10		-	
MU39.12	+0	4	15	+10	5	15	+20	6	15	+30	7	15
MU39.14	+0	4	15	+10	5	15		-			-	
MU41.01	+5	3	10		-			-			-	
MU41.02	+5	2	10	+15	6	10		-			-	
MU41.03	+0	4	10		-		+20	2	10		-	
MU42.02		-			-		+20	4	10	+30	5	15
MU42.03	+0	4	15	+10	5	15	+20	6	15	+30	7	15
MU42.05	+0	25	10	+10	26	10	+20	27	10	+30	28	10
MU42.09		-		+15	4	20	+23	2	10		-	
MU42.11		-		+15	4	10		-		+38	2	10
MU42.15		-			-			-			-	
MU42.16		-		+10	4	15	+20	5	15	+30	6	15
MU42.17	+0	4	10		-			-			-	
MU42.19	+0	4	15		-			-			-	
MU43.04		-		+10	4	15	+20	5	15		-	
MU44.02	+0	4	15	+10	5	15	+20	6	15		-	
MU44.04		-		+10	4	15	+20	5	15	+30	6	15
MU45.09		-		+10	2	10		-			-	

continued

Cell	Threshold			+10 dB			+20 dB			+30 dB		
	dB	F#	T	dB	F#	T	dB	F#	T	db	F#	T
MU46.11		-			-		+25	2	10		-	
MU46.12		-		+10	4	15	+20	5	15	+30	6	15
MU46.13		-		+10	6	15	+20	7	15	+30	8	15
MU47.05		-		+15	2	10	+25	4	10	+35	5	10
MU47.08	+0	2	10	+10	5	10	+20	6	10	+30	7	10
MU48.01		-		+10	5	10	+20	4	10		-	
MU48.05	+0	4	15	+10	5	15	+20	6	15	+30	2	10
UW132.08	+0	15	15	+10	14	15	+20	10	15	+30	13	15
UW134.04	+0	10	15	+10	11	15	+20	12	15	+30	13	15
UW170.04	+3	9	10	+13	10	10	+23	11	10	+33	12	10
UW170.06	+5	12	10	+15	13	10	+25	14	10	+35	15	10
UW170.09	+0	15	10	+10	16	10	+20	17	10	+30	18	10
UW170.12	+0	9	10	+10	10	10		-			-	
UW180.01	+0	37	10	+10	38	10		-			-	
UW181.07	+0	7	20	+10	8	20	+20	9	20	+30	10	20
UW181.08	+0	8	20	+10	9	20	+20	10	20	+30	11	20
UW181.09	+0	9	15	+10	10	15	+20	11	15	+30	12	15
UW184.03	+1	9	10	+11	10	10	+21	11	10	+31	12	10
UW184.07	+0	9	10	+10	10	10	+20	11	10	+30	12	10
UW184.10	+8	41	10	+18	42	10	+28	43	10	+38	44	10
UW184.13	+0	19	10	+10	20	10	+20	21	10	+30	22	10
UW193.01	+2	8	15	+12	9	15	+22	10	15	+32	11	15
UW219.01	+5	20	15	+15	21	15	+25	22	15		-	
UW219.06	+5	16	15	+15	17	15	+25	11	15	+35	25	15
UW219.08	+5	23	15	+15	25	15	+25	28	15	+35	30	15
UW221.03	+5	15	15	+15	16	15	+25	17	15		-	
UW223.01	+5	11	15	+15	12	15		-			-	
UW223.02	+5	6	15	+15	7	15	+25	8	15	+35	9	15
UW223.03	+8	8	15	+18	9	15	+28	10	15	+38	11	15
UW223.07		-		+15	11	15	+25	12	15	+35	13	15
UW223.09	+5	8	15	+15	9	15	+25	10	15	+35	11	15
UW228.04	+0	8	15	+10	9	15	+20	10	15		-	
UW228.05		-		+10	12	15	+20	13	15		-	
UW231.01	+5	9	15	+15	10	15	+25	11	15	+35	12	15
UW231.02		-		+10	9	15	+20	10	15	+30	11	15
UW231.03	+7	11	15	+17	12	15		-			-	
UW231.04		-		+10	6	15	+20	7	15	+30	8	15
UW231.06	+0	7	15	+10	8	15	+20	9	15		-	
UW231.07	+5	12	15	+15	13	15	+25	14	15	+35	15	15
UW235.01	+8	7	15	+18	8	15	+28	9	15		-	
UW235.02	+5	8	15	+15	9	15	+25	10	15		-	
UW287.02		-		+10	17	15	+20	19	15	+30	21	15
UW287.04	+7	9	15	+17	10	15	+27	11	15	+37	18	15

continued

Cell	Threshold			+10 dB			+20 dB			+30 dB		
	dB	F#	T	dB	F#	T	dB	F#	T	db	F#	T
UW296.01		-		+10	10	15	+20	11	15		-	
UW296.03		-		+15	16	15	+25	17	15	+35	18	15
UW296.04		-		+15	14	15		-			-	
UW296.06	+5	11	15	+15	13	15	+25	15	15		-	
UW301.02		-		+10	6	15	+20	7	15	+30	8	15
UW323.02	+0	7	15	+10	8	15	+20	9	15		-	
UW323.03		-		+10	12	15	+20	13	15	+30	14	15
UW323.04	+0	7	15	+10	8	15	+20	9	15		-	
UW328.01	+7	9	20	+17	10	20		-			-	
UW328.02	+5	12	20	+15	13	20	+25	14	20		-	
UW328.04	+0	6	20	+10	7	20	+20	8	20		-	
UW328.05	+5	8	20	+15	9	20	+25	10	20		-	
UW336.01	+2	8	20	+12	9	20		-			-	
UW336.07		-		+10	7	20	+20	8	20	+30	9	20
UW378.06		-		+10	4	15		-			-	
UW381.02	+5	28	20	+15	29	20	+25	9	15		-	
UW381.12	+1	5	15		-			-			-	
UW381.13		-		+10	6	20	+20	7	20	+30	8	20
UW389.03		-		+10	4	15		-			-	
UW389.09	+5	7	15		-			-			-	
UW397.01	+5	10	20	+15	11	20		-			-	
UW397.06	+5	9	20	+15	20	20		-			-	
UW397.09	+5	11	20		-			-			-	
UW400.03	+0	23	15	+10	22	15		-			-	
UW400.07	+5	9	20	+15	10	20		-			-	
UW400.08	+5	4	20	+15	5	20		-			-	
UW400.10		-		+10	6	20	+20	7	20	+30	30	20

SpikeDB: Extracellular Electrophysiology Database and Data Analyzer

D

D.1 Availability

SpikeDB is open source software available at `http://spikedb.aubie.ca` and downloadable as compiled versions for Microsoft Windows and Mac OS X, or as source code that can be compiled on Linux.

D.2 Overview

SpikeDB is a database and data analysis application for use in electrophysiological labs that employ custom data acquisition software, Spike, maintained by Brandon Warren at the University of Washington. SpikeDB is useful for organizing data files from multiple cells and animals and for quickly viewing the results of each recording session (Fig. D.1) or for population level analysis (Fig. D.2). For analysis, SpikeDB integrates the Python scripting language to enable users to write data analysis scripts that operate over their entire collection (or a subset of) their data. For example, mean spike counts per stimulus can be calculated and graphed directly in SpikeDB by the code in Listing D.1. Statistical analysis can be enhanced with well known python modules such as SciPy.
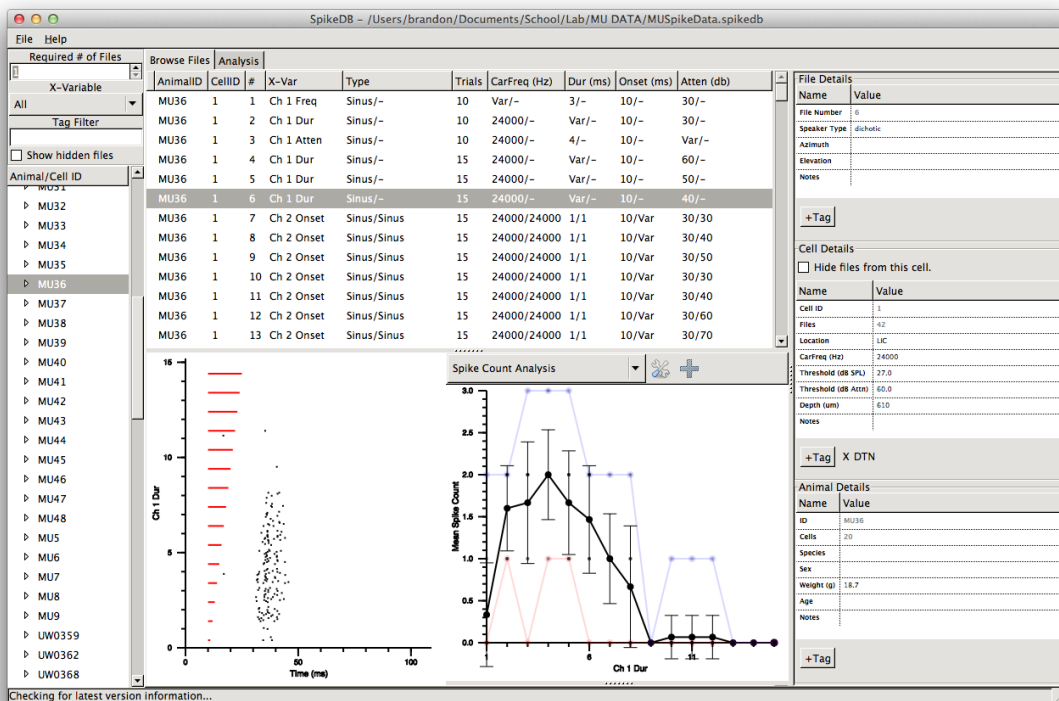
Figure D.1: Screenshot of SpikeDB showing a spike raster display and the spike count information.
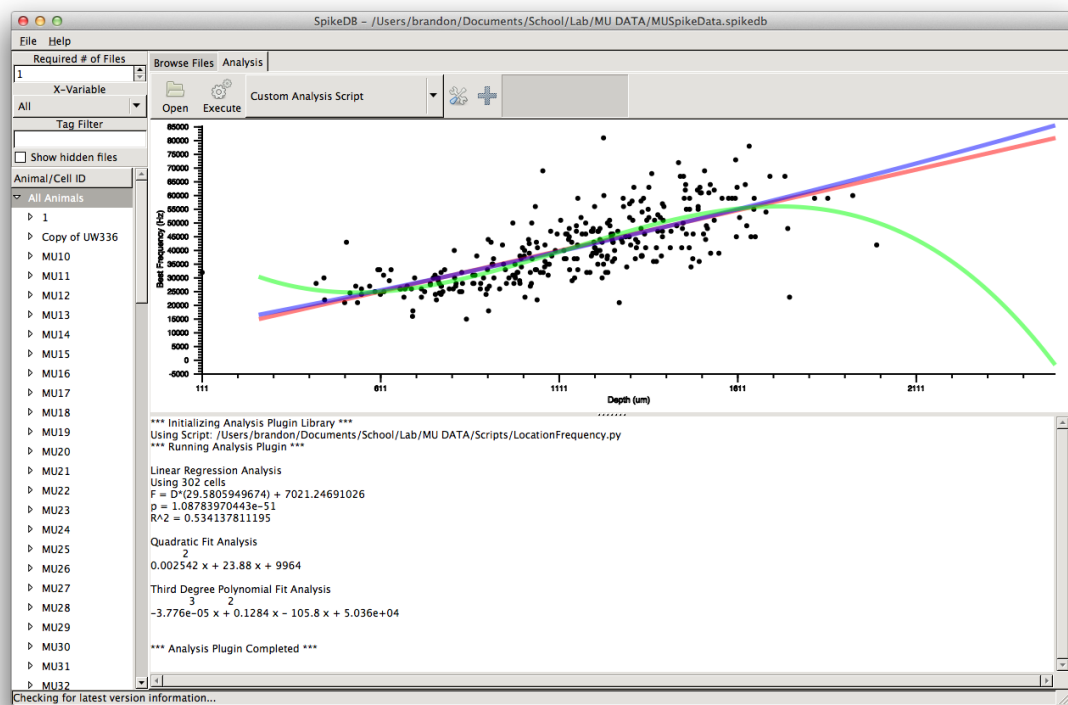
Figure D.2: Screenshot of SpikeDB showing population data (best excitatory frequency vs electrode depth).

Listing D.1: meanSpikeCount.py

```python
### Mean Spike Count
def SpikeDBRun():
  # Get selected files only
  files = SpikeDB.getFiles(True)

  # Plot means for each file.
  for f in files:
    # Create placeholder lists
    means = []
    err = []
    x = []

  # Calculate the mean and standard deviation
  # for each trial in the file
  for t in f['trials']:

    # Placeholder for the spike counts
    count = []

    # Get the X value
    x.append(t['xvalue'])

    # Get the spike counts for each pass
    for p in t['passes']:
      count.append(len(p))
      # Calculate the mean and standard devations
      means.append(SpikeDB.mean(count))
      err.append(SpikeDB.stddev(count))

    # Plot this file
    SpikeDB.plotXLabel(f['xvar'])
    SpikeDB.plotYLabel('Mean Spike Count')
    SpikeDB.plotLine(x,means,err)
```